NASA/TP-1999-209693

Subsonic Aerodynamic Assessment of Vortex Flow Management Devices on a High-Speed Civil Transport Configuration

Bryan A. Campbell, Zachary T. Applin, and Guy T. Kemmerly
Langley Research Center, Hampton, Virginia

National Aeronautics and
Space Administration

Langley Research Center
Hampton, Virginia 23681-2199

December 1999

Available from:

NASA Center for AeroSpace Information (CASI)
7121 Standard Drive
Hanover, MD 21076-1320
(301) 621-0390

National Technical Information Service (NTIS)
5285 Port Royal Road
Springfield, VA 22161-2171
(703) 605-6000

Contents

Abstract

An experimental investigation of the effects of leading-edge vortex management devices on the subsonic performance of a high-speed civil transport (HSCT) configuration was conducted in the Langley 14- by 22-Foot Subsonic Tunnel. Data were obtained over a Mach number range of 0.14 to 0.27, with corresponding chord Reynolds numbers of 3.08×10^6 to 5.47×10^6. The test model was designed for a cruise Mach number of 2.7. During the subsonic high-lift phase of flight, vortical flow dominates the upper surface flow structure, and during vortex breakdown, this flow causes adverse pitch-up and a reduction of usable lift. The experimental results showed that the beneficial effects of small leading-edge vortex management devices located near the model reference center were insufficient to substantially affect the resulting aerodynamic forces and moments. However, devices located at or near the wing apex region demonstrated potential for pitch control with little effect on overall lift.

Introduction

During the past 20 years, the airline market growth indicator of annual revenue per passenger miles has approximately tripled. Based on this steady growth, a projection of future activity indicates similar trends for the next 20 years, with long-range international travel being the fastest growing sector (ref. 1). Hence, to effectively meet this projected demand, there has been an increase in the efforts to develop the technology and increase the practicality of long-range supersonic transports.

The Concorde of the French and British governments has proven the feasibility of civil supersonic flight as well as provided an operational data base in a commercial environment from which to grow. However, the Concorde does not comply with the paradigm of current standards in such areas as environmental acceptability, range, payload capability, and passenger cost. Therefore, NASA, together with U.S. industry, has embarked on a research program to develop a future supersonic commercial transport, called a high-speed civil transport (HSCT), which meets or exceeds current standards for community noise, sonic booms, and atmospheric effects as well as maintains economic competitiveness with future long-range subsonic transports.

A major facet of this research involves substantially reducing the community noise levels associated with such an aircraft. Community noise, or the perceived noise at ground level, can be divided into three major areas: (1) sonic boom, which currently prohibits supersonic flight over land, (2) propulsion noise, which is generated particularly during takeoff, and (3) aerodynamic airframe noise, which is associated with high-lift devices and landing gear during takeoff and landing. As a result of the Supersonic Cruise Research (SCR) Program of the 1970's and 1980's, considerable knowledge and experience have been gained in these areas. (See refs. 2 to 9.)

While advancement continues in these three areas, simultaneous research efforts are underway to improve the overall lift and drag characteristics and thus improve the time-to-climb. Decreasing this time for a given power setting can minimize the area and duration of the ground-level perceived noise through noise attenuation. Improvements in aircraft lift and drag also positively impact other design considerations, such as engine power settings, range, approach speed, angle-of-attack range, and subsonic maneuverability. However, the wing geometry associated with efficient supersonic cruise typically incorporates many design features, such as high leading-edge wing sweep, low aspect ratio, and relatively thin airfoils with low camber. These features can conflict with the requirements for subsonic high lift and stability and control, particularly during the takeoff, loiter, and landing phases. During these phases, having high aspect ratios, moderate-to-high leading- and trailing-edge wing camber, and good control effectiveness is desirable.

Over the past years, a blending of technologies has resulted in high-lift devices being used on both the leading and the trailing edge of a highly swept wing planform (refs. 10 to 12). These devices can be deflected for increased camber. Additionally, using planform breaks or cranks, which reduce the leading-edge sweep on the outboard wing, has effectively increased the overall wing aspect ratio while maintaining design wing loading. Several independent studies, however, have revealed inherent problems resulting from such wing geometries. For example, reference 3 examined high levels of effective dihedral, C_{l_β}, which can result in Dutch roll instabilities and reversals in pilot-commanded roll rates. In references 10 and 11, a study of similar wing designs demonstrated that the vortex generation accompanying this wing design at low-to-moderate angles of attack produces high levels of localized vortex-induced suction over the upper surface. As angle of attack increases, progressive vortex breakdown occurs, particularly on the outboard wing panel. This breakdown can result in pitching-moment nonlinearities that limit the usable lift to levels well below the maximum lift coefficient, $C_{L,\mathrm{max}}$.

References 10 and 11 also noted the following aerodynamic behaviors associated with the outboard wing section: (1) high aerodynamic loading and boundary-layer build-up lead to early flow separation, (2) the apex vortex generated on the inboard section can induce a strong sidewash on the outboard wing section that adds to separated flow, and (3) the apex vortex can also induce a vertical velocity component on the outboard crank vortex to lift it away from the surface and thus produces rapid and pronounced lift loss on the outer panel. All three behaviors contribute to pitching-moment instabilities and aileron ineffectiveness. Therefore, to achieve the desired subsonic lift and drag improvements, an effective method is needed to delay the onset of vortex flow separation or to control the vortex-dominated flow field in a manner that preserves low-speed stability and control.

Methods including (1) blunt (i.e., large radius) leading-edge flaps deflected into the upwash field both uniformly and variably as a function of span, (2) leading-edge slats, and (3) combinations of these with trailing-edge flap deflections have been attempted with partial success. This paper describes the application and effectiveness of additional aerodynamic devices designed for vortex management.

The results presented herein were acquired in the Langley 14- by 22-Foot Subsonic Tunnel (ref. 13). Data were obtained with and without leading- and trailing-edge flap deflections (both without vertical tails) for an angle-of-attack range from -4° to 20° over a Mach number range of 0.14 to 0.27. The Reynolds number, based on the mean aerodynamic chord, ranged from 3.08×10^6 to 5.47×10^6.

Symbols

a	speed of sound, ft/sec
b	wing span, ft
C_A	axial-force coefficient, Axial force/$q_\infty S$
C_D	drag coefficient, Drag/$q_\infty S$
C_L	lift coefficient, Lift/$q_\infty S$
C_{L_α}	lift-curve slope, per deg
C_l	rolling-moment coefficient, Rolling moment/$q_\infty Sb$
C_m	pitching-moment coefficient, Pitching moment/$q_\infty S\bar{c}$
C_N	normal-force coefficient, Normal force/$q_\infty S$
C_n	yawing-moment coefficient, Yawing moment/$q_\infty Sb$
C_Y	side-force coefficient, Side force/$q_\infty S$
$\bar{c}$	mean aerodynamic chord, ft
D	drag, lb
L	lift, lb
L/D	lift-drag ratio
M	Mach number, V_∞/a
q	dynamic pressure, psf
R	Reynolds number, $\rho V_\infty \bar{c}/\mu$
S	wing reference area, ft^2
V_∞	velocity, ft/sec
α	angle of attack, deg
α_{break}	angle of attack at which an abrupt change occurs in slope of an aerodynamic force or moment curve, deg
β	angle of sideslip, deg
δ	flap deflection angle, normal to hinge line (positive down), deg
μ	viscosity, lb-sec/ft^2
ρ	density, slugs/ft^3

Derivatives:

C_{l_β}	$= \partial C_l/\delta\beta$, per deg
C_{n_β}	$= \partial C_n/\delta\beta$, per deg
C_{Y_β}	$= \partial C_Y/\partial\beta$, per deg

Subscripts:

L	leading edge
max	maximum

T	trailing edge
∞	free-stream conditions

Abbreviations:

AF-1	apex flap 1 (see fig. 29)
AF-2	apex flap 2 (see fig. 29)
AF-3	apex flap 3 (see fig. 29)
$\frac{1}{2}$AF-1	variation of AF-1 (see fig. 29)
FBS	forebody strake
HSCT	high-speed civil transport
PC	pylon vortex generator located at leading-edge break corresponding to crank
PI	pylon vortex generator located inboard of crank
PVG	pylon vortex generator
SCR	Supersonic Cruise Research
WF	upper surface wing fence
WS	wing strake

Model Description

Figure 1 shows the geometric characteristics of the model tested in this investigation, and figure 2 shows the model mounted in the Langley 14- by 22-Foot Subsonic Tunnel. This model represents the last iteration of the SCR Program and incorporates the required twist and camber for a design cruise speed of Mach 2.7. The wing has an inboard sweep of 73.02° and an outboard sweep of 60.00°. The leading-edge radius, which is large inboard, gradually decreases to a sharp edge outboard. The trailing edge is sharp for the entire span. The wing has full-span segmented leading-edge flaps (fig. 3(a)), and the trailing-edge flap system is composed of partial-span segments to accommodate engine nacelle placement. (See fig. 3(b).)

Tests were conducted for three configurations: flaps undeflected (cruise-wing), leading-edge flaps deflected 30°, and leading- and trailing-edge flaps deflected 30° and 20°, respectively, for high lift and approach. During this investigation, the model had no canards, horizontal tails, or engine nacelles. Table 1 shows the geometric characteristics of the baseline configuration. The wing aerodynamic reference area is defined by extending the inboard leading edge and the outboard trailing edge of the cruise configuration planform projection to the centerline. The surface coordinates of the model are presented in table 2 in the Langley Wireframe Geometry Standard (LaWGS) format, which is described in reference 14.

Several leading-edge vortex management devices were tested on the two configurations with the leading-edge flaps deflected. These devices, shown in figures 4 and 5, include pylon vortex generators (PVG's), wing strakes, upper surface fences, and apex flaps. All of these devices except the apex flaps were mounted close to the leading-edge crank. The apex flaps were mounted at the wing apex near the junction of the wing and fuselage.

Test Conditions and Instrumentation

Tests were conducted in the Langley 14- by 22-Foot Subsonic Tunnel (ref. 13) with the following Mach numbers, dynamic pressures, and average Reynolds numbers based on the wing mean aerodynamic chord:

Mach number, M	Dynamic pressure, q, psf	Reynolds number, R
0.14	30	3.1×10^6
.18	50	3.9
.22	70	4.6
.25	90	5.0
.27	110	5.5

The tests were conducted over an angle-of-attack range of −4° to 20°. For selected configurations, angle-of-attack sweeps were conducted at sideslip angles of ±5°. All configurations had zero roll angle.

A six-component strain-gauge balance mounted inside the fuselage measured the forces and moments. Appendix A presents the accuracy of this strain-gauge balance. The angle of attack was set by the pitch and height assembly of the model support system. This angle was measured with an accelerometer installed in the model, and the angle of sideslip was measured with a digital encoder mounted to the turntable gearing mechanism.

Base pressures were measured with a static pressure manifold fitted to the outer perimeter of the fuselage base, and chamber pressure was measured with a static tube inside the fuselage cavity. These pressures were measured throughout the test to correct the data to a condition of free-stream pressure acting over the total model base. The data were corrected for jet-boundary and blockage effects according to the methods of references 15 and 16. No corrections were made for flow angularity or flow interference for the local support system.

Results and Discussion

Appendix B presents the complete tabulated force and moment results obtained in this wind tunnel investigation, along with an associated configuration index. The following sections present a discussion of the results, which are shown in the figures as follows:

	Figure
Lateral divergence investigation	6
Tunnel dynamic pressure effects	7
Transition grit effects	8 and 9
Flap effects	10
PVG effects	14
Dual PVG effects	16 to 18
Wing strake effects	21 and 22
Wing fence effects	24 and 25
Wing fence with PVG effects	27 and 28
90° apex flap effects	33
115° apex flap effects	34 and 35
One-half 115° apex flap effects	37
Lateral aerodynamic effects without devices	38 and 39
Lateral aerodynamic effects with one-half 115° apex flap	40 and 41

Lateral Divergence Investigation

Before investigating the effectiveness of the vortex management devices, we addressed the issue of model safety. Concerns of model stability resulted from the long slender forebody and the nature of its vortex shedding. Typically, the transition from symmetric to asymmetric vortex shedding from slender forebodies at moderate-to-high angles of attack can result in the rapid onset of large oscillatory side forces for sting-mounted models. The associated rapid increase in yawing moment can jeopardize the balance-sting support. Therefore, methods were sought to minimize the magnitude of the asymmetric vortex shedding and hence minimize the potentially damaging model dynamics.

References 17 and 18 propose helical strakes and elliptic forebody shaping as possible solutions to this problem. However, these methods generally targeted angles of attack above 25°, which are beyond the expected angle for transition to asymmetric vortex shedding of 16° for this model. Hence, simple tab-like forebody strakes were used to correct asymmetric vortex shedding.

As shown in figure 6(a), the addition of forebody strakes had little effect on the longitudinal aerodynamic data; only slight increases in pitching moment occurred. The lateral aerodynamic data (fig. 6(b)) demonstrated the effectiveness of the strakes. The forebody strakes stabilized the model from the potentially hazardous dynamic forces associated with asymmetric vortex shedding at the higher angles of attack tested. Also, as shown in figures 7(a) and 7(b), the sensitivity to variations in tunnel dynamic pressure was generally small and confined to the lateral aerodynamic data.

The data showed that abrupt changes in yawing moment did not occur until after 20°, and observed large-scale model oscillations did not occur until 22.5° (see fig. 6(b)). Thus, the forebody strakes were deemed unnecessary for the remainder of this test and hence were removed. Their removal also prevented any possible contamination of the flow fields associated with the vortex management devices for the wing.

Effect of Transition Grit

Traditionally, subsonic models having relatively low leading-edge sweep angles and limited angle-of-attack range were gritted according to the method of reference 19 to properly simulate laminar-to-turbulent boundary-layer transition. Applying this method typically required strips of grit near airfoil leading edges and a ring of grit on the fuselage nose. However, highly swept configurations, such as the model used in this test, are usually dominated by vortical flow. Hence, the location of transition grit depends on where flow reattachment occurs. Also, the nose ring transition strip may not be effective in simulating transition on long slender forebodies.

To resolve these issues of grit placement, tests were conducted in which the entire model upper surface and entire forebody were lightly sprinkled with No. 60 grit. These results were then compared with the no-grit test results. As shown in figure 8, the addition of grit had little effect on the longitudinal aerodynamic data but exhibited changes in the lateral aerodynamic data. Figure 9 shows that these lateral aerodynamic changes are a function of dynamic pressure and that C_l, C_n, and C_Y decrease as dynamic pressure increases.

Although these results are not from an isolated forebody test, the trends coincide with those presented in reference 20, which summarized the work of references 21 and 22 on the side-force variations as a function of cross-flow Reynolds number on an ogive cylinder. Reference 20, however, showed that geometric perturbations in the nose apex geometry were a major factor in lateral divergence repeatability difficulties for slender forebodies. Therefore, because of the uncertainty of transition grit application repeatability and possible erosion during the test, the issue of lateral divergence repeatability was addressed by performing all subsequent testing without transition grit.

Effect of Leading- and Trailing-Edge Flap Deflections

Figure 10 shows the results for the cruise-wing configuration with the undeflected flaps ($\delta_L = 0°$, $\delta_T = 0°$), the configuration with the deflected full-span leading-edge flaps ($\delta_L = 30°$, $\delta_T = 0°$), and the configuration with the deflected partial-span trailing-edge flaps ($\delta_L = 30°$, $\delta_T = 20°$). In figure 10(a), C_{L_α} changed from 0.034 to 0.041 at $\alpha = 2°$ for the cruise-wing configuration; this change shows that the onset of upper surface vorticity has occurred. This onset is also indicated by a corresponding break in pitching moment. As angle of attack increases, two additional inflections in nose-up pitch occur: one at $\alpha \approx 6°$ and another at $\alpha \approx 12°$. These last two inflections are less severe than the initial pitching-moment break and indicate a redistribution of upper surface vortex location relative to the moment reference center. In reference 10, a study of a similar wing demonstrated that the vortex generation that accompanies these highly swept, cranked-wing designs at low-to-moderate angles of attack produces high levels of localized vortex-induced suction over the upper surface of the inner and outer wing panels. As angle of attack is furthur increased, vortex breakdown begins to occur on the outboard wing panel. This breakdown can result in pitching-moment nonlinearities that limit the usable lift to levels well below the $C_{L,\max}$. Additionally, high aerodynamic loading and boundary-layer buildup lead to early flow separation on the outboard wing panel and thus also contribute to pitching-moment inflections.

Deflecting the leading-edge flaps into the upwash field produces a weaker apex (or inboard) vortex system at the same angle of attack; hence, less overall lift and less nose-up pitching moment are produced. However, the trends of α_{break} for pitching moment tend to remain the same. The addition of trailing-edge flap deflection has the effect of delaying the α_{break} for pitching moment to about 14° and thus extending the usable lift range. Figure 10(b) shows the effect on lateral performance. In general, flap deflections tend to produce slight asymmetric flow characteristics that are within the angle-of-attack range of importance to this test. However, the addition of a vertical tail should improve the lateral-directional stability characteristics.

The efficiency of this flap configuration over the C_L range generally considered for HSCT high lift (i.e., $C_L = 0.4$ to 0.8) is shown in the drag polar in figure 10(a) as well as the lift-drag plots in figure 10(c). For example, a drag reduction of about 200 counts at $C_L = 0.5$ occurs with the leading-edge flaps deflected 30°, whereas a drag reduction of about 310 counts occurs with the leading-edge and trailing-edge flaps deflected 30° and 20°, respectively.

Effect of Pylon Vortex Generator

Figure 11, which is reproduced from reference 10, shows the subsonic flow-field interaction of the apex vortex system with the outboard crank vortex system. As shown at high angles of attack, the apex vortex can induce a vertical velocity component on the outboard crank vortex to lift it off; thus, rapid and pronounced lift loss is produced on the outer wing panel. Such vortex dynamics can contribute to both pitching-moment instabilities and aileron ineffectiveness. Therefore, an innovative method needs to be developed to delay the onset of flow separation on the outboard wing panel or to control the separation in such a way as to preserve low-speed stability and control.

Previous work investigated methods designed to promote attached flow, such as blunt (i.e., large radius) leading-edge flaps deflected into the upwash, both uniformly and variably as a function of span (refs. 3 and 23); leading-edge slats (ref. 7); and combinations with trailing-edge flap deflections (ref. 6), all with partial success. Therefore, vortex management devices intended to either reduce or alleviate the apex vortex influence on the outboard crank vortex were tested on this HSCT model. Several of these devices were previously tested on similar planform configurations, and the results are reported in references 10 and 11.

One such device, called a pylon vortex generator (fig. 12), is intended to generate a vortex that rotates in the opposite sense of the apex vortex to induce a downward velocity component on the crank vortex to resist its lift-off tendency. As shown in figures 13(a) and 13(b), a PVG was located at the leading-edge break point of each wing and aligned parallel to the streamwise velocity component. Figure 14 shows the results of the single PVG compared with those of the baseline. In general, a single PVG proved ineffective in significantly altering the pitch-up characteristics of this model. However, it was effective in reducing the C_l, C_n, and C_Y of the flapped configuration at high angles of attack.

To induce a more powerful downward velocity component on the crank vortex, an additional PVG was installed at a location inboard of the PVG located at the crank. (See figs. 15(a) and (b).) Figure 16 demonstrates that the addition of an inboard PVG had a slight negative effect on the overall performance, which is particularly evident in the quantities of C_L and L/D. At the higher angles of attack, the inboard PVG probably produced a vortex that passed under the wing surface and directly reduced lift and increased drag. Figure 17 shows that with the trailing-edge flaps set to 0°, the PVG's provided no additional benefits. As shown in figure 18, these results are consistent with the dynamic pressure variation trends observed for the cruise wing with transition grit in figure 9, which demonstrates no noticeable effects of dynamic pressure on the wing with the PVG's installed.

Effect of Wing Strake

A variation of the PVG concept is to generate a vortex near the crank that rotates in the same sense as the apex vortex. At moderate angles of attack, this vortex behaves similar to those produced by the wing root strakes of high-performance aircraft (i.e., F-16 or F-18) by energizing the stalling flow on the tip panel or in this case the outer wing panel. Figure 19 illustrates the device and the desired flow field. This device, called a wing strake herein, is shown mounted to the model in figures 20(a) and (b).

Figure 21 shows the effect of the wing strake on the performance of the high-lift configuration ($\delta_L = 30°$, $\delta_T = 20°$). As shown in the figure, the wing strake tends to slightly smooth the pitch-up characteristics, but it does not lessen the overall pitching-moment magnitude. Also, the slight increase in lift is negated by a corresponding increase in drag; thus, no overall L/D benefits are produced over the high-lift range (i.e., $C_L = 0.4$ to 0.8). The lateral characteristics are similar to those shown in figure 16(b) for the inboard and outboard PVG's. With the exception of small differences in the lateral data at high angles of attack, the results are consistent with the results in figure 22 for the configuration with the trailing-edge flaps undeflected.

Effect of Wing Fence

The devices reported on thus far relied on aerodynamic means to suppress the influence of the inboard vortex on that of the outboard crank. Another device, an upper surface wing fence shown in figure 23, attempted to suppress the vortex interaction by placing a physical boundary between them.

Figure 24 shows the effects of the wing fence on the high-lift configuration. Overall, the wing fence had little effect on the pitching-moment characteristics, but its presence did tend to decrease lift at the higher angles of attack. The corresponding change in L/D was negligible over the C_L range of interest. The associated lateral aerodynamic data also show little change in performance. Setting the trailing-edge flaps to 0° (fig. 25) resulted in only small pitching-moment benefits that are confined to the higher angles of attack; hence, no improvement in overall L/D occurred.

The performance of the wing fence is possibly a function of its relative angle to the inboard vortex core trajectory or the local surface velocity components. However, testing these parameters was beyond the scope of this investigation.

Effect of Device Combination

A combination of the wing fence and the PVG located at the crank was investigated. Their relative positioning is shown in figure 26. The aerodynamic results presented in figures 27 and 28 demonstrate that the effects are small when compared with the basic deflected flap configurations; hence, no appreciable benefits are obtained by combining these devices.

Effect of Apex Flaps

An alternate approach to wing vortex management is to redirect the vortex-induced suction force and hence directly impact the overall lift and drag characteristics. In previous research, a concept known as vortex flaps was used to achieve this form of vortex management. These flaps were designed to utilize sharp leading edges that were deflected downward relative to the wing plane to reduce configuration drag by rotating the vortex-induced suction force forward. Reference 24 provides a more detailed discussion on the design of such flaps. Although the downward deflection of vortex flaps can produce significant performance improvements, a variation of this concept demonstrated that upward deflections of sharp leading-edge flaps on the order of 120° to 160° (or 60° to 20° measured from the upper surface of the wing) can produce additional aerodynamic benefits for shorter approach and landing through increased lift and drag. (See refs. 17 and 25.)

In this investigation, a derivative of the upward deflected flap was tested. However, as shown in figure 29, the flap spans were confined to the apex region of the wing; hence, the flaps are called apex flaps. Figures 30 to 32 are photographs of these flaps. The leading- and trailing-edge flap deflections shown were not the only configurations tested. The apex flaps were tested at two deflection angles, 90° and 115°, measured from the upper surface of the wing, just aft of the leading edge.

The objective was to provide a means to directly affect pitch control for rotation during takeoff and for flare during landing, all with minimal effect on the overall lift characteristics. Figure 33 shows the results of the 90° apex flaps on the cruise configuration. Over the C_L range of 0.4 to 0.8, the apex flaps can provide significant increases in nose-up pitching moment. For example, depending on the flap geometry, C_m increased about 47 to 66 percent at $C_L = 0.5$. Similarly, C_m increased about 18 to 30 percent at $C_L = 0.8$. The apex flap with the largest area (AF-1) provided the most nose-up pitch control for rotation. This positive increment in pitching moment was accomplished with little effect on lift; however, the corresponding increase in drag resulted in overall L/D degradation; thus, the prolonged usefulness of this drag is limited during takeoff. Such a device can be momentarily deployed to provide the initial takeoff rotation. Once that has been achieved, the flap can be stowed to allow induced vortex lift to provide additional nose-up pitch. Also, as previous results have shown, the effects on lateral stability were relatively small and should easily be overcome by a sufficient vertical tail. Similar results are obtained with the 115° apex flaps. (See fig. 34.)

Figure 35 shows the influence of deflecting the leading-edge flap 30° with AF-1 deployed 115°. Adding the apex flap to the deflected leading-edge flap increases the magnitude of both the pitching moment and the lift. However, the resulting increase in drag again degrades the L/D performance.

Data were also acquired for a variation of the AF-1 apex flap. (See fig. 36.) This flap variation is referred to as the $\frac{1}{2}$AF-1, and it was only used for the configuration with the leading-edge flaps deflected 30°. Figure 37 shows the longitudinal and lateral data for this flap on both deflected flap configurations. The magnitudes of the effects caused by the $\frac{1}{2}$AF-1 flap are about half those of the AF-1.

Effect of Sideslip

Figures 38 through 40 show the results of yaw on the tailless model for $\beta = 0°$, $-5°$, and $5°$. Two salient features are the differences in the rolling and yawing moments of the deflected leading-edge configuration (fig. 39) when compared with those of the cruise-wing configuration (fig. 38). The decreased rolling moment and increased yawing moment can be attributed to the increased geometric anhedral coupled with the forward rotation of the induced vortex-lift vector by the flap.

The addition of the $\frac{1}{2}$AF-1 deflected 115° on the configuration with the deflected leading-edge flap produced a C_l increment (see fig. 40) comparable with that for the cruise-wing configuration but produced little change to C_n. Also, the level of C_Y increased at the high angles of attack. This phenomenon is possibly produced by the inward migration of the windward wing-apex vortex and its subsequent interaction with the centerbody.

Figure 41 presents the lateral-directional stability derivatives. As shown, deflecting the leading-edge flap 30° results in a slight decrement in the roll stability magnitude. This result contradicts the finding in reference 2 and can be attributed to differences in flap geometry as well as possible variations in vortex trajectory. The data in figure 41 also show a reduction in C_{n_β} due to the leading-edge flap deflection, which increased the forward projected wing area ahead of the moment reference center.

The addition of the apex flaps tends to restore the general magnitude of C_{l_β} and C_{Y_β} to those of the cruise-wing configuration up to moderate angles of attack. At higher angles, the local anhedral reduction caused by the apex flaps produces a favorable increment in roll stability with little effect on C_{n_β}.

Summary of Results

During the subsonic high-lift testing of a high-speed civil transport (HSCT) model, the upper surface flow structure associated with the highly swept wing was found to be dominated by vortex flow, which during vortex breakdown, particularly on the outer wing panel, causes adverse pitch-up and a reduction of usable lift. As a consequence, tests were conducted to investigate the impact of leading-edge vortex management devices on the subsonic performance of this HSCT model. The results of this investigation are summarized as follows:

1. The relatively small vortex management devices, which were located near the wing leading-edge crank and near the model moment reference center, had little positive effect on the overall aerodynamic performance within the bounds of this investigation.

2. Apex flaps, located at the wing apex region, proved effective in achieving significant nose-up pitch control with little change in the overall lift; however, the corresponding increase in drag resulted in an overall lift-drag degradation. Although this degradation limits the prolonged usefulness of the flaps during the takeoff phase of operation, the momentary deployment of such a device can provide sufficient pitching moment for rotation at takeoff and for flare during landing.

3. The deflection of leading-edge and trailing-edge flaps had the most impact on delaying adverse pitch-up than any of the devices tested. Furthermore, positive deflections of the leading-edge and trailing-edge flaps produced a significant reduction in drag over the lift-coefficient range of 0.4 to 0.8 (e.g., 200 to 310 drag counts at 0.5).

These results demonstrate that the need still exists for increasing control power for nose down pitch while maintaining high levels of lift. One likely source is to extend the aft fuselage sufficiently to provide the necessary moment arm for a horizontal tail. The incorporation of a horizontal tail on HSCT configurations can pose sonic boom penalties, but the subsonic stability benefits can warrant its use. Other areas for potential pitch control power include improving the effectiveness of the outer wing panel to produce high levels of lift aft of the moment reference center and totally or partially suppressing the main wing vortex. Further investigation into these areas may provide the necessary high-lift pitch control required for HSCT vehicles.

NASA Langley Research Center
Hampton, VA 23681-0001
May 4, 1993

Table 1. Geometric Characteristics of Model

Aspect ratio	1.838
Reference area, ft^2	9.293
Gross area, ft^2	10.210
Span, ft	4.133
Root chord, ft	5.492
Tip chord, ft	0.529
Reference mean aerodynamic chord, ft	2.937
Leading-edge sweep, deg, at—	
Body station 1.738 ft	73.02
Body station 6.651 ft	60.00

Table 2. Surface Coordinates for Model

[Coordinates are presented in Langley Wireframe Geometry Standard (LaWGS) format]

MODEL CRUISE CONFIGURATION
INBOARD-WING

0 21 26 0 0.000 0.000 0.000 0.000 0.000 0.000 1.000 1.000
1.000 0

24.594	0.000	5.493	24.594	−0.834	5.637	24.594	−0.975	5.693
24.594	−1.005	5.707	24.594	−1.022	5.714	24.594	−1.033	5.719
24.594	−1.041	5.724	24.594	−1.049	5.727	24.594	−1.056	5.731
24.594	−1.063	5.735	24.594	−1.070	5.738	24.594	−1.078	5.742
24.594	−1.085	5.746	24.594	−1.092	5.749	24.594	−1.099	5.753
24.594	−1.106	5.757	24.594	−1.113	5.761	24.594	−1.120	5.766
24.594	−1.128	5.770	24.594	−1.138	5.776	24.594	−1.153	5.785
24.594	−1.180	5.803	24.594	−1.345	5.925	24.594	−2.082	6.912
24.594	−2.067	8.546	24.594	0.000	9.900	28.000	0.000	5.071
28.000	−0.741	5.194	28.000	−1.371	5.070	28.000	−1.889	4.908
28.000	−2.145	4.857	28.000	−2.194	4.890	28.000	−2.202	4.901
28.000	−2.206	4.908	28.000	−2.209	4.916	28.000	−2.211	4.923
28.000	−2.213	4.931	28.000	−2.214	4.939	28.000	−2.214	4.947
28.000	−2.213	4.955	28.000	−2.212	4.963	28.000	−2.209	4.971
28.000	−2.207	4.978	28.000	−2.204	4.986	28.000	−2.201	4.994
28.000	−2.197	5.003	28.000	−2.183	5.035	28.000	−2.070	5.202
28.000	−1.736	5.843	28.000	−2.273	6.945	28.000	−2.026	8.510
28.000	0.000	9.662	32.000	0.000	4.579	32.000	−0.694	4.704
32.000	−1.307	4.597	32.000	−1.905	4.399	32.000	−2.495	4.220
32.000	−3.002	3.988	32.000	−3.305	3.886	32.000	−3.382	3.900
32.000	−3.390	3.915	32.000	−3.392	3.923	32.000	−3.394	3.931
32.000	−3.395	3.939	32.000	−3.394	3.947	32.000	−3.394	3.955
32.000	−3.393	3.963	32.000	−3.391	3.971	32.000	−3.390	3.979
32.000	−3.388	3.987	32.000	−3.386	3.995	32.000	−3.381	4.012
32.000	−3.330	4.109	32.000	−2.930	4.608	32.000	−1.993	5.715
32.000	−2.319	6.891	32.000	−1.892	8.323	32.000	0.000	9.221
36.000	0.000	4.089	36.000	−0.653	4.209	36.000	−1.227	4.098
36.000	−1.793	3.917	36.000	−2.360	3.738	36.000	−2.928	3.566
36.000	−3.484	3.360	36.000	−4.013	3.147	36.000	−4.423	2.991
36.000	−4.575	3.022	36.000	−4.589	3.052	36.000	−4.590	3.063
36.000	−4.589	3.071	36.000	−4.588	3.079	36.000	−4.587	3.086
36.000	−4.585	3.094	36.000	−4.582	3.102	36.000	−4.580	3.109
36.000	−4.576	3.120	36.000	−4.556	3.159	36.000	−4.365	3.406
36.000	−3.462	4.233	36.000	−2.042	5.416	36.000	−2.265	6.607
36.000	−1.717	7.909	36.000	0.000	8.648	40.000	0.000	3.557
40.000	−0.573	3.649	40.000	−1.079	3.558	40.000	−1.596	3.419
40.000	−2.195	3.260	40.000	−3.183	2.987	40.000	−4.776	2.480
40.000	−5.637	2.169	40.000	−5.808	2.154	40.000	−5.831	2.169
40.000	−5.836	2.178	40.000	−5.838	2.186	40.000	−5.839	2.194
40.000	−5.839	2.202	40.000	−5.838	2.210	40.000	−5.836	2.218
40.000	−5.834	2.230	40.000	−5.826	2.256	40.000	−5.776	2.335
40.000	−5.559	2.576	40.000	−4.907	3.143	40.000	−3.588	4.019
40.000	−2.077	5.042	40.000	−2.177	6.243	40.000	−1.534	7.427
40.000	0.000	8.027	44.000	0.000	3.019	44.000	−0.434	3.055
44.000	−0.821	2.987	44.000	−1.226	2.905	44.000	−1.750	2.802
44.000	−2.905	2.567	44.000	−5.251	1.997	44.001	−6.700	1.584
44.000	−7.010	1.541	44.000	−7.055	1.562	44.000	−7.060	1.574

44.000	−7.060	1.583	44.000	−7.060	1.591	44.000	−7.060	1.599
44.000	−7.059	1.607	44.000	−7.057	1.617	44.000	−7.052	1.632
44.000	−7.028	1.673	44.000	−6.912	1.799	44.000	−6.502	2.146
44.000	−5.491	2.797	44.000	−3.834	3.661	44.000	−2.133	4.623
44.000	−2.129	5.821	44.000	−1.412	6.908	44.000	0.000	7.422
48.000	0.000	2.417	48.000	−0.429	2.471	48.000	−0.818	2.413
48.000	−1.227	2.344	48.000	−1.784	2.255	48.000	−3.125	2.052
48.000	−5.993	1.516	48.000	−7.815	1.139	48.000	−8.206	1.085
48.000	−8.267	1.098	48.000	−8.277	1.110	48.000	−8.280	1.118
48.000	−8.281	1.126	48.000	−8.281	1.134	48.000	−8.280	1.143
48.000	−8.278	1.154	48.000	−8.269	1.178	48.000	−8.218	1.248
48.000	−7.987	1.444	48.000	−7.288	1.876	48.000	−5.893	2.538
48.000	−3.967	3.326	48.000	−2.165	4.171	48.000	−2.113	5.369
48.000	−1.376	6.423	48.000	0.000	6.907	52.000	0.000	1.853
52.000	−0.417	1.921	52.000	−0.797	1.882	52.000	−1.204	1.830
52.000	−1.787	1.763	52.000	−3.313	1.601	52.000	−6.724	1.122
52.000	−8.937	0.797	52.000	−9.414	0.734	52.000	−9.488	0.751
52.000	−9.500	0.763	52.000	−9.503	0.772	52.000	−9.504	0.780
52.000	−9.503	0.788	52.000	−9.502	0.797	52.000	−9.498	0.812
52.000	−9.476	0.847	52.000	−9.365	0.948	52.000	−8.965	1.215
52.000	−7.945	1.686	52.000	−6.238	2.290	52.000	−4.133	2.964
52.000	−2.198	3.670	52.000	−2.127	4.867	52.000	−1.383	5.919
52.000	0.000	6.404	56.000	0.000	1.318	56.000	−0.310	1.374
56.000	−0.597	1.383	56.000	−0.915	1.361	56.000	−1.444	1.327
56.000	−3.125	1.231	56.000	−7.229	0.838	56.000	−10.003	0.529
56.000	−10.616	0.465	56.000	−10.710	0.491	56.000	−10.724	0.506
56.000	−10.725	0.516	56.000	−10.724	0.524	56.000	−10.723	0.533
56.000	−10.721	0.543	56.000	−10.712	0.564	56.000	−10.663	0.618
56.000	−10.454	0.771	56.000	−9.795	1.093	56.000	−8.422	1.554
56.000	−6.462	2.074	56.000	−4.231	2.612	56.000	−2.255	3.230
56.000	−2.161	4.426	56.000	−1.400	5.474	56.000	0.000	5.960
60.000	0.000	0.823	60.000	−0.354	0.891	60.000	−0.681	0.897
60.000	−1.044	0.882	60.000	−1.643	0.864	60.000	−3.526	0.845
60.000	−8.088	0.581	60.000	−11.149	0.314	60.000	−11.824	0.254
60.000	−11.929	0.274	60.000	−11.944	0.288	60.000	−11.946	0.298
60.000	−11.946	0.306	60.000	−11.945	0.315	60.000	−11.942	0.329
60.000	−11.922	0.359	60.000	−11.819	0.440	60.000	−11.447	0.656
60.000	−10.470	1.021	60.000	−8.773	1.432	60.000	−6.630	1.844
60.000	−4.325	2.274	60.000	−2.319	2.874	60.000	−2.194	4.068
60.000	−1.414	5.107	60.000	0.000	5.587	64.000	0.000	0.412
64.000	−0.570	0.520	64.000	−1.091	0.531	64.000	−1.657	0.507
64.000	−2.470	0.493	64.000	−4.601	0.506	64.000	−9.344	0.348
64.000	−12.397	0.151	64.000	−13.052	0.156	64.000	−13.150	0.183
64.000	−13.166	0.196	64.000	−13.168	0.205	64.000	−13.168	0.214
64.000	−13.167	0.224	64.000	−13.160	0.243	64.000	−13.112	0.285
64.000	−12.908	0.390	64.000	−12.276	0.618	64.000	−10.945	0.966
64.000	−8.988	1.295	64.000	−6.732	1.616	64.000	−4.385	1.962
64.000	−2.340	2.404	64.000	−2.257	3.605	64.000	−1.499	4.699
64.000	0.000	5.241	68.000	0.000	0.045	68.000	−0.913	0.243
68.000	−1.748	0.276	68.000	−2.633	0.263	68.000	−3.764	0.262
68.000	−6.156	0.256	68.000	−10.858	0.139	68.000	−13.707	0.117
68.000	−14.290	0.150	68.000	−14.373	0.178	68.000	−14.387	0.189
68.000	−14.389	0.198	68.000	−14.389	0.207	68.000	−14.387	0.220

68.000	−14.369	0.248	68.000	−14.269	0.315	68.000	−13.899	0.463
68.000	−12.921	0.640	68.000	−11.236	0.884	68.000	−9.089	1.138
68.000	−6.762	1.375	68.000	−4.386	1.601	68.000	−2.331	1.905
68.000	−2.312	3.114	68.000	−1.588	4.271	68.000	0.000	4.882
72.000	0.000	−0.301	72.000	−1.149	0.006	72.000	−2.205	0.082
72.000	−3.324	0.091	72.000	−4.695	0.107	72.000	−7.328	0.090
72.000	−12.151	−0.008	72.000	−14.965	0.114	72.000	−15.523	0.123
72.000	−15.601	0.149	72.000	−15.610	0.161	72.000	−15.610	0.171
72.001	−15.609	0.181	72.001	−15.602	0.200	72.000	−15.553	0.242
72.000	−15.350	0.347	72.000	−14.710	0.531	72.000	−13.345	0.641
72.000	−11.370	0.768	72.000	−9.098	0.928	72.000	−6.729	1.051
72.000	−4.338	1.175	72.000	−2.282	1.414	72.000	−2.350	2.626
72.000	−1.684	3.859	72.000	0.000	4.536	76.000	0.000	−0.607
76.000	−1.378	−0.166	76.000	−2.676	−0.070	76.000	−4.037	−0.051
76.000	−5.655	−0.033	76.000	−8.527	−0.045	76.000	−13.450	−0.050
76.000	−16.212	0.063	76.000	−16.741	0.081	76.000	−16.812	0.102
76.000	−16.826	0.109	76.000	−16.831	0.115	76.000	−16.832	0.128
76.000	−16.819	0.161	76.000	−16.711	0.227	76.000	−16.317	0.367
76.000	−15.310	0.550	76.000	−13.582	0.571	76.000	−11.409	0.561
76.000	−9.068	0.619	76.000	−6.681	0.676	76.000	−4.284	0.741
76.000	−2.246	0.930	76.000	−2.396	2.139	76.000	−1.778	3.447
76.000	0.000	4.224	79.810	0.000	−0.880	79.810	−1.524	−0.339
79.810	−2.958	−0.196	79.810	−4.483	−0.176	79.810	−6.277	−0.156
79.810	−9.371	−0.175	79.810	−14.529	−0.056	79.810	−17.378	0.016
79.810	−17.912	0.059	79.810	−17.981	0.085	79.810	−17.991	0.097
79.810	−17.995	0.105	79.810	−17.991	0.122	79.810	−17.942	0.166
79.810	−17.716	0.243	79.810	−17.042	0.386	79.810	−15.652	0.492
79.810	−13.661	0.387	79.810	−11.382	0.281	79.810	−9.009	0.282
79.810	−6.614	0.300	79.810	−4.216	0.329	79.810	−2.184	0.497
79.810	−2.406	1.699	79.810	−1.853	3.078	79.810	0.000	3.936
80.500	0.000	−0.925	80.500	−1.545	−0.358	80.500	−3.005	−0.217
80.500	−4.558	−0.197	80.500	−6.387	−0.178	80.500	−9.550	−0.197
80.500	−14.832	−0.054	80.500	−17.753	0.017	80.500	−18.302	0.070
80.500	−18.376	0.088	80.500	−18.390	0.094	80.500	−18.394	0.102
80.500	−18.386	0.120	80.500	−18.307	0.149	80.500	−18.026	0.224
80.500	−17.244	0.367	80.500	−15.736	0.472	80.500	−13.678	0.343
80.500	−11.376	0.225	80.500	−8.997	0.219	80.500	−6.601	0.230
80.500	−4.202	0.256	80.500	−2.167	0.418	80.500	−2.405	1.619
80.500	−1.866	3.010	80.500	0.000	3.888	81.500	0.000	−0.987
81.500	−1.571	−0.386	81.500	−3.069	−0.246	81.500	−4.658	−0.229
81.500	−6.533	−0.211	81.500	−9.792	−0.222	81.500	−15.263	−0.058
81.500	−18.297	0.016	81.500	−18.868	0.078	81.500	−18.946	0.092
81.500	−18.962	0.095	81.500	−18.969	0.100	81.500	−18.952	0.116
81.500	−18.838	0.139	81.500	−18.458	0.206	81.500	−17.499	0.338
81.500	−15.823	0.430	81.500	−13.680	0.263	81.500	−11.351	0.132
81.500	−8.965	0.117	81.500	−6.568	0.123	81.500	−4.169	0.143
81.500	−2.135	0.298	81.500	−2.399	1.494	81.500	−1.883	2.903
81.500	0.000	3.807	82.500	0.000	−1.053	82.500	−1.605	−0.422
82.500	−3.138	−0.275	82.500	−4.766	−0.261	82.500	−6.690	−0.243
82.500	−10.049	−0.249	82.500	−15.706	−0.066	82.500	−18.850	0.019
82.500	−19.443	0.086	82.500	−19.524	0.097	82.500	−19.540	0.099
82.500	−19.547	0.103	82.500	−19.519	0.117	82.500	−19.356	0.133
82.500	−18.851	0.195	82.500	−17.698	0.322	82.500	−15.864	0.383

Table 2. Continued

82.500	−13.654	0.185	82.500	−11.304	0.046	82.500	−8.914	0.021
82.500	−6.515	0.024	82.500	−4.116	0.039	82.500	−2.089	0.195
82.500	−2.390	1.382	82.500	−1.897	2.808	82.500	0.001	3.738
83.500	0.000	−1.119	83.500	−1.648	−0.468	83.500	−3.206	−0.299
83.500	−4.877	−0.290	83.500	−6.854	−0.272	83.500	−10.314	−0.281
83.500	−16.154	−0.075	83.500	−19.403	0.019	83.500	−20.017	0.090
83.500	−20.101	0.099	83.500	−20.118	0.100	83.500	−20.125	0.104
83.500	−20.083	0.118	83.500	−19.859	0.130	83.500	−19.208	0.184
83.500	−17.863	0.304	83.500	−15.898	0.326	83.500	−13.637	0.108
83.500	−11.274	−0.046	83.500	−8.880	−0.069	83.500	−6.481	−0.075
83.500	−4.081	−0.067	83.500	−2.049	0.090	83.500	−2.378	1.271
83.500	−1.910	2.714	83.500	0.001	3.665	86.000	0.000	−1.294
86.000	−1.708	−0.537	86.000	−3.338	−0.363	86.000	−5.116	−0.360
86.000	−7.215	−0.335	86.000	−10.932	−0.346	86.000	−17.255	−0.100
86.000	−20.789	0.007	86.000	−21.459	0.090	86.000	−21.551	0.099
86.000	−21.568	0.102	86.000	−21.569	0.111	86.000	−21.460	0.128
86.000	−20.990	0.144	86.000	−19.895	0.199	86.000	−18.113	0.257
86.000	−15.919	0.166	86.000	−13.586	−0.098	86.000	−11.203	−0.250
86.000	−8.806	−0.287	86.000	−6.406	−0.308	86.000	−4.007	−0.304
86.000	−1.992	−0.165	86.000	−2.338	1.010	86.000	−1.930	2.488
86.000	0.000	3.486	86.766	0.000	−1.344	86.766	−1.786	−0.522
86.709	−4.048	−0.323	86.641	−6.554	−0.305	86.594	−9.063	−0.333
86.594	−12.384	−0.309	86.594	−18.036	−0.103	86.594	−21.194	0.029
86.594	−21.794	0.086	86.594	−21.874	0.105	86.594	−21.889	0.111
86.594	−21.896	0.114	86.594	−21.787	0.124	86.594	−21.319	0.142
86.594	−20.229	0.194	86.594	−18.453	0.241	86.594	−16.267	0.176
86.594	−13.942	−0.069	86.594	−11.570	−0.241	86.594	−9.182	−0.283
86.637	−6.697	−0.304	86.706	−4.153	−0.323	86.766	−2.009	−0.214
86.766	−2.348	0.943	86.766	−1.901	2.381	86.766	0.000	3.365

OUTBOARD-WING

1 9 26 0 0.000 0.000 0.000 0.000 0.000 0.000 1.000 1.000
1.000 0

86.594	−8.286	−0.293	86.594	−10.461	−0.336	86.594	−12.625	−0.303
86.594	−14.741	−0.156	86.594	−16.732	−0.099	86.594	−18.428	−0.104
86.594	−19.654	−0.079	86.594	−20.411	−0.035	86.594	−20.871	0.002
86.594	−21.203	0.029	86.594	−21.491	0.052	86.594	−21.766	0.081
86.594	−21.762	0.126	86.594	−21.488	0.136	86.594	−21.211	0.147
86.594	−20.923	0.161	86.594	−20.608	0.177	86.594	−20.226	0.194
86.594	−19.696	0.212	86.594	−18.901	0.229	86.594	−17.733	0.247
86.594	−16.177	0.170	86.594	−14.327	−0.010	86.594	−12.299	−0.204
86.594	−10.175	−0.261	86.594	−8.286	−0.293	88.000	−13.455	−0.299
88.000	−14.932	−0.161	88.000	−16.406	−0.115	88.000	−17.851	−0.108
88.000	−19.208	−0.126	88.000	−20.364	−0.109	88.000	−21.198	−0.064
88.000	−21.714	−0.029	88.000	−22.027	0.002	88.000	−22.252	0.031
88.000	−22.447	0.057	88.000	−22.634	0.082	88.000	−22.634	0.118
88.000	−22.447	0.124	88.000	−22.258	0.130	88.000	−22.062	0.135
88.000	−21.847	0.142	88.000	−21.587	0.151	88.000	−21.226	0.164
88.000	−20.683	0.177	88.000	−19.886	0.196	88.000	−18.823	0.203
88.000	−16.405	0.067	88.000	−15.090	−0.052	88.000	−14.260	−0.167
88.000	−13.455	−0.299	90.000	−15.738	−0.140	90.000	−17.131	−0.106
90.000	−18.403	−0.105	90.000	−19.649	−0.133	90.000	−20.820	−0.133
90.000	−21.816	−0.109	90.000	−22.536	−0.065	90.000	−22.980	−0.028

Table 2. Continued

90.000	−23.250	−0.001	90.000	−23.444	0.020	90.000	−23.613	0.042
90.000	−23.774	0.062	90.000	−23.784	0.098	90.000	−23.623	0.104
90.000	−23.459	0.109	90.000	−23.290	0.114	90.000	−23.105	0.120
90.000	−22.880	0.126	90.000	−22.569	0.135	90.000	−22.101	0.146
90.000	−21.413	0.153	90.000	−20.496	0.157	90.000	−19.401	0.139
90.000	−18.203	0.085	90.000	−16.957	−0.021	90.000	−15.738	−0.140
91.588	−17.551	−0.082	91.588	−18.760	−0.060	91.588	−19.904	−0.097
91.588	−21.024	−0.114	91.588	−22.077	−0.118	91.588	−22.973	−0.123
91.588	−23.620	−0.080	91.588	−24.019	−0.048	91.588	−24.262	−0.022
91.588	−24.436	0.003	91.588	−24.587	0.026	91.588	−24.730	0.057
91.588	−24.723	0.087	91.587	−24.578	0.088	91.587	−24.431	0.092
91.587	−24.279	0.097	91.587	−24.113	0.101	91.588	−23.910	0.106
91.588	−23.631	0.111	91.588	−23.211	0.119	91.588	−22.595	0.138
91.588	−21.780	0.138	91.588	−20.791	0.129	91.588	−19.719	0.100
91.588	−18.604	0.026	91.588	−17.551	−0.082	92.000	−18.021	−0.069
92.000	−19.206	−0.086	92.000	−20.266	−0.109	92.000	−21.305	−0.126
92.000	−22.280	−0.126	92.000	−23.111	−0.104	92.000	−23.711	−0.071
92.000	−24.081	−0.046	92.000	−24.306	−0.026	92.000	−24.468	−0.009
92.000	−24.609	0.008	92.000	−24.743	0.030	92.001	−24.737	0.074
92.001	−24.603	0.085	92.000	−24.467	0.095	92.000	−24.326	0.102
92.000	−24.172	0.108	92.000	−23.985	0.111	92.000	−23.725	0.114
92.000	−23.336	0.119	92.000	−22.765	0.123	92.000	−22.003	0.123
92.000	−21.094	0.110	92.000	−20.098	0.073	92.000	−19.060	0.014
92.000	−18.021	−0.069	94.000	−20.304	−0.023	94.000	−21.088	−0.049
94.000	−21.803	−0.072	94.000	−22.503	−0.091	94.000	−23.161	−0.105
94.000	−23.721	−0.105	94.000	−24.127	−0.099	94.000	−24.377	−0.094
94.000	−24.530	−0.088	94.000	−24.639	−0.083	94.000	−24.735	−0.078
94.000	−24.800	−0.039	94.000	−24.800	0.052	94.000	−24.747	0.100
94.000	−24.655	0.102	94.000	−24.560	0.103	94.000	−24.456	0.104
94.000	−24.330	0.104	94.000	−24.154	0.104	94.000	−23.891	0.104
94.000	−23.504	0.102	94.000	−22.987	0.096	94.000	−22.371	0.080
94.000	−21.696	0.058	94.000	−20.993	0.024	94.000	−20.304	−0.023
96.000	−22.588	0.012	96.000	−22.972	−0.013	96.000	−23.331	−0.027
96.000	−23.683	−0.041	96.000	−24.013	−0.054	96.000	−24.294	−0.063
96.000	−24.497	−0.070	96.000	−24.623	−0.074	96.000	−24.699	−0.076
96.000	−24.755	−0.076	96.000	−24.800	−0.070	96.000	−24.800	−0.024
96.000	−24.800	0.021	96.000	−24.800	0.067	96.000	−24.766	0.084
96.000	−24.718	0.084	96.000	−24.666	0.083	96.000	−24.603	0.082
96.000	−24.515	0.083	96.000	−24.385	0.082	96.000	−24.195	0.077
96.000	−23.941	0.070	96.000	−23.638	0.060	96.000	−23.305	0.048
96.000	−22.958	0.034	96.000	−22.588	0.012	96.345	−22.981	0.005
96.345	−23.279	−0.010	96.345	−23.577	−0.020	96.345	−23.869	−0.029
96.345	−24.143	−0.038	96.345	−24.377	−0.046	96.345	−24.546	−0.052
96.345	−24.650	−0.055	96.345	−24.714	−0.057	96.345	−24.759	−0.058
96.345	−24.799	−0.057	96.345	−24.800	−0.019	96.345	−24.800	0.019
96.345	−24.800	0.056	96.345	−24.763	0.059	96.345	−24.723	0.058
96.345	−24.680	0.057	96.345	−24.627	0.055	96.345	−24.554	0.053
96.345	−24.445	0.050	96.345	−24.284	0.046	96.345	−24.069	0.040
96.345	−23.813	0.033	96.345	−23.532	0.025	96.345	−23.240	0.017
96.345	−22.981	0.005	97.938	−24.800	0.000	97.938	−24.800	0.000
97.938	−24.800	0.000	97.938	−24.800	0.000	97.938	−24.800	0.000
97.938	−24.800	0.000	97.938	−24.800	0.000	97.938	−24.800	0.000
97.938	−24.800	0.000	97.938	−24.800	0.000	97.938	−24.800	0.000

Table 2. Continued

97.938	−24.800	0.000	97.938	−24.800	0.000	97.938	−24.800	0.000
97.938	−24.800	0.000	97.938	−24.800	0.000	97.938	−24.800	0.000
97.938	−24.800	0.000	97.938	−24.800	0.000	97.938	−24.800	0.000
97.938	−24.800	0.000	97.938	−24.800	0.000	97.938	−24.800	0.000
97.938	−24.800	0.000	97.938	−24.800	0.000	97.938	−24.800	0.000

FOREBODY

2 19 26 0 0.000 0.000 0.000 0.000 0.000 0.000 1.000 1.000

1.000 0

0.400	0.000	8.381	0.400	0.000	8.381	0.400	0.000	8.381
0.400	0.000	8.381	0.400	0.000	8.381	0.400	0.000	8.381
0.400	0.000	8.381	0.400	0.000	8.381	0.400	0.000	8.381
0.400	0.000	8.381	0.400	0.000	8.381	0.400	0.000	8.381
0.400	0.000	8.381	0.400	0.000	8.381	0.400	0.000	8.381
0.400	0.000	8.381	0.400	0.000	8.381	0.400	0.000	8.381
0.400	0.000	8.381	0.400	0.000	8.381	0.400	0.000	8.381
0.400	0.000	8.381	0.400	0.000	8.381	0.400	0.000	8.381
0.400	0.000	8.381	0.400	0.000	8.381	0.425	0.000	8.341
0.425	−0.005	8.341	0.425	−0.010	8.342	0.425	−0.015	8.344
0.425	−0.019	8.346	0.425	−0.024	8.349	0.425	−0.027	8.352
0.425	−0.031	8.356	0.425	−0.034	8.360	0.425	−0.036	8.364
0.425	−0.038	8.369	0.425	−0.039	8.374	0.425	−0.040	8.379
0.425	−0.040	8.384	0.425	−0.039	8.389	0.425	−0.038	8.394
0.425	−0.036	8.398	0.425	−0.034	8.403	0.425	−0.031	8.407
0.425	−0.027	8.410	0.425	−0.023	8.414	0.425	−0.019	8.416
0.425	−0.014	8.418	0.425	−0.009	8.420	0.425	−0.004	8.421
0.425	0.000	8.421	0.450	0.000	8.321	0.450	−0.008	8.321
0.450	−0.015	8.323	0.450	−0.022	8.325	0.450	−0.029	8.328
0.450	−0.035	8.333	0.450	−0.041	8.337	0.450	−0.046	8.343
0.450	−0.051	8.349	0.450	−0.054	8.356	0.450	−0.057	8.363
0.450	−0.059	8.370	0.450	−0.060	8.378	0.450	−0.060	8.385
0.450	−0.059	8.393	0.450	−0.057	8.400	0.450	−0.054	8.407
0.450	−0.050	8.414	0.450	−0.046	8.420	0.450	−0.041	8.425
0.450	−0.035	8.430	0.450	−0.028	8.434	0.450	−0.021	8.437
0.450	−0.014	8.439	0.450	−0.007	8.441	0.450	0.000	8.441
0.500	0.000	8.306	0.500	−0.009	8.307	0.500	−0.019	8.308
0.500	−0.028	8.311	0.500	−0.036	8.315	0.500	−0.044	8.320
0.500	−0.052	8.327	0.500	−0.058	8.333	0.500	−0.064	8.341
0.500	−0.068	8.349	0.500	−0.071	8.358	0.500	−0.074	8.367
0.500	−0.075	8.377	0.500	−0.075	8.386	0.500	−0.074	8.396
0.500	−0.071	8.405	0.500	−0.068	8.414	0.500	−0.063	8.422
0.500	−0.057	8.429	0.500	−0.051	8.436	0.500	−0.043	8.442
0.500	−0.035	8.447	0.500	−0.027	8.451	0.500	−0.018	8.454
0.500	−0.008	8.456	0.500	0.000	8.456	0.900	0.000	8.246
0.900	−0.017	8.247	0.900	−0.034	8.250	0.900	−0.050	8.256
0.900	−0.065	8.263	0.900	−0.080	8.272	0.900	−0.093	8.283
0.900	−0.104	8.295	0.900	−0.114	8.309	0.900	−0.122	8.324
0.900	−0.129	8.340	0.900	−0.133	8.357	0.900	−0.135	8.374
0.900	−0.135	8.391	0.900	−0.132	8.407	0.900	−0.128	8.424
0.900	−0.122	8.440	0.900	−0.113	8.455	0.900	−0.103	8.468
0.900	−0.091	8.481	0.900	−0.078	8.491	0.900	−0.063	8.500
0.900	−0.048	8.507	0.900	−0.032	8.512	0.900	−0.015	8.515
0.900	0.000	8.516	1.400	0.000	8.171	1.400	−0.026	8.173

Table 2. Continued

1.400	−0.052	8.178	1.400	−0.078	8.186	1.400	−0.102	8.197
1.400	−0.124	8.211	1.400	−0.144	8.228	1.400	−0.162	8.248
1.400	−0.178	8.269	1.400	−0.191	8.293	1.400	−0.200	8.317
1.400	−0.207	8.343	1.400	−0.210	8.369	1.400	−0.209	8.396
1.400	−0.206	8.422	1.400	−0.199	8.448	1.400	−0.189	8.472
1.400	−0.176	8.495	1.400	−0.160	8.517	1.400	−0.142	8.536
1.400	−0.121	8.552	1.400	−0.099	8.566	1.400	−0.075	8.577
1.400	−0.049	8.585	1.400	−0.023	8.590	1.400	0.000	8.591
2.000	0.000	8.087	2.000	−0.034	8.095	2.000	−0.068	8.104
2.000	−0.101	8.117	2.000	−0.132	8.134	2.000	−0.160	8.155
2.000	−0.186	8.179	2.000	−0.208	8.206	2.000	−0.227	8.236
2.000	−0.242	8.268	2.000	−0.254	8.301	2.000	−0.262	8.335
2.000	−0.266	8.370	2.000	−0.266	8.405	2.000	−0.262	8.440
2.000	−0.254	8.475	2.000	−0.242	8.508	2.000	−0.226	8.539
2.000	−0.206	8.568	2.000	−0.183	8.595	2.000	−0.157	8.618
2.000	−0.129	8.639	2.000	−0.098	8.657	2.000	−0.065	8.670
2.000	−0.031	8.676	2.000	0.000	8.675	4.000	0.000	7.788
4.000	−0.087	7.798	4.000	−0.148	7.814	4.000	−0.203	7.835
4.000	−0.256	7.862	4.000	−0.306	7.895	4.000	−0.352	7.932
4.000	−0.394	7.975	4.000	−0.431	8.021	4.000	−0.463	8.071
4.000	−0.490	8.124	4.000	−0.511	8.180	4.000	−0.526	8.238
4.000	−0.536	8.296	4.000	−0.541	8.356	4.000	−0.539	8.415
4.000	−0.530	8.474	4.000	−0.515	8.532	4.000	−0.494	8.587
4.000	−0.468	8.641	4.000	−0.437	8.691	4.000	−0.400	8.738
4.000	−0.352	8.787	4.000	−0.241	8.863	4.000	−0.116	8.909
4.000	0.000	8.922	6.000	0.000	7.538	6.000	−0.128	7.548
6.000	−0.206	7.566	6.000	−0.276	7.589	6.000	−0.343	7.619
6.000	−0.406	7.655	6.000	−0.467	7.697	6.000	−0.522	7.744
6.000	−0.574	7.796	6.000	−0.621	7.853	6.000	−0.662	7.913
6.000	−0.698	7.977	6.000	−0.727	8.044	6.000	−0.750	8.114
6.000	−0.766	8.185	6.000	−0.775	8.258	6.000	−0.778	8.331
6.000	−0.775	8.404	6.000	−0.765	8.477	6.000	−0.748	8.548
6.000	−0.726	8.618	6.000	−0.697	8.685	6.000	−0.650	8.771
6.000	−0.469	8.967	6.000	−0.230	9.086	6.000	0.000	9.122
8.000	0.000	7.326	8.000	−0.208	7.350	8.000	−0.300	7.375
8.000	−0.375	7.403	8.000	−0.447	7.437	8.000	−0.516	7.477
8.000	−0.582	7.522	8.000	−0.644	7.572	8.000	−0.701	7.627
8.000	−0.753	7.687	8.000	−0.800	7.751	8.000	−0.842	7.819
8.000	−0.878	7.891	8.000	−0.908	7.964	8.000	−0.931	8.041
8.000	−0.949	8.118	8.000	−0.962	8.197	8.000	−0.968	8.276
8.000	−0.969	8.356	8.000	−0.963	8.435	8.000	−0.950	8.514
8.000	−0.932	8.592	8.000	−0.893	8.704	8.000	−0.668	9.021
8.000	−0.336	9.222	8.000	0.000	9.283	10.000	0.000	7.132
10.000	−0.270	7.166	10.000	−0.376	7.195	10.000	−0.457	7.225
10.000	−0.536	7.261	10.000	−0.612	7.302	10.000	−0.684	7.350
10.000	−0.753	7.403	10.000	−0.817	7.461	10.000	−0.876	7.524
10.000	−0.930	7.592	10.000	−0.979	7.664	10.000	−1.021	7.739
10.000	−1.058	7.817	10.000	−1.090	7.898	10.000	−1.115	7.981
10.000	−1.134	8.065	10.000	−1.147	8.151	10.000	−1.153	8.237
10.000	−1.153	8.324	10.000	−1.146	8.410	10.000	−1.134	8.496
10.000	−1.101	8.630	10.000	−0.845	9.058	10.000	−0.430	9.334
10.000	0.000	9.416	12.000	0.000	6.915	12.000	−0.300	6.947
12.000	−0.403	6.975	12.000	−0.477	7.000	12.000	−0.550	7.030

Table 2. Continued

12.000	−0.621	7.064	12.000	−0.690	7.102	12.000	−0.757	7.144
12.000	−0.820	7.191	12.000	−0.881	7.241	12.000	−0.938	7.296
12.000	−0.992	7.353	12.000	−1.042	7.414	12.000	−1.088	7.478
12.000	−1.132	7.544	12.000	−1.171	7.612	12.000	−1.206	7.682
12.000	−1.237	7.755	12.000	−1.264	7.829	12.000	−1.286	7.905
12.000	−1.304	7.981	12.000	−1.318	8.059	12.000	−1.331	8.218
12.000	−1.147	8.913	12.000	−0.616	9.396	12.000	0.000	9.542
14.000	0.000	6.699	14.000	−0.323	6.732	14.000	−0.415	6.754
14.000	−0.474	6.771	14.000	−0.532	6.791	14.000	−0.590	6.813
14.000	−0.647	6.837	14.000	−0.703	6.864	14.000	−0.757	6.894
14.000	−0.810	6.925	14.000	−0.862	6.959	14.000	−0.912	6.996
14.000	−0.960	7.034	14.000	−1.007	7.074	14.000	−1.052	7.116
14.000	−1.096	7.160	14.000	−1.137	7.206	14.000	−1.177	7.253
14.000	−1.214	7.303	14.000	−1.250	7.353	14.000	−1.283	7.405
14.000	−1.315	7.458	14.000	−1.395	7.621	14.000	−1.447	8.621
14.000	−0.847	9.422	14.000	0.000	9.666	16.000	0.000	6.479
16.000	−0.380	6.517	16.000	−0.471	6.538	16.000	−0.520	6.552
16.000	−0.568	6.567	16.000	−0.617	6.584	16.000	−0.664	6.602
16.000	−0.711	6.622	16.000	−0.758	6.644	16.000	−0.803	6.667
16.000	−0.848	6.692	16.000	−0.891	6.718	16.000	−0.934	6.746
16.000	−0.976	6.774	16.000	−1.018	6.805	16.000	−1.058	6.836
16.000	−1.097	6.869	16.000	−1.135	6.902	16.000	−1.173	6.937
16.000	−1.209	6.973	16.000	−1.244	7.010	16.000	−1.278	7.048
16.000	−1.402	7.207	16.000	−1.666	8.398	16.000	−1.027	9.438
16.000	0.000	9.761	18.000	0.000	6.260	18.000	−0.501	6.318
18.000	−0.598	6.345	18.000	−0.638	6.358	18.000	−0.678	6.372
18.000	−0.718	6.387	18.000	−0.757	6.404	18.000	−0.796	6.421
18.000	−0.834	6.440	18.000	−0.872	6.459	18.000	−0.909	6.480
18.000	−0.946	6.502	18.000	−0.982	6.524	18.000	−1.017	6.547
18.000	−1.052	6.571	18.000	−1.087	6.596	18.000	−1.120	6.622
18.000	−1.154	6.648	18.000	−1.186	6.676	18.000	−1.218	6.703
18.000	−1.250	6.732	18.000	−1.281	6.761	18.000	−1.429	6.917
18.000	−1.838	8.249	18.000	−1.162	9.461	18.000	0.000	9.858
20.000	0.000	6.043	20.000	−0.620	6.127	20.000	−0.721	6.160
20.000	−0.751	6.171	20.000	−0.780	6.183	20.000	−0.810	6.195
20.000	−0.839	6.208	20.000	−0.867	6.221	20.000	−0.896	6.235
20.000	−0.924	6.249	20.000	−0.952	6.264	20.000	−0.980	6.279
20.000	−1.008	6.295	20.000	−1.035	6.311	20.000	−1.062	6.328
20.000	−1.088	6.345	20.000	−1.115	6.363	20.000	−1.141	6.381
20.000	−1.167	6.399	20.000	−1.192	6.418	20.000	−1.217	6.437
20.000	−1.242	6.457	20.000	−1.412	6.609	20.000	−1.978	8.060
20.000	−1.296	9.456	20.000	0.000	9.910	22.000	0.000	5.802
22.000	−0.726	5.917	22.000	−0.831	5.958	22.000	−0.853	5.967
22.000	−0.875	5.977	22.000	−0.897	5.987	22.000	−0.919	5.997
22.000	−0.940	6.008	22.000	−0.962	6.018	22.000	−0.983	6.029
22.000	−1.004	6.041	22.000	−1.025	6.052	22.000	−1.046	6.064
22.000	−1.067	6.076	22.000	−1.087	6.088	22.000	−1.108	6.100
22.000	−1.128	6.113	22.000	−1.149	6.126	22.000	−1.169	6.139
22.000	−1.188	6.152	22.000	−1.208	6.166	22.000	−1.228	6.180
22.000	−1.415	6.329	22.000	−2.102	7.879	22.000	−1.408	9.426
22.000	0.000	9.946	24.000	0.000	5.568	24.000	−0.842	5.711
24.000	−0.954	5.760	24.000	−0.970	5.768	24.000	−0.985	5.775
24.000	−1.000	5.783	24.000	−1.015	5.791	24.000	−1.030	5.799

Table 2. Concluded

24.000	−1.044	5.808	24.000	−1.059	5.816	24.000	−1.074	5.825
24.000	−1.088	5.834	24.000	−1.103	5.843	24.000	−1.117	5.852
24.000	−1.131	5.861	24.000	−1.146	5.870	24.000	−1.160	5.879
24.000	−1.174	5.889	24.000	−1.188	5.898	24.000	−1.202	5.908
24.000	−1.216	5.918	24.000	−1.230	5.927	24.000	−1.426	6.079
24.000	−2.210	7.711	24.000	−1.498	9.371	24.000	0.000	9.930
24.594	0.000	5.493	24.594	−0.827	5.634	24.594	−0.939	5.678
24.594	−0.954	5.684	24.594	−0.969	5.691	24.594	−0.984	5.697
24.594	−0.999	5.704	24.594	−1.014	5.711	24.594	−1.029	5.718
24.594	−1.044	5.725	24.594	−1.058	5.732	24.594	−1.073	5.740
24.594	−1.087	5.747	24.594	−1.102	5.755	24.594	−1.116	5.763
24.594	−1.130	5.771	24.594	−1.144	5.780	24.594	−1.158	5.789
24.594	−1.172	5.797	24.594	−1.186	5.806	24.594	−1.199	5.815
24.594	−1.213	5.825	24.594	−1.411	5.980	24.594	−2.227	7.631
24.594	−1.520	9.327	24.594	0.000	9.900			

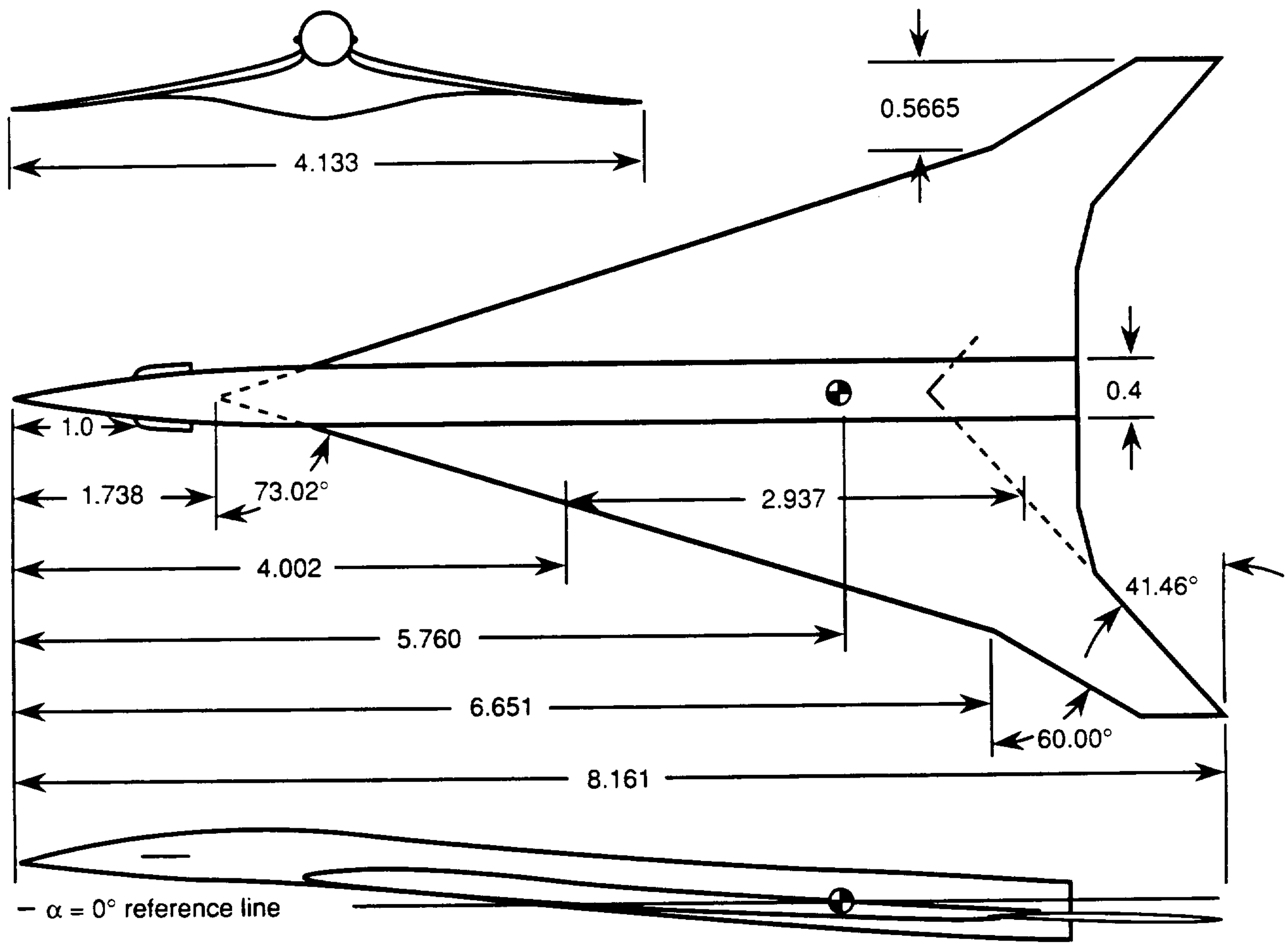

Figure 1. Geometric characteristics of model. All linear dimensions are in feet.

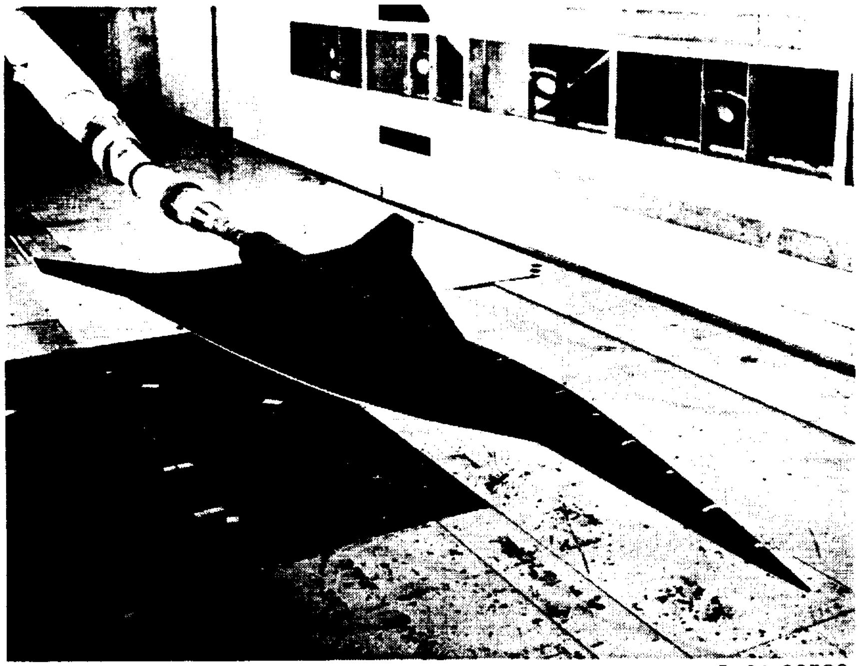

L-91-00500

(a) Side view.

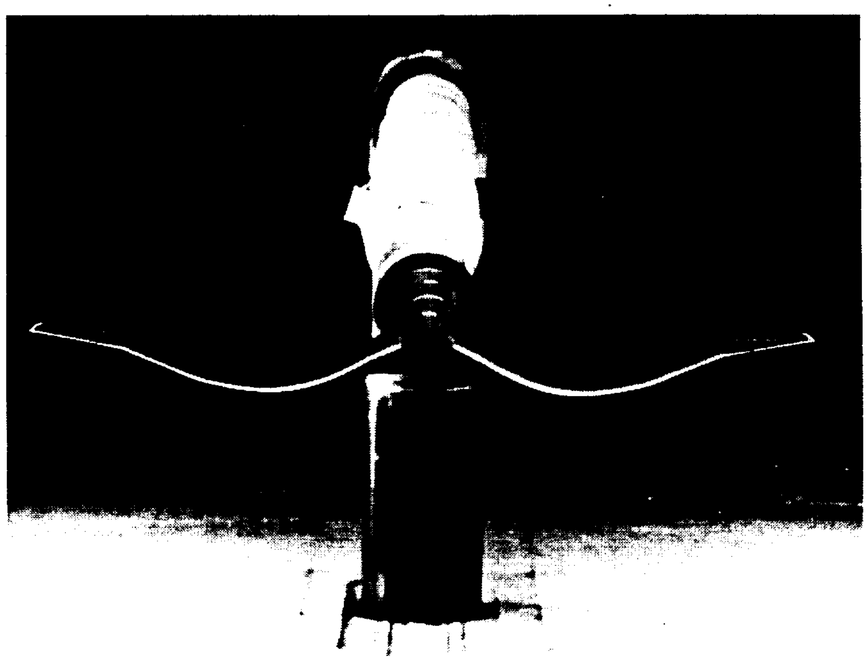

L-91-00482

(b) Front view.

Figure 2. Baseline configuration of model mounted in the 14- by 22-Foot Subsonic Tunnel.

L-91-00505

(a) Front view.

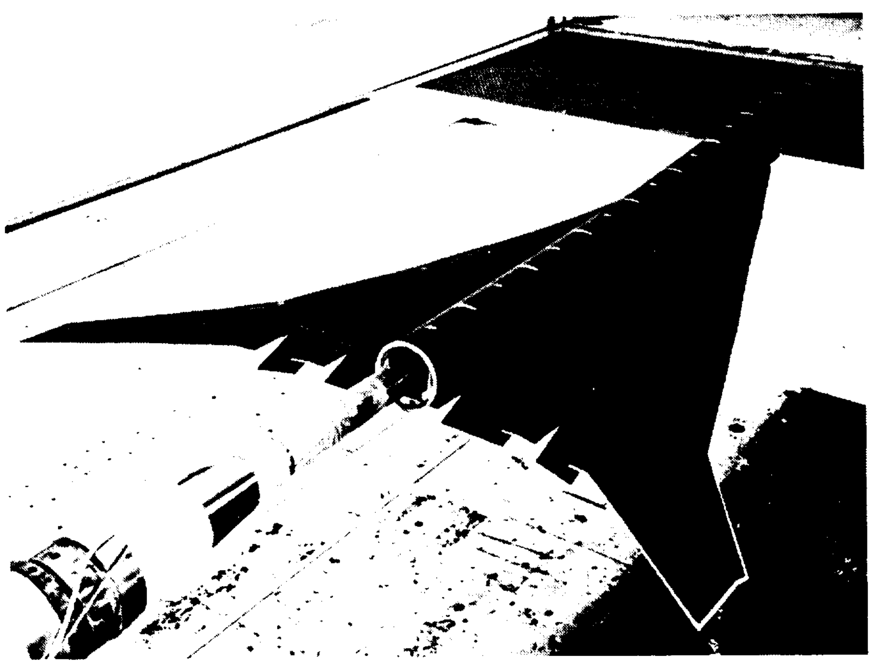

L-91-00477

(b) Aft view.

Figure 3. Deflected flap configuration with $\delta_L = 30^\circ$, $\delta_T = 20^\circ$.

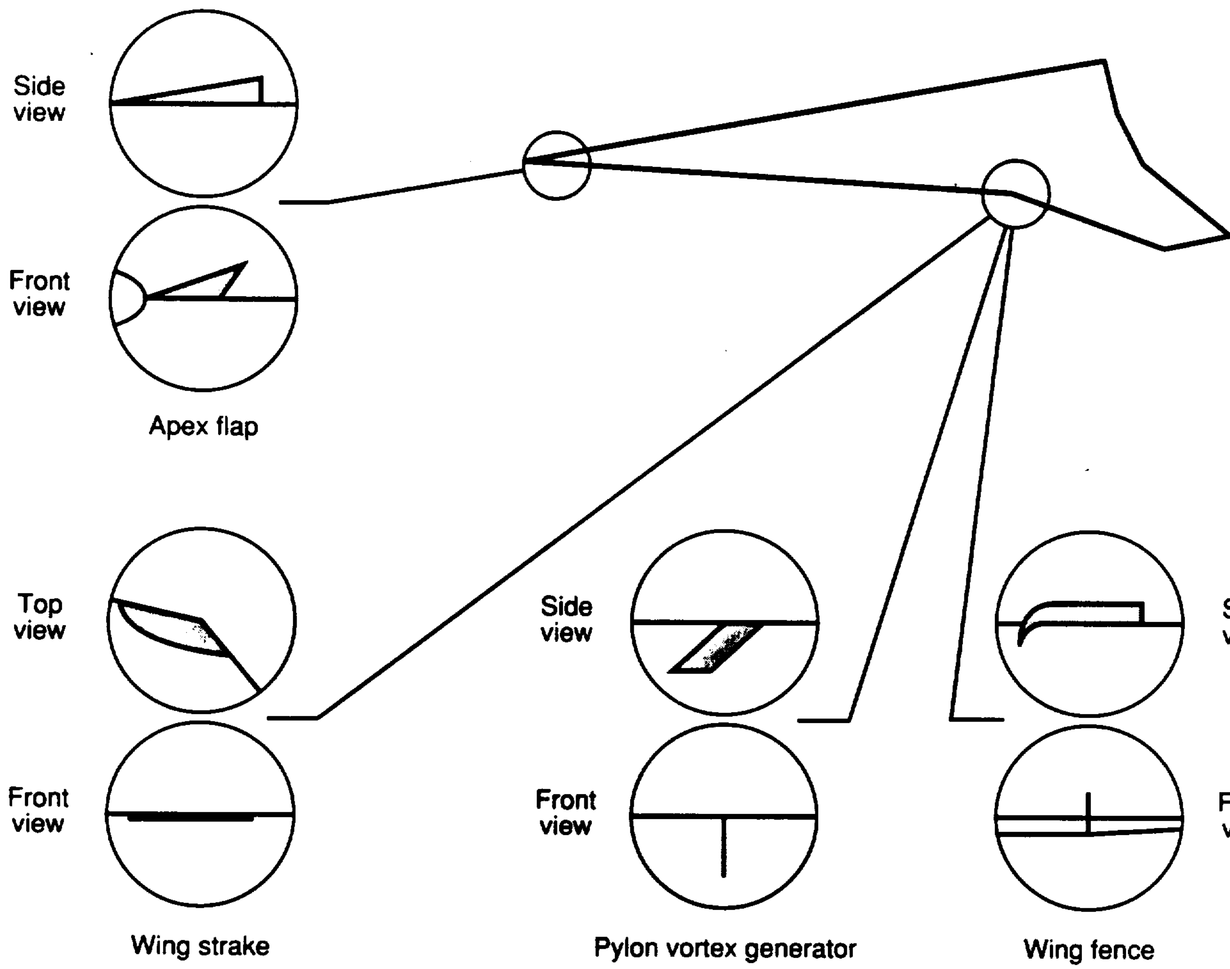

Figure 4. Vortex management devices tested during this investigation.

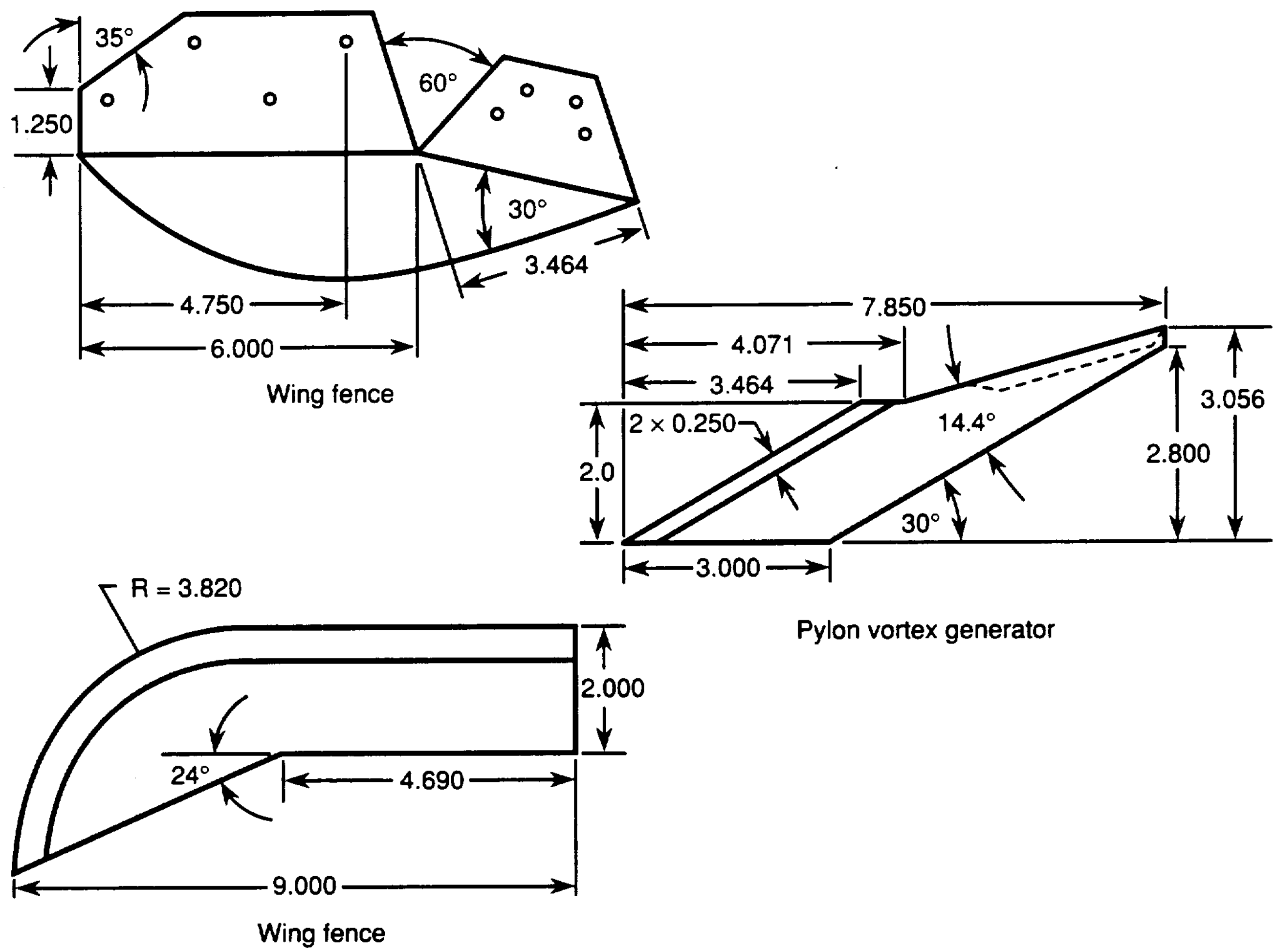

Figure 5. Geometric characteristics of vortex management devices applied to leading-edge crank. Linear dimensions are in inches.

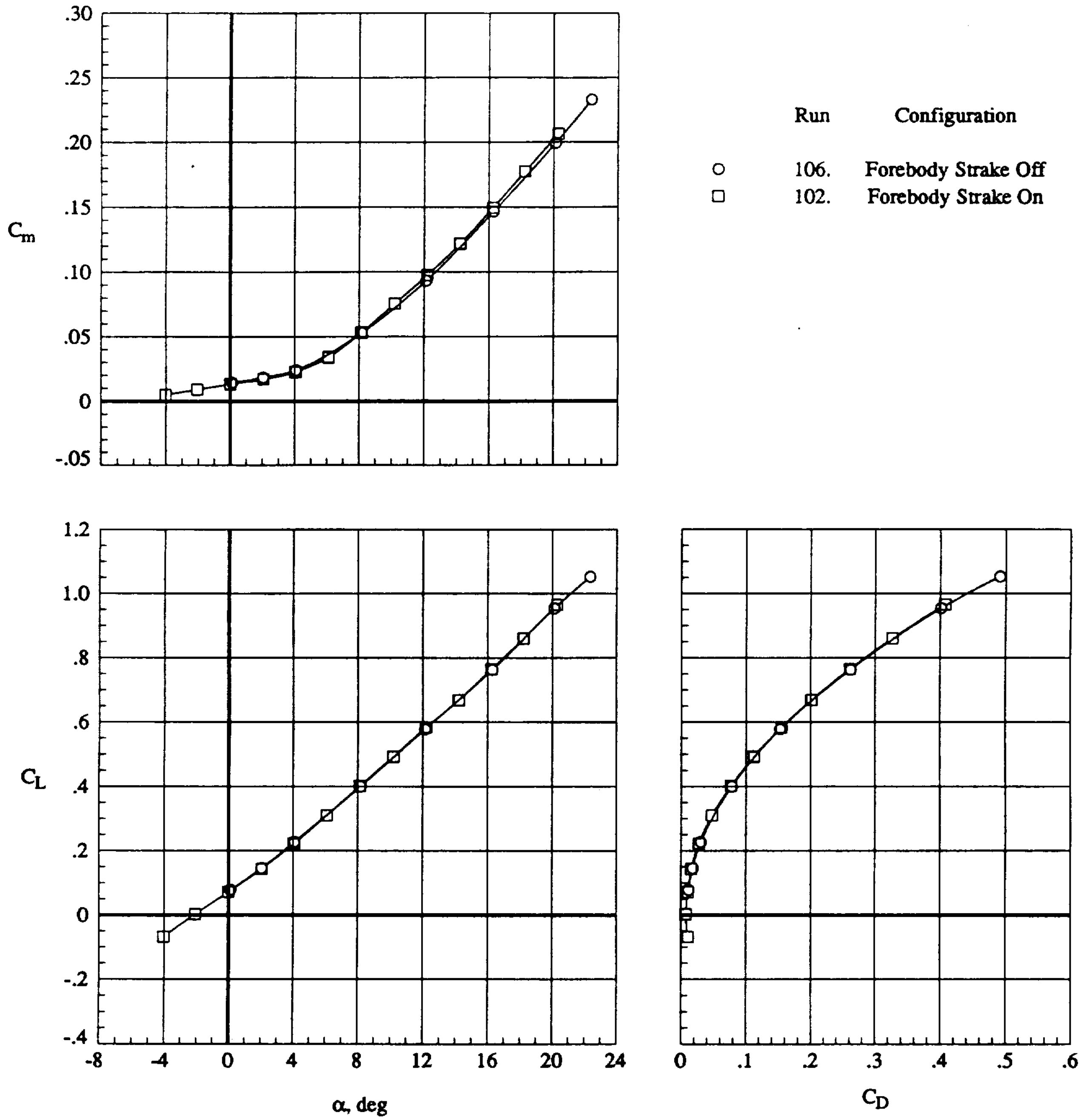

(a) Longitudinal aerodynamics.

Figure 6. Effect of forebody strakes with $\delta_L = 0°$ and $\delta_T = 0°$ at q = 70 psf.

	Run	β, deg	Configuration
○	106.	0.	Forebody Strake Off
□	102.	0.	Forebody Strake On

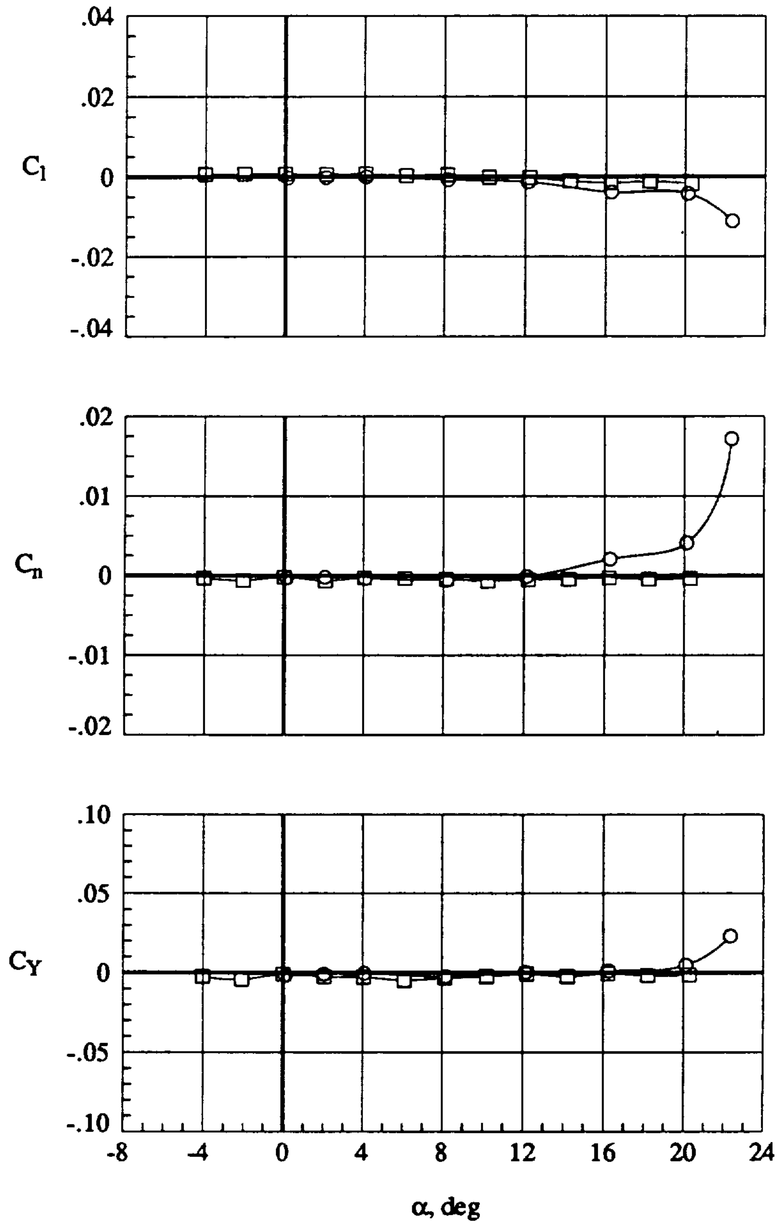

(b) Lateral aerodynamics.

Figure 6. Concluded.

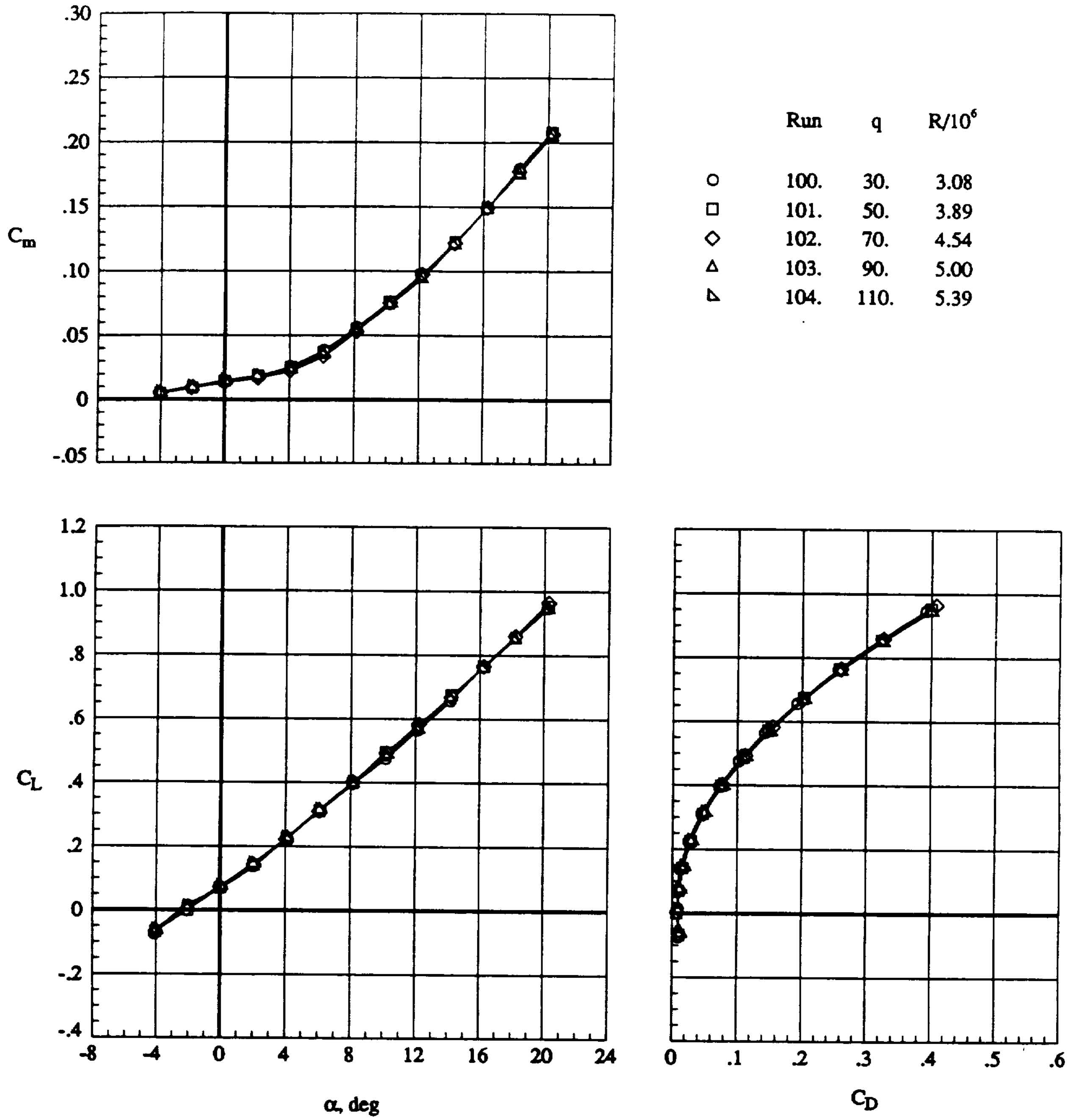

(a) Longitudinal aerodynamics.

Figure 7. Effect of tunnel dynamic pressure with forebody strakes in place, $\delta_L = 0°$ and $\delta_T = 0°$.

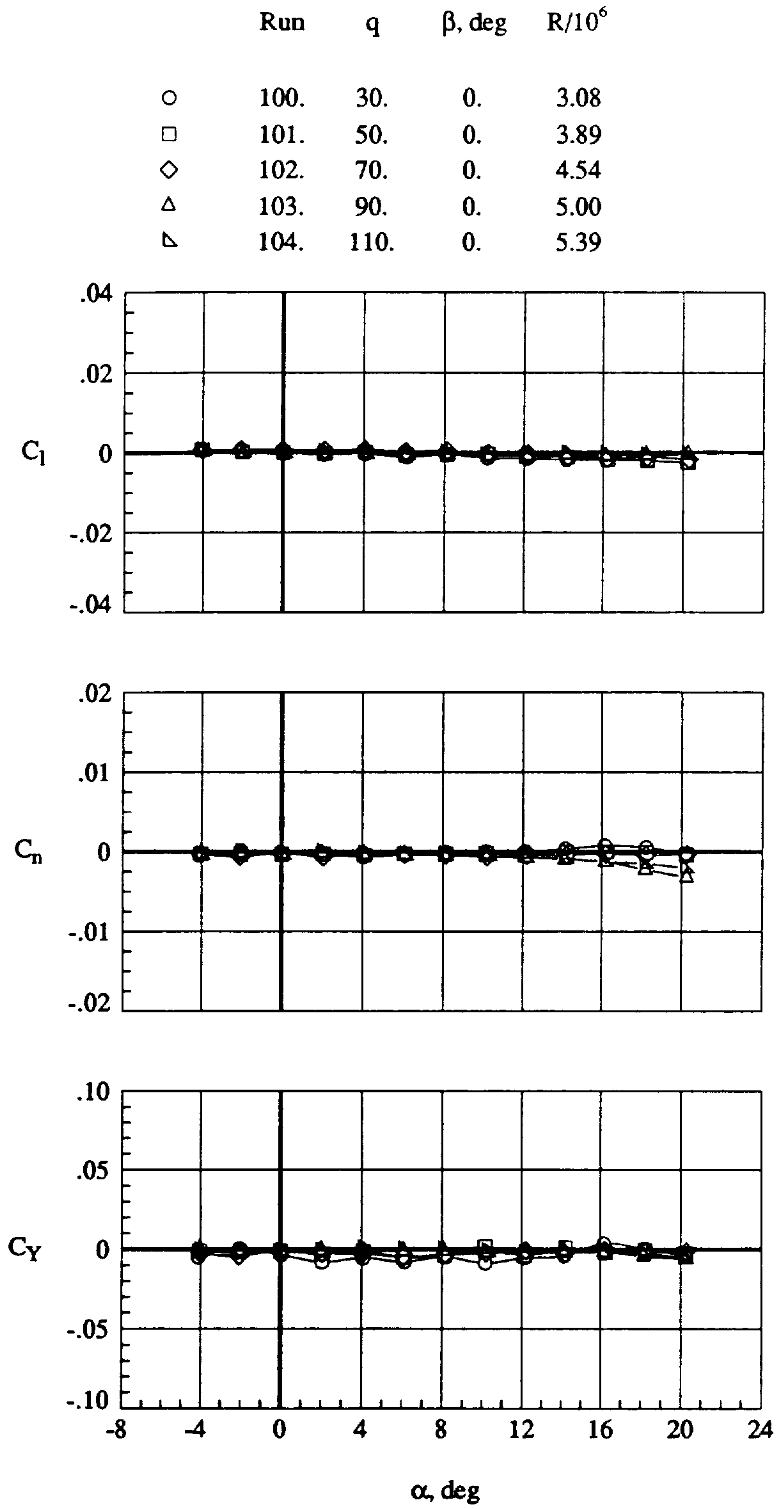

(b) Lateral aerodynamics.

Figure 7. Concluded.

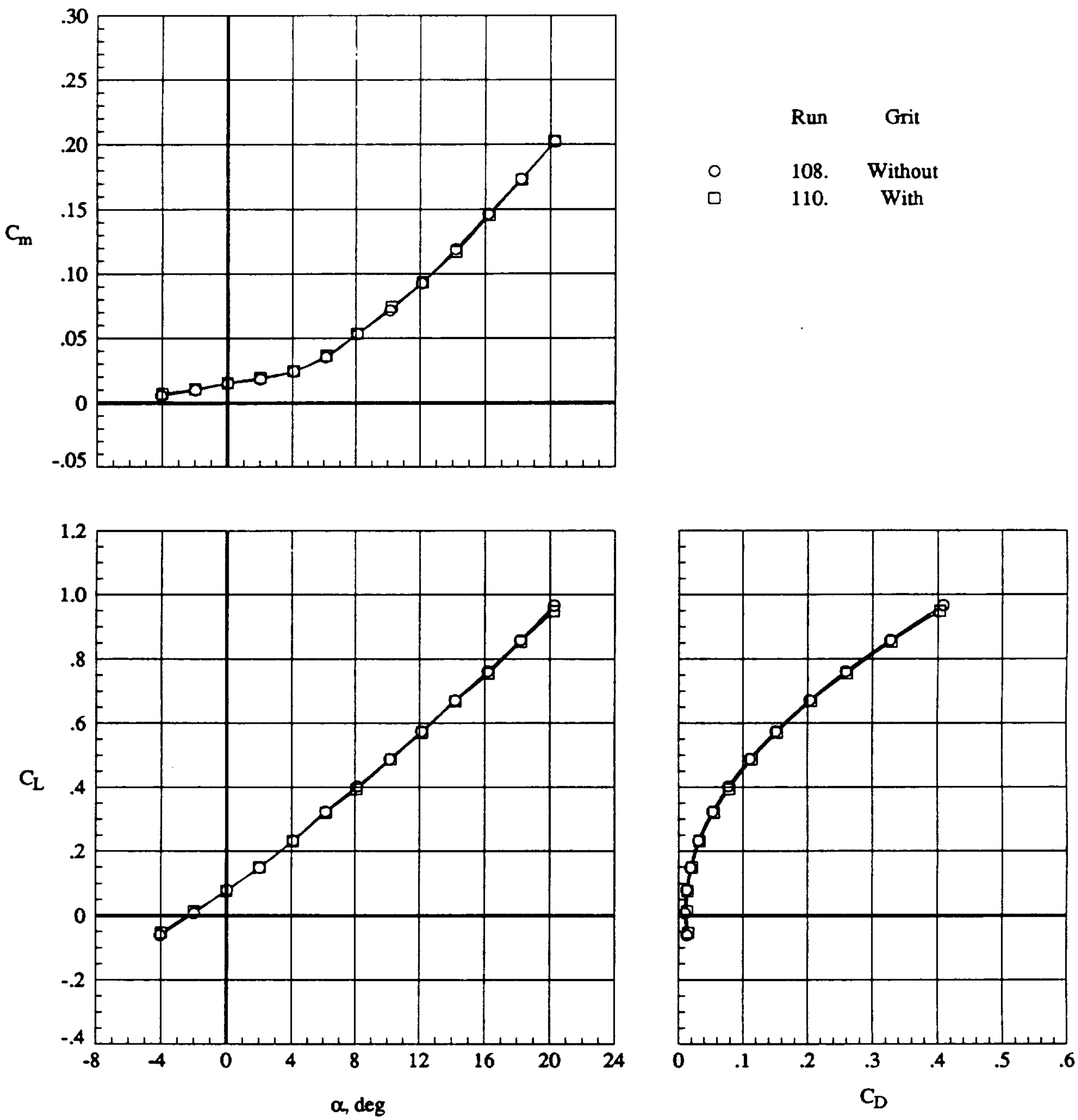

(a) Longitudinal aerodynamics.

Figure 8. Effect of boundary-layer transition grit with $\delta_L = 0°$ and $\delta_T = 0°$ at q = 70 psf.

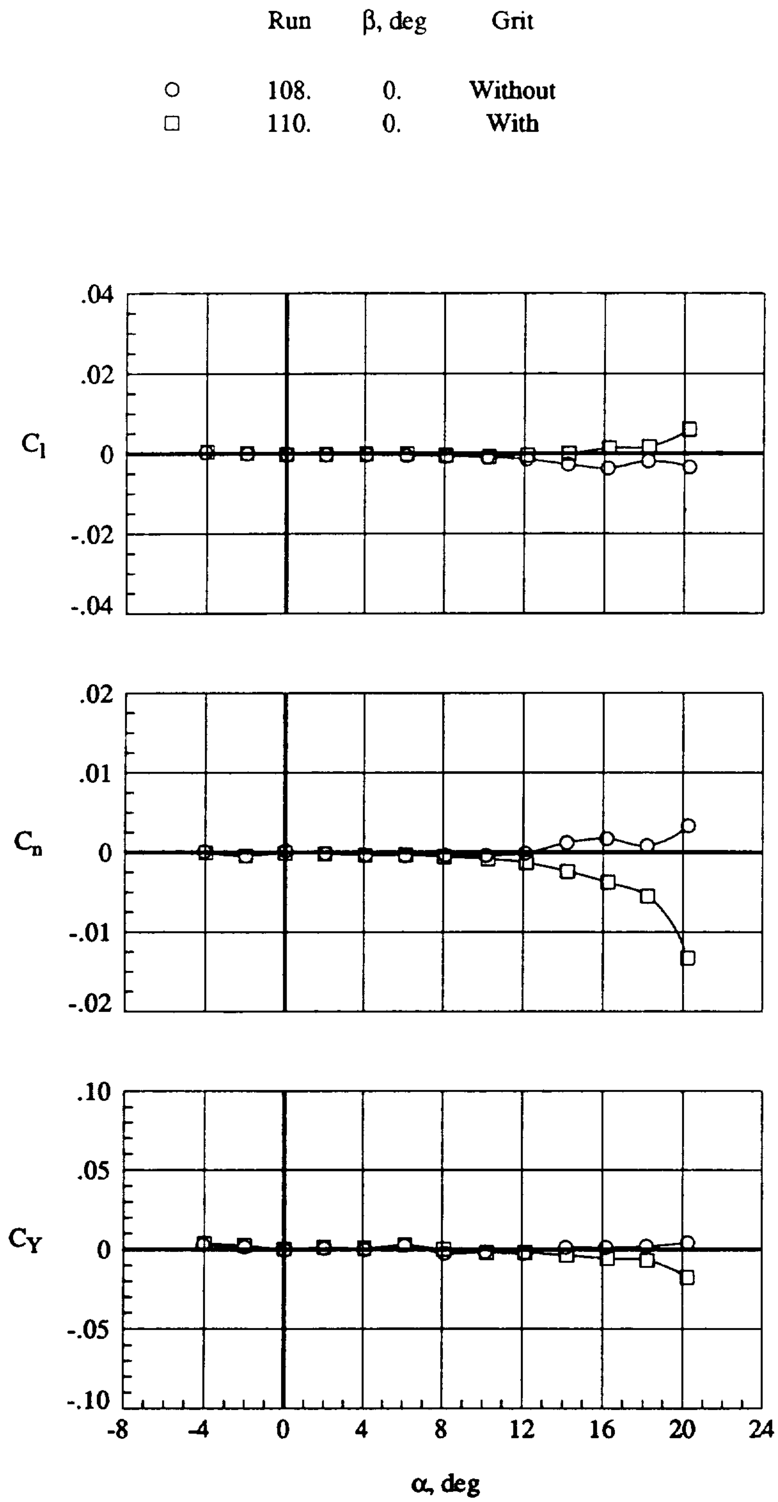

(b) Lateral aerodynamics.

Figure 8. Concluded.

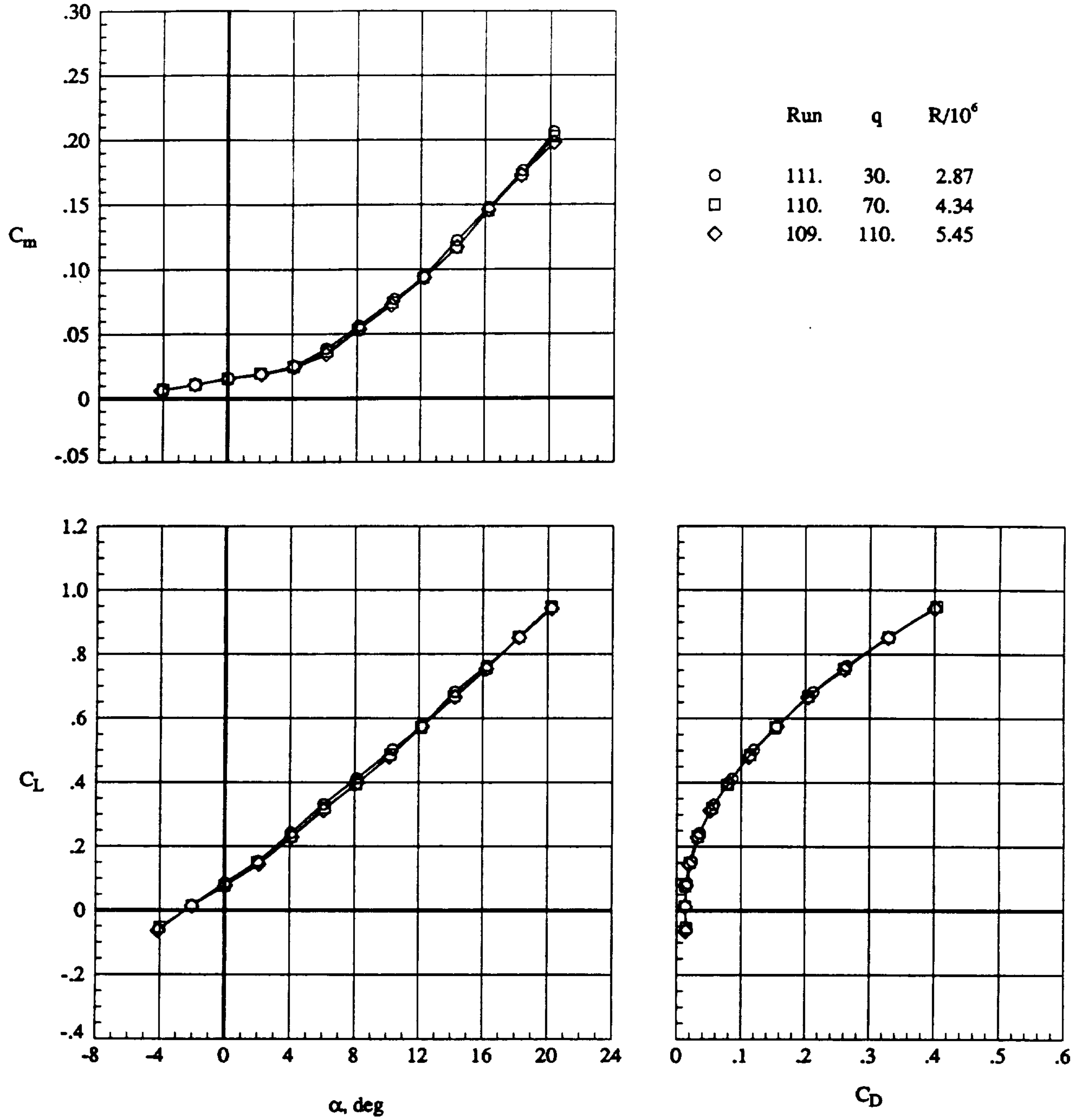

(a) Longitudinal aerodynamics.

Figure 9. Effect of tunnel dynamic pressure with boundary-layer transition grit in place with $\delta_L = 0^\circ$ and $\delta_T = 0^\circ$.

	Run	q	β, deg	$R/10^6$
○	111.	30.	0.	2.87
□	110.	70.	0.	4.34
◇	109.	110.	0.	5.45

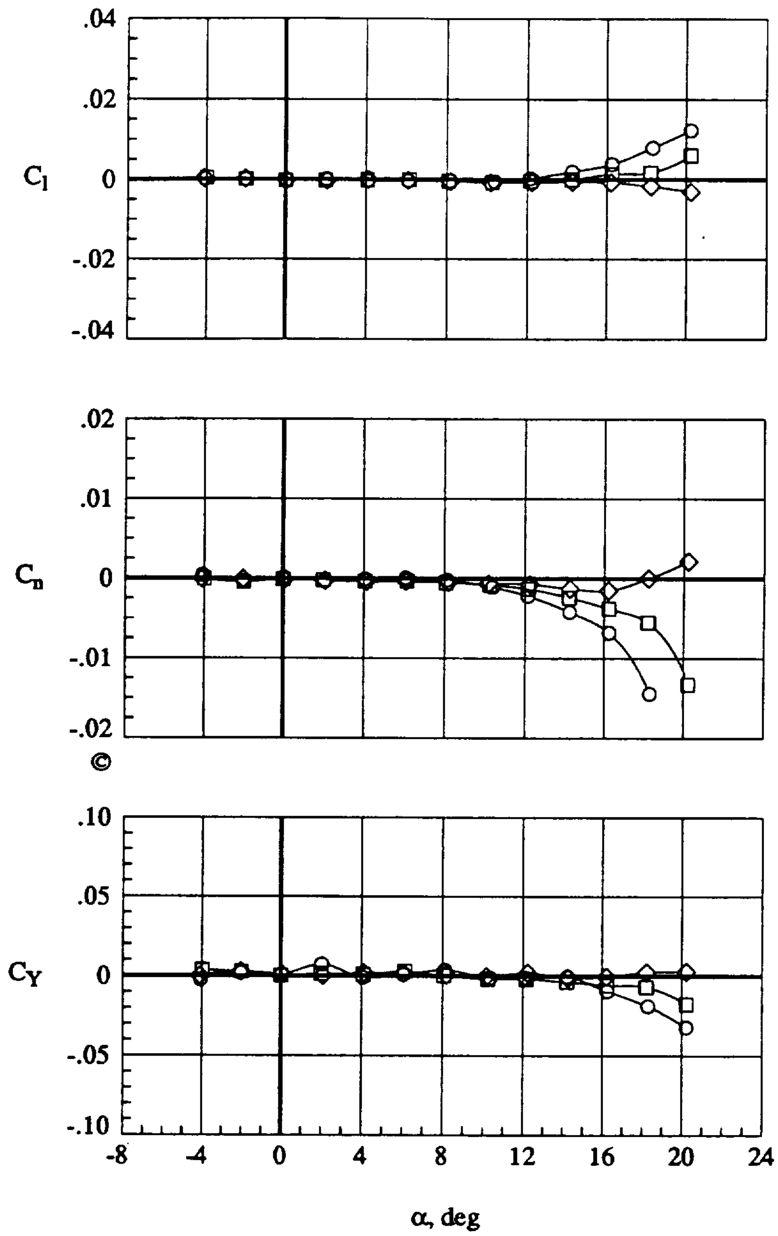

(b) Lateral aerodynamics.

Figure 9. Concluded.

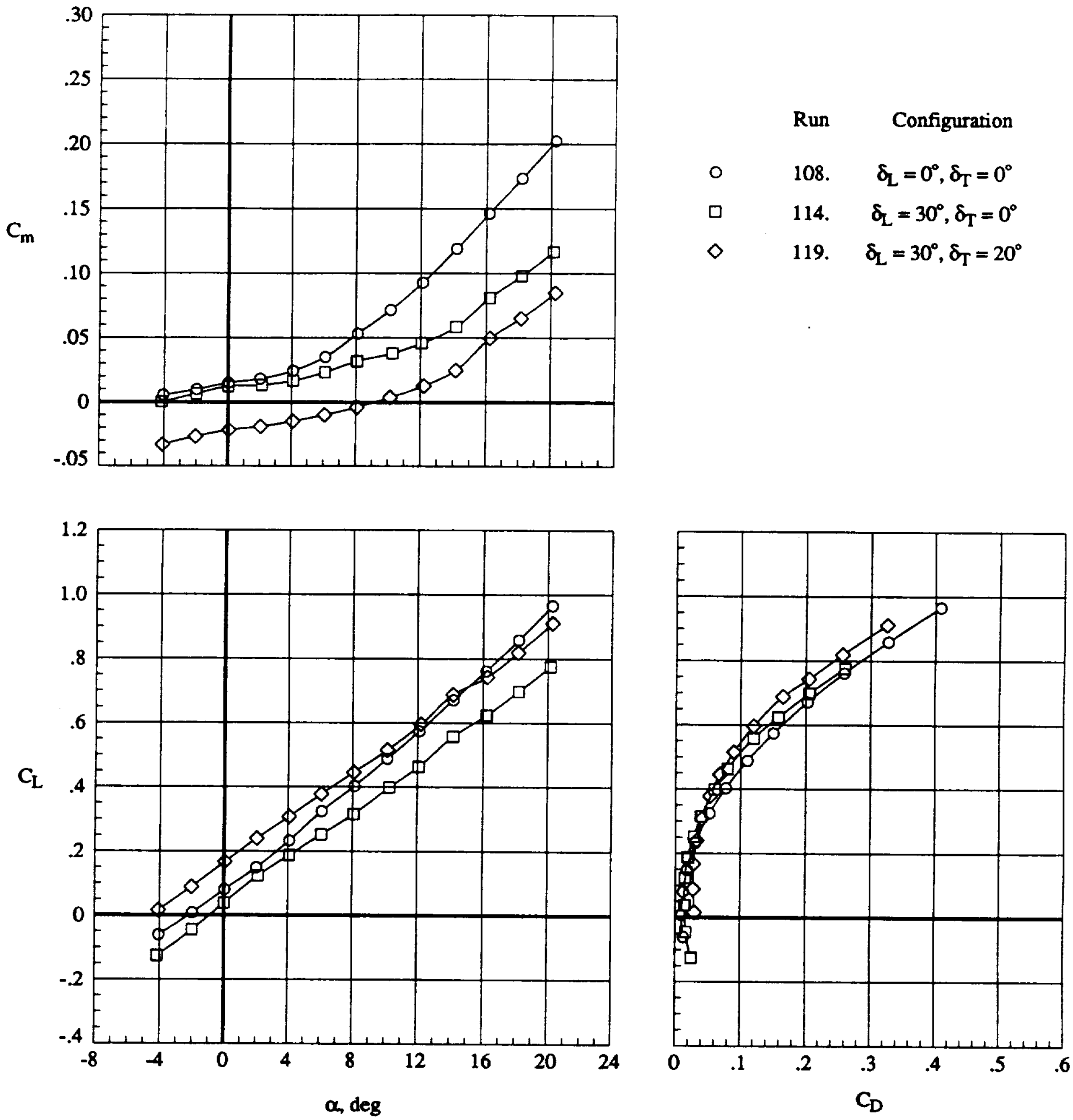

(a) Longitudinal aerodynamics.

Figure 10. Effect of leading-edge and trailing-edge flap deflections at q = 70 psf.

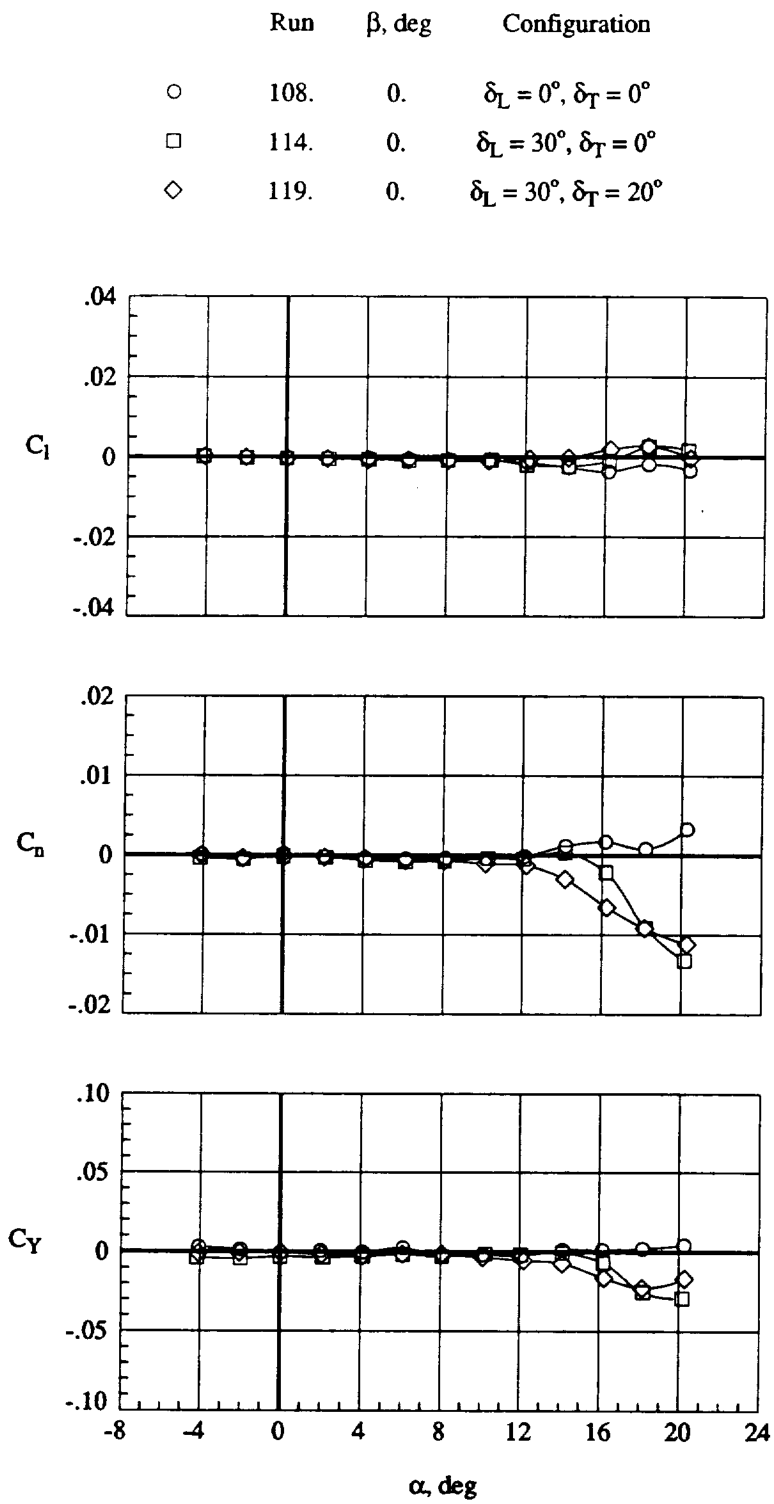

(b) Lateral aerodynamics.

Figure 10. Continued.

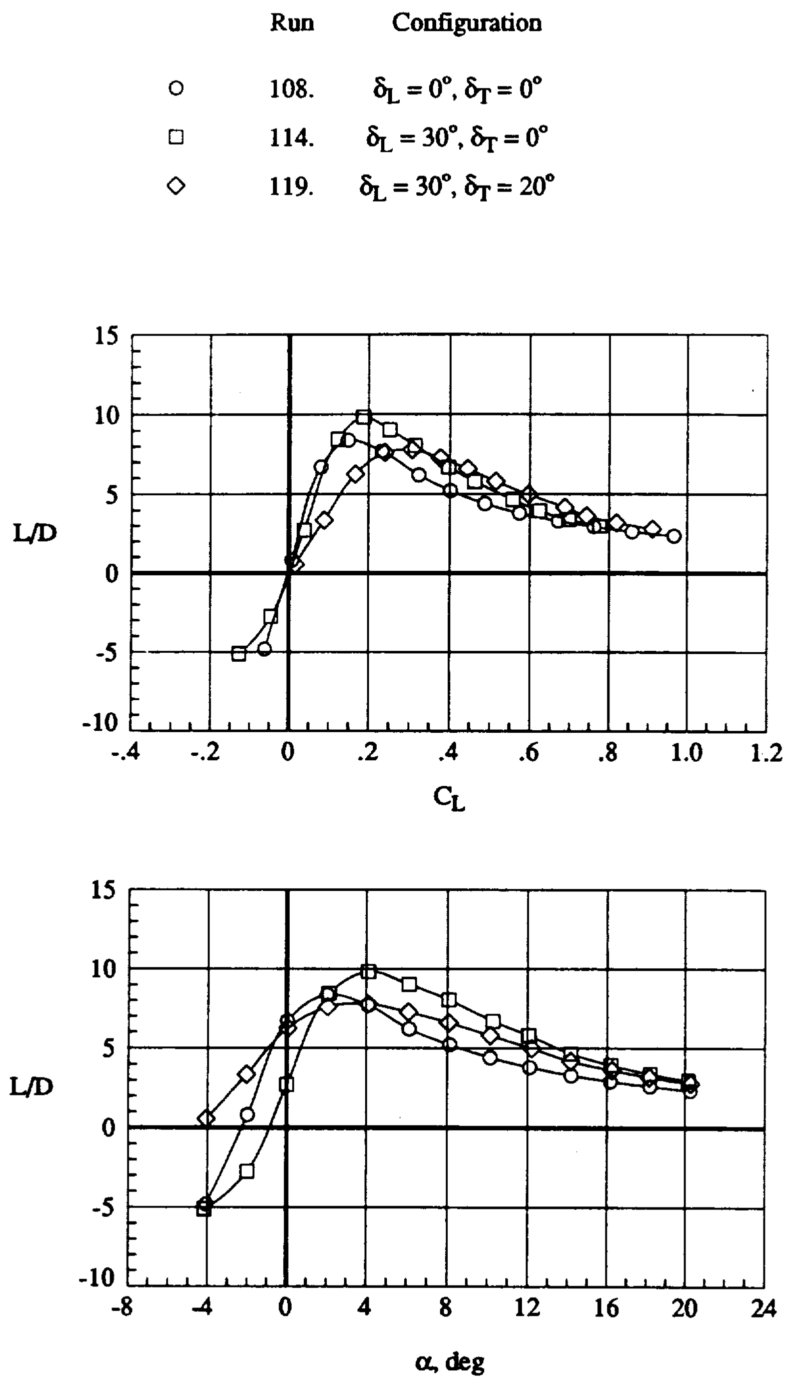

(c) Lift-drag performance.

Figure 10. Concluded.

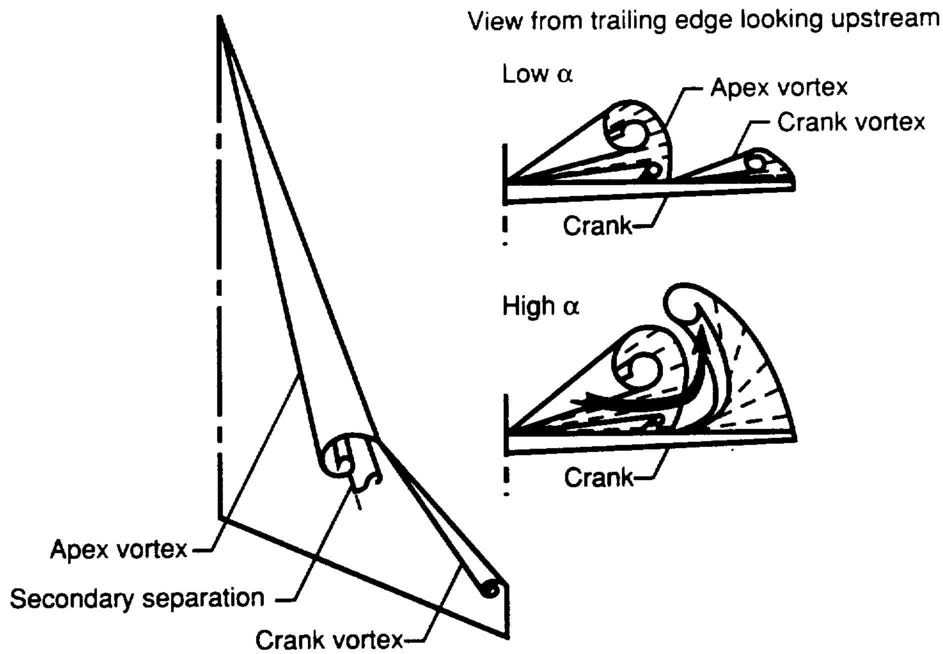

Figure 11. Hypothesized development of leading-edge vortices on a cranked wing.

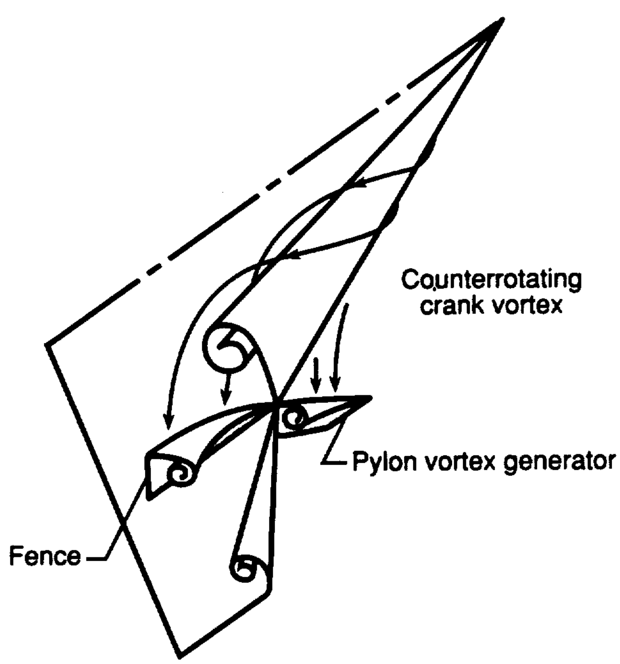

Figure 12. Hypothesized flow structure in presence of pylon vortex generator and upper surface wing fence.

L-91-00507

(a) Full view.

L-91-00493

(b) Close-up view.

Figure 13. Model with pylon vortex generator.

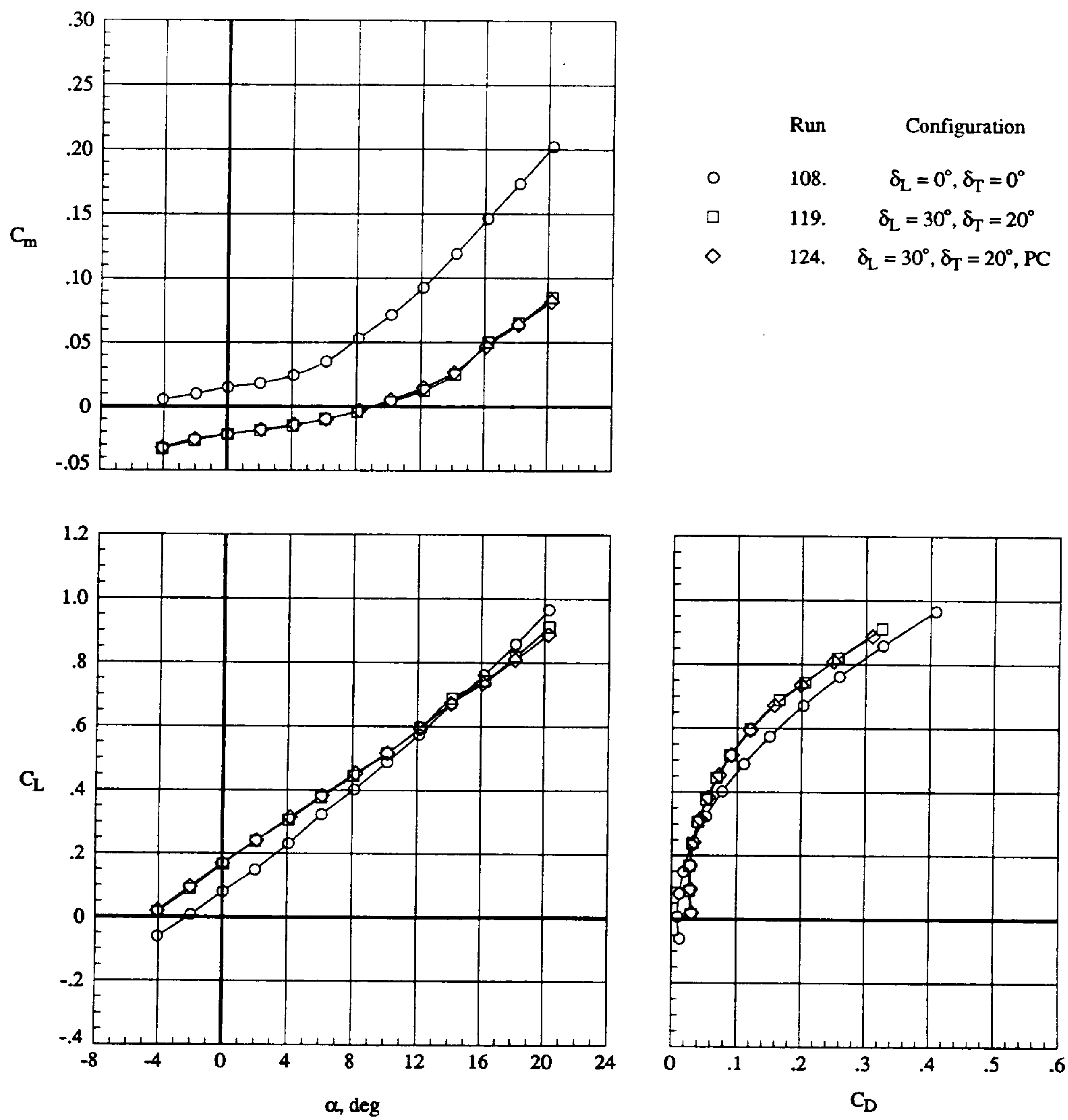

(a) Longitudinal aerodynamics.

Figure 14. Effect of pylon vortex generator at wing crank; q = 70 psf.

	Run	β, deg	Configuration
○	108.	0.	$\delta_L = 0°, \delta_T = 0°$
□	119.	0.	$\delta_L = 30°, \delta_T = 20°$
◇	124.	0.	$\delta_L = 30°, \delta_T = 20°$, PC

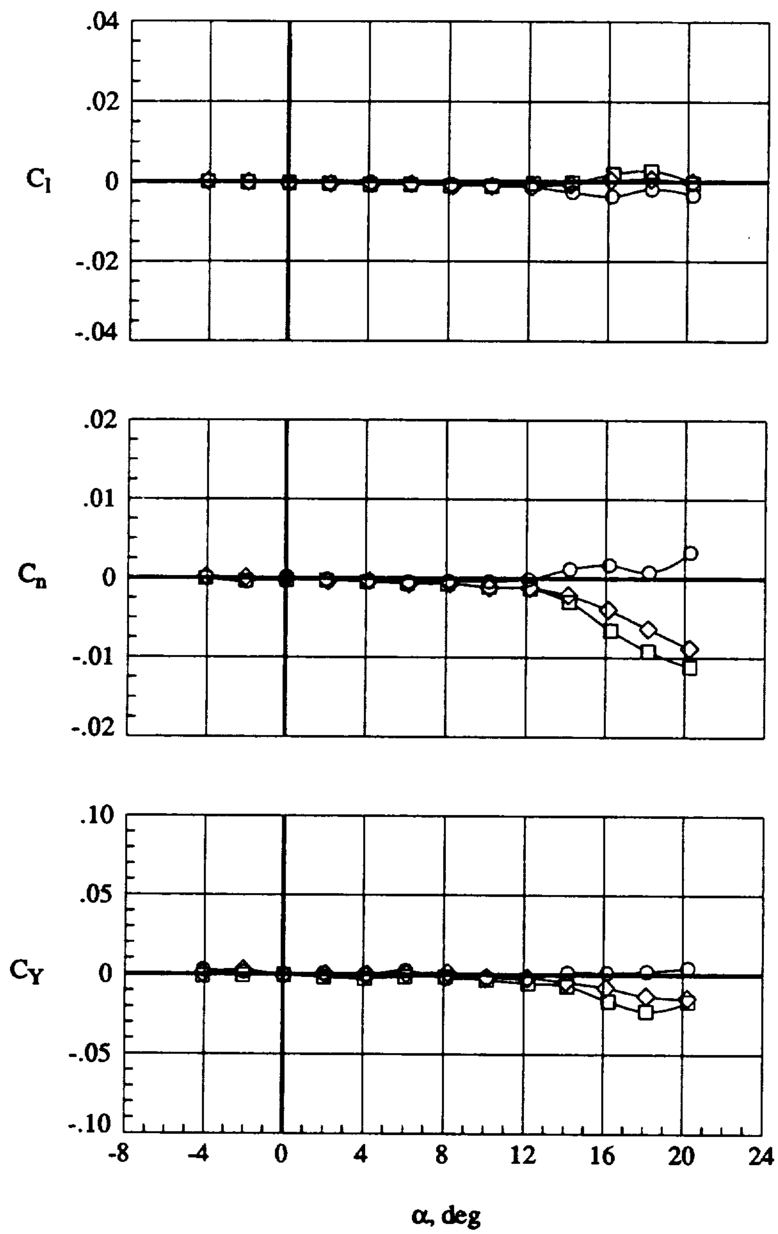

(b) Lateral aerodynamics.

Figure 14. Continued.

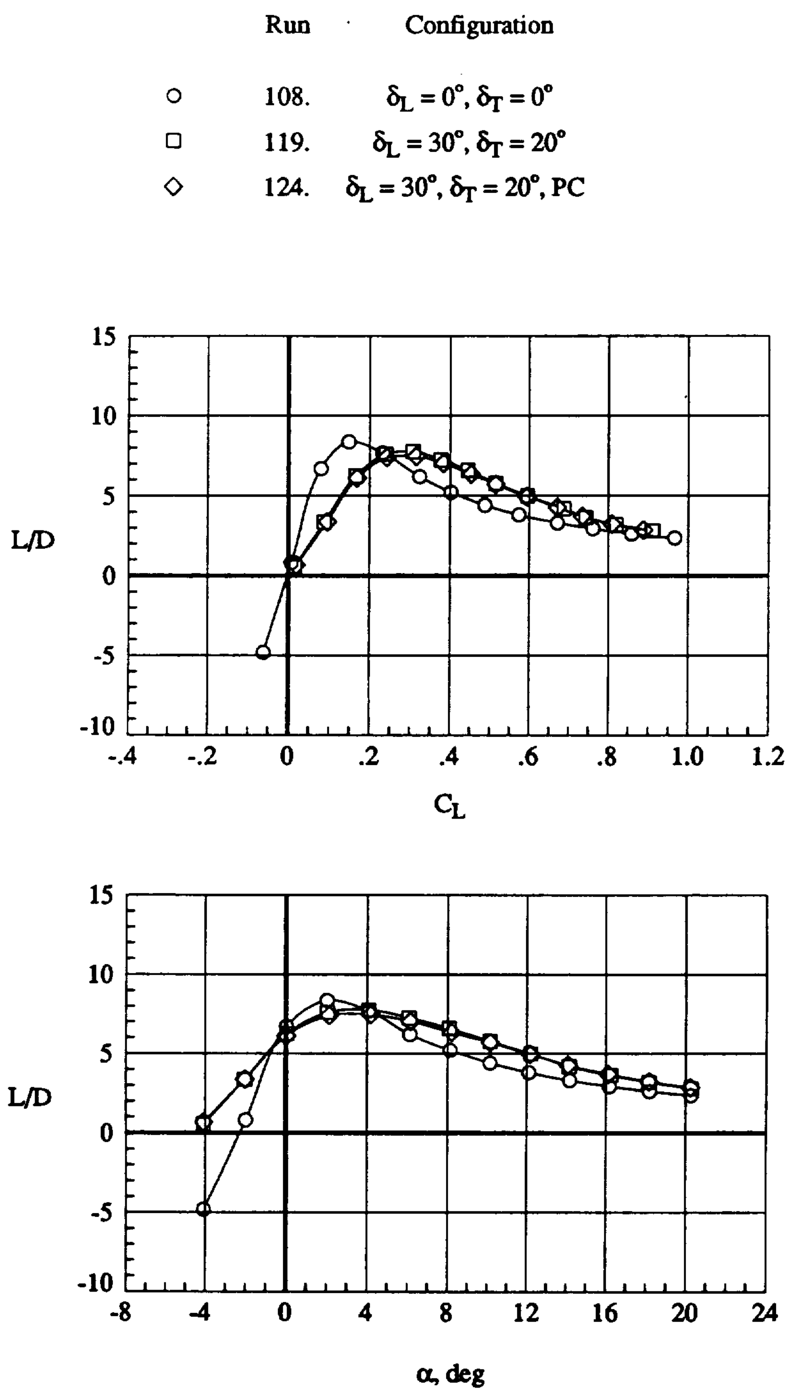

(c) Lift-drag performance.

Figure 14. Concluded.

L-91-00504

(a) Full view.

L-91-00495

(b) Close-up view.

Figure 15. Model with both inboard and outboard pylon vortex generators.

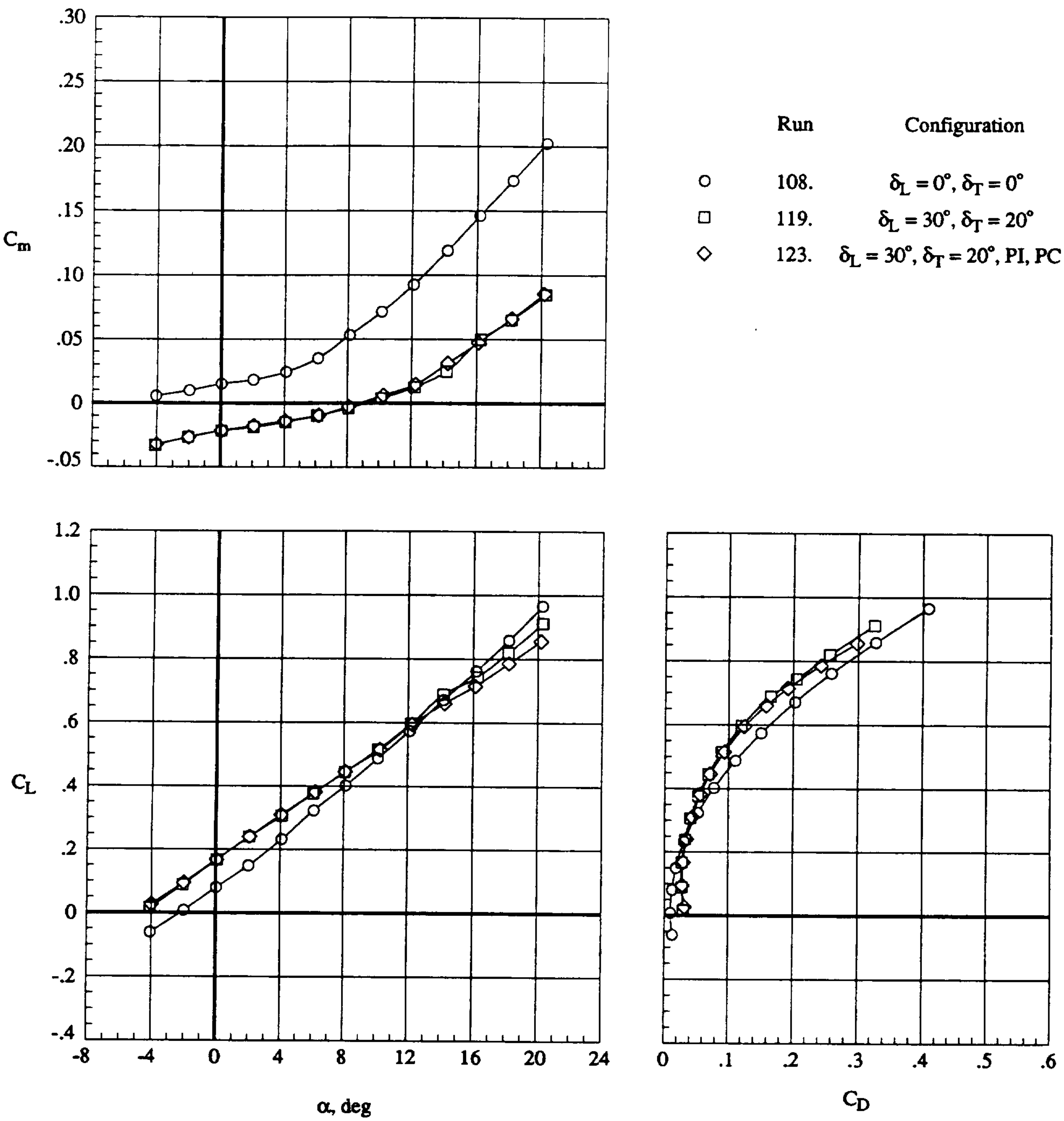

(a) Longitudinal aerodynamics.

Figure 16. Effect of both inboard and crank pylon vortex generators at q = 70 psf.

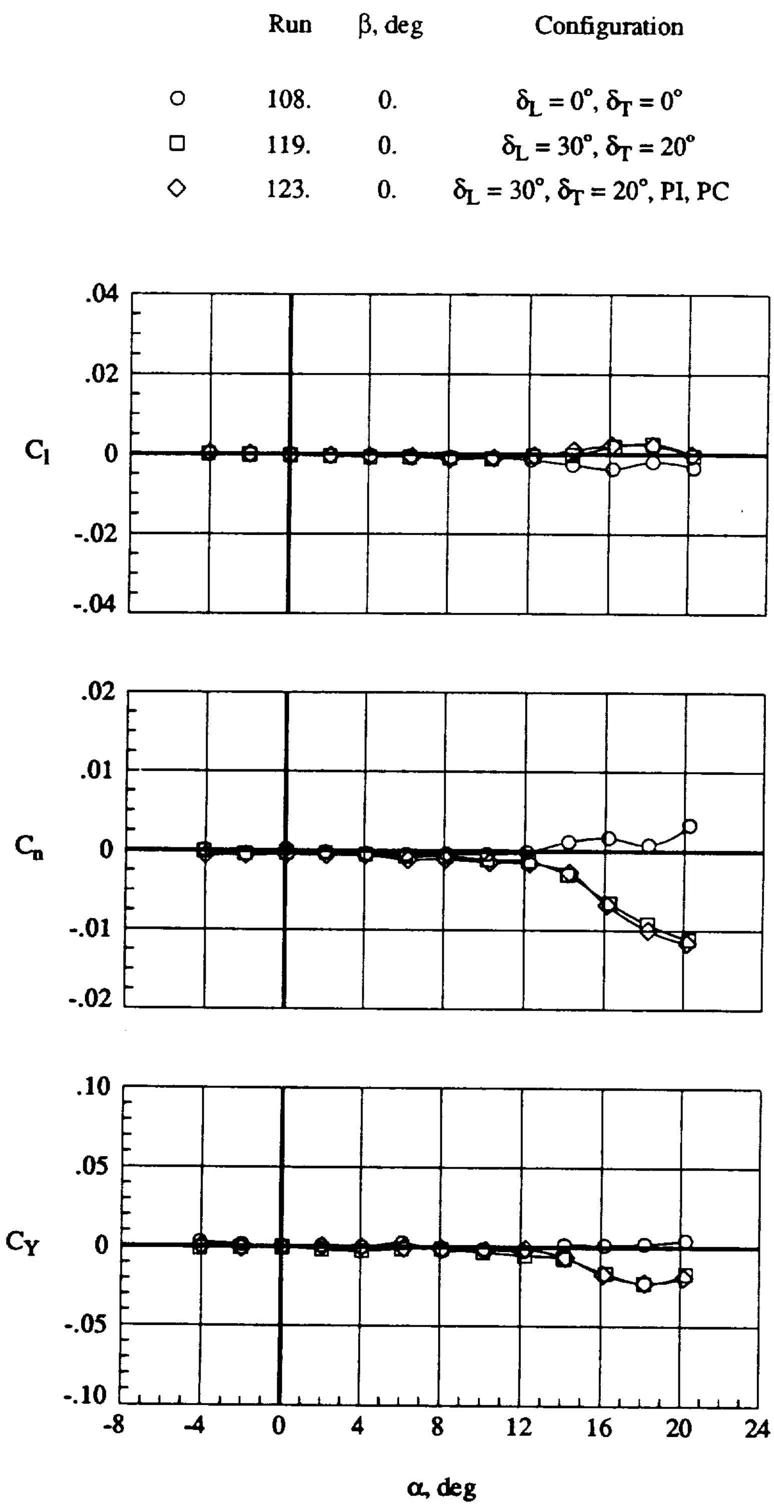

(b) Lateral aerodynamics.

Figure 16. Continued.

	Run	Configuration
○	108.	$\delta_L = 0°, \delta_T = 0°$
□	119.	$\delta_L = 30°, \delta_T = 20°$
◇	123.	$\delta_L = 30°, \delta_T = 20°$, PI, PC

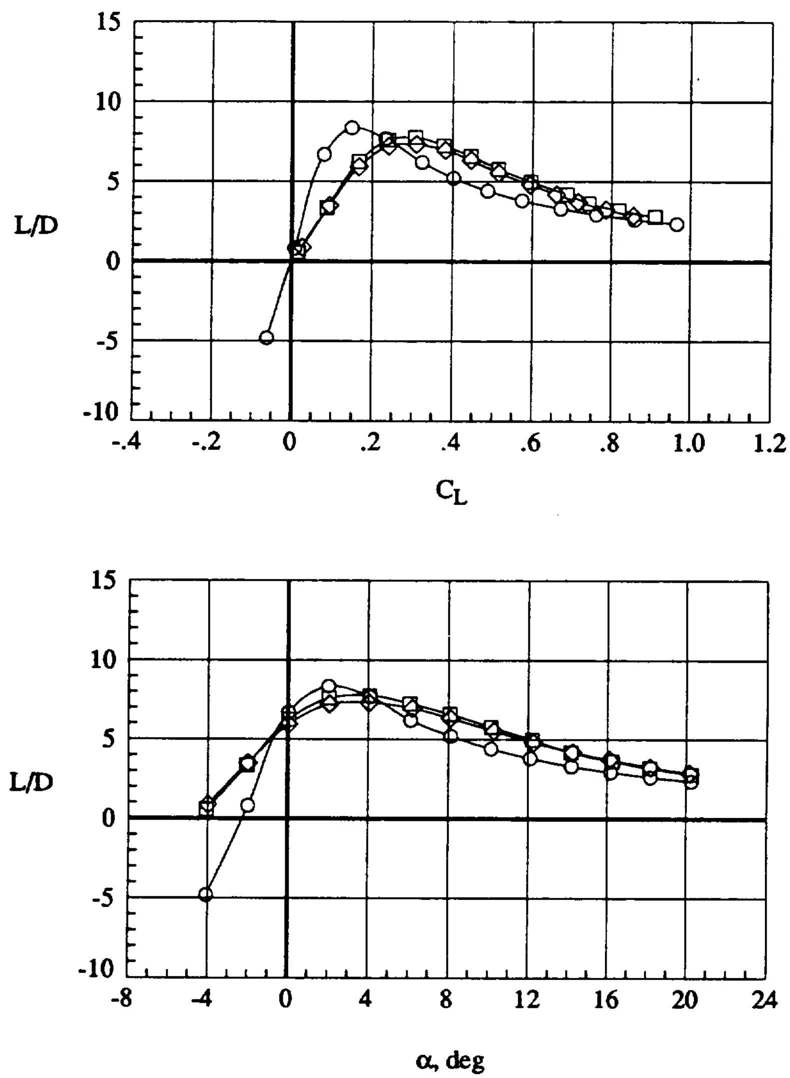

(c) Lift-drag performance.

Figure 16. Concluded.

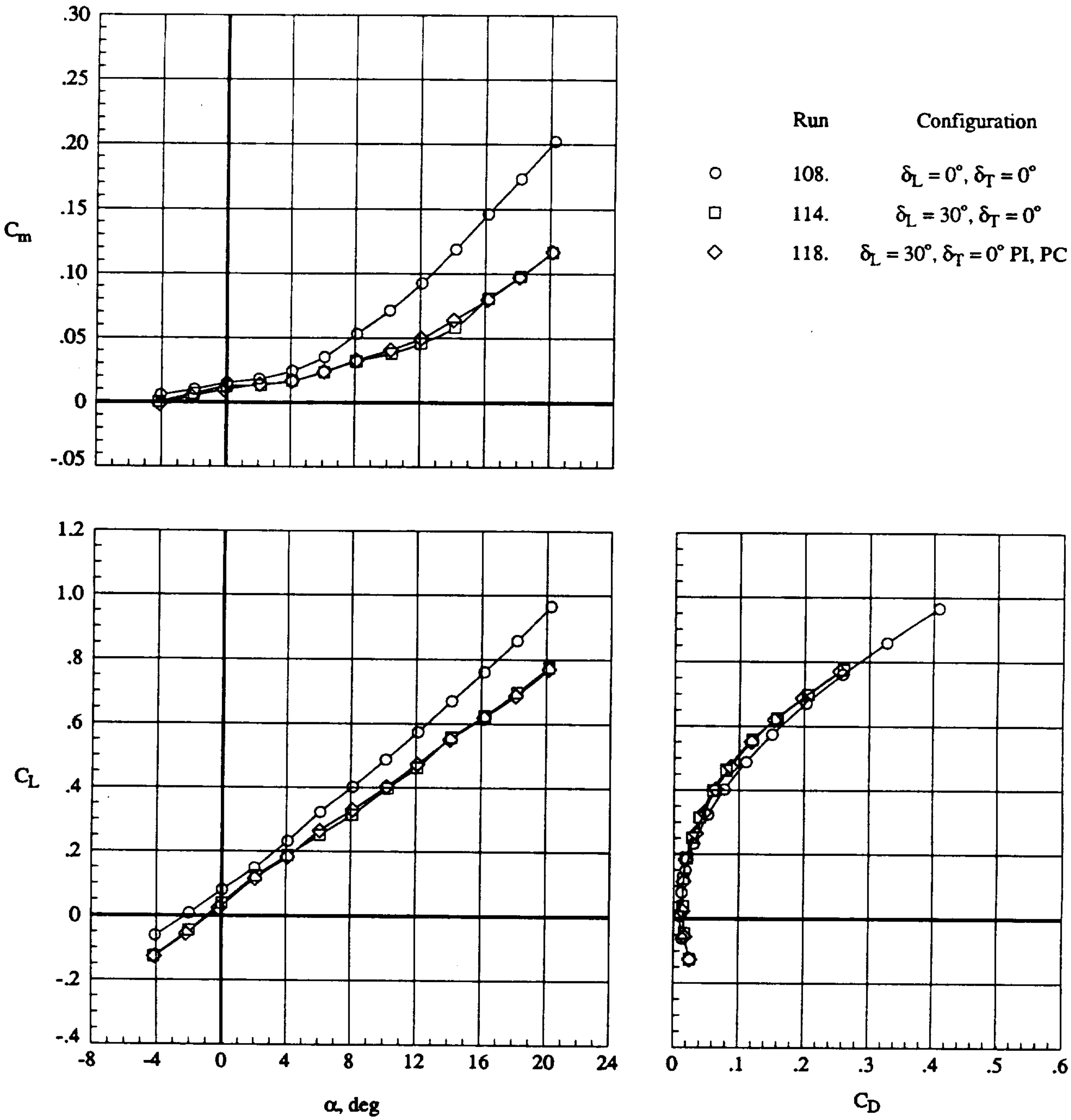

(a) Longitudinal aerodynamics.

Figure 17. Effect of both inboard and crank pylon vortex generators without trailing-edge flap deflection at q = 70 psf.

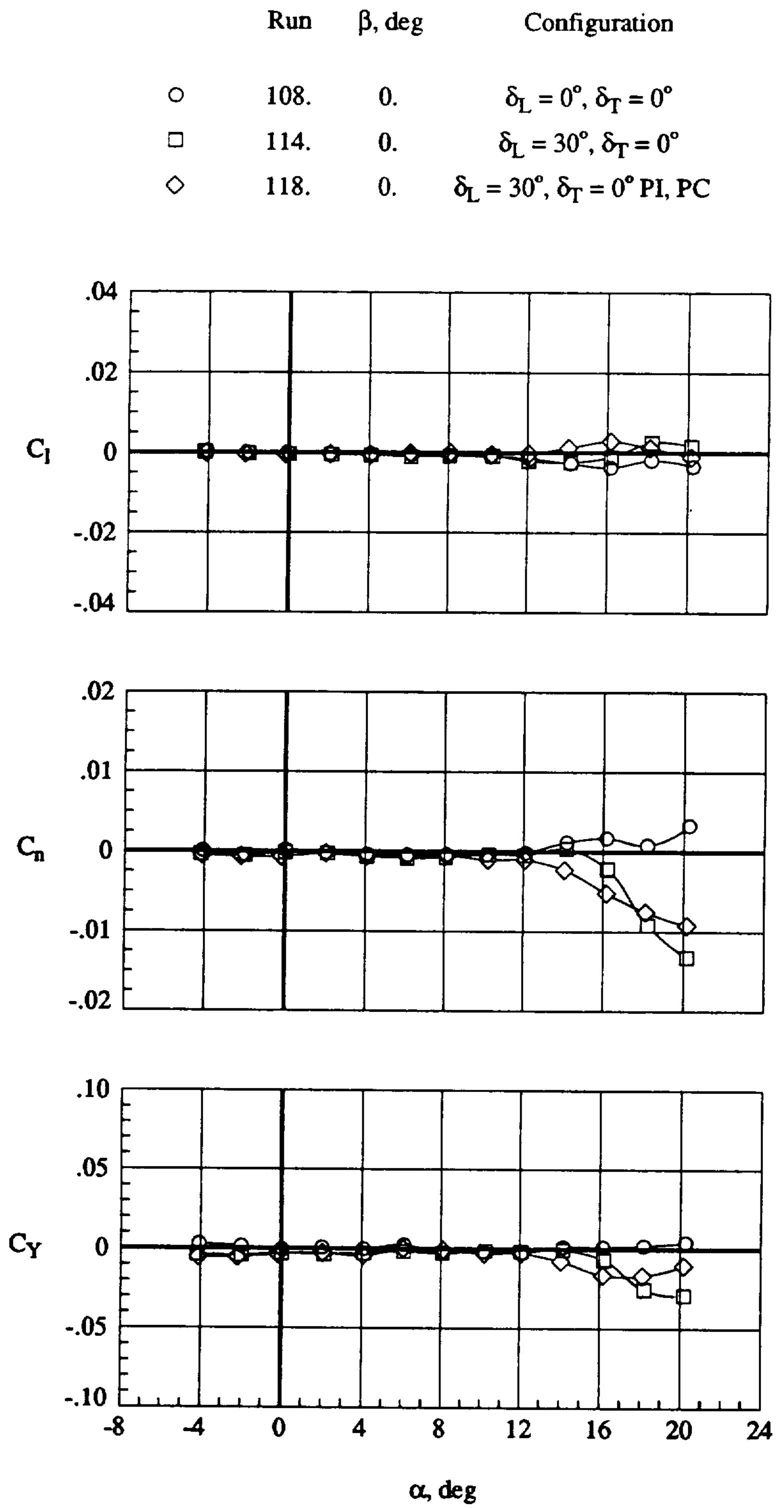

(b) Lateral aerodynamics.

Figure 17. Continued.

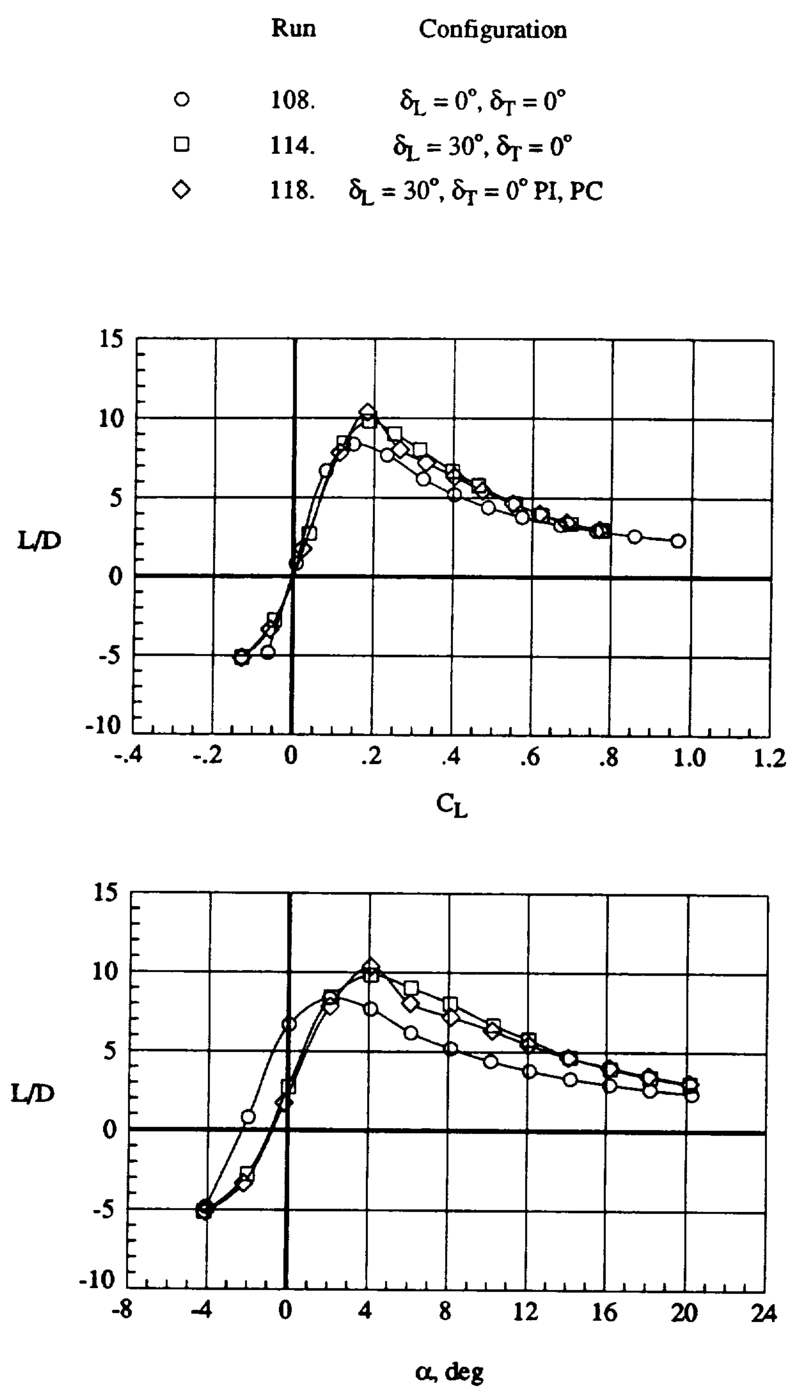

(c) Lift-drag performance.

Figure 17. Concluded.

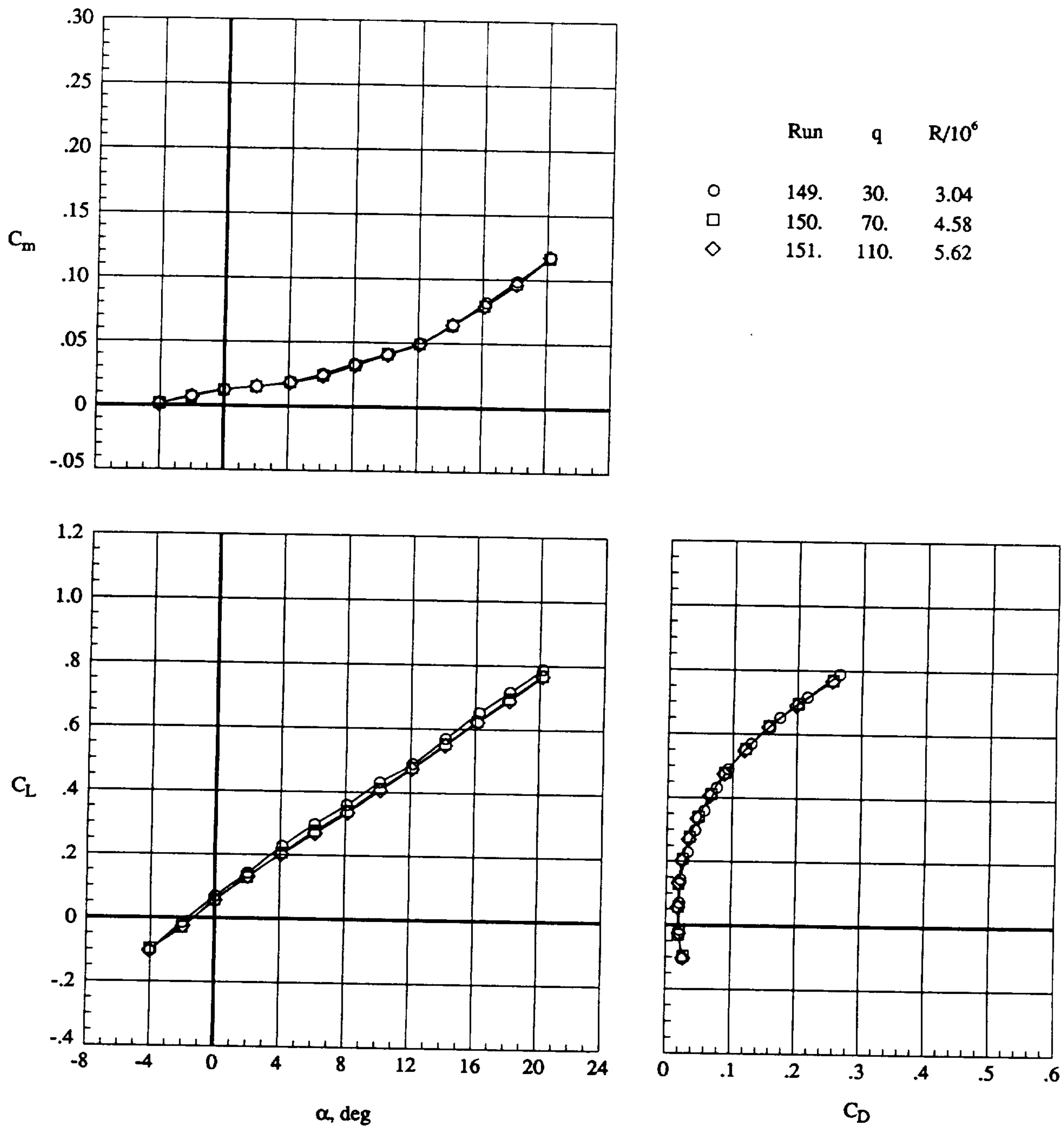

(a) Longitudinal aerodynamics.

Figure 18. Effect of tunnel dynamic pressure on both inboard and crank pylon vortex generators with $\delta_L = 30^\circ$ and $\delta_T = 0^\circ$.

	Run	q	β, deg	$R/10^6$
○	149.	30.	0.	3.04
□	150.	70.	0.	4.58
◇	151.	110.	0.	5.62

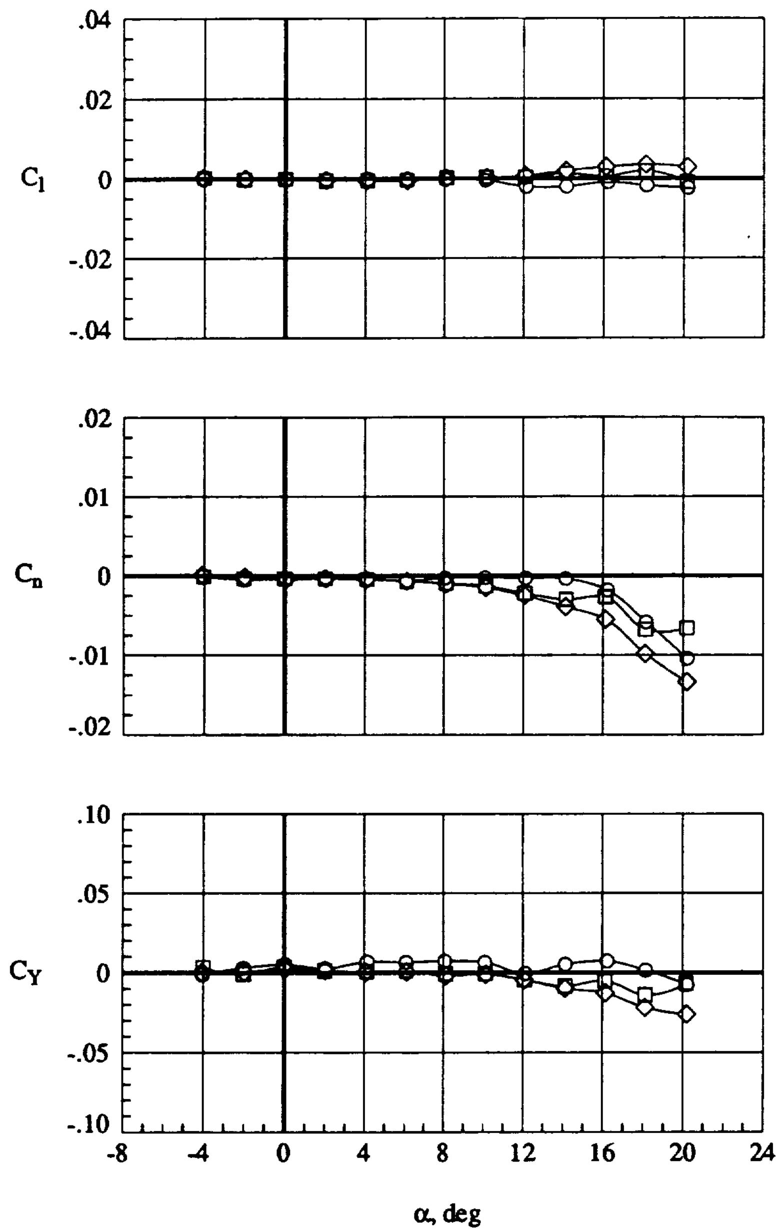

(b) Lateral aerodynamics.

Figure 18. Concluded.

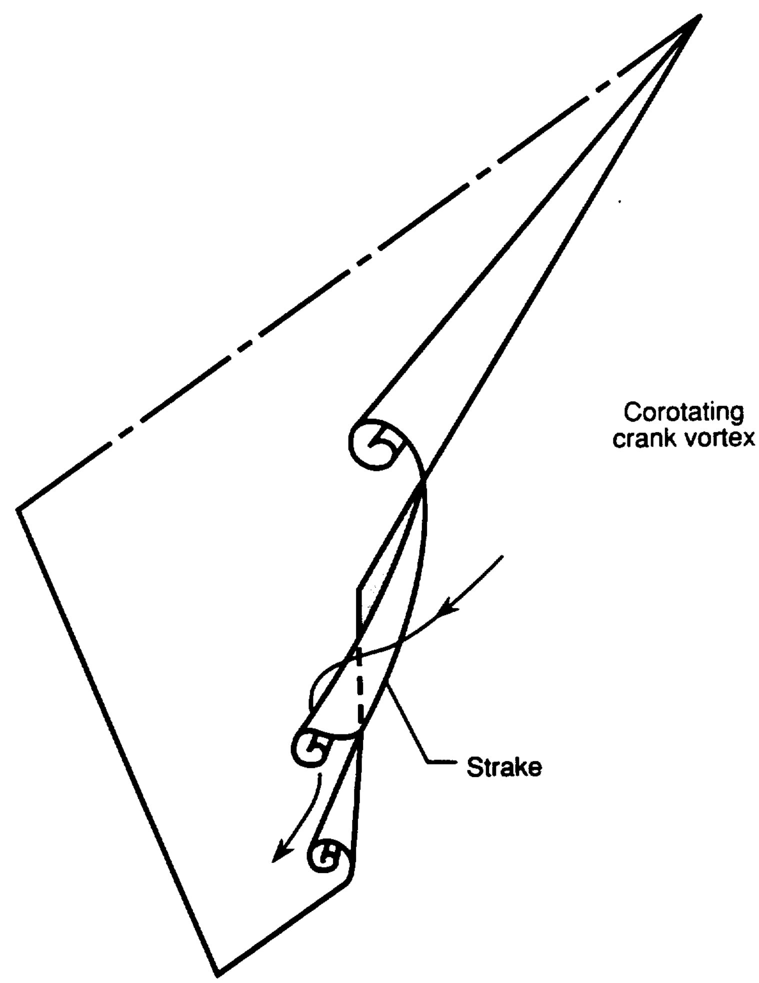

Figure 19. Hypothesized flow structure in presence of wing strake.

L-91-00512

(a) Full view.

L-91-00487

(b) Close-up view.

Figure 20. Model with wing strake.

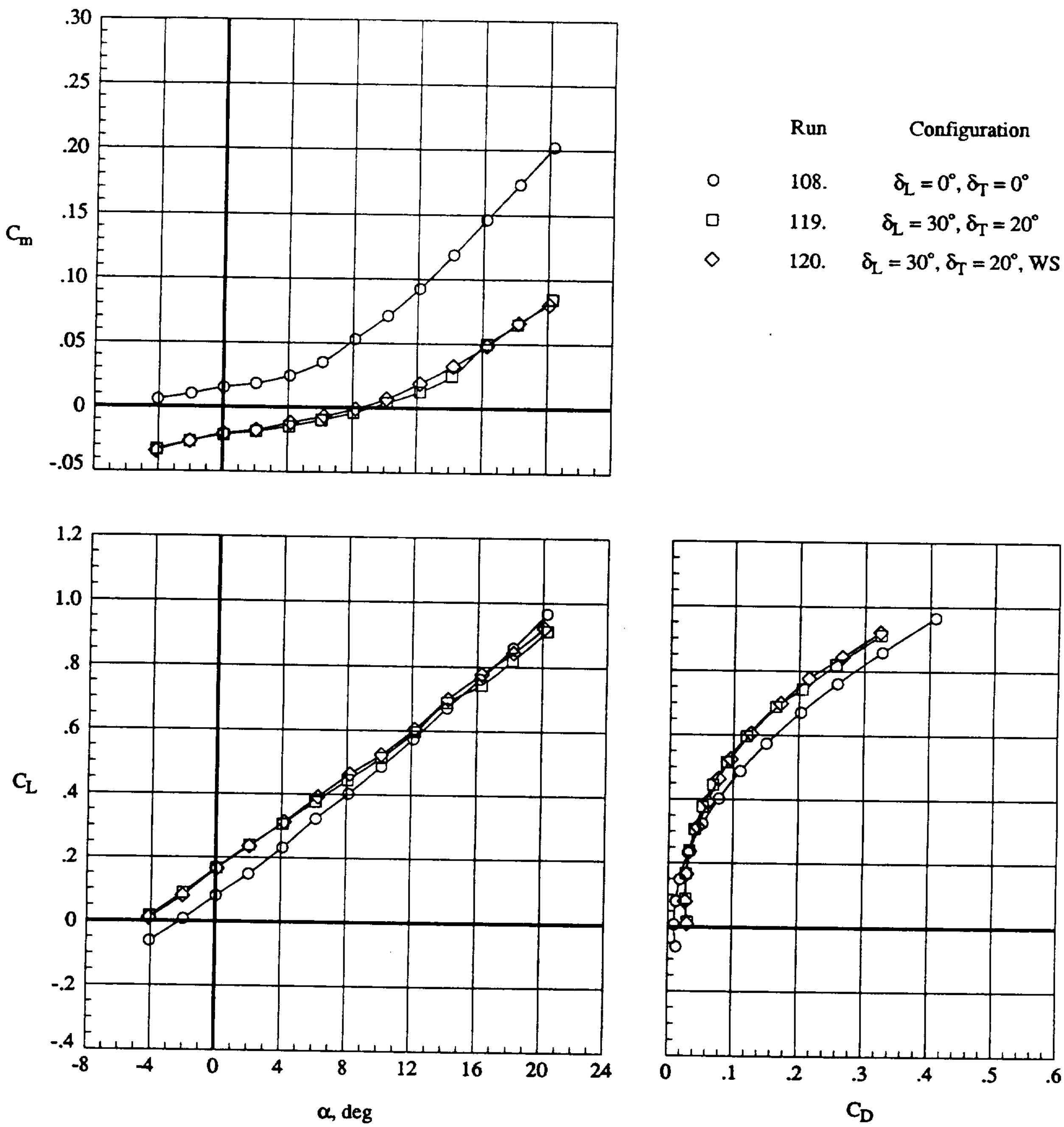

(a) Longitudinal aerodynamics.

Figure 21. Effect of wing strake located at wing crank; q = 70 psf.

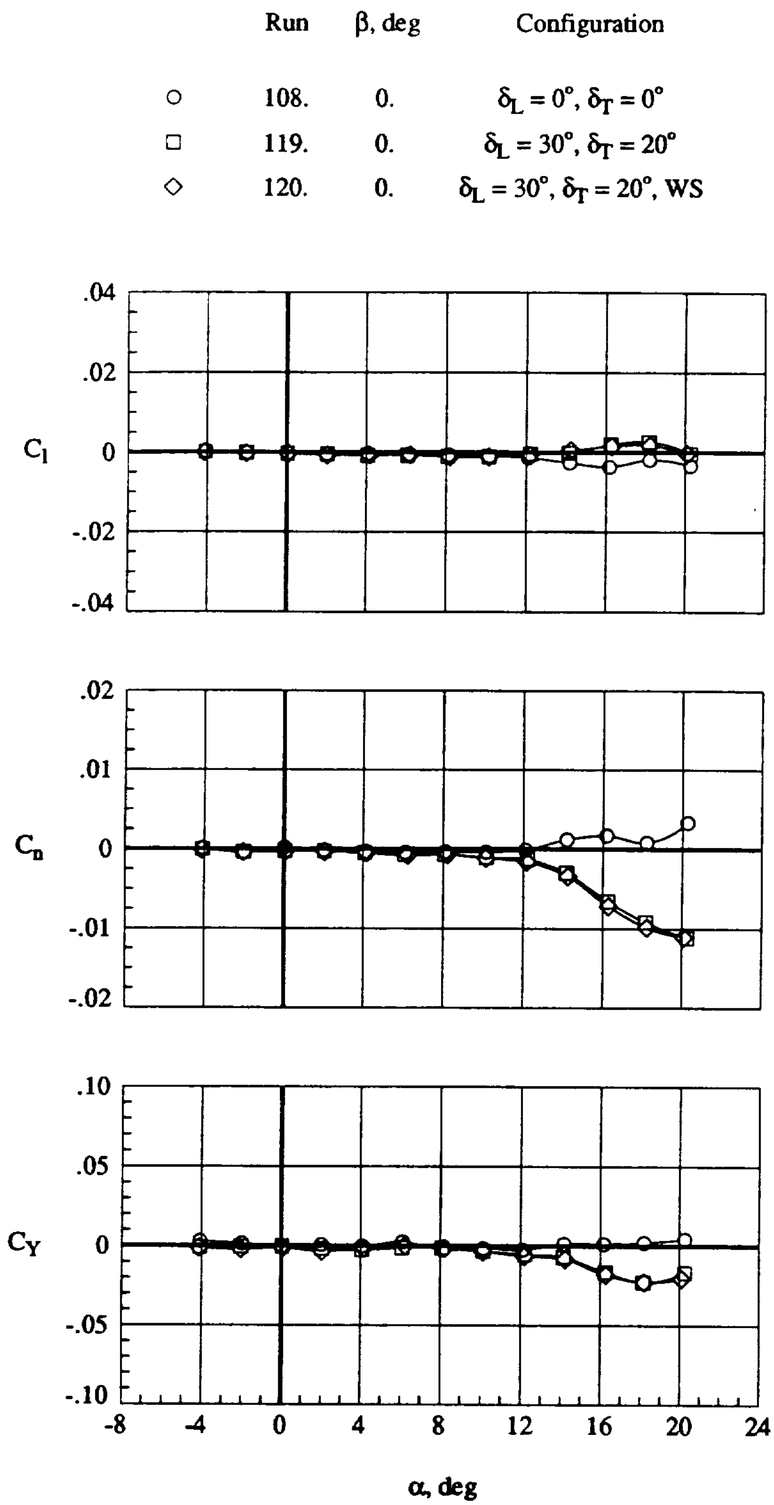

(b) Lateral aerodynamics.

Figure 21. Continued.

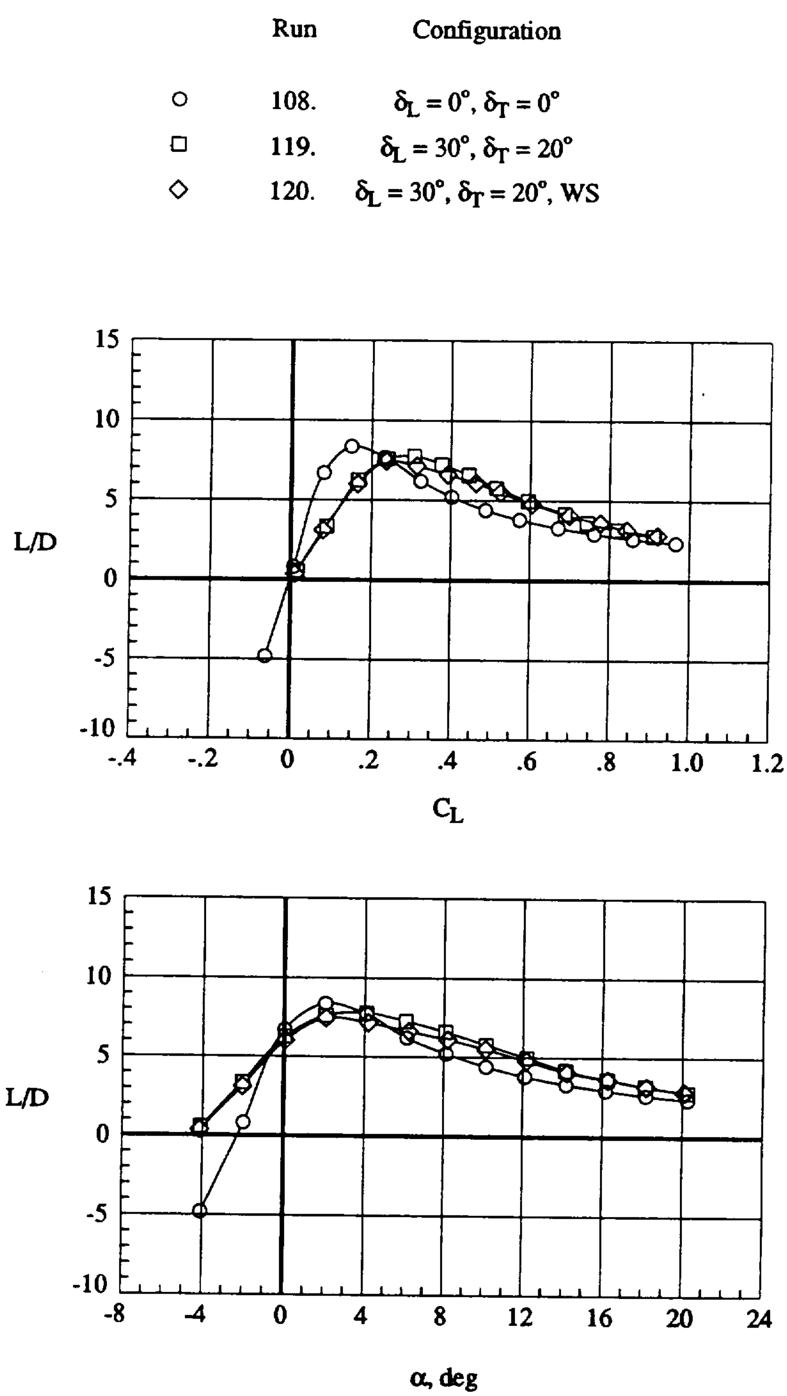

(c) Lift-drag performance.

Figure 21. Concluded.

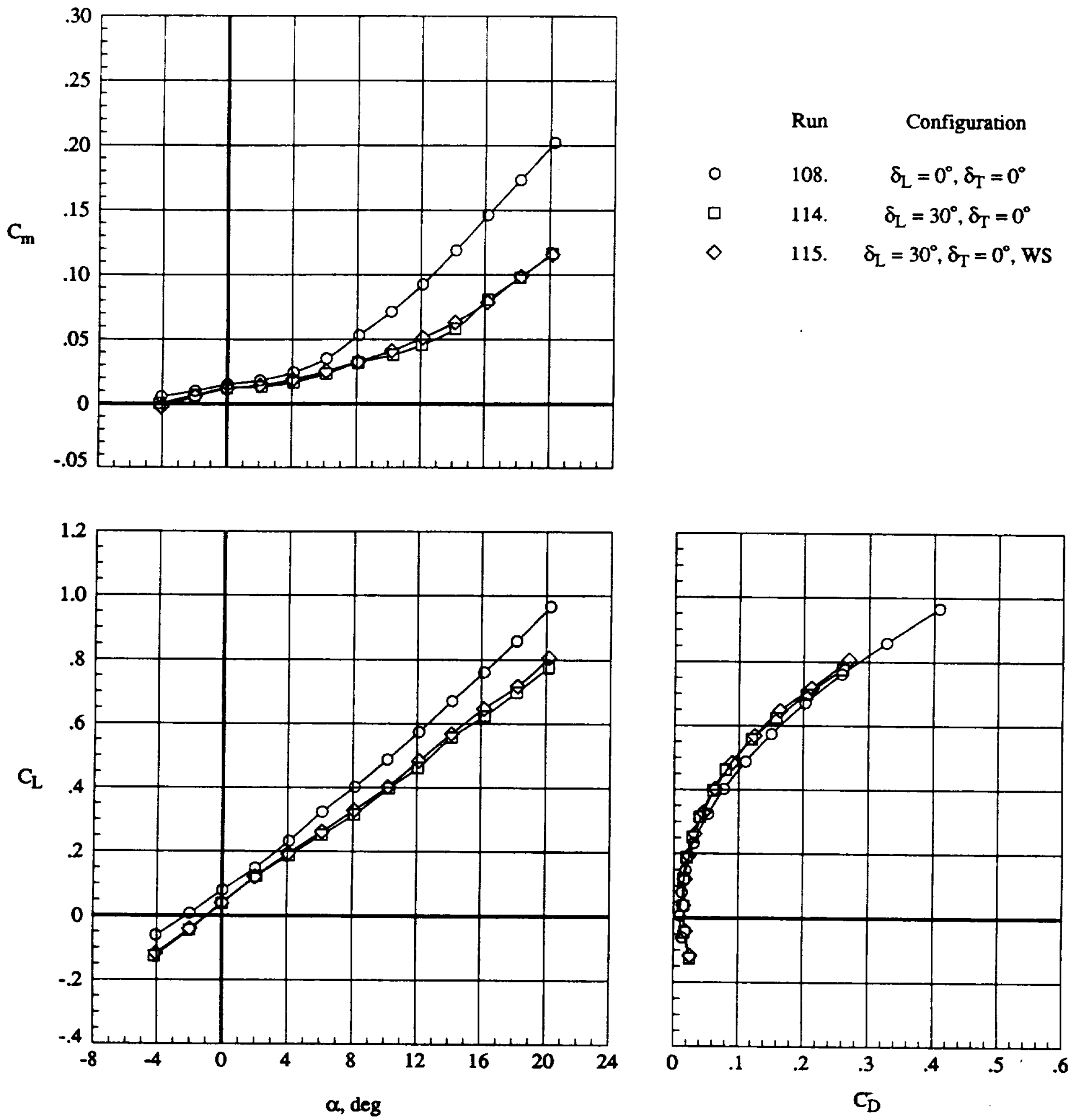

(a) Longitudinal aerodynamics.

Figure 22. Effect of wing strake located at wing crank without trailing-edge flap deflection; q = 70 psf.

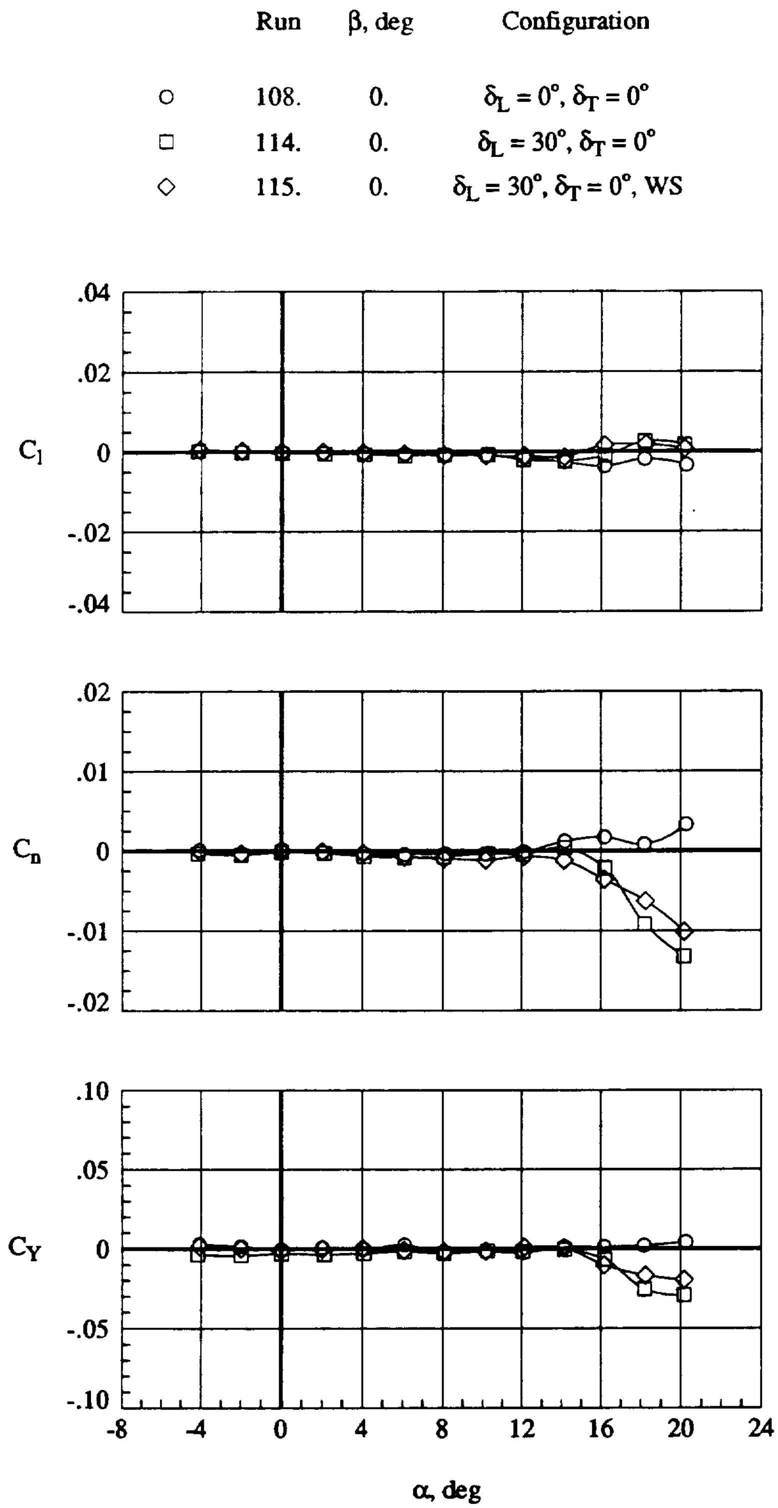

(b) Lateral aerodynamics.

Figure 22. Continued.

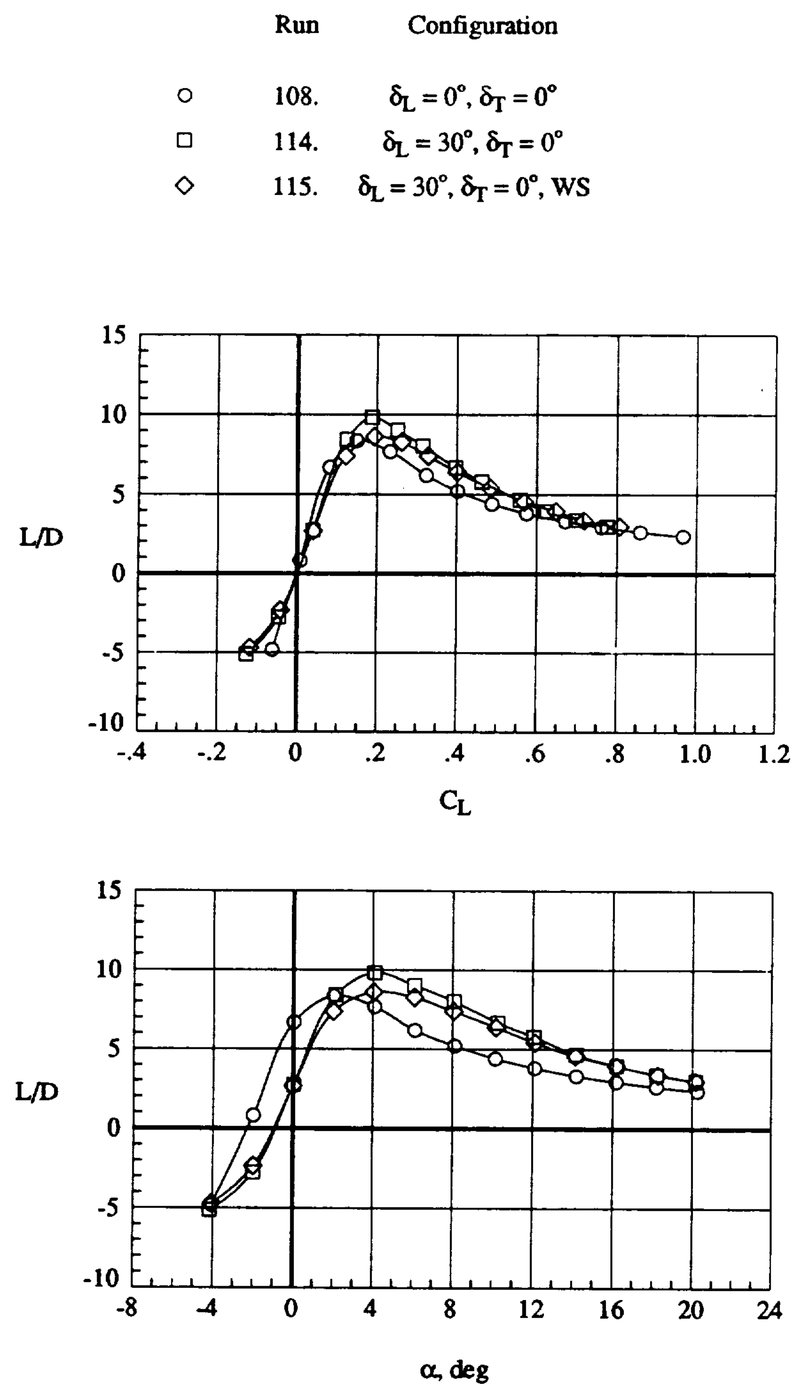

(c) Lift-drag performance.

Figure 22. Concluded.

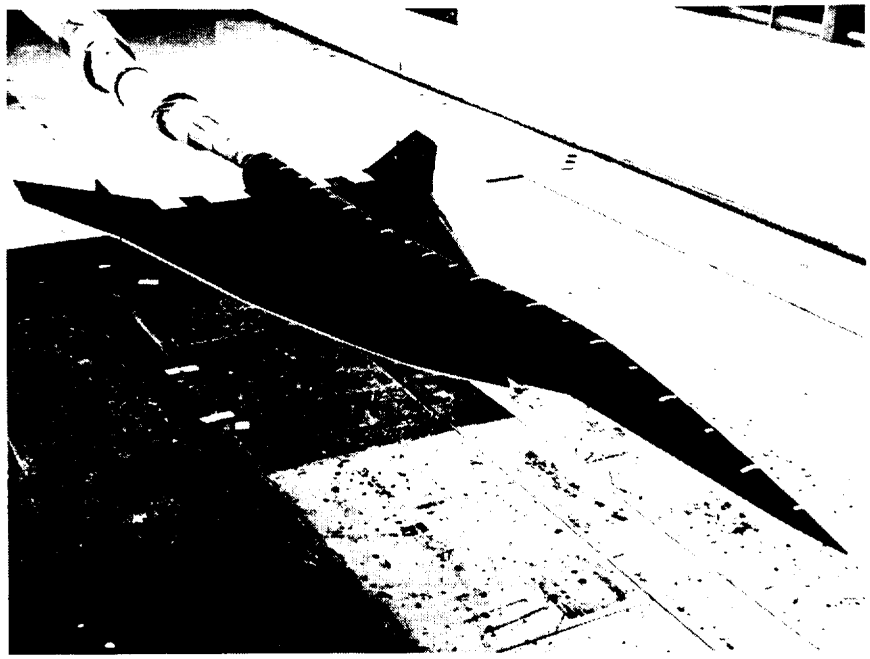

L-91-00496

(a) Full view.

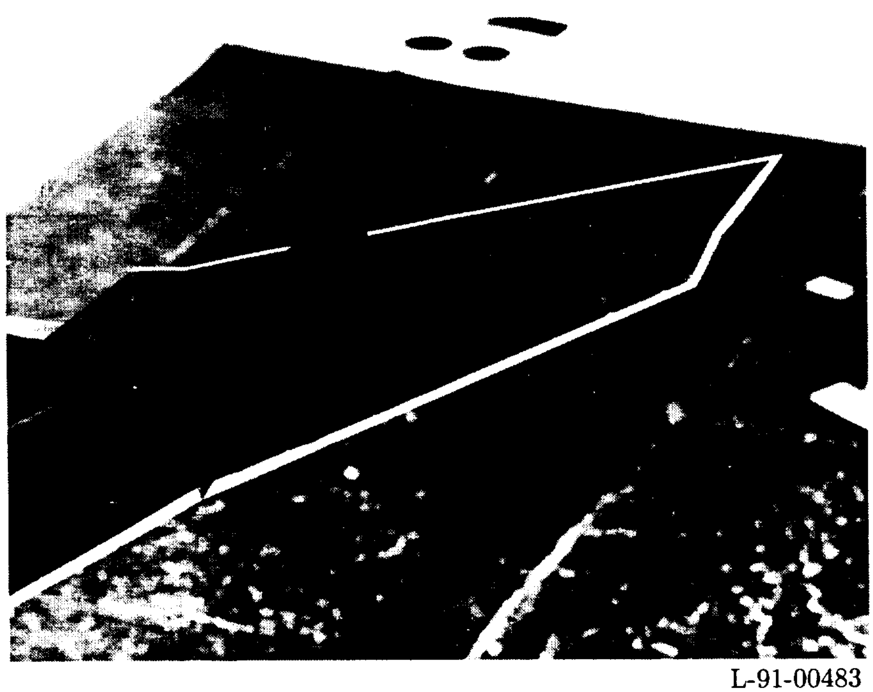

L-91-00483

(b) Close-up view.

Figure 23. Model with upper surface wing fence.

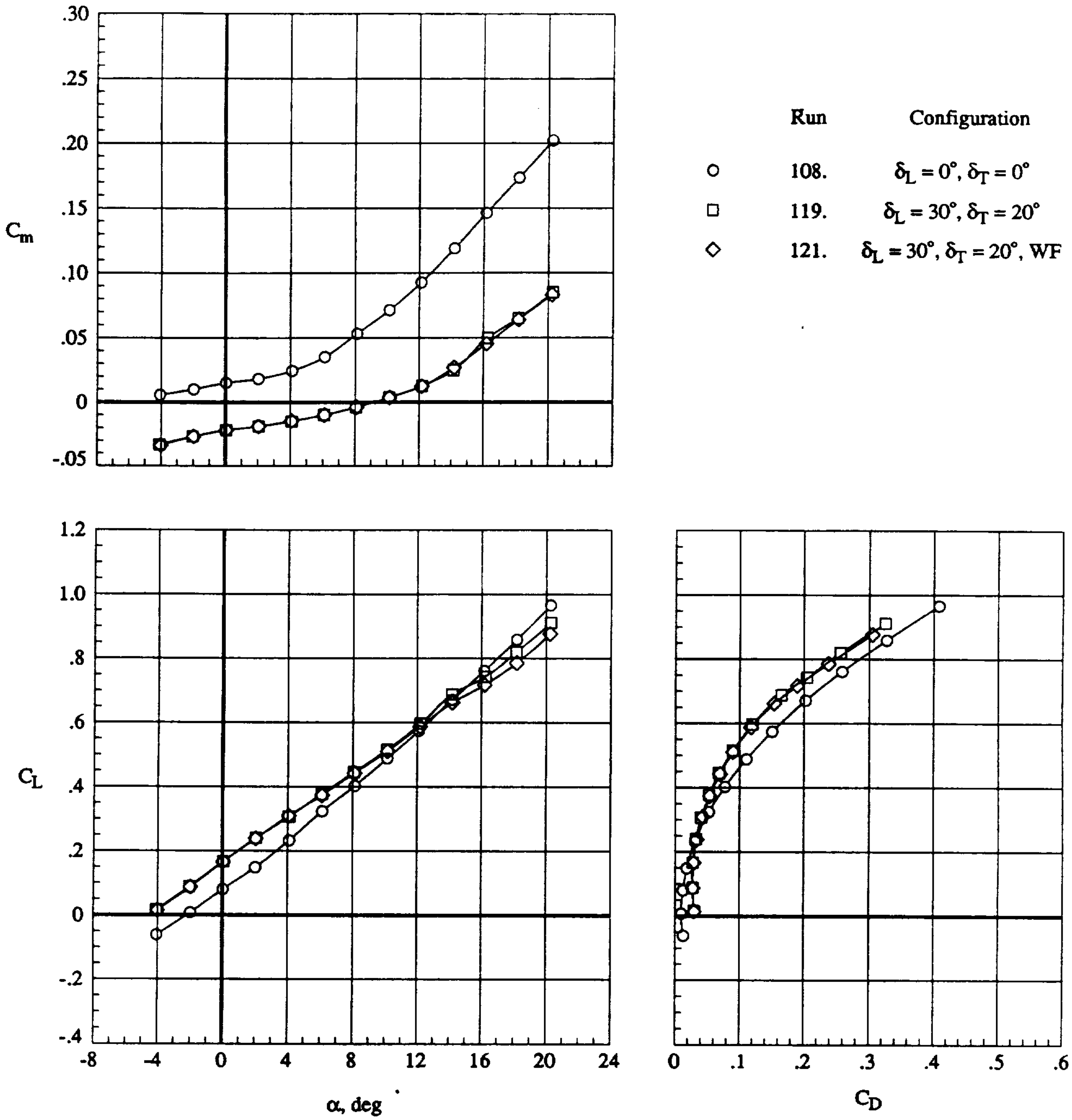

(a) Longitudinal aerodynamics.

Figure 24. Effect of wing fence located at wing crank; q = 70 psf.

	Run	β, deg	Configuration
○	108.	0.	$\delta_L = 0°, \delta_T = 0°$
□	119.	0.	$\delta_L = 30°, \delta_T = 20°$
◇	121.	0.	$\delta_L = 30°, \delta_T = 20°$, WF

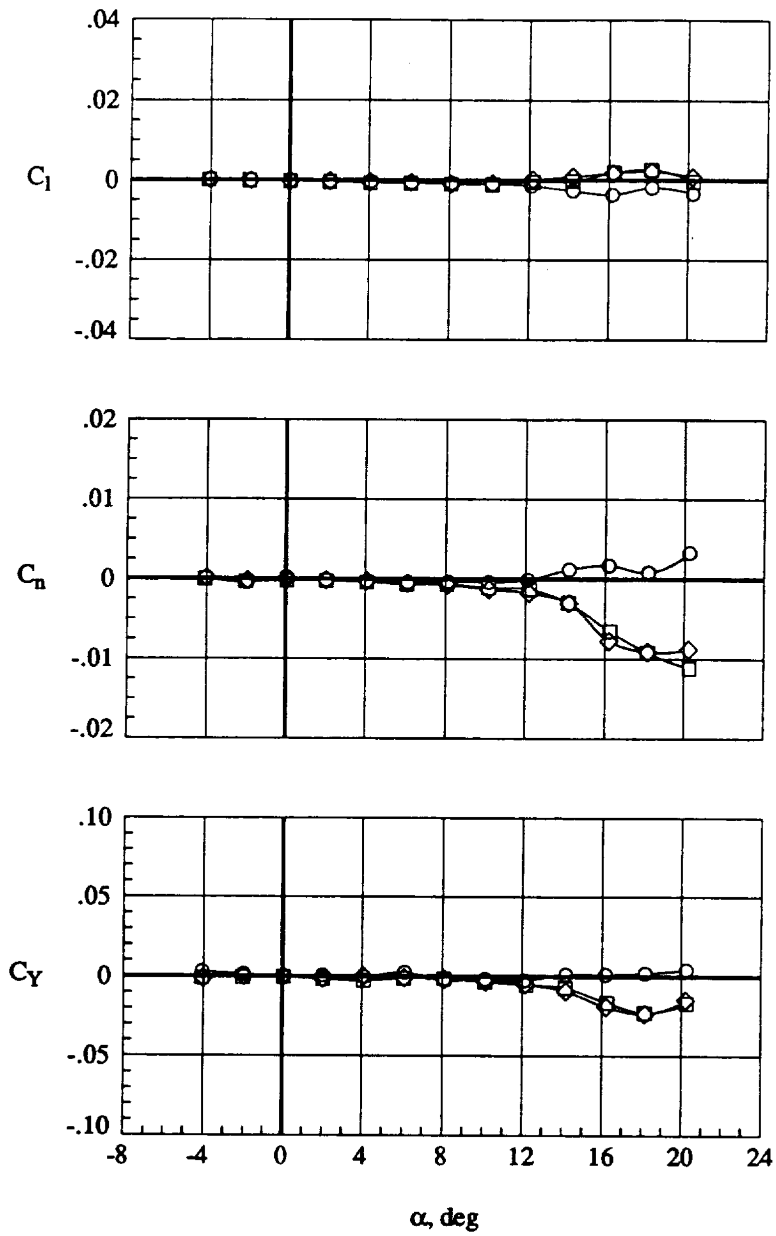

(b) Lateral aerodynamics.

Figure 24. Continued.

	Run	Configuration
○	108.	$\delta_L = 0°, \delta_T = 0°$
□	119.	$\delta_L = 30°, \delta_T = 20°$
◇	121.	$\delta_L = 30°, \delta_T = 20°$, WF

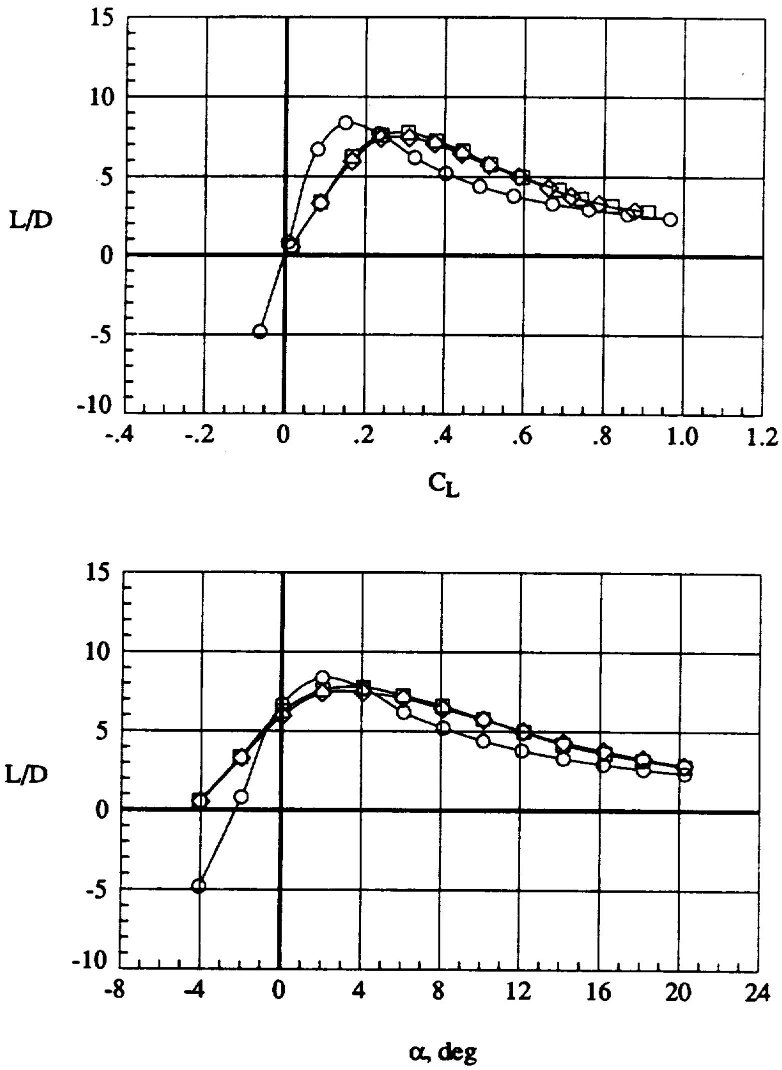

(c) Lift-drag performance.

Figure 24. Concluded.

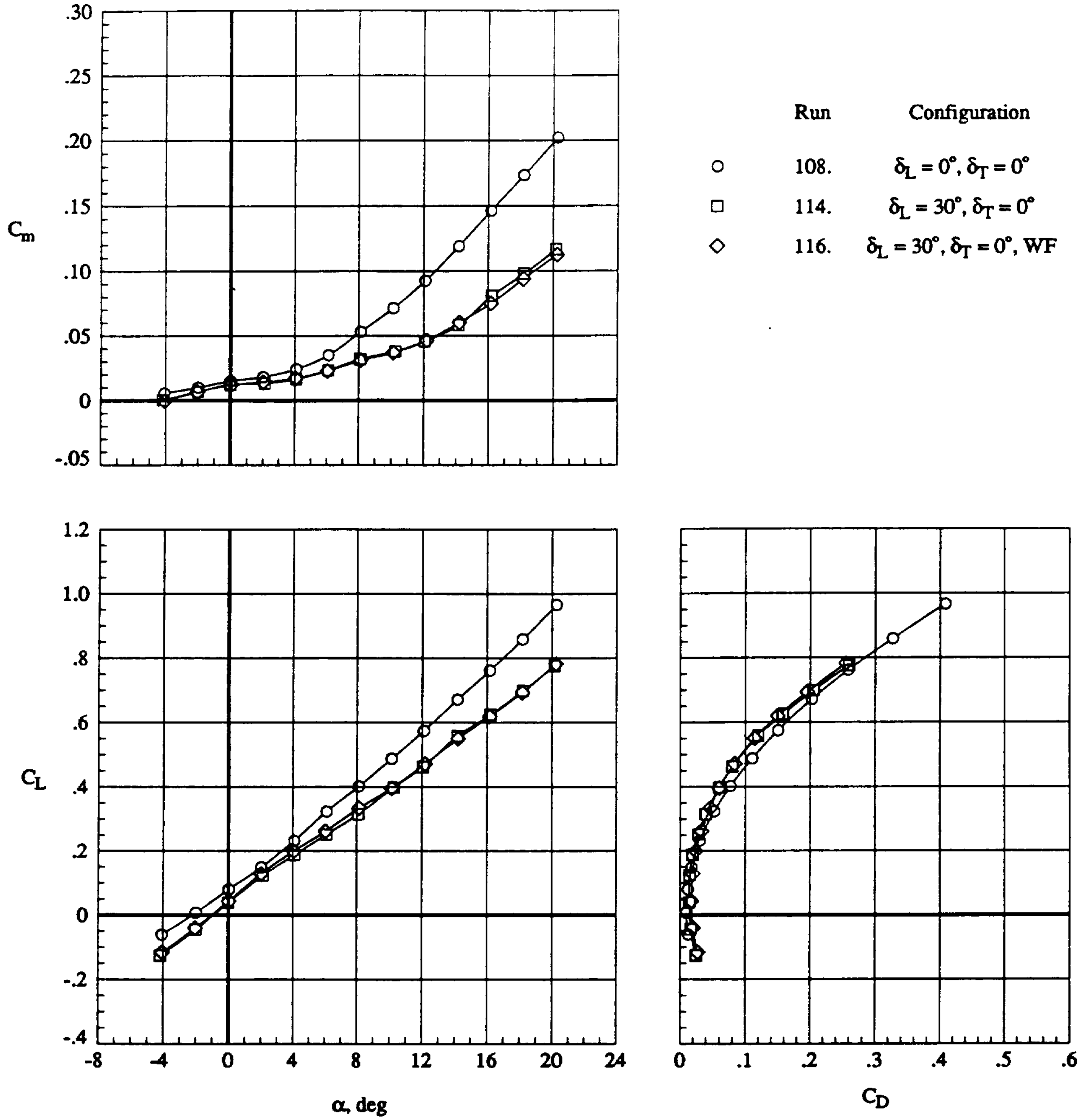

(a) Longitudinal aerodynamics.

Figure 25. Effect of wing fence located at wing crank without trailing-edge flap deflection; q = 70 psf.

	Run	β, deg	Configuration
○	108.	0.	$\delta_L = 0^\circ, \delta_T = 0^\circ$
□	114.	0.	$\delta_L = 30^\circ, \delta_T = 0^\circ$
◇	116.	0.	$\delta_L = 30^\circ, \delta_T = 0^\circ$, WF

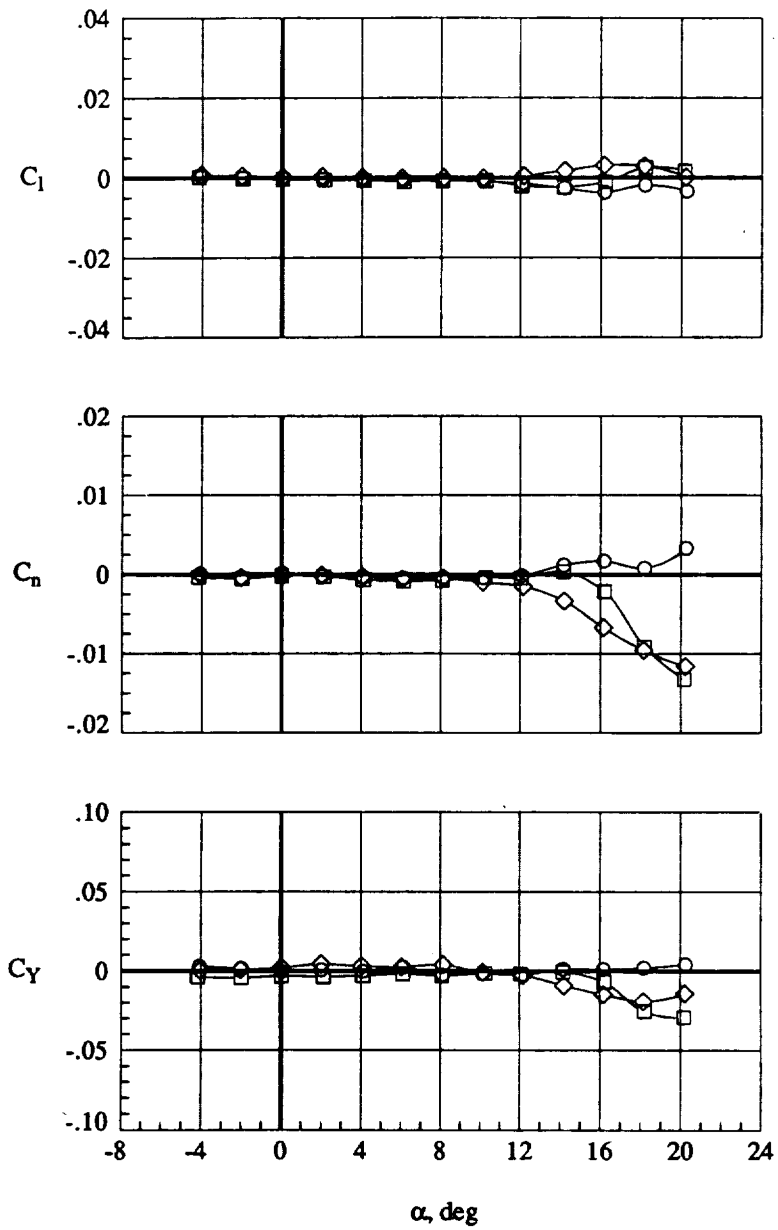

(b) Lateral aerodynamics.

Figure 25. Continued.

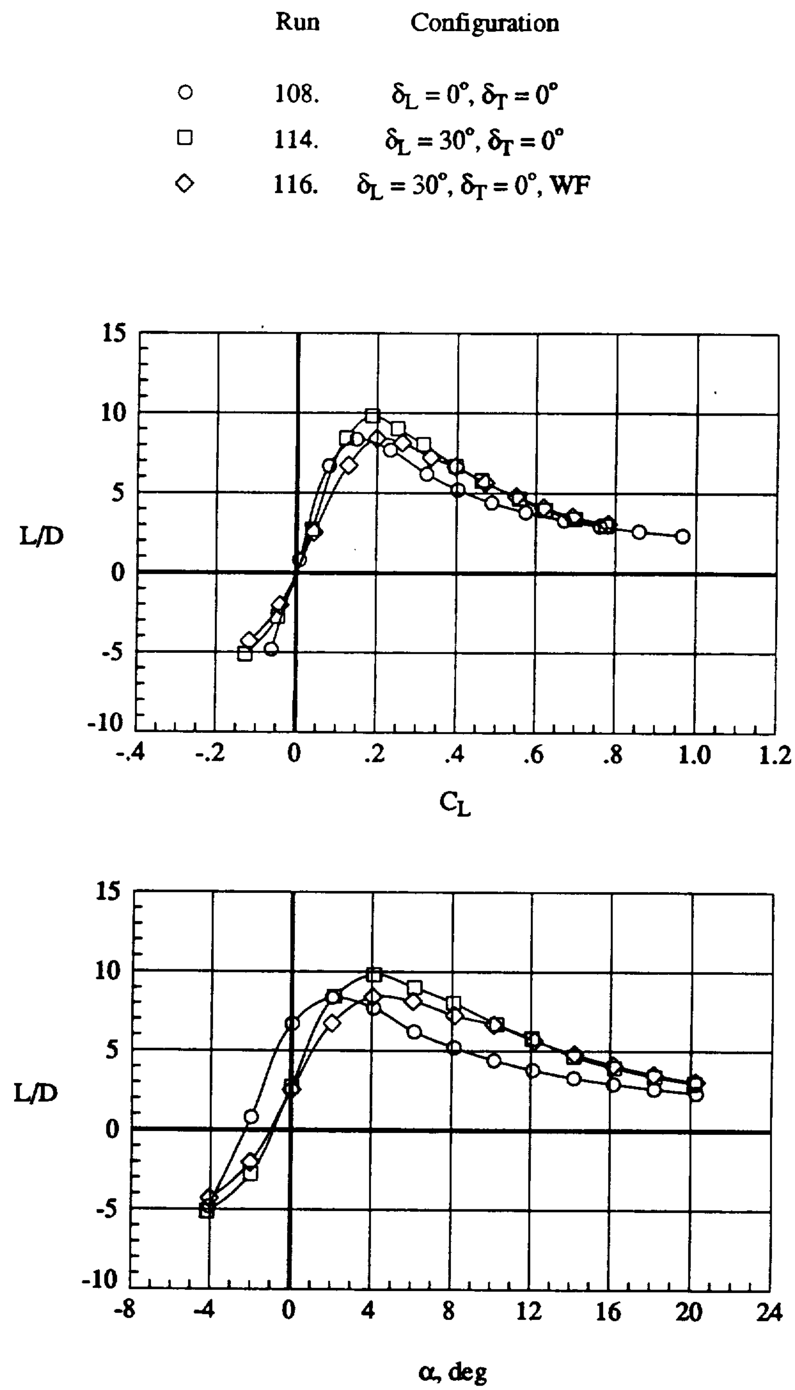

(c) Lift-drag performance.

Figure 25. Concluded.

L-91-00514

(a) Full view.

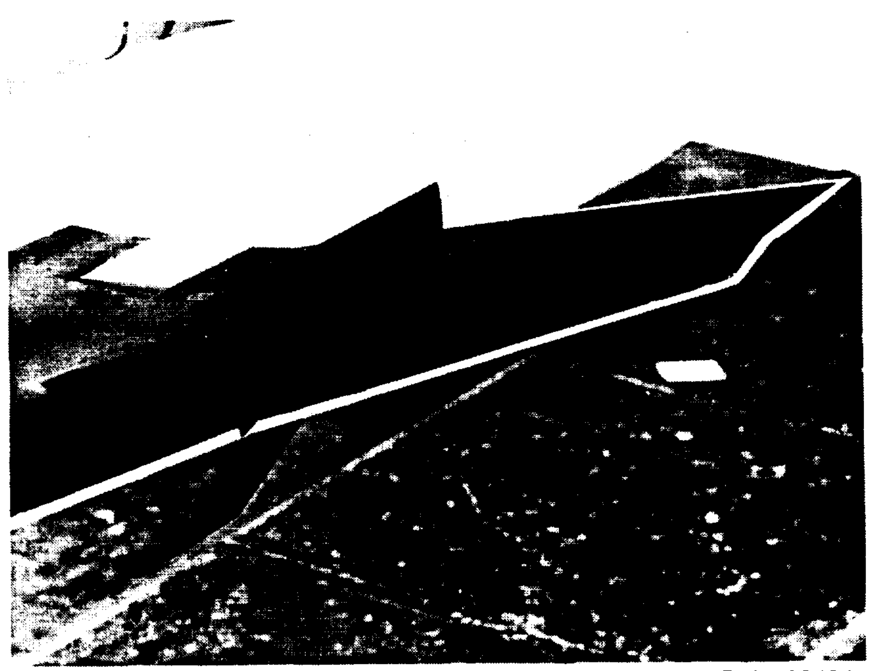

L-91-00484

(b) Close-up view.

Figure 26. Model with wing fence and pylon vortex generator located at crank.

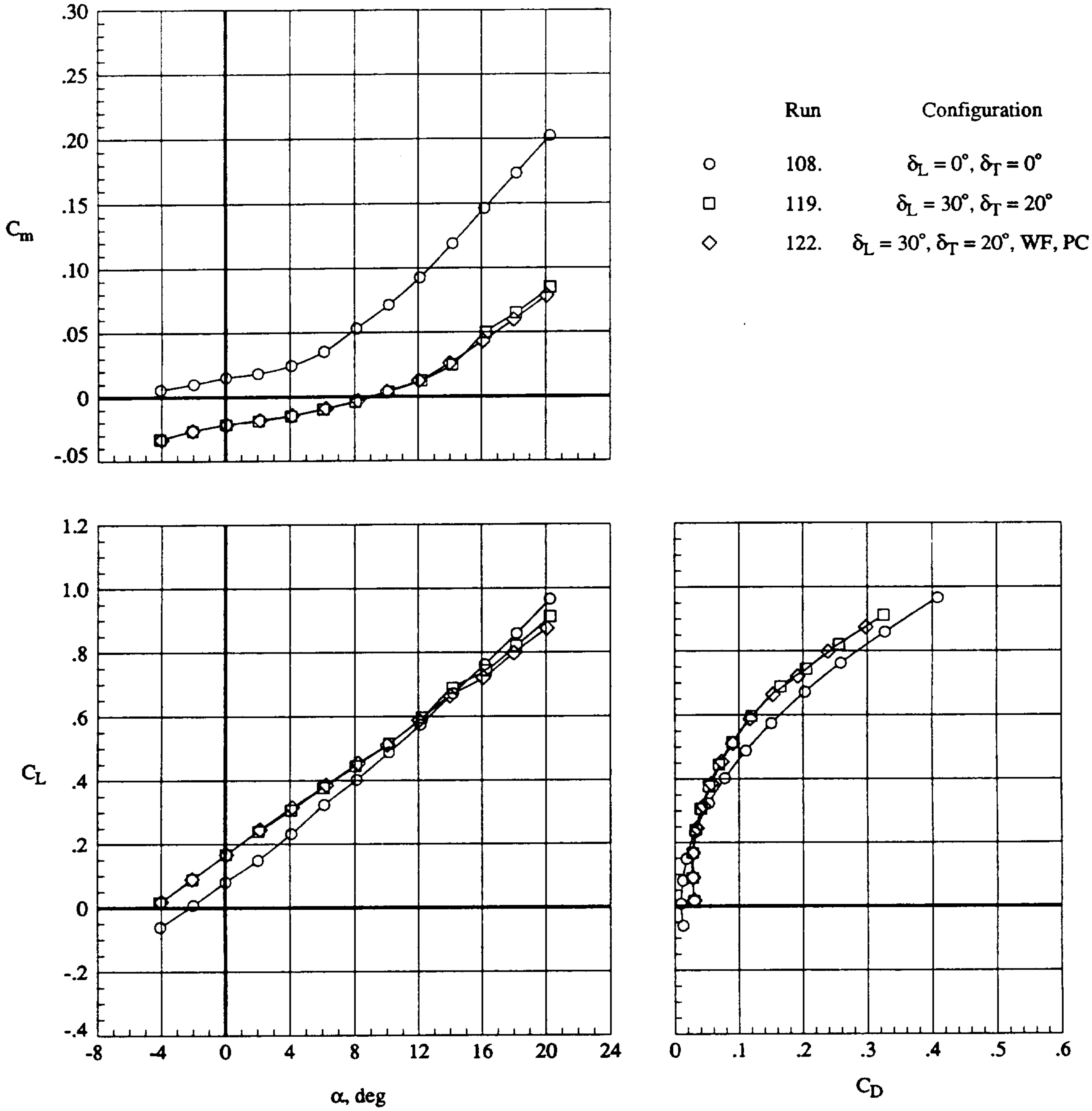

(a) Longitudinal aerodynamics.

Figure 27. Effect of wing fence and pylon vortex generator located at wing crank; q = 70 psf.

	Run	β, deg	Configuration
○	108.	0.	$\delta_L = 0°, \delta_T = 0°$
□	119.	0.	$\delta_L = 30°, \delta_T = 20°$
◇	122.	0.	$\delta_L = 30°, \delta_T = 20°$, WF, PC

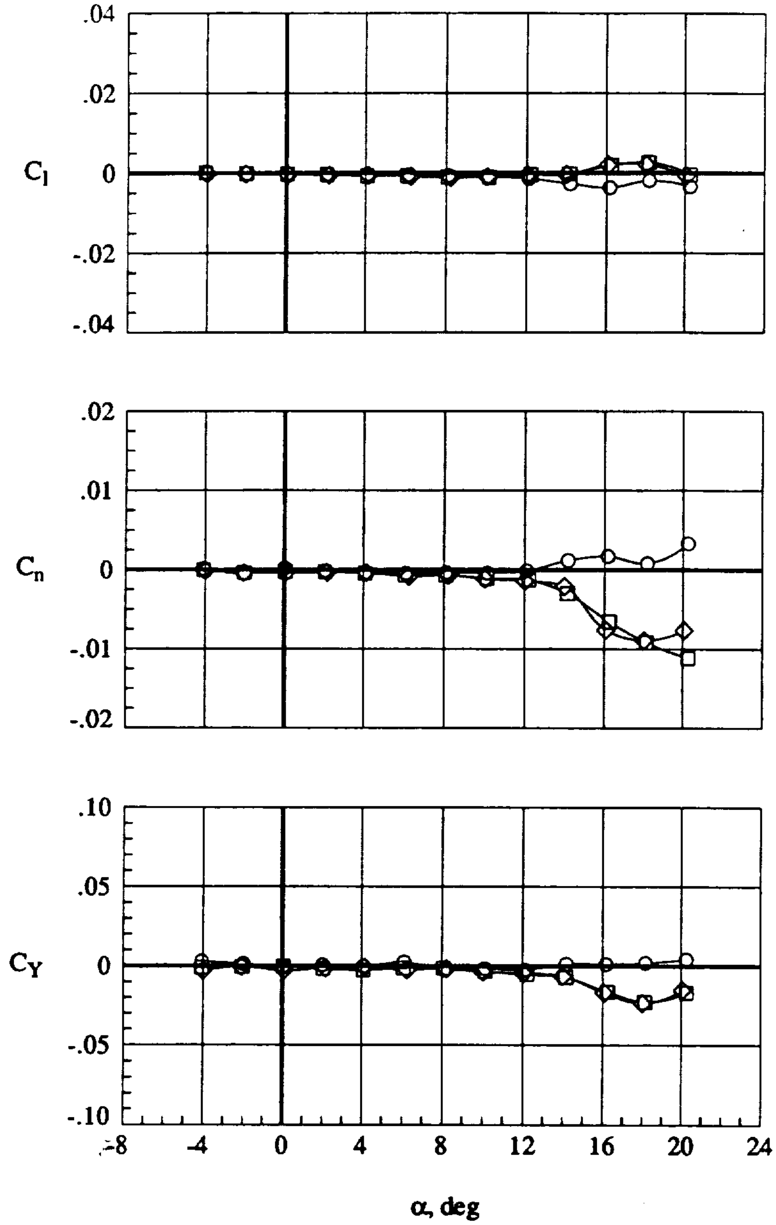

(b) Lateral aerodynamics.

Figure 27. Continued.

	Run	Configuration
○	108.	$\delta_L = 0°$, $\delta_T = 0°$
□	119.	$\delta_L = 30°$, $\delta_T = 20°$
◇	122.	$\delta_L = 30°$, $\delta_T = 20°$, WF, PC

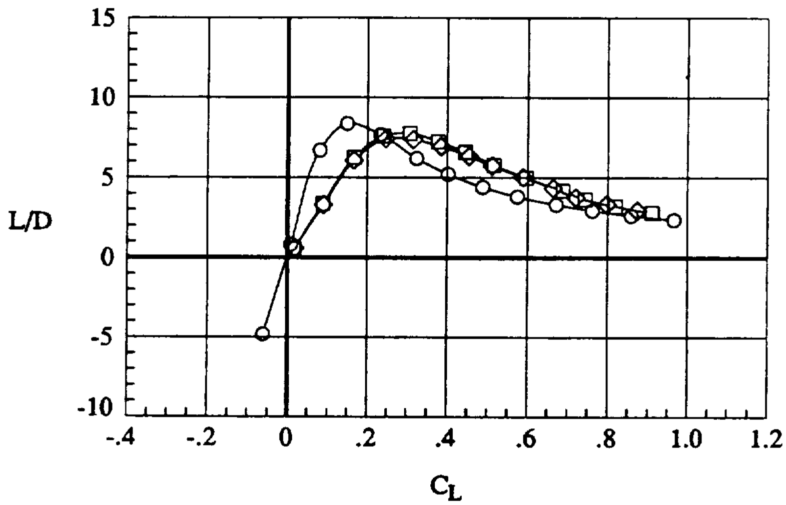

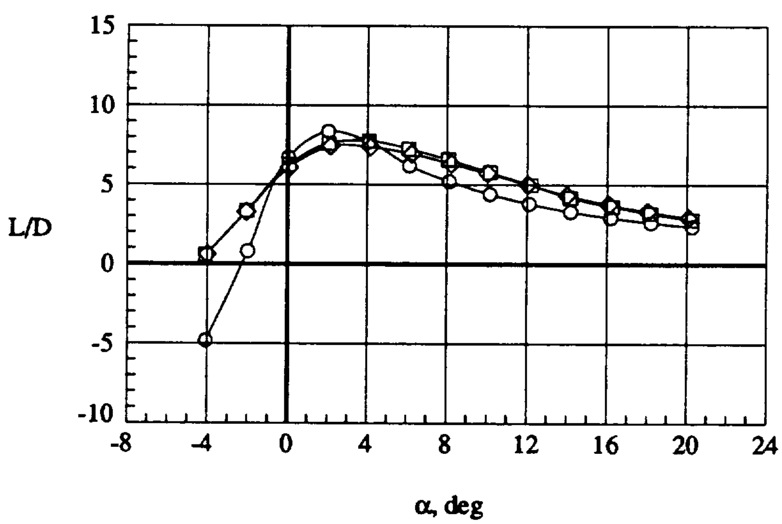

(c) Lift-drag performance.

Figure 27. Concluded.

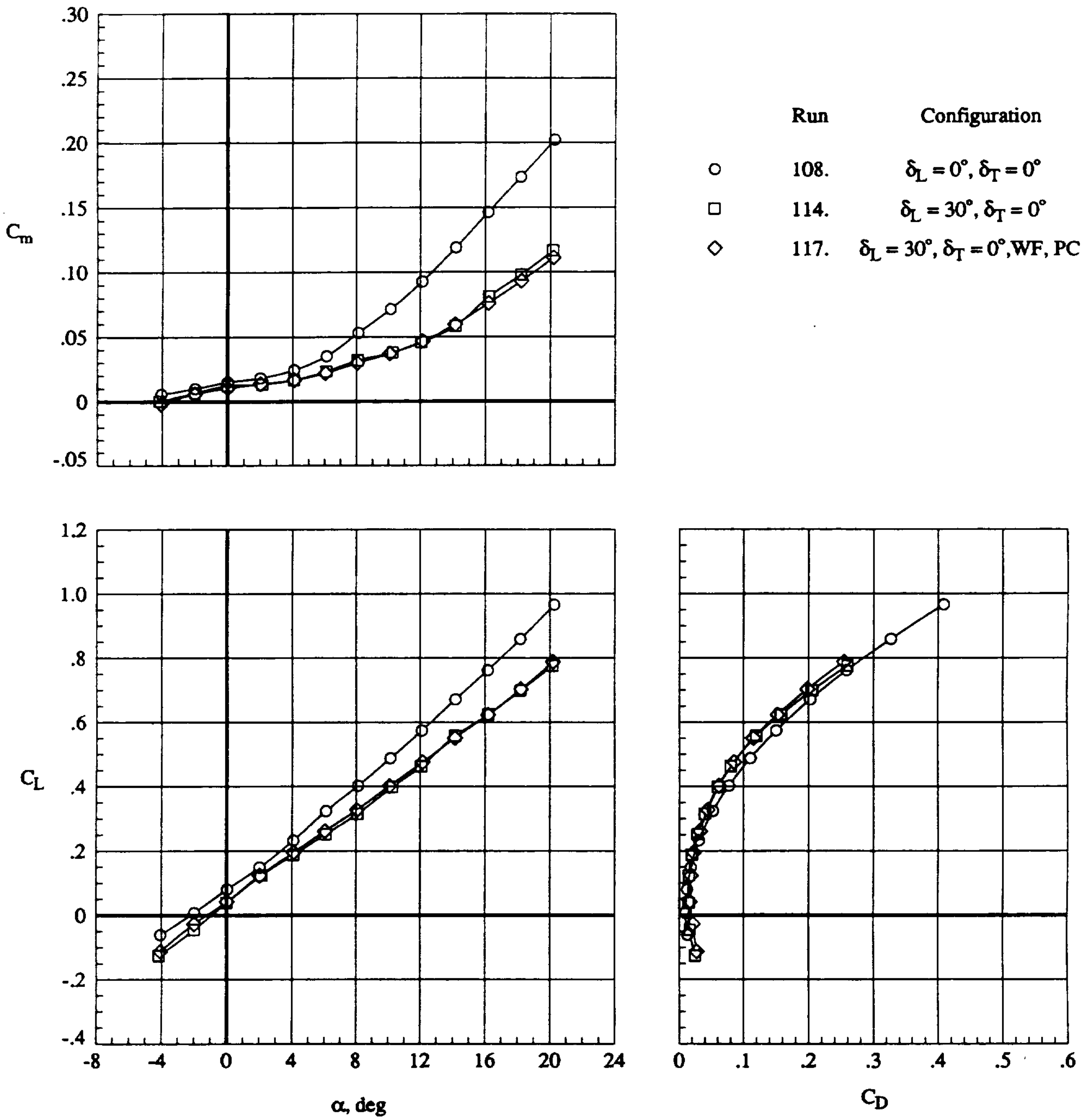

(a) Longitudinal aerodynamics.

Figure 28. Effect of wing fence and pylon vortex generator located at wing crank without trailing-edge flap deflection; q = 70 psf.

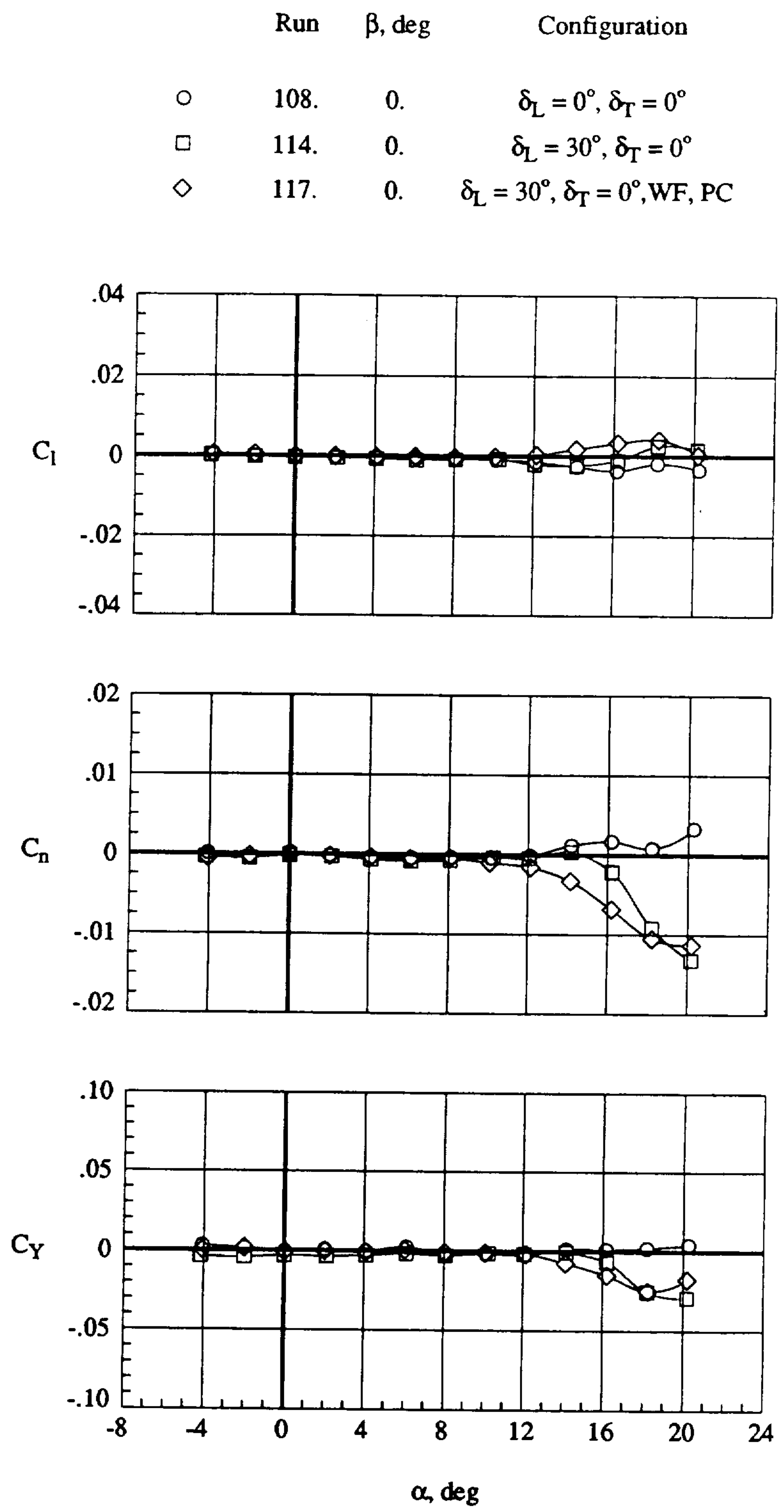

(b) Lateral aerodynamics.

Figure 28. Continued.

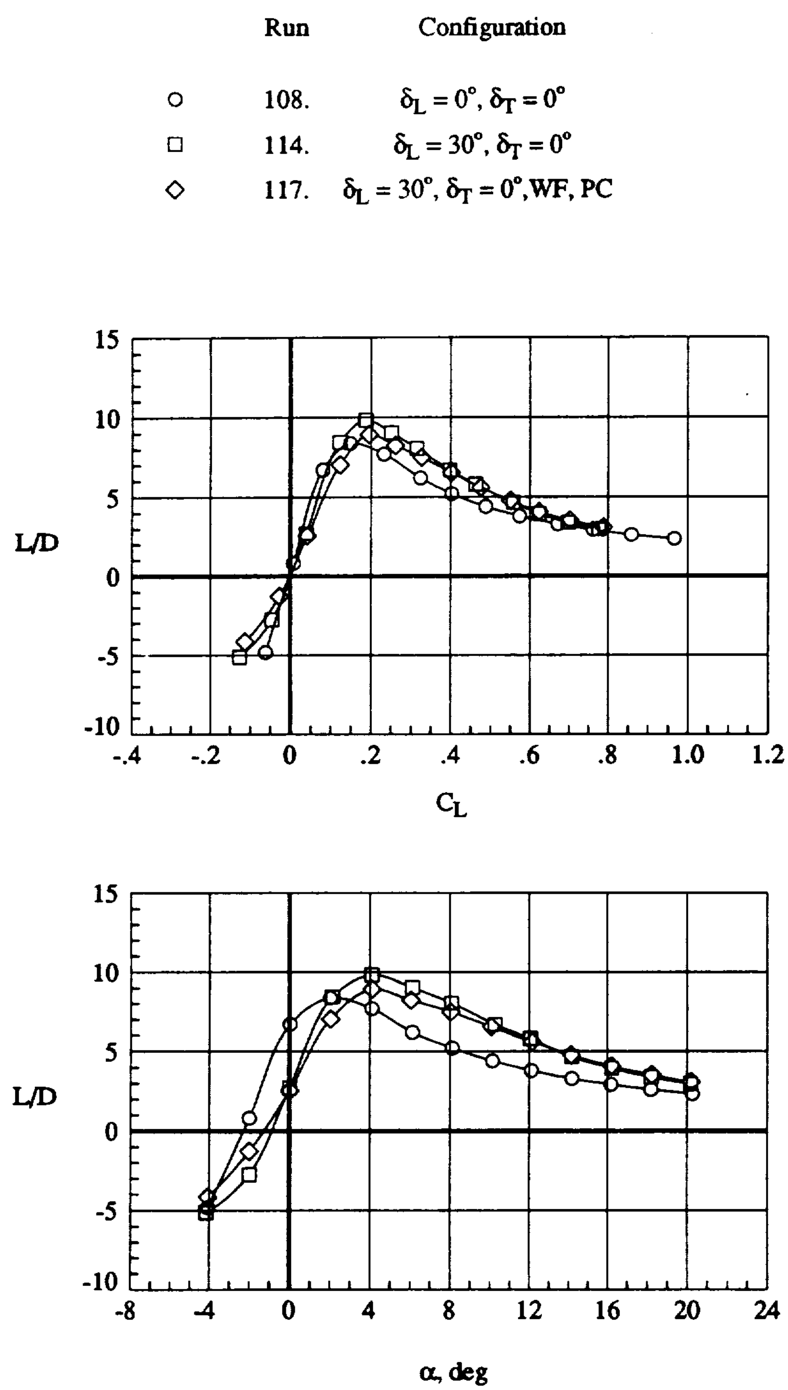

(c) Lift-drag performance.

Figure 28. Concluded.

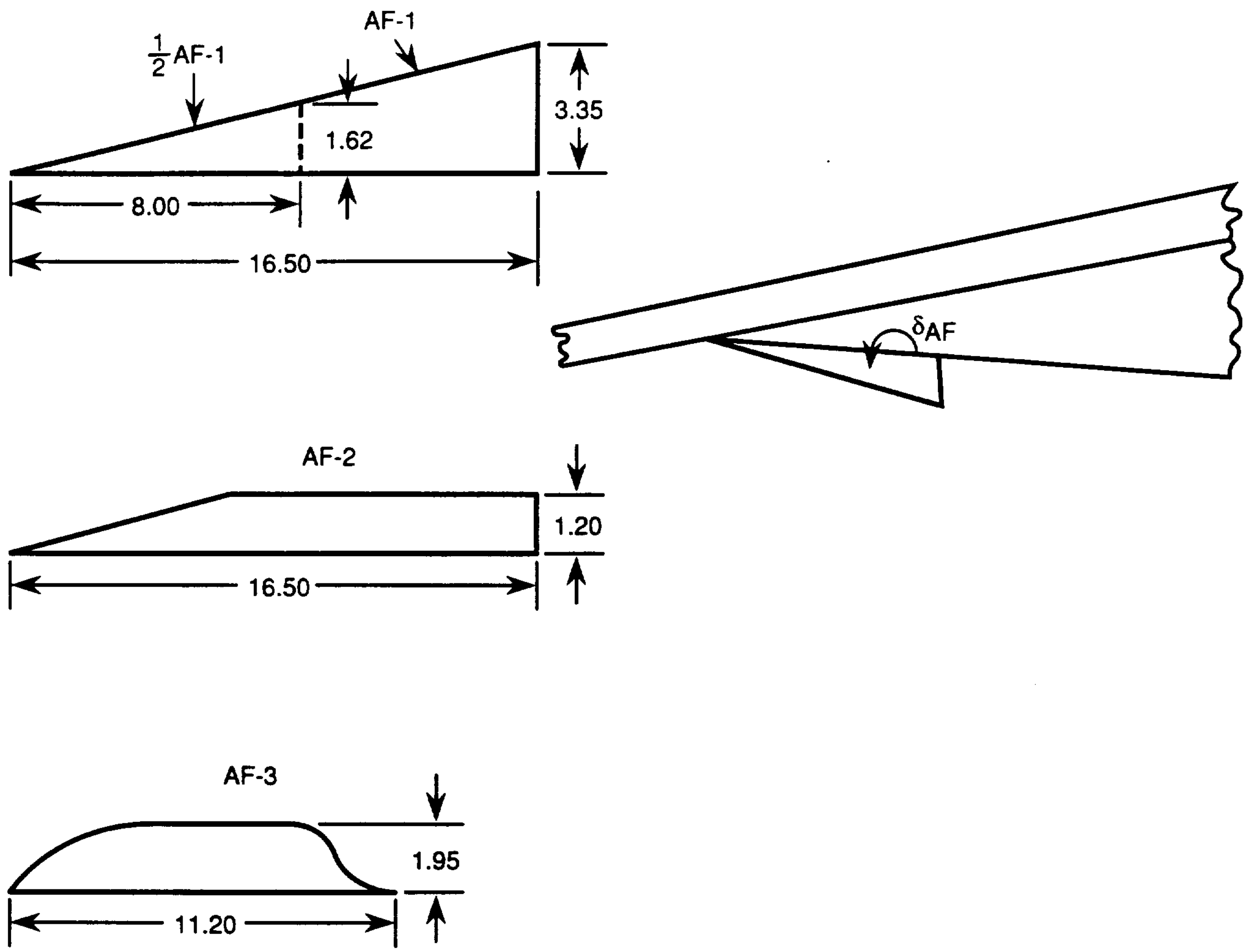

Figure 29. Geometric characteristics of apex flaps tested during this investigation. Linear dimensions are in inches.

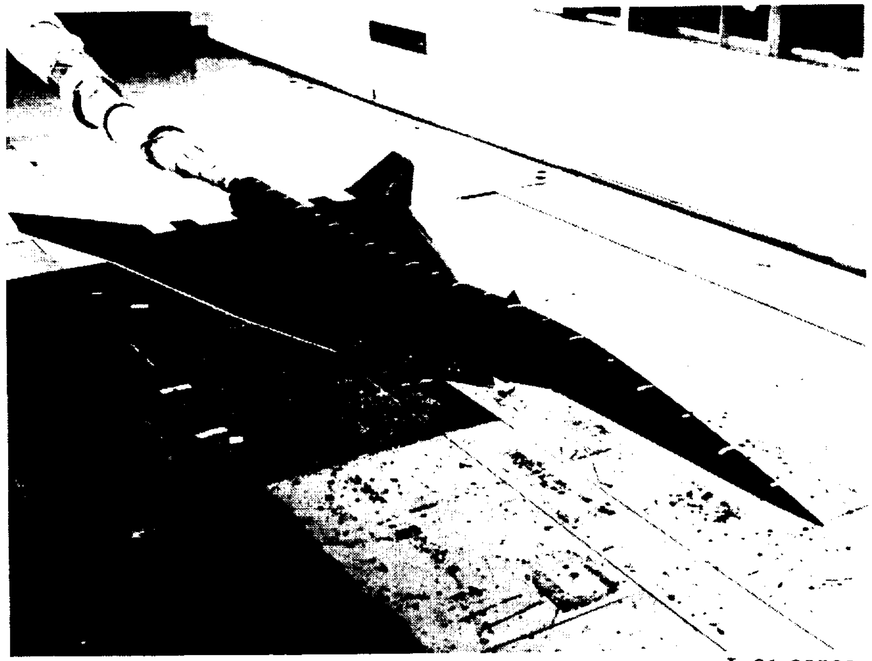

L-91-00509

(a) Full view.

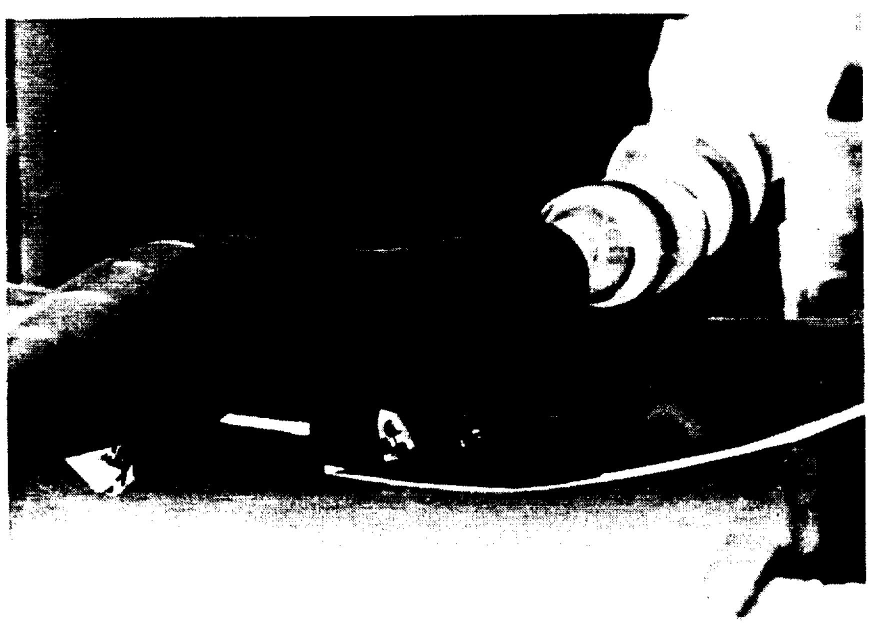

L-91-00492

(b) Close-up view.

Figure 30. Model with apex flap 1.

L-91-00508

(a) Full view.

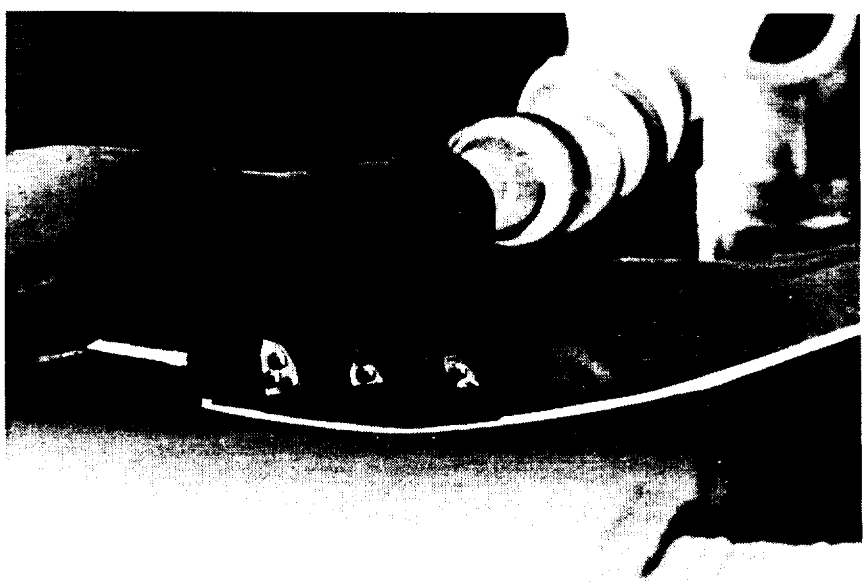

L-91-00476

(b) Close-up view.

Figure 31. Model with apex flap 2.

L-91-00499

(a) Full view.

L-91-00480

(b) Close-up view.

Figure 32. Model with apex flap 3.

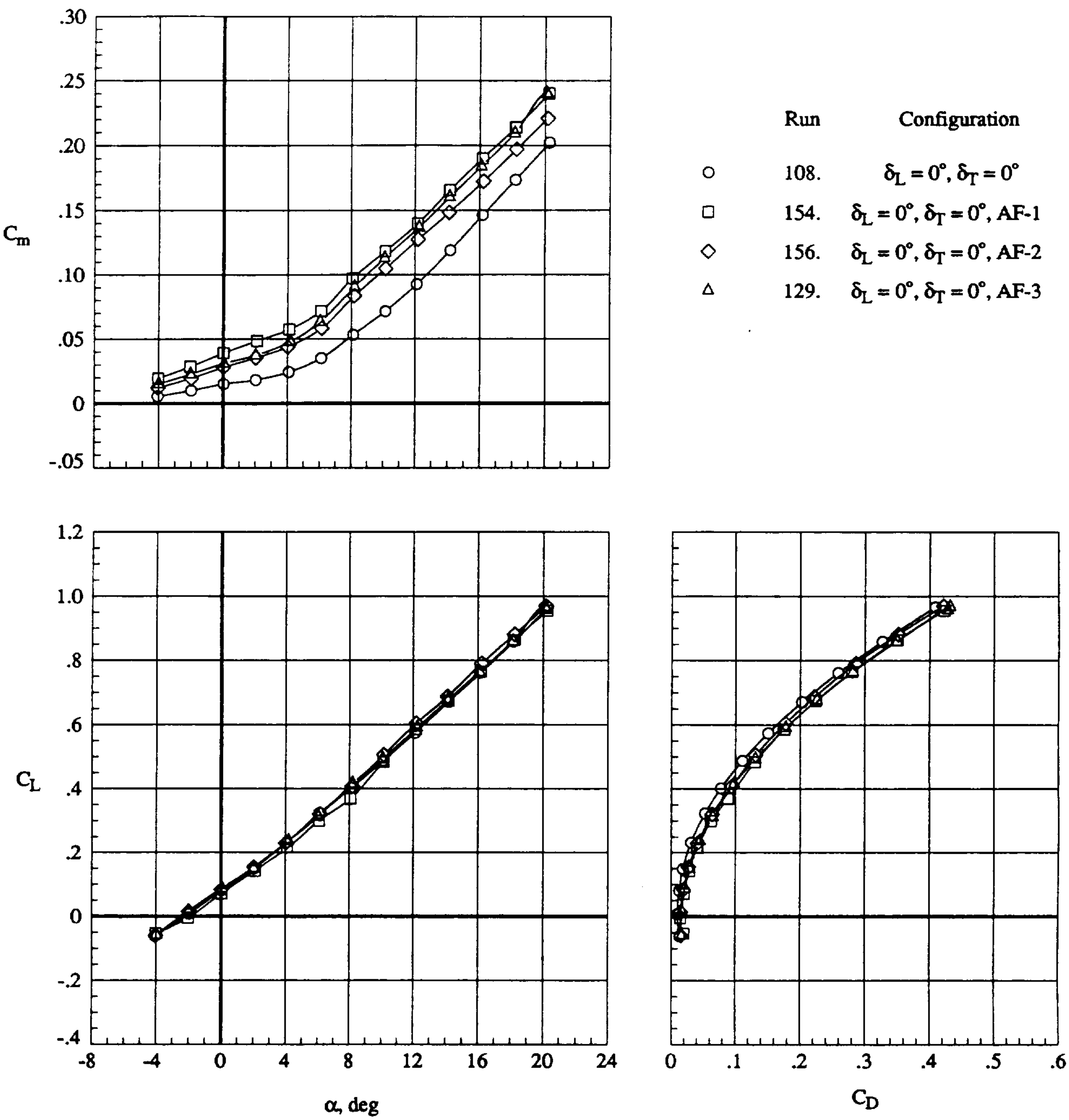

(a) Longitudinal aerodynamics.

Figure 33. Effect of 90° apex flaps at q = 70 psf.

	Run	β, deg	Configuration
○	108.	0.	$\delta_L = 0°, \delta_T = 0°$
□	154.	0.	$\delta_L = 0°, \delta_T = 0°$, AF-1
◇	156.	0.	$\delta_L = 0°, \delta_T = 0°$, AF-2
△	129.	0.	$\delta_L = 0°, \delta_T = 0°$, AF-3

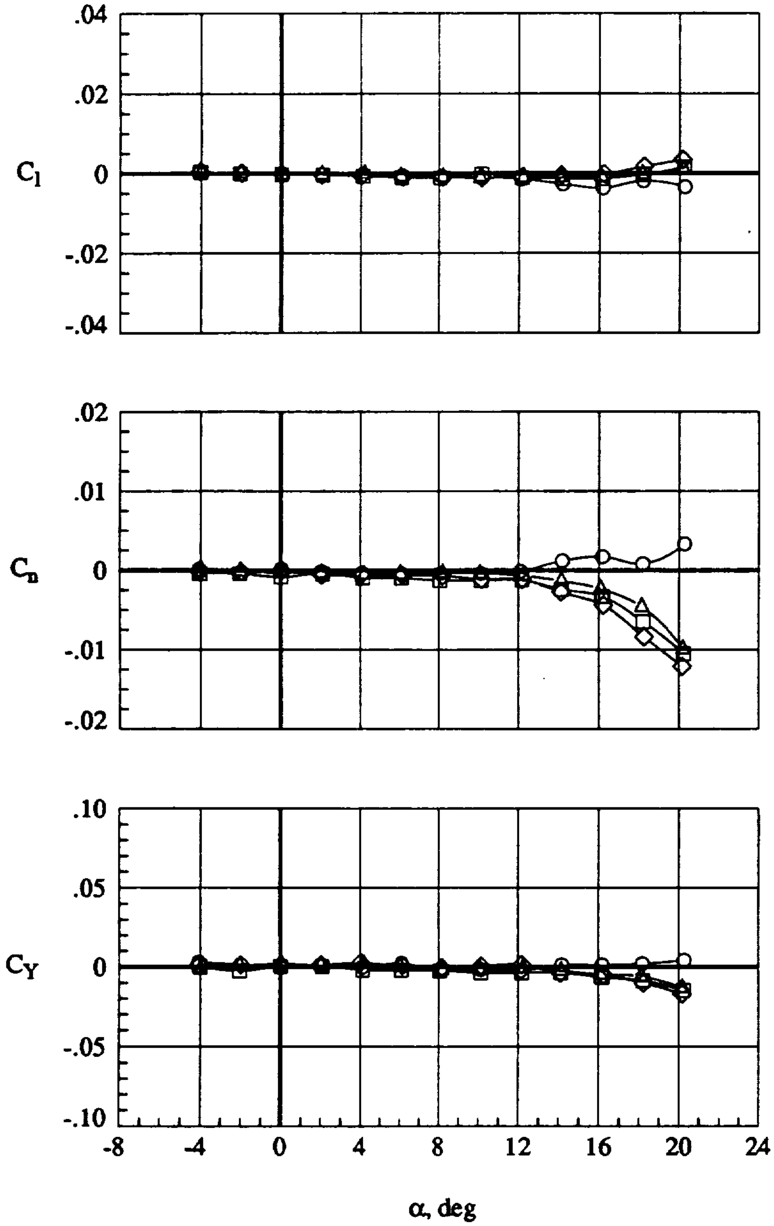

(b) Lateral aerodynamics.

Figure 33. Continued.

	Run	Configuration
○	108.	$\delta_L = 0°, \delta_T = 0°$
□	154.	$\delta_L = 0°, \delta_T = 0°$, AF-1
◇	156.	$\delta_L = 0°, \delta_T = 0°$, AF-2
△	129.	$\delta_L = 0°, \delta_T = 0°$, AF-3

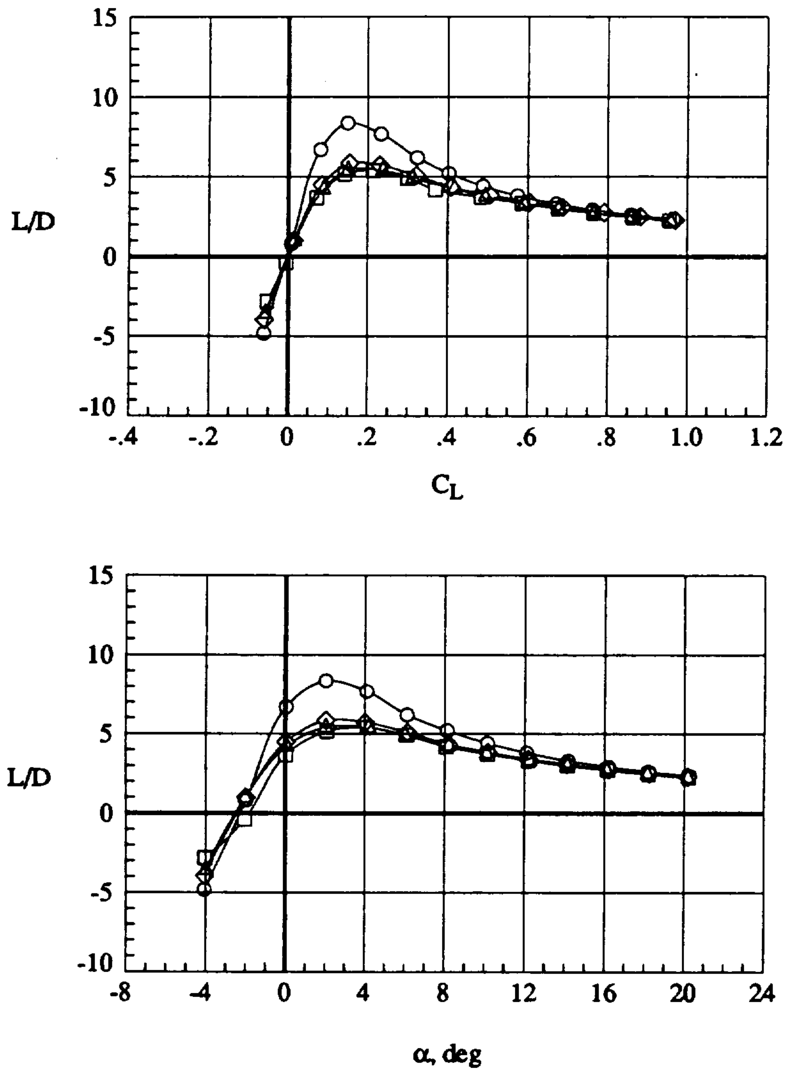

(c) Lift-drag performance.

Figure 33. Concluded.

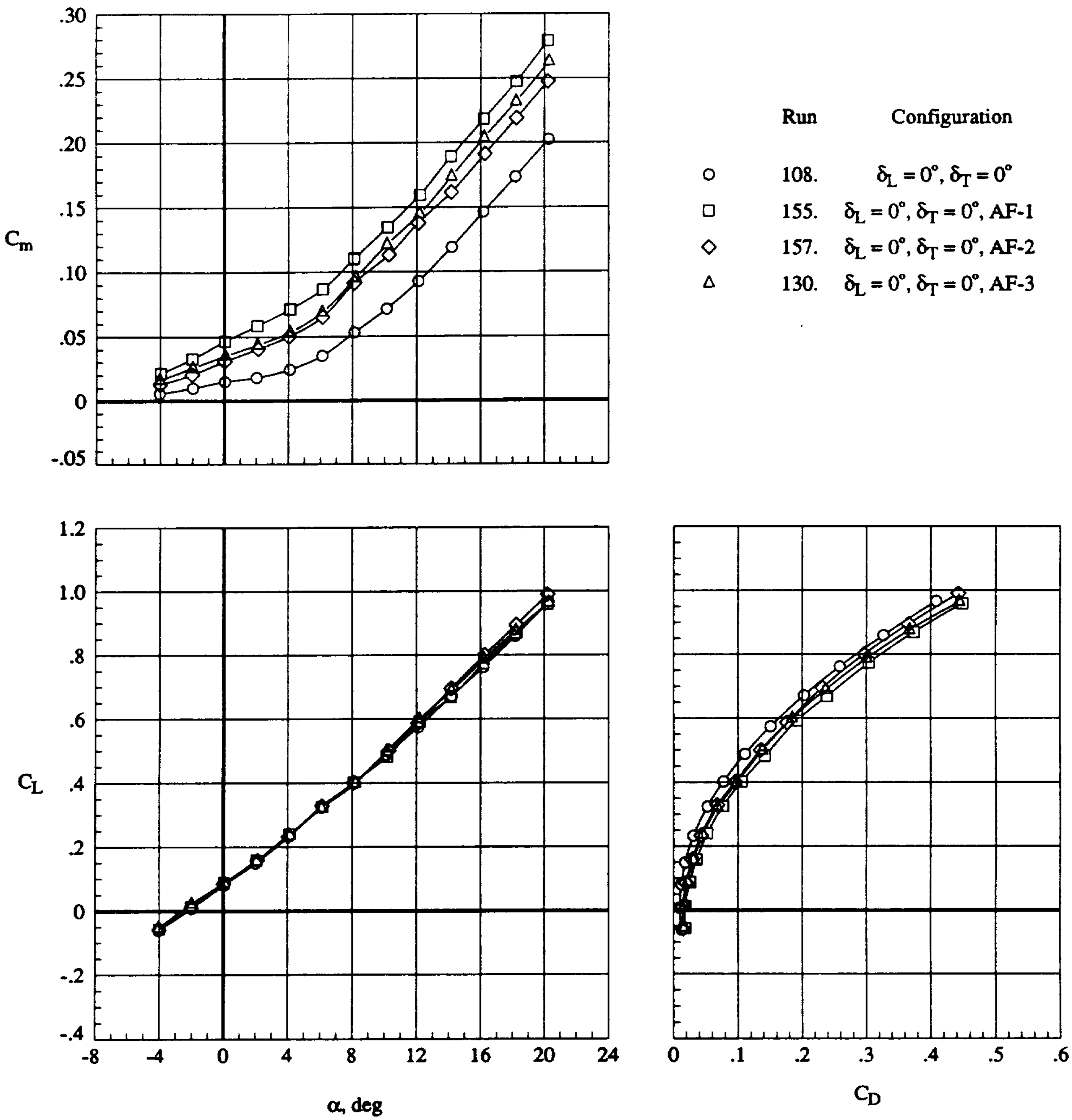

(a) Longitudinal aerodynamics.

Figure 34. Effect of 115° apex flaps with $\delta_L = 0°$ and $\delta_T = 0°$ at q = 70 psf.

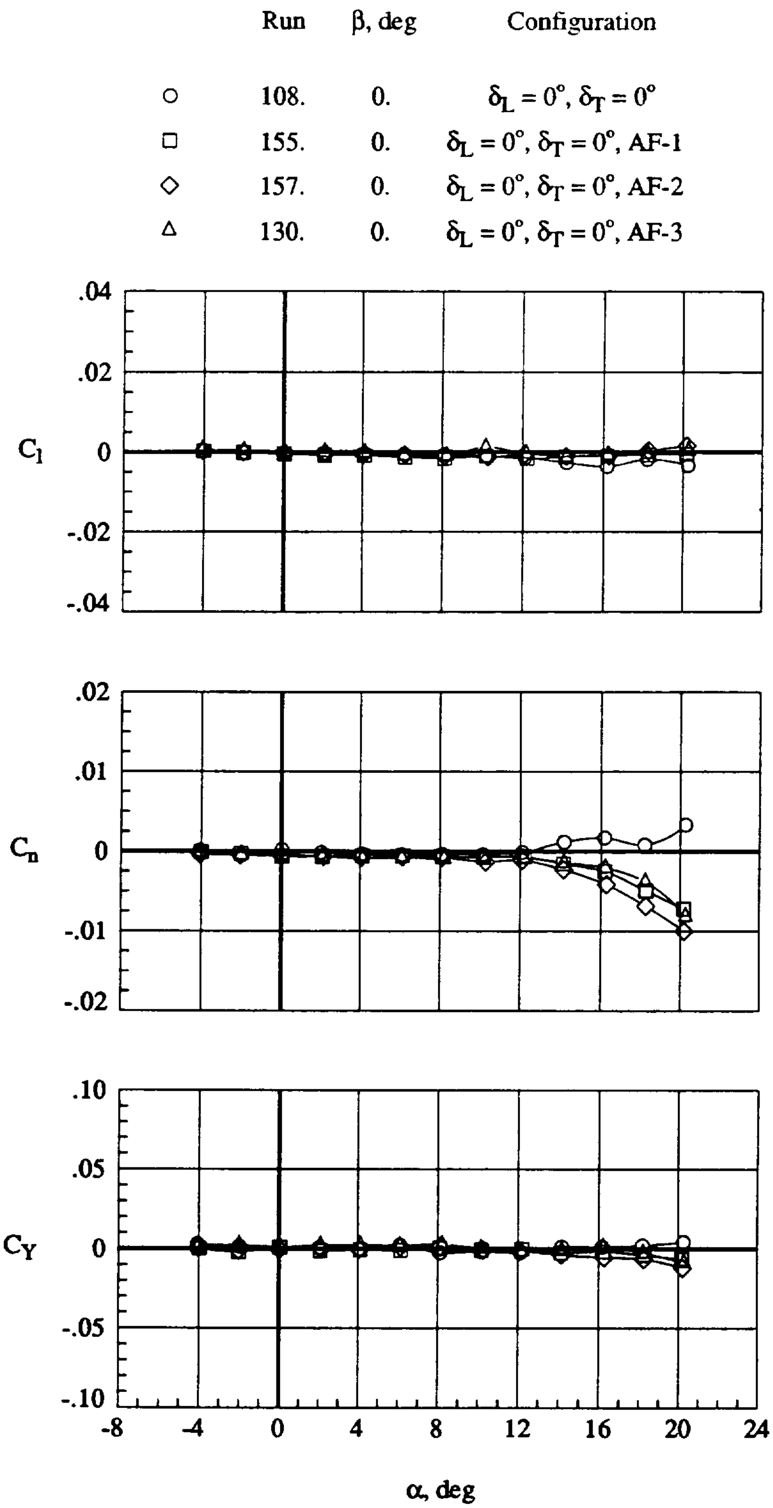

(b) Lateral aerodynamics.

Figure 34. Continued.

	Run	Configuration
○	108.	$\delta_L = 0°, \delta_T = 0°$
□	155.	$\delta_L = 0°, \delta_T = 0°$, AF-1
◇	157.	$\delta_L = 0°, \delta_T = 0°$, AF-2
△	130.	$\delta_L = 0°, \delta_T = 0°$, AF-3

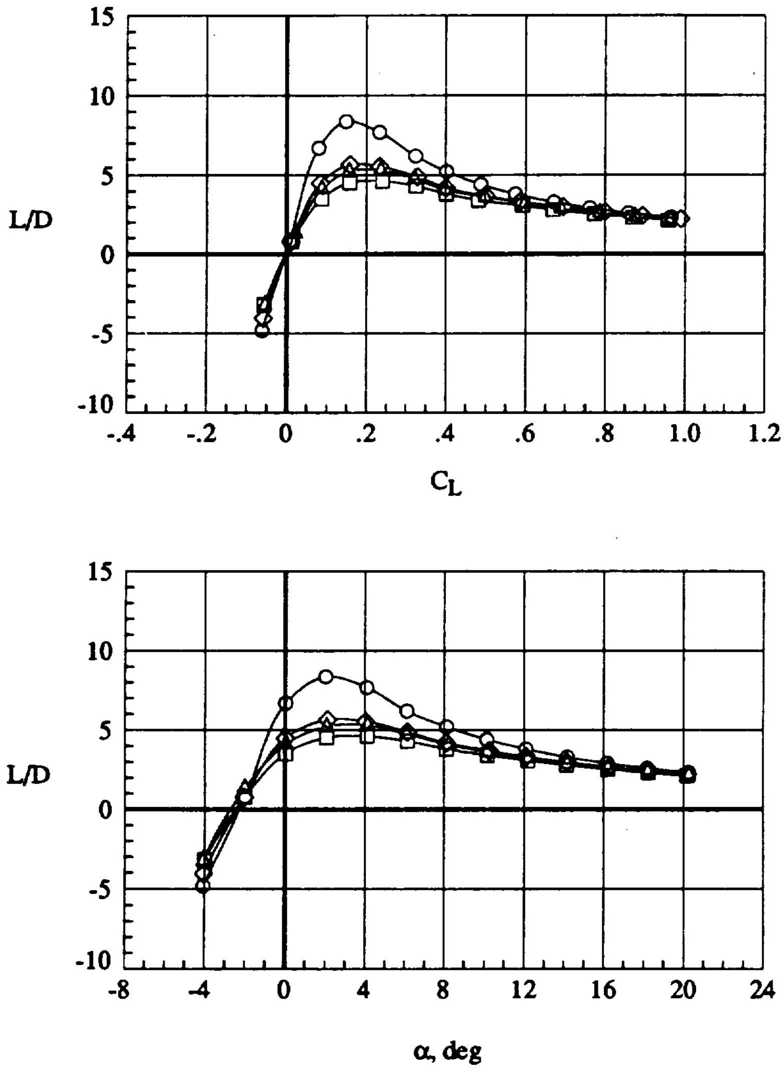

(c) Lift-drag performance.

Figure 34. Concluded.

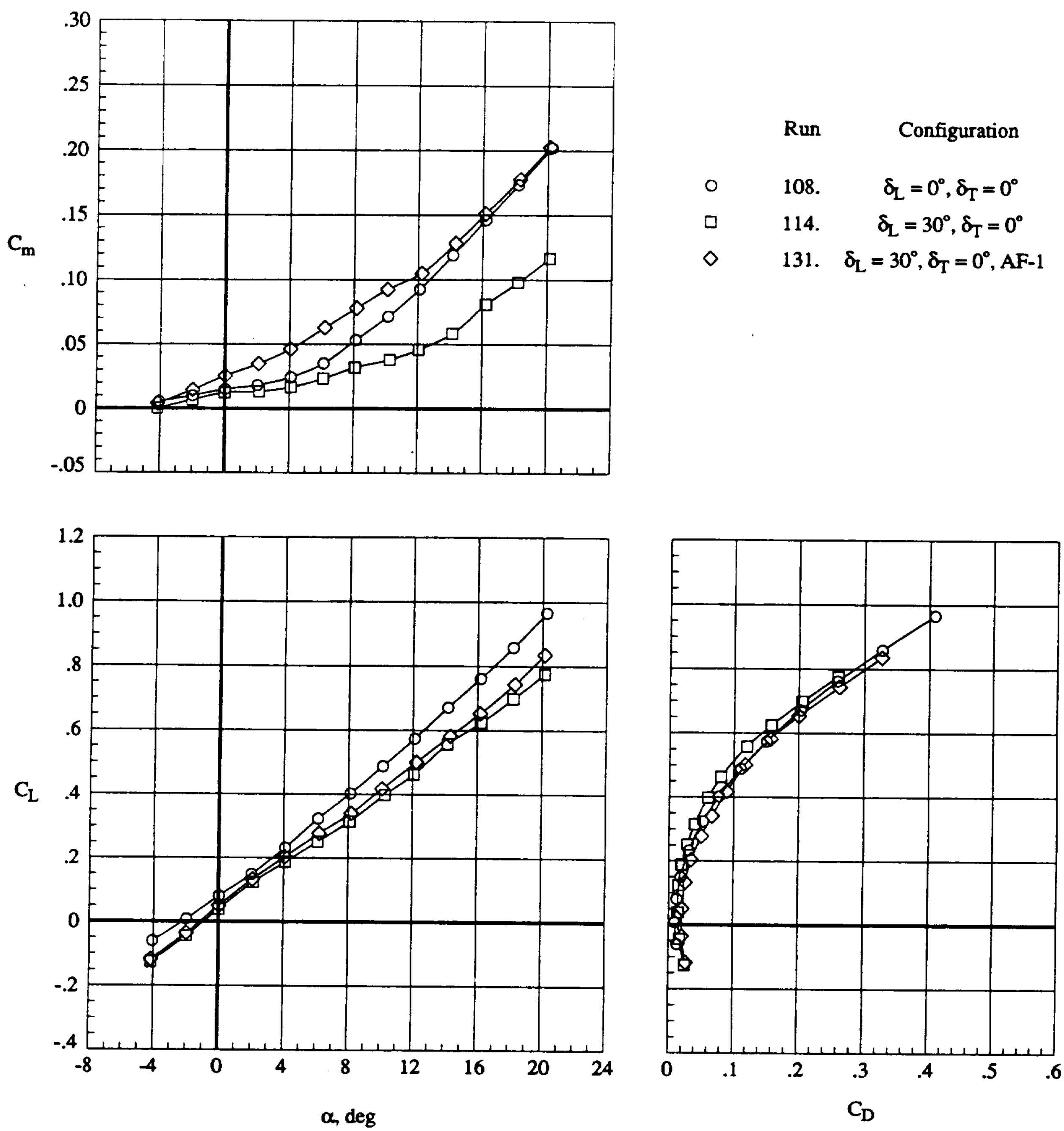

(a) Longitudinal aerodynamics.

Figure 35. Effect of AF-1 flap deflected 115° with $\delta_L = 30°$ and $\delta_T = 0°$ at q = 70 psf.

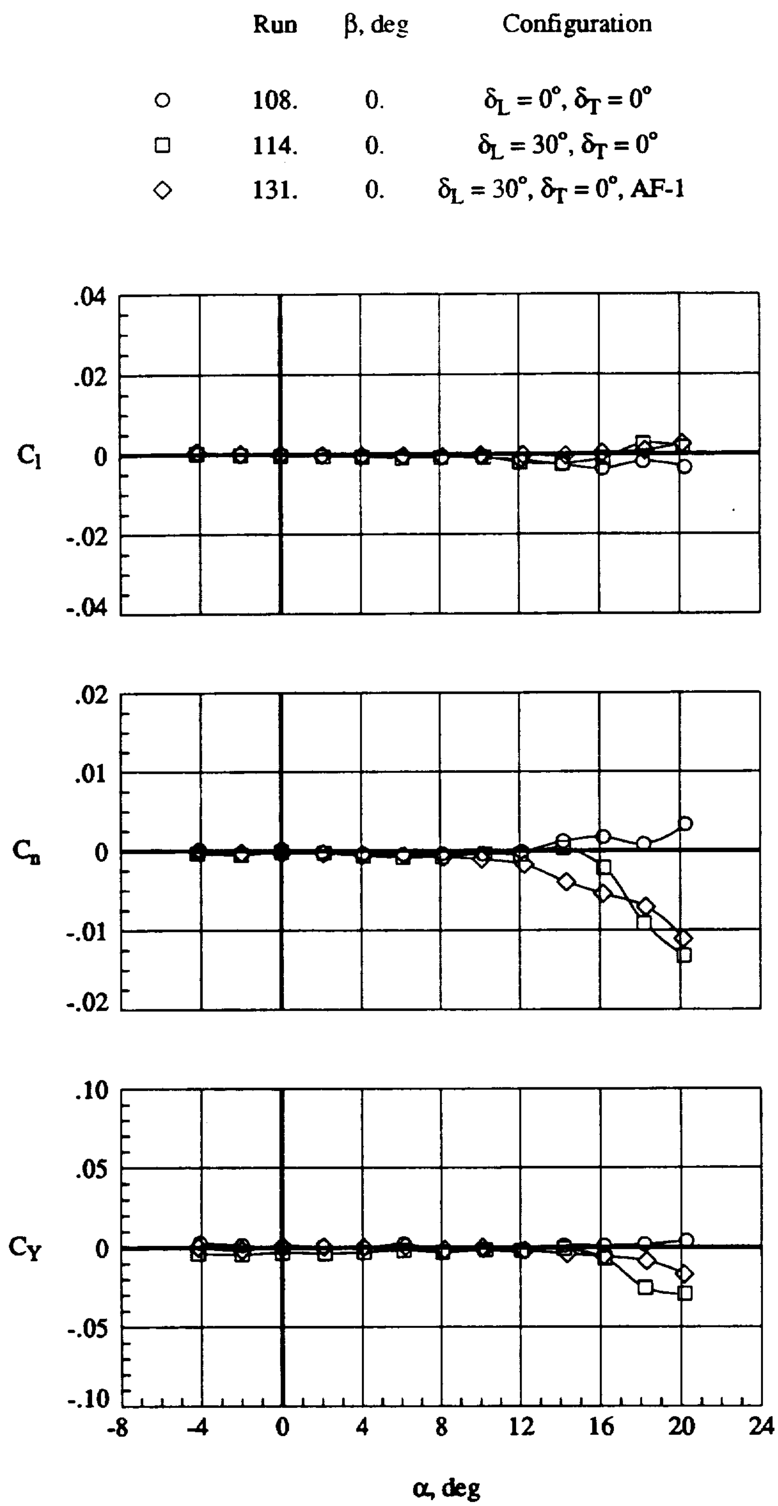

(b) Lateral aerodynamics.

Figure 35. Continued.

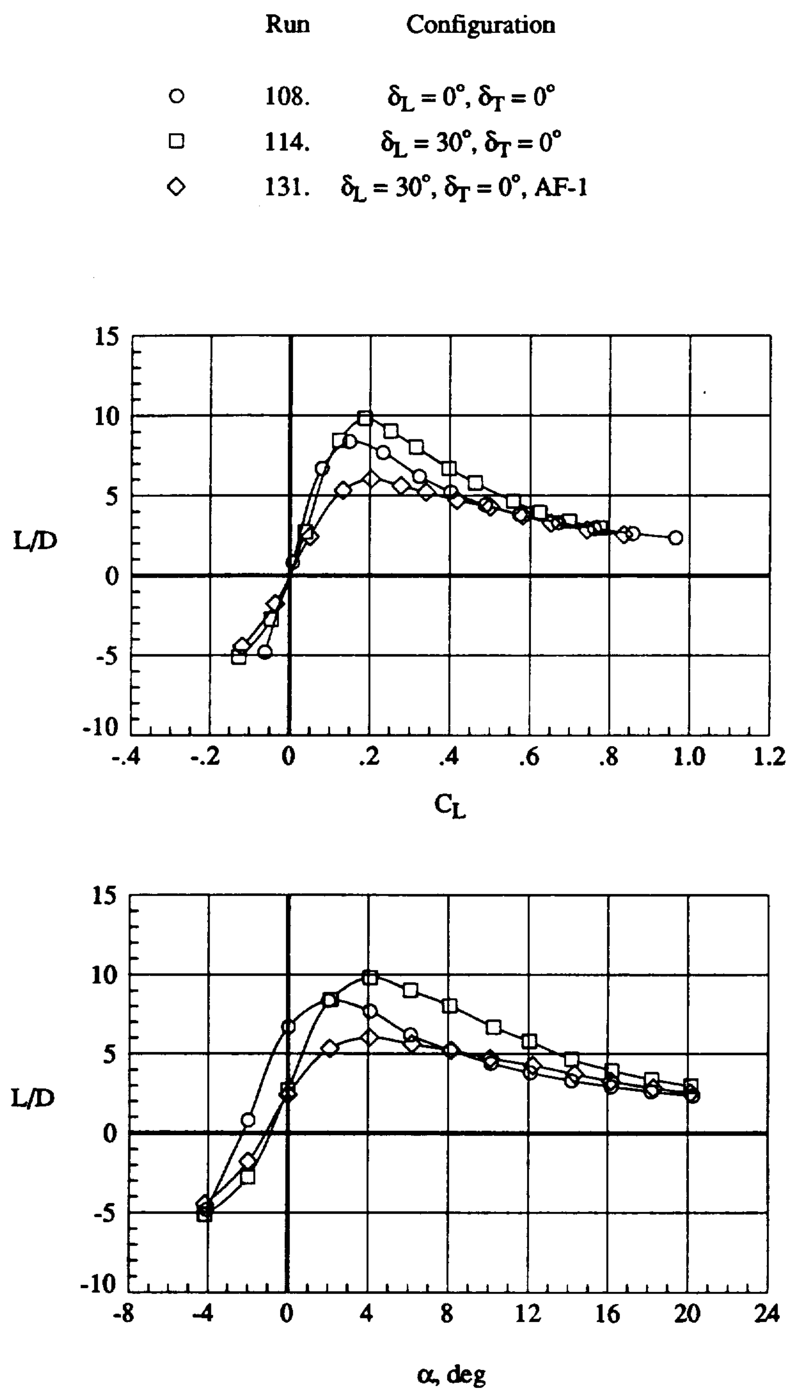

(c) Lift-drag performance.

Figure 35. Concluded.

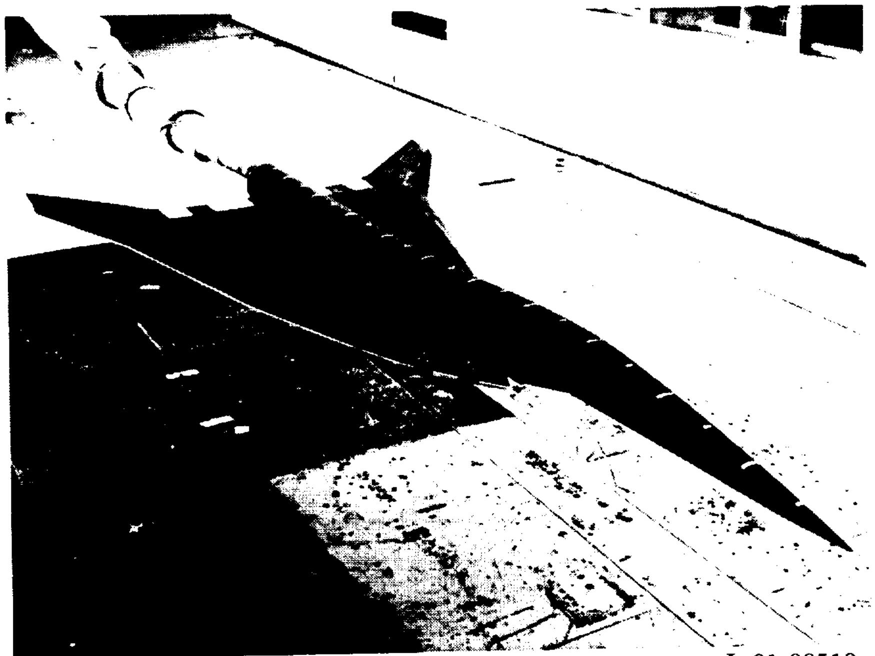

L-91-00510

(a) Full view.

L-91-00486

(b) Close-up view.

Figure 36. Model with $\frac{1}{2}$AF-1.

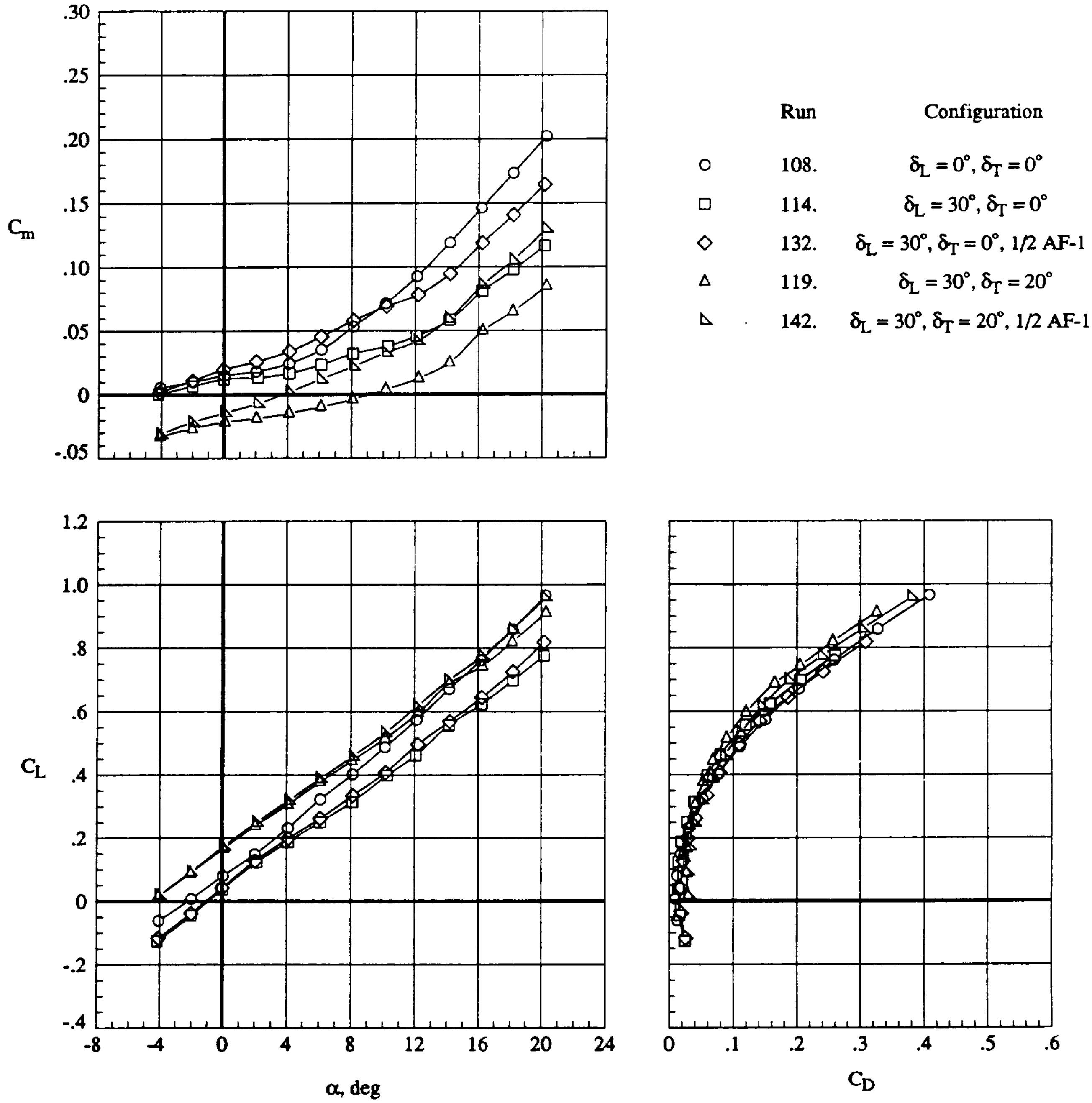

(a) Longitudinal aerodynamics.

Figure 37. Effect of 115° apex flaps altered to represent approximately one-half the area of AF-1; q = 70 psf.

	Run	β, deg	Configuration
○	108.	0.	$\delta_L = 0°, \delta_T = 0°$
□	114.	0.	$\delta_L = 30°, \delta_T = 0°$
◇	132.	0.	$\delta_L = 30°, \delta_T = 0°$, 1/2 AF-1
△	119.	0.	$\delta_L = 30°, \delta_T = 20°$
◺	142.	0.	$\delta_L = 30°, \delta_T = 20°$, 1/2 AF-1

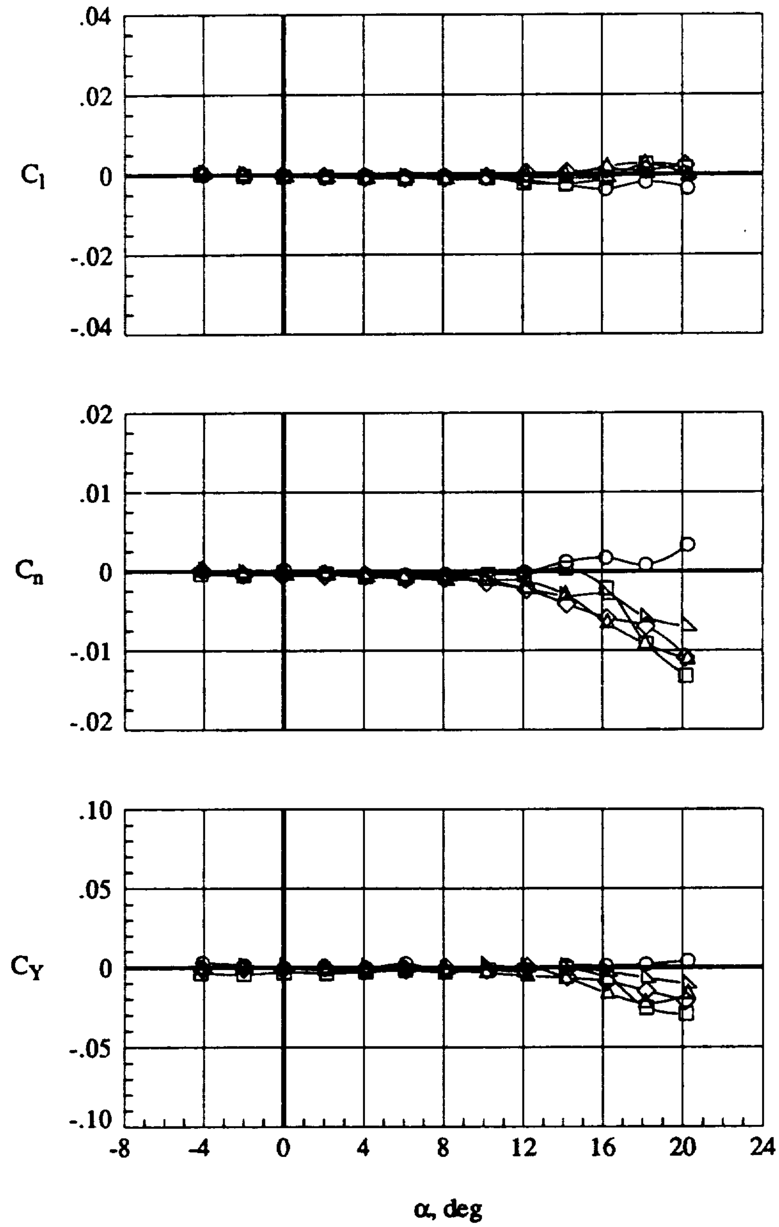

(b) Lateral aerodynamics.

Figure 37. Continued.

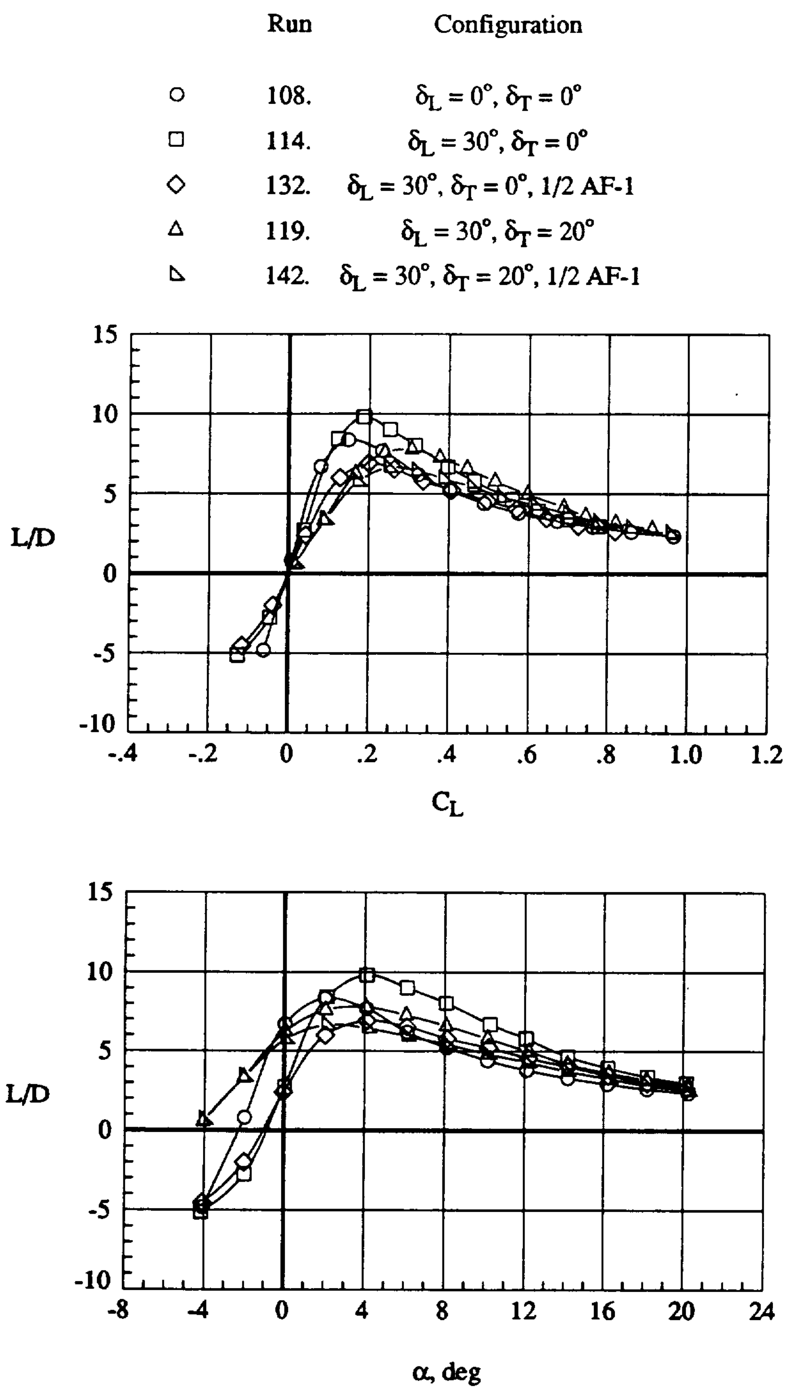

(c) Lift-drag performance.

Figure 37. Concluded.

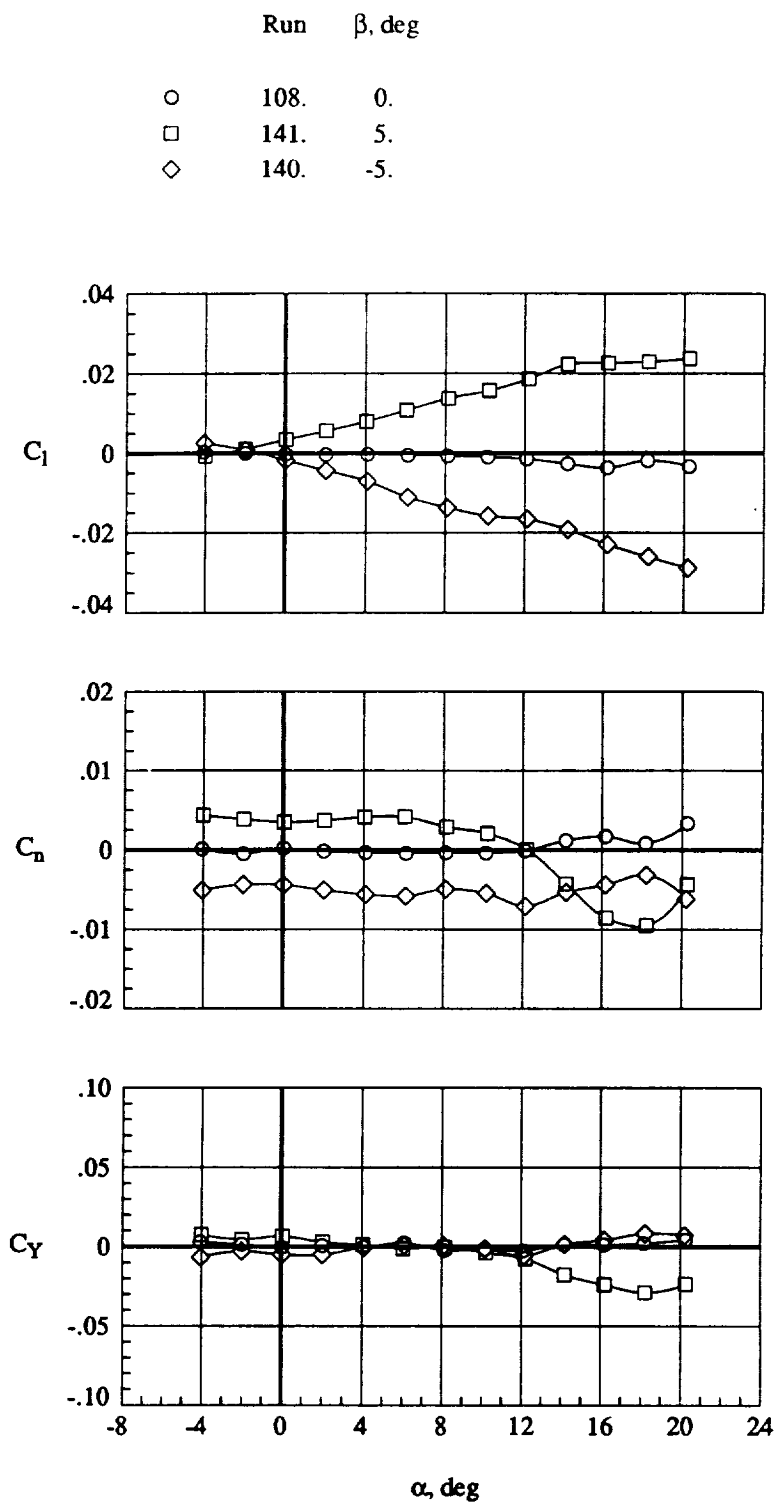

Figure 38. Lateral aerodynamics for wing with $\delta_L = 0°$ and $\delta_T = 0°$, without vortex devices, at q = 70 psf.

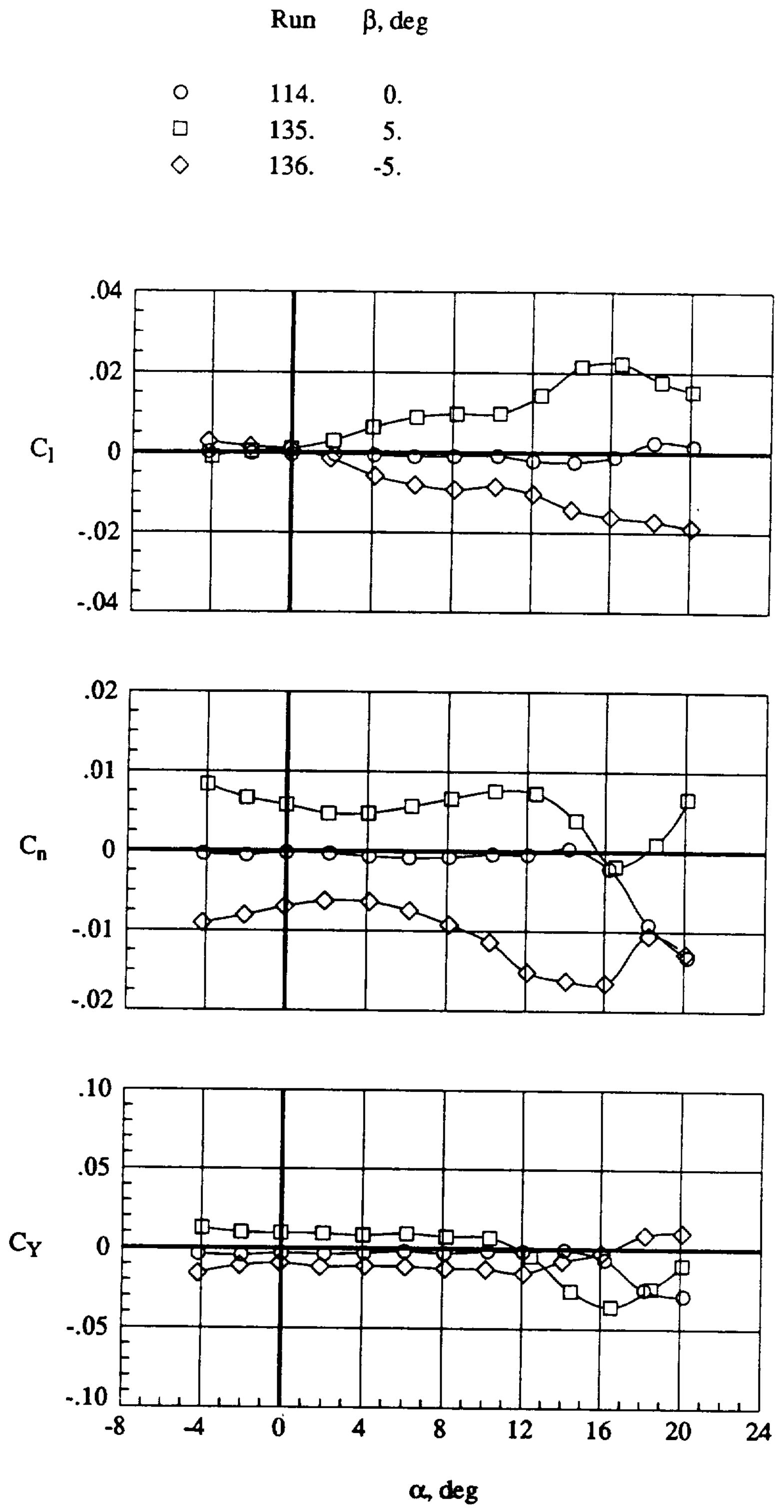

Figure 39. Lateral aerodynamics for wing with $\delta_L = 30°$ and $\delta_T = 0°$, without vortex devices, at q = 70 psf.

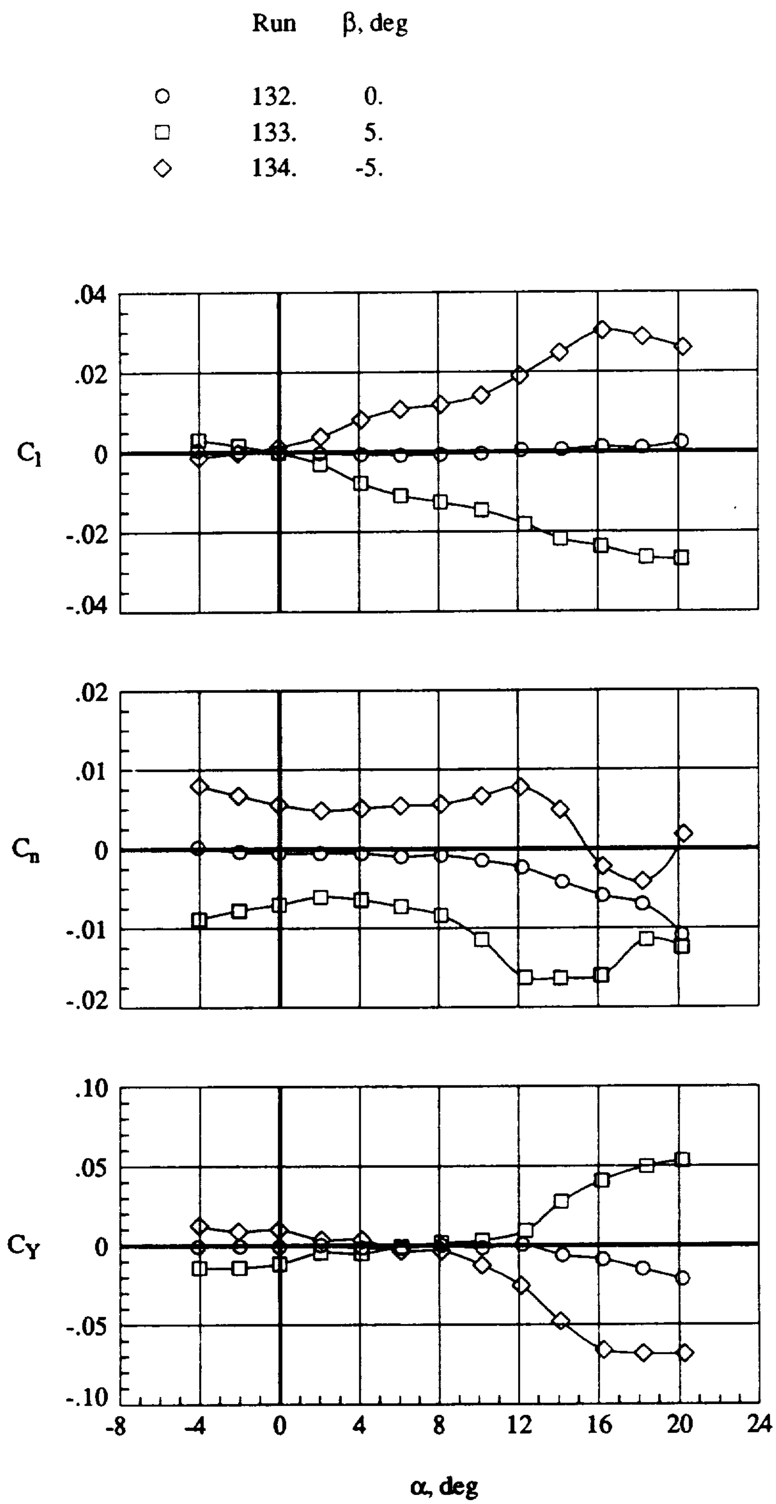

Figure 40. Lateral aerodynamics for wing with $\delta_L = 30°$ and $\delta_T = 0°$, and one-half 115° apex flap, at q = 70 psf.

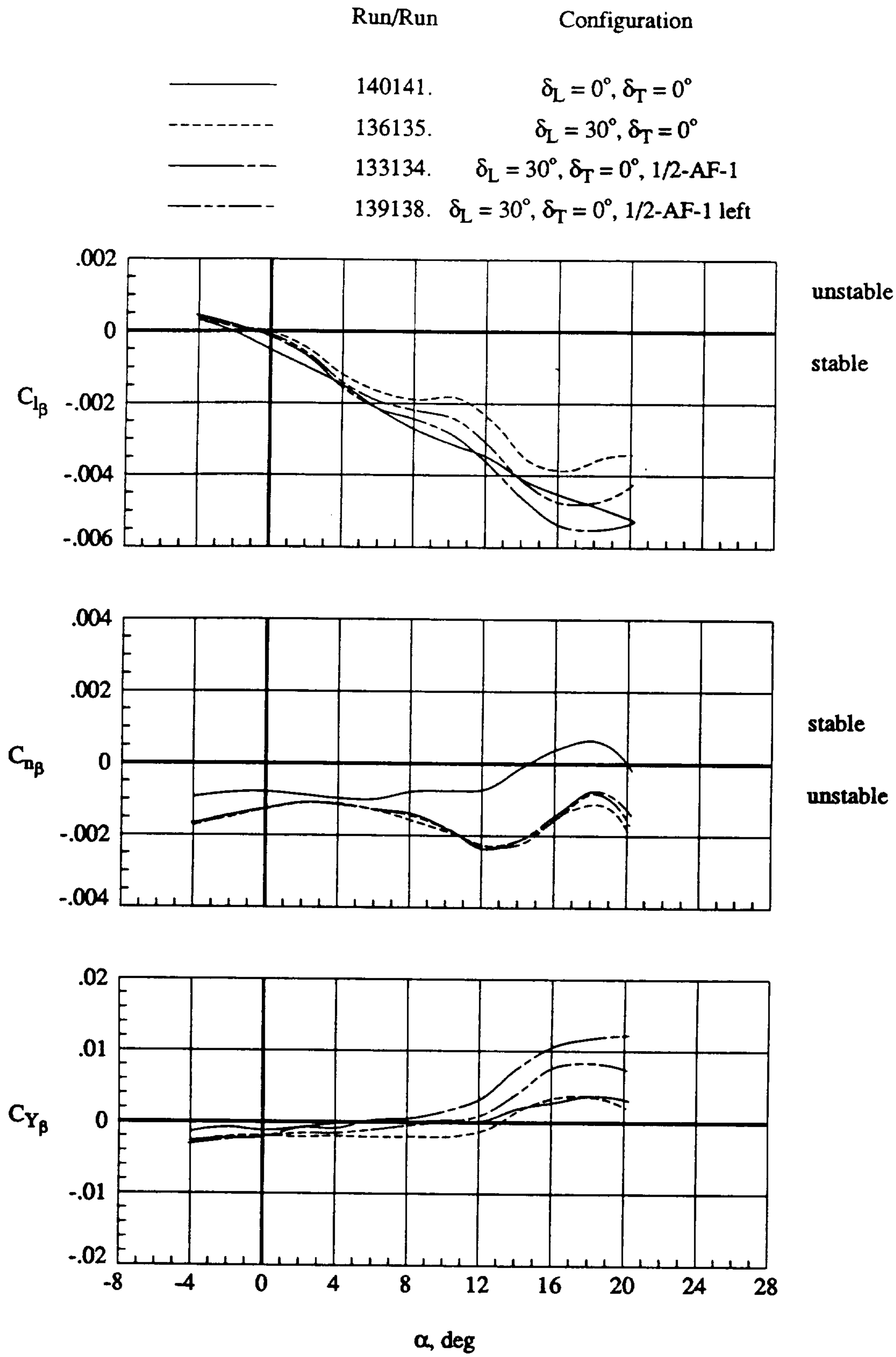

Figure 41. Lateral stability derivatives with one-half 115° apex flap at q = 70 psf.

Appendix A

Instrumentation Accuracy

Forces and moments were measured with a six-component strain-gauge balance identified as NASA LaRC VST-3. The load limit and error range for each component are as follows:

Component	Max load range	Error range, percent
Normal Force	3 000 lb	0.6
Axial Force	500 lb	0.75
Pitching Moment	10 000 in-lb	0.5
Rolling Moment	7 500 in-lb	1.1
Yawing Moment	4 500 in-lb	1.4
Side Force	1 800 lb	0.8

Base and chamber pressures were measured with ±5-psid transducers that had accuracies of ±0.5 percent. The angle-of-attack sensor had an accuracy of ±0.01°. Tunnel and atmospheric conditions were measured with standard facility instrumentation as described in reference 13.

Appendix B

Tabulated Force and Moment Results

Table B1. Index to Tabulated Data

[Unless specified, all data were acquired at $\alpha = -4°$ to $20°$, in $2°$ increments]

Run	q, psf	β, deg	δ_L, deg	δ_T, deg	Device
100	30	0	0	0	FBS
101	50	0	0	0	FBS
102	70	0	0	0	FBS
103	90	0	0	0	FBS
104	110	0	0	0	FBS
[a]106	70	0	0	0	
107	110	0	0	0	
108	70	0	0	0	
[b]109	110	0	0	0	
[b]110	70	0	0	0	
[b]111	30	0	0	0	
114	70	0	30	0	
115	70	0	30	0	WS
116	70	0	30	0	WF
117	70	0	30	0	WF, PC
118	70	0	30	0	PC, PI
119	70	0	30	20	
120	70	0	30	20	WS
121	70	0	30	20	WF
122	70	0	30	20	WF, PC
123	70	0	30	20	PC, PI
124	70	0	30	20	PC
129	70	0	0	0	AF-3 at 90°
130	70	0	0	0	AF-3 at 115°
131	70	0	30	0	AF-1 at 115°

[a]Run 106 had an abbreviated α range of 0°, 2°, 4°, 8°, 12°, 16°, 20°, and 22°.

[b]Runs 109, 110, and 111 had transition grit lightly applied to the entire wing upper surface and the entire forebody.

Table B1. Concluded

Run	q, psf	β, deg	δ_L, deg	δ_T, deg	Device
132	70	0	30	0	$\frac{1}{2}$AF-1 at 115°
133	70	+5	30	0	$\frac{1}{2}$AF-1 at 115°
134	70	−5	30	0	$\frac{1}{2}$AF-1 at 115°
135	70	−5	30	0	
136	70	+5	30	0	
[c]137	70	0	30	0	$\frac{1}{2}$AF-1 at 115°
[c]138	70	−5	30	0	$\frac{1}{2}$AF-1 at 115°
[c]139	70	+5	30	0	$\frac{1}{2}$AF-1 at 115°
140	70	+5	0	0	
141	70	−5	0	0	
142	70	0	30	20	$\frac{1}{2}$AF-1 at 115°
146	30	0	30	0	
147	70	0	30	0	
148	110	0	30	0	
149	30	0	30	0	PC, PI
150	70	0	30	0	PC, PI
151	110	0	30	0	PC, PI
154	70	0	0	0	AF-1 at 90°
155	70	0	0	0	AF-1 at 115°
156	70	0	0	0	AF-2 at 90°
157	70	0	0	0	AF-2 at 115°

[c]Runs 137, 138, and 139 were obtained with $\frac{1}{2}$AF-1 device at 115° on the left wing only.

Table B2. Tabulated Force and Moment Data

[Langley 14- by 22-Foot Subsonic Tunnel: test 376]

Run	Point	$R/10^6$	M	q	α	β	C_N	C_A	C_L	C_D	C_m	C_l	C_n	C_Y	L/D
100.	2.	3.10	0.14	30.01	−4.11	0.00	−0.0756	0.0043	−0.0751	0.0097	0.0050	0.0005	−0.0005	−0.0050	−7.27
100.	3.	3.10	0.14	30.25	−2.02	0.00	0.0147	0.0094	0.0150	0.0089	0.0103	0.0005	0.0001	0.0004	1.59
100.	4.	3.09	0.14	30.13	0.05	0.00	0.0686	0.0083	0.0686	0.0083	0.0144	−0.0002	−0.0002	−0.0037	7.69
100.	5.	3.08	0.14	30.01	2.05	0.00	0.1371	0.0073	0.1367	0.0122	0.0181	−0.0005	−0.0004	−0.0080	10.68
100.	6.	3.09	0.14	30.13	4.07	0.00	0.2251	0.0092	0.2238	0.0252	0.0261	−0.0004	−0.0007	−0.0056	8.66
100.	7.	3.09	0.14	30.25	6.14	0.00	0.3139	0.0114	0.3109	0.0449	0.0386	−0.0012	−0.0004	−0.0079	6.80
100.	8.	3.08	0.14	30.25	8.16	0.00	0.4016	0.0152	0.3953	0.0721	0.0563	−0.0006	−0.0001	−0.0050	5.42
100.	9.	3.07	0.14	30.14	10.16	0.00	0.4855	0.0169	0.4749	0.1023	0.0756	−0.0013	0.0000	−0.0088	4.60
100.	10.	3.06	0.14	30.03	12.14	0.00	0.5819	0.0212	0.5644	0.1431	0.0972	−0.0015	0.0000	−0.0055	3.91
100.	11.	3.07	0.14	30.15	14.17	0.00	0.6836	0.0263	0.6564	0.1929	0.1214	−0.0018	0.0004	−0.0042	3.38
100.	12.	3.06	0.14	30.16	16.17	0.00	0.8039	0.0340	0.7626	0.2565	0.1487	−0.0019	0.0008	0.0036	2.95
100.	13.	3.04	0.14	29.83	18.24	0.00	0.9153	0.0380	0.8574	0.3226	0.1798	−0.0022	0.0005	0.0004	2.64
100.	14.	3.05	0.14	30.06	20.19	0.00	1.0235	0.0410	0.9465	0.3917	0.2077	−0.0026	−0.0003	−0.0042	2.40
101.	1.	3.90	0.18	50.26	−4.03	0.00	−0.0683	0.0063	−0.0677	0.0111	0.0049	0.0007	−0.0003	−0.0011	−6.03
101.	2.	3.89	0.18	50.03	−2.01	0.00	−0.0006	0.0077	−0.0004	0.0077	0.0092	0.0001	−0.0003	−0.0016	−0.05
101.	3.	3.87	0.18	49.68	0.02	0.00	0.0704	0.0100	0.0704	0.0100	0.0147	0.0000	−0.0003	−0.0012	7.01
101.	4.	3.88	0.18	49.91	2.06	0.00	0.1421	0.0103	0.1417	0.0154	0.0187	−0.0002	−0.0003	−0.0030	9.20
101.	5.	3.89	0.18	50.26	4.09	0.00	0.2264	0.0121	0.2249	0.0282	0.0256	0.0001	−0.0004	−0.0015	7.96
101.	6.	3.89	0.18	50.15	6.09	0.00	0.3126	0.0138	0.3094	0.0469	0.0369	−0.0006	−0.0003	−0.0049	6.57
101.	7.	3.90	0.18	50.38	8.14	0.00	0.4046	0.0177	0.3981	0.0749	0.0551	−0.0006	−0.0003	−0.0038	5.30
101.	8.	3.90	0.18	50.40	10.16	0.00	0.5068	0.0241	0.4946	0.1131	0.0759	−0.0004	−0.0002	0.0017	4.36
101.	9.	3.89	0.18	50.28	12.13	0.00	0.5899	0.0250	0.5715	0.1484	0.0971	−0.0009	−0.0004	−0.0040	3.84
101.	10.	3.89	0.18	50.41	14.24	0.00	0.7040	0.0315	0.6746	0.2037	0.1230	−0.0012	0.0000	0.0010	3.30
101.	11.	3.88	0.18	50.08	16.26	0.00	0.8062	0.0344	0.7643	0.2587	0.1495	−0.0018	0.0000	−0.0022	2.94
101.	12.	3.89	0.18	50.32	18.24	0.00	0.9138	0.0396	0.8555	0.3237	0.1776	−0.0020	−0.0001	−0.0008	2.63
101.	13.	3.88	0.18	50.11	20.25	0.00	1.0321	0.0450	0.9527	0.3995	0.2079	−0.0025	−0.0004	−0.0025	2.37
102.	1.	4.56	0.22	69.92	−4.03	0.00	−0.0689	0.0059	−0.0683	0.0107	0.0051	0.0006	−0.0003	−0.0024	−6.34
102.	2.	4.55	0.22	69.92	−2.07	0.00	0.0022	0.0076	0.0025	0.0075	0.0090	0.0007	−0.0006	−0.0042	0.33
102.	3.	4.55	0.22	69.92	0.00	0.00	0.0720	0.0107	0.0720	0.0107	0.0131	0.0007	−0.0002	−0.0009	6.78
102.	4.	4.55	0.22	70.04	2.06	0.00	0.1437	0.0108	0.1432	0.0160	0.0170	0.0005	−0.0007	−0.0025	9.06
102.	5.	4.54	0.22	70.04	4.05	0.00	0.2236	0.0118	0.2222	0.0276	0.0226	0.0007	−0.0003	−0.0028	8.10
102.	6.	4.54	0.22	69.93	6.09	0.00	0.3139	0.0146	0.3106	0.0478	0.0340	0.0003	−0.0004	−0.0047	6.51
102.	7.	4.54	0.22	70.17	8.15	0.00	0.4082	0.0192	0.4013	0.0769	0.0531	0.0005	−0.0004	−0.0034	5.22
102.	8.	4.53	0.22	70.41	10.20	0.00	0.5048	0.0233	0.4927	0.1123	0.0754	−0.0002	−0.0007	−0.0024	4.38
102.	9.	4.52	0.22	70.08	12.21	0.00	0.6026	0.0279	0.5830	0.1547	0.0977	−0.0003	−0.0005	−0.0009	3.76
102.	10.	4.53	0.22	70.44	14.22	0.00	0.6978	0.0308	0.6688	0.2013	0.1219	−0.0011	−0.0004	−0.0024	3.31
102.	11.	4.52	0.22	70.11	16.23	0.00	0.8073	0.0365	0.7649	0.2607	0.1496	−0.0015	−0.0003	−0.0005	2.92
102.	12.	4.52	0.22	70.36	18.22	0.00	0.9189	0.0413	0.8599	0.3265	0.1774	−0.0012	−0.0005	−0.0019	2.62
102.	13.	4.51	0.22	70.16	20.29	0.00	1.0461	0.0476	0.9646	0.4075	0.2062	−0.0018	−0.0003	−0.0014	2.36
103.	2.	5.03	0.25	90.05	−4.03	0.00	−0.0607	0.0083	−0.0600	0.0125	0.0058	0.0005	−0.0002	0.0007	−4.93
103.	3.	5.03	0.25	90.28	−1.98	0.00	0.0084	0.0090	0.0087	0.0087	0.0099	0.0000	−0.0003	−0.0019	1.05
103.	4.	5.01	0.25	89.82	0.03	0.00	0.0737	0.0114	0.0737	0.0114	0.0149	−0.0001	−0.0003	−0.0010	6.74
103.	5.	5.02	0.25	90.17	2.01	0.00	0.1455	0.0127	0.1450	0.0178	0.0188	−0.0001	−0.0003	−0.0004	8.38
103.	6.	5.00	0.25	89.71	4.14	0.00	0.2284	0.0132	0.2268	0.0297	0.0245	−0.0001	−0.0005	−0.0010	7.77
103.	7.	5.01	0.25	90.52	6.09	0.00	0.3181	0.0163	0.3146	0.0499	0.0350	−0.0005	−0.0003	−0.0009	6.35
103.	8.	5.00	0.25	90.19	8.09	0.00	0.4049	0.0205	0.3979	0.0773	0.0533	−0.0003	−0.0005	−0.0007	5.17
103.	9.	5.00	0.25	90.32	10.16	0.00	0.4929	0.0232	0.4811	0.1098	0.0730	−0.0007	−0.0006	−0.0022	4.39
103.	10.	5.00	0.25	90.56	12.19	0.00	0.5922	0.0273	0.5731	0.1517	0.0949	−0.0006	−0.0008	−0.0024	3.78

Table B2. Continued

Run	Point	$R/10^6$	M	q	α	β	C_N	C_A	C_L	C_D	C_m	C_l	C_n	C_Y	L/D
103.	11.	5.00	0.25	90.47	14.12	0.00	0.6949	0.0328	0.6659	0.2014	0.1201	−0.0006	−0.0010	−0.0009	3.30
103.	12.	4.99	0.25	90.15	16.16	0.00	0.8025	0.0378	0.7603	0.2596	0.1482	−0.0010	−0.0013	−0.0015	2.92
103.	13.	4.99	0.25	90.29	18.18	0.00	0.9110	0.0425	0.8523	0.3246	0.1759	−0.0005	−0.0023	−0.0044	2.62
103.	14.	4.98	0.25	90.09	20.24	0.00	1.0281	0.0478	0.9480	0.4006	0.2064	−0.0003	−0.0032	−0.0060	2.36
104.	1.	5.45	0.27	109.83	−4.03	0.00	−0.0640	0.0071	−0.0634	0.0116	0.0051	0.0003	−0.0004	−0.0012	−5.64
104.	2.	5.45	0.27	110.06	−2.03	0.00	0.0089	0.0096	0.0092	0.0093	0.0099	0.0000	−0.0002	−0.0020	1.04
104.	3.	5.43	0.27	110.29	0.03	0.00	0.0754	0.0118	0.0754	0.0118	0.0147	−0.0001	−0.0004	−0.0018	6.69
104.	4.	5.43	0.27	110.18	2.02	0.00	0.1468	0.0126	0.1463	0.0178	0.0187	−0.0002	−0.0001	−0.0017	8.51
104.	5.	5.42	0.27	110.07	4.06	0.00	0.2272	0.0135	0.2257	0.0295	0.0236	−0.0003	−0.0003	0.0001	7.79
104.	6.	5.41	0.27	110.08	6.10	0.00	0.3180	0.0166	0.3144	0.0503	0.0351	−0.0006	−0.0005	−0.0008	6.31
104.	7.	5.41	0.27	109.98	8.08	0.00	0.4058	0.0207	0.3989	0.0775	0.0532	−0.0004	−0.0004	−0.0009	5.18
104.	8.	5.41	0.27	110.34	10.24	0.00	0.5016	0.0244	0.4892	0.1132	0.0749	−0.0007	−0.0006	−0.0018	4.33
104.	9.	5.36	0.27	110.01	12.12	0.00	0.5875	0.0277	0.5686	0.1504	0.0939	−0.0007	−0.0008	−0.0031	3.78
104.	10.	5.33	0.27	110.15	14.15	0.00	0.6985	0.0338	0.6691	0.2036	0.1204	−0.0004	−0.0009	−0.0019	3.28
104.	11.	5.33	0.27	110.30	16.14	0.00	0.8016	0.0390	0.7592	0.2603	0.1482	−0.0006	−0.0013	−0.0024	2.91
104.	12.	5.30	0.27	110.79	18.15	0.00	0.9088	0.0442	0.8498	0.3251	0.1750	−0.0007	−0.0015	−0.0028	2.61
104.	13.	5.29	0.27	110.48	20.19	0.00	1.0250	0.0488	0.9452	0.3996	0.2046	−0.0006	−0.0021	−0.0056	2.36
106.	2.	4.26	0.22	69.92	0.12	0.00	0.0784	0.0117	0.0784	0.0119	0.0145	−0.0003	−0.0003	−0.0019	6.88
106.	3.	4.25	0.22	70.04	2.05	0.00	0.1462	0.0129	0.1456	0.0181	0.0183	−0.0003	−0.0002	−0.0009	8.27
106.	4.	4.25	0.22	70.04	4.08	0.00	0.2286	0.0142	0.2270	0.0305	0.0239	−0.0001	−0.0004	−0.0004	7.55
106.	5.	4.24	0.22	69.94	8.17	0.00	0.4070	0.0203	0.4000	0.0780	0.0529	−0.0[illegible]	−0.0006	−0.0024	5.15
106.	6.	4.25	0.22	70.43	12.14	0.00	0.5971	0.0279	0.5779	0.1528	0.0933	−0.0013	−0.0001	0.0002	3.78
106.	7.	4.22	0.22	69.77	16.28	0.00	0.8057	0.0376	0.7628	0.2620	0.1468	−0.0039	0.0021	0.0012	2.90
106.	8.	4.23	0.22	70.28	20.13	0.00	1.0335	0.0486	0.9537	0.4013	0.1993	−0.0043	0.0041	0.0048	2.37
106.	9.	4.21	0.22	69.63	22.36	0.00	1.1600	0.0538	1.0523	0.4911	0.2330	−0.0111	0.0172	0.0230	2.13
107.	1.	5.22	0.27	110.18	−4.07	0.00	−0.0610	0.0080	−0.0603	0.0123	0.0059	0.0003	−0.0004	0.0005	−5.04
107.	2.	5.20	0.27	109.94	−2.03	0.00	0.0083	0.0097	0.0086	0.0094	0.0102	−0.0001	−0.0003	−0.0020	0.96
107.	3.	5.20	0.27	110.29	−0.06	0.00	0.0723	0.0117	0.0723	0.0116	0.0147	−0.0003	−0.0003	−0.0021	6.54
107.	4.	5.19	0.27	110.29	2.05	0.00	0.1461	0.0129	0.1455	0.0181	0.0179	−0.0003	−0.0002	−0.0016	8.28
107.	5.	5.18	0.27	109.95	4.09	0.00	0.2262	0.0131	0.2247	0.0292	0.0226	−0.0004	−0.0005	−0.0010	7.82
107.	6.	5.18	0.27	110.19	6.11	0.00	0.3209	0.0168	0.3172	0.0508	0.0342	−0.0008	−0.0005	−0.0007	6.30
107.	7.	5.17	0.27	110.32	8.16	0.00	0.4100	0.0209	0.4029	0.0788	0.0527	−0.0007	−0.0005	−0.0010	5.14
107.	8.	5.16	0.27	109.88	10.14	0.00	0.4997	0.0251	0.4875	0.1127	0.0719	−0.0007	−0.0004	0.0004	4.33
107.	9.	5.16	0.27	110.47	12.14	0.00	0.5927	0.0277	0.5736	0.1518	0.0918	−0.0011	−0.0001	−0.0017	3.78
107.	10.	5.15	0.27	110.16	14.18	0.00	0.6975	0.0333	0.6680	0.2031	0.1188	−0.0024	0.0012	−0.0002	3.29
107.	11.	5.15	0.27	110.31	16.31	0.00	0.8061	0.0380	0.7630	0.2628	0.1476	−0.0056	0.0048	0.0037	2.90
107.	12.	5.14	0.27	110.24	18.25	0.00	0.9158	0.0441	0.8560	0.3287	0.1745	−0.0085	0.0107	0.0116	2.60
107.	13.	5.13	0.27	110.51	20.24	0.00	1.0276	0.0498	0.9470	0.4022	0.2034	−0.0114	0.0161	0.0172	2.35
108.	2.	4.32	0.22	70.16	−4.07	0.00	−0.0618	0.0085	−0.0611	0.0129	0.0056	0.0003	0.0001	0.0029	−4.82
108.	3.	4.30	0.22	70.04	−1.98	0.00	0.0073	0.0100	0.0076	0.0097	0.0100	−0.0001	−0.0005	0.0015	0.81
108.	4.	4.29	0.22	70.04	0.03	0.00	0.0801	0.0123	0.0801	0.0124	0.0151	−0.0003	0.0002	−0.0005	6.70
108.	5.	4.29	0.22	70.04	2.02	0.00	0.1491	0.0129	0.1485	0.0182	0.0182	−0.0004	−0.0002	0.0006	8.37
108.	6.	4.28	0.22	70.04	4.09	0.00	0.2341	0.0139	0.2325	0.0306	0.0244	−0.0003	−0.0003	−0.0002	7.69
108.	7.	4.26	0.22	69.59	6.11	0.00	0.3276	0.0177	0.3239	0.0525	0.0351	−0.0005	−0.0004	0.0024	6.20
108.	8.	4.28	0.22	70.06	8.12	0.00	0.4091	0.0198	0.4022	0.0774	0.0532	−0.0007	−0.0003	−0.0025	5.21
108.	9.	4.28	0.22	70.41	10.14	0.00	0.4997	0.0230	0.4878	0.1107	0.0714	−0.0010	−0.0004	−0.0017	4.41
108.	10.	4.26	0.22	69.96	12.11	0.00	0.5928	0.0269	0.5740	0.1506	0.0926	−0.0014	−0.0001	−0.0025	3.81
108.	11.	4.27	0.22	70.33	14.18	0.00	0.7007	0.0322	0.6715	0.2029	0.1190	−0.0027	0.0012	0.0013	3.30
108.	12.	4.25	0.22	69.88	16.18	0.00	0.8036	0.0364	0.7617	0.2588	0.1464	−0.0037	0.0017	0.0012	2.93
108.	13.	4.27	0.22	70.60	18.19	0.00	0.9179	0.0425	0.8587	0.3269	0.1734	−0.0019	0.0008	0.0021	2.62

Table B2. Continued

Run	Point	$R/10^6$	M	q	α	β	C_N	C_A	C_L	C_D	C_m	C_l	C_n	C_Y	L/D
108.	14.	4.25	0.22	70.16	20.26	0.00	1.0476	0.0486	0.9660	0.4084	0.2023	−0.0034	0.0033	0.0042	2.35
109.	2.	5.51	0.27	109.83	−4.12	0.00	−0.0658	0.0091	−0.0650	0.0138	0.0060	0.0003	0.0000	0.0000	−4.83
109.	3.	5.49	0.27	109.72	−2.02	0.00	0.0118	0.0135	0.0123	0.0131	0.0107	0.0002	−0.0001	0.0026	0.97
109.	4.	5.48	0.27	109.95	0.05	0.00	0.0771	0.0144	0.0771	0.0144	0.0155	−0.0002	−0.0002	0.0013	5.53
109.	5.	5.48	0.27	110.07	2.09	0.00	0.1454	0.0139	0.1448	0.0192	0.0185	−0.0003	−0.0003	0.0002	7.75
109.	6.	5.46	0.27	109.61	4.14	0.00	0.2312	0.0162	0.2294	0.0328	0.0243	−0.0001	−0.0004	0.0019	7.09
109.	7.	5.46	0.27	110.08	6.08	0.00	0.3159	0.0187	0.3121	0.0520	0.0342	−0.0002	−0.0004	0.0016	6.05
109.	8.	5.45	0.27	109.75	8.19	0.00	0.4064	0.0224	0.3990	0.0800	0.0538	−0.0005	−0.0005	0.0005	5.01
109.	9.	5.45	0.27	110.34	10.16	0.00	0.4917	0.0253	0.4795	0.1117	0.0722	−0.0008	−0.0007	−0.0004	4.30
109.	10.	5.43	0.27	109.91	12.23	0.00	0.5946	0.0307	0.5746	0.1560	0.0935	−0.0008	−0.0007	0.0020	3.68
109.	11.	5.44	0.27	110.27	14.26	0.00	0.6953	0.0341	0.6655	0.2044	0.1172	−0.0007	−0.0013	−0.0012	3.25
109.	12.	5.44	0.27	110.53	16.21	0.00	0.7956	0.0399	0.7528	0.2605	0.1461	−0.0008	−0.0015	−0.0004	2.88
109.	13.	5.41	0.27	110.11	18.24	0.00	0.9116	0.0457	0.8515	0.3287	0.1725	−0.0017	0.0000	0.0024	2.58
109.	14.	5.41	0.27	110.61	20.24	0.00	1.0223	0.0499	0.9419	0.4005	0.1979	−0.0031	0.0021	0.0027	2.34
110.	1.	4.34	0.22	70.04	−3.99	0.00	−0.0540	0.0112	−0.0531	0.0149	0.0071	0.0004	−0.0001	0.0036	−3.63
110.	2.	4.34	0.22	70.04	−1.99	0.00	0.0124	0.0136	0.0129	0.0131	0.0107	0.0001	−0.0004	0.0026	1.01
110.	3.	4.34	0.22	69.93	0.00	0.00	0.0766	0.0142	0.0766	0.0142	0.0153	−0.0003	−0.0001	0.0002	5.56
110.	4.	4.34	0.22	69.81	2.02	0.00	0.1511	0.0156	0.1505	0.0210	0.0196	−0.0002	−0.0002	0.0014	7.35
110.	5.	4.34	0.22	70.05	4.08	0.00	0.2326	0.0163	0.2309	0.0328	0.0246	−0.0002	−0.0003	0.0008	7.12
110.	6.	4.34	0.22	70.05	6.15	0.00	0.3244	0.0207	0.3204	0.0553	0.0365	0.0000	−0.0003	0.0028	5.84
110.	7.	4.35	0.22	70.41	8.08	0.00	0.4001	0.0227	0.3930	0.0787	0.0533	−0.0005	−0.0006	0.0001	5.01
110.	8.	4.34	0.22	70.19	10.24	0.00	0.4992	0.0259	0.4867	0.1143	0.0741	−0.0008	−0.0008	−0.0020	4.26
110.	9.	4.35	0.22	70.20	12.16	0.00	0.5904	0.0299	0.5709	0.1535	0.0934	−0.0004	−0.0013	−0.0020	3.72
110.	10.	4.35	0.22	70.21	14.22	0.00	0.6984	0.0347	0.6685	0.2052	0.1172	0.0000	−0.0024	−0.0037	3.25
110.	11.	4.35	0.22	70.46	16.24	0.00	0.7974	0.0389	0.7547	0.2604	0.1455	0.0014	−0.0038	−0.0057	2.89
110.	12.	4.34	0.22	70.13	18.22	0.00	0.9138	0.0454	0.8538	0.3289	0.1729	0.0017	−0.0055	−0.0069	2.59
110.	13.	4.34	0.22	70.26	20.24	0.00	1.0293	0.0504	0.9483	0.4034	0.2024	0.0060	−0.0133	−0.0176	2.34
111.	1.	2.87	0.14	30.25	−4.08	0.00	−0.0611	0.0115	−0.0602	0.0159	0.0063	0.0001	0.0004	−0.0023	−3.82
111.	2.	2.87	0.14	30.13	−2.02	0.00	0.0139	0.0147	0.0144	0.0142	0.0107	0.0000	−0.0004	0.0018	1.03
111.	3.	2.87	0.14	30.13	0.03	0.00	0.0861	0.0169	0.0861	0.0169	0.0158	−0.0002	0.0001	0.0009	5.19
111.	4.	2.87	0.14	30.14	2.04	0.00	0.1553	0.0186	0.1545	0.0241	0.0191	0.0002	−0.0003	0.0072	6.50
111.	5.	2.86	0.14	29.90	4.07	0.00	0.2442	0.0182	0.2422	0.0355	0.0257	−0.0004	−0.0001	−0.0010	6.88
111.	6.	2.87	0.14	29.91	6.08	0.00	0.3357	0.0226	0.3314	0.0580	0.0386	−0.0004	0.0001	0.0008	5.73
111.	7.	2.87	0.14	29.91	8.13	0.00	0.4202	0.0270	0.4121	0.0862	0.0562	−0.0004	−0.0002	0.0036	4.79
111.	8.	2.89	0.14	30.26	10.37	0.00	0.5156	0.0273	0.5023	0.1197	0.0768	−0.0005	−0.0011	−0.0011	4.19
111.	9.	2.89	0.14	30.27	12.14	0.00	0.5948	0.0313	0.5749	0.1557	0.0944	0.0003	−0.0022	−0.0011	3.68
111.	10.	2.88	0.14	30.04	14.25	0.00	0.7130	0.0379	0.6817	0.2122	0.1224	0.0020	−0.0042	−0.0003	3.20
111.	11.	2.88	0.14	30.05	16.24	0.00	0.8069	0.0397	0.7636	0.2638	0.1481	0.0038	−0.0068	−0.0095	2.88
111.	12.	2.88	0.14	30.17	18.31	0.00	0.9135	0.0447	0.8532	0.3294	0.1763	0.0079	−0.0144	−0.0188	2.58
111.	13.	2.86	0.14	29.71	20.23	0.00	1.0251	0.0495	0.9447	0.4009	0.2062	0.0123	−0.0226	−0.0321	2.35
114.	1.	4.63	0.22	69.81	−4.16	0.00	−0.1273	0.0156	−0.1258	0.0248	0.0003	0.0002	−0.0003	−0.0036	−5.12
114.	2.	4.62	0.22	69.81	−1.99	0.00	−0.0458	0.0152	−0.0452	0.0168	0.0067	−0.0002	−0.0005	−0.0043	−2.74
114.	3.	4.61	0.22	69.69	0.01	0.00	0.0385	0.0146	0.0385	0.0146	0.0123	−0.0004	−0.0002	−0.0031	2.72
114.	4.	4.61	0.22	70.04	2.13	0.00	0.1232	0.0104	0.1227	0.0150	0.0133	−0.0005	−0.0003	−0.0036	8.42
114.	5.	4.59	0.22	69.58	4.10	0.00	0.1883	0.0060	0.1874	0.0195	0.0167	−0.0007	−0.0007	−0.0029	9.83
114.	6.	4.59	0.22	69.58	6.11	0.00	0.2533	0.0013	0.2518	0.0283	0.0233	−0.0010	−0.0008	−0.0018	9.02
114.	7.	4.54	0.22	70.15	8.08	0.00	0.3175	−0.0051	0.3151	0.0396	0.0319	−0.0009	−0.0007	−0.0029	8.04
114.	8.	4.50	0.22	69.81	10.26	0.00	0.4023	−0.0121	0.3981	0.0598	0.0379	−0.0008	−0.0004	−0.0015	6.69
114.	9.	4.49	0.22	69.82	12.06	0.00	0.4689	−0.0185	0.4624	0.0800	0.0457	−0.0020	−0.0004	−0.0018	5.79
114.	10.	4.48	0.22	70.18	14.17	0.00	0.5699	−0.0204	0.5575	0.1197	0.0582	−0.0024	0.0004	−0.0006	4.66

Table B2. Continued

Run	Point	$R/10^6$	M	q	α	β	C_N	C_A	C_L	C_D	C_m	C_l	C_n	C_Y	L/D
114.	11.	4.48	0.22	70.18	16.22	0.00	0.6433	−0.0227	0.6240	0.1579	0.0807	−0.0010	−0.0022	−0.0068	3.95
114.	12.	4.46	0.22	70.30	18.21	0.00	0.7276	−0.0231	0.6984	0.2054	0.0979	0.0025	−0.0091	−0.0255	3.39
114.	13.	4.46	0.22	70.20	20.17	0.00	0.8181	−0.0237	0.7761	0.2598	0.1167	0.0016	−0.0132	−0.0292	2.98
115.	2.	4.55	0.22	69.93	−4.07	0.00	−0.1190	0.0169	−0.1175	0.0253	−0.0025	0.0005	−0.0001	0.0016	−4.70
115.	3.	4.54	0.22	70.16	−1.98	0.00	−0.0415	0.0166	−0.0409	0.0180	0.0056	0.0002	−0.0003	0.0001	−2.33
115.	4.	4.53	0.22	69.93	0.00	0.00	0.0397	0.0155	0.0397	0.0155	0.0118	0.0000	−0.0001	−0.0011	2.66
115.	5.	4.52	0.22	69.70	2.02	0.00	0.1214	0.0127	0.1209	0.0170	0.0143	−0.0001	−0.0001	−0.0002	7.39
115.	6.	4.52	0.22	70.16	4.04	0.00	0.1943	0.0093	0.1931	0.0230	0.0187	−0.0002	−0.0003	0.0003	8.61
115.	7.	4.52	0.22	70.27	6.10	0.00	0.2636	0.0042	0.2617	0.0322	0.0253	−0.0006	−0.0007	−0.0011	8.26
115.	8.	4.50	0.22	69.93	8.07	0.00	0.3315	−0.0017	0.3285	0.0449	0.0326	−0.0008	−0.0010	−0.0018	7.39
115.	9.	4.51	0.22	70.51	10.17	0.00	0.4068	−0.0089	0.4020	0.0631	0.0410	−0.0010	−0.0012	−0.0015	6.40
115.	10.	4.50	0.22	70.17	12.12	0.00	0.4918	−0.0140	0.4837	0.0896	0.0513	−0.0011	−0.0007	0.0010	5.41
115.	11.	4.50	0.22	70.41	14.14	0.00	0.5816	−0.0181	0.5684	0.1245	0.0632	−0.0014	−0.0012	0.0005	4.56
115.	12.	4.49	0.22	70.18	16.18	0.00	0.6674	−0.0231	0.6474	0.1638	0.0787	0.0016	−0.0036	−0.0104	3.95
115.	13.	4.49	0.22	70.19	18.25	0.00	0.7481	−0.0230	0.7176	0.2125	0.0988	0.0018	−0.0063	−0.0168	3.37
115.	14.	4.48	0.22	69.98	20.18	0.00	0.8504	−0.0255	0.8070	0.2695	0.1154	0.0006	−0.0101	−0.0196	2.98
116.	2.	4.51	0.22	70.05	−4.05	0.00	−0.1177	0.0191	−0.1160	0.0274	−0.0006	0.0007	0.0000	0.0003	−4.29
116.	3.	4.51	0.22	70.28	−2.02	0.00	−0.0409	0.0188	−0.0402	0.0202	0.0066	0.0005	−0.0004	0.0008	−2.04
116.	4.	4.50	0.22	70.05	0.03	0.00	0.0439	0.0179	0.0439	0.0179	0.0119	0.0002	−0.0001	0.0022	2.54
116.	5.	4.49	0.22	70.05	2.02	0.00	0.1291	0.0152	0.1285	0.0197	0.0142	0.0003	0.0000	0.0043	6.72
116.	6.	4.48	0.22	70.04	4.04	0.00	0.2003	0.0102	0.1991	0.0243	0.0172	0.0001	−0.0002	0.0030	8.42
116.	7.	4.48	0.22	70.16	6.05	0.00	0.2644	0.0050	0.2624	0.0328	0.0229	−0.0001	−0.0006	0.0025	8.13
116.	8.	4.48	0.22	70.16	8.13	0.00	0.3376	−0.0011	0.3343	0.0467	0.0310	−0.0001	−0.0005	0.0040	7.23
116.	9.	4.47	0.22	70.05	10.14	0.00	0.4004	−0.0108	0.3960	0.0599	0.0369	−0.0001	−0.0010	−0.0008	6.64
116.	10.	4.46	0.22	70.05	12.18	0.00	0.4786	−0.0178	0.4716	0.0836	0.0464	0.0005	−0.0015	−0.0026	5.65
116.	11.	4.48	0.22	70.51	14.21	0.00	0.5614	−0.0241	0.5501	0.1144	0.0603	0.0018	−0.0033	−0.0091	4.80
116.	12.	4.47	0.22	70.40	16.16	0.00	0.6362	−0.0280	0.6189	0.1502	0.0749	0.0031	−0.0067	−0.0147	4.12
116.	13.	4.46	0.22	70.07	18.16	0.00	0.7195	−0.0299	0.6930	0.1958	0.0938	0.0029	−0.0096	−0.0190	3.53
116.	14.	4.43	0.22	69.40	20.23	0.00	0.8225	−0.0314	0.7826	0.2550	0.1123	0.0001	−0.0116	−0.0141	3.06
117.	2.	4.48	0.22	69.93	−4.07	0.00	−0.1141	0.0194	−0.1125	0.0274	−0.0020	0.0004	−0.0005	0.0001	−4.16
117.	3.	4.46	0.22	69.93	−1.99	0.00	−0.0277	0.0205	−0.0270	0.0215	0.0059	0.0004	−0.0002	0.0017	−1.29
117.	4.	4.43	0.22	69.81	0.02	0.00	0.0418	0.0170	0.0418	0.0170	0.0104	0.0000	−0.0001	−0.0007	2.55
117.	5.	4.43	0.22	69.81	2.03	0.00	0.1240	0.0139	0.1235	0.0183	0.0137	−0.0001	−0.0002	−0.0002	7.02
117.	6.	4.44	0.22	70.15	4.11	0.00	0.1964	0.0085	0.1953	0.0226	0.0167	−0.0002	−0.0004	−0.0011	8.91
117.	7.	4.43	0.22	69.93	6.04	0.00	0.2633	0.0047	0.2614	0.0324	0.0219	−0.0001	−0.0005	0.0005	8.22
117.	8.	4.43	0.22	69.93	8.04	0.00	0.3304	−0.0020	0.3274	0.0443	0.0298	−0.0004	−0.0005	−0.0010	7.48
117.	9.	4.43	0.22	70.28	10.08	0.00	0.4060	−0.0095	0.4014	0.0617	0.0370	−0.0002	−0.0010	−0.0010	6.54
117.	10.	4.44	0.22	70.51	12.15	0.00	0.4826	−0.0167	0.4753	0.0853	0.0467	0.0003	−0.0016	−0.0017	5.58
117.	11.	4.44	0.22	70.40	14.15	0.00	0.5626	−0.0228	0.5511	0.1154	0.0595	0.0018	−0.0033	−0.0075	4.78
117.	12.	4.43	0.22	70.40	16.20	0.00	0.6413	−0.0271	0.6234	0.1529	0.0757	0.0033	−0.0068	−0.0151	4.07
117.	13.	4.42	0.22	69.84	18.23	0.00	0.7299	−0.0315	0.7031	0.1984	0.0930	0.0041	−0.0105	−0.0249	3.53
117.	14.	4.42	0.22	69.86	20.20	0.00	0.8276	−0.0334	0.7883	0.2545	0.1111	0.0003	−0.0113	−0.0177	3.09
118.	3.	4.34	0.22	70.27	−4.11	0.00	−0.1282	0.0159	−0.1267	0.0251	−0.0016	−0.0002	−0.0005	−0.0054	−5.13
118.	4.	4.33	0.22	70.15	−2.17	0.00	−0.0569	0.0153	−0.0562	0.0174	0.0045	−0.0003	−0.0007	−0.0055	−3.33
118.	5.	4.32	0.22	70.04	−0.18	0.00	0.0231	0.0141	0.0231	0.0140	0.0095	−0.0005	−0.0007	−0.0037	1.73
118.	6.	4.31	0.22	70.15	2.06	0.00	0.1148	0.0111	0.1143	0.0153	0.0139	−0.0004	−0.0003	−0.0028	7.85
118.	7.	4.31	0.22	70.15	4.08	0.00	0.1832	0.0052	0.1824	0.0183	0.0165	−0.0007	−0.0006	−0.0045	10.37
118.	8.	4.28	0.22	70.04	6.08	0.00	0.2670	0.0054	0.2650	0.0337	0.0238	−0.0001	−0.0006	−0.0002	8.04
118.	9.	4.27	0.22	69.81	8.11	0.00	0.3339	−0.0006	0.3307	0.0466	0.0325	0.0000	−0.0005	−0.0006	7.20
118.	10.	4.23	0.22	69.70	10.20	0.00	0.4076	−0.0083	0.4026	0.0640	0.0407	−0.0004	−0.0010	−0.0032	6.35

Table B2. Continued

Run	Point	$R/10^6$	M	q	α	β	C_N	C_A	C_L	C_D	C_m	C_l	C_n	C_Y	L/D
118.	11.	4.23	0.22	69.82	12.07	0.00	0.4808	−0.0138	0.4731	0.0870	0.0496	−0.0002	−0.0010	−0.0029	5.46
118.	12.	4.24	0.22	70.06	14.07	0.00	0.5632	−0.0188	0.5509	0.1187	0.0640	0.0012	−0.0023	−0.0078	4.66
118.	13.	4.24	0.22	70.29	16.17	0.00	0.6378	−0.0247	0.6195	0.1540	0.0798	0.0028	−0.0052	−0.0165	4.03
118.	14.	4.25	0.22	70.53	18.11	0.00	0.7144	−0.0266	0.6873	0.1968	0.0971	0.0012	−0.0075	−0.0168	3.49
118.	15.	4.23	0.22	69.98	20.16	0.00	0.8107	−0.0274	0.7704	0.2537	0.1169	−0.0011	−0.0092	−0.0104	3.03
119.	2.	4.65	0.22	70.05	−4.08	0.00	0.0138	0.0308	0.0160	0.0298	−0.0331	0.0001	0.0000	−0.0010	0.55
119.	3.	4.65	0.22	70.16	−2.03	0.00	0.0874	0.0305	0.0884	0.0274	−0.0267	−0.0001	−0.0003	−0.0006	3.35
119.	4.	4.64	0.22	70.16	0.05	0.00	0.1668	0.0276	0.1668	0.0277	−0.0216	−0.0003	−0.0002	−0.0004	6.25
119.	5.	4.63	0.22	70.04	2.05	0.00	0.2406	0.0240	0.2396	0.0326	−0.0189	−0.0005	−0.0003	−0.0019	7.59
119.	6.	4.63	0.22	70.39	4.09	0.00	0.3090	0.0184	0.3069	0.0404	−0.0148	−0.0008	−0.0004	−0.0026	7.77
119.	7.	4.63	0.22	70.50	6.08	0.00	0.3807	0.0125	0.3772	0.0528	−0.0098	−0.0008	−0.0007	−0.0014	7.25
119.	8.	4.62	0.22	70.16	8.08	0.00	0.4502	0.0051	0.4450	0.0683	−0.0040	−0.0010	−0.0007	−0.0014	6.59
119.	9.	4.61	0.22	70.04	10.14	0.00	0.5228	−0.0025	0.5151	0.0896	0.0037	−0.0011	−0.0011	−0.0035	5.79
119.	10.	4.60	0.22	69.93	12.21	0.00	0.6081	−0.0087	0.5962	0.1201	0.0127	−0.0005	−0.0013	−0.0054	4.98
119.	11.	4.60	0.22	70.06	14.16	0.00	0.7075	−0.0085	0.6881	0.1648	0.0248	−0.0002	−0.0030	−0.0072	4.18
119.	12.	4.60	0.22	70.07	16.26	0.00	0.7707	−0.0115	0.7431	0.2047	0.0497	0.0019	−0.0066	−0.0165	3.63
119.	13.	4.59	0.22	69.96	18.16	0.00	0.8584	−0.0119	0.8193	0.2562	0.0649	0.0027	−0.0092	−0.0227	3.19
119.	14.	4.59	0.22	69.99	20.28	0.00	0.9674	−0.0108	0.9112	0.3252	0.0848	−0.0004	−0.0111	−0.0168	2.80
120.	3.	4.56	0.22	69.94	−4.14	0.00	0.0081	0.0302	0.0103	0.0296	−0.0345	−0.0001	−0.0001	−0.0013	0.36
120.	4.	4.54	0.22	69.70	−2.04	0.00	0.0787	0.0295	0.0797	0.0267	−0.0268	−0.0003	−0.0004	−0.0022	3.11
120.	5.	4.54	0.22	69.81	0.07	0.00	0.1653	0.0284	0.1653	0.0286	−0.0207	−0.0003	−0.0003	−0.0014	6.01
120.	6.	4.54	0.22	69.93	2.06	0.00	0.2372	0.0243	0.2362	0.0328	−0.0179	−0.0008	−0.0004	−0.0036	7.44
120.	7.	4.54	0.22	69.93	4.17	0.00	0.3158	0.0219	0.3134	0.0449	−0.0120	−0.0007	−0.0005	−0.0016	7.14
120.	8.	4.54	0.22	69.93	6.23	0.00	0.3964	0.0173	0.3922	0.0603	−0.0069	−0.0007	−0.0008	−0.0001	6.60
120.	9.	4.53	0.22	69.93	8.19	0.00	0.4700	0.0100	0.4638	0.0769	−0.0010	−0.0012	−0.0007	−0.0016	6.09
120.	10.	4.55	0.22	70.51	10.12	0.00	0.5337	0.0022	0.5250	0.0960	0.0069	−0.0012	−0.0012	−0.0038	5.51
120.	11.	4.54	0.22	70.40	12.18	0.00	0.6182	−0.0037	0.6050	0.1268	0.0190	−0.0007	−0.0016	−0.0066	4.79
120.	12.	4.55	0.22	70.52	14.23	0.00	0.7199	−0.0051	0.6991	0.1721	0.0325	0.0004	−0.0034	−0.0084	4.07
120.	13.	4.52	0.22	69.60	16.28	0.00	0.8060	−0.0113	0.7768	0.2151	0.0484	0.0015	−0.0072	−0.0182	3.61
120.	14.	4.53	0.22	70.08	18.20	0.00	0.8847	−0.0111	0.8439	0.2659	0.0662	0.0018	−0.0098	−0.0228	3.17
120.	15.	4.53	0.22	69.98	20.10	0.00	0.9766	−0.0125	0.9215	0.3238	0.0806	−0.0004	−0.0110	−0.0203	2.84
121.	2.	4.69	0.22	70.28	−4.01	0.00	0.0129	0.0305	0.0150	0.0296	−0.0339	0.0001	0.0001	−0.0013	0.52
121.	3.	4.67	0.22	70.05	−1.97	0.00	0.0865	0.0305	0.0875	0.0275	−0.0267	−0.0001	−0.0002	0.0000	3.30
121.	4.	4.66	0.22	70.05	0.04	0.00	0.1658	0.0289	0.1658	0.0290	−0.0218	−0.0002	−0.0001	0.0003	5.95
121.	5.	4.65	0.22	69.81	2.05	0.00	0.2392	0.0247	0.2382	0.0333	−0.0187	−0.0004	−0.0002	−0.0014	7.40
121.	6.	4.64	0.22	69.70	4.06	0.00	0.3113	0.0206	0.3091	0.0426	−0.0145	−0.0006	−0.0003	0.0003	7.44
121.	7.	4.66	0.22	70.50	6.10	0.00	0.3772	0.0137	0.3736	0.0537	−0.0100	−0.0006	−0.0006	−0.0009	7.08
121.	8.	4.65	0.22	70.27	8.10	0.00	0.4472	0.0067	0.4418	0.0696	−0.0038	−0.0010	−0.0008	−0.0017	6.42
121.	9.	4.65	0.22	70.51	10.15	0.00	0.5182	−0.0016	0.5104	0.0898	0.0036	−0.0008	−0.0013	−0.0033	5.73
121.	10.	4.65	0.22	70.62	12.17	0.00	0.5988	−0.0086	0.5872	0.1178	0.0123	0.0002	−0.0017	−0.0049	5.00
121.	11.	4.65	0.22	70.74	14.19	0.00	0.6796	−0.0132	0.6621	0.1538	0.0269	0.0009	−0.0030	−0.0093	4.31
121.	12.	4.64	0.22	70.29	16.20	0.00	0.7420	−0.0179	0.7176	0.1899	0.0452	0.0018	−0.0077	−0.0191	3.78
121.	13.	4.64	0.22	70.30	18.18	0.00	0.8211	−0.0191	0.7860	0.2380	0.0638	0.0022	−0.0091	−0.0234	3.30
121.	14.	4.62	0.22	69.98	20.24	0.00	0.9282	−0.0170	0.8768	0.3051	0.0828	0.0008	−0.0088	−0.0148	2.87
122.	2.	4.64	0.22	70.28	−4.00	0.00	0.0156	0.0317	0.0178	0.0305	−0.0334	−0.0002	−0.0002	−0.0031	0.60
122.	3.	4.64	0.22	70.51	−2.06	0.00	0.0887	0.0316	0.0898	0.0284	−0.0265	−0.0003	−0.0004	−0.0006	3.28
122.	4.	4.63	0.22	70.27	0.08	0.00	0.1665	0.0284	0.1664	0.0286	−0.0216	−0.0005	−0.0004	−0.0029	6.07
122.	5.	4.63	0.22	70.50	2.15	0.00	0.2471	0.0251	0.2460	0.0343	−0.0180	−0.0005	−0.0004	−0.0014	7.42
122.	6.	4.61	0.22	70.16	4.15	0.00	0.3176	0.0210	0.3153	0.0439	−0.0143	−0.0006	−0.0004	−0.0009	7.36
122.	7.	4.59	0.22	69.81	6.25	0.00	0.3892	0.0142	0.3854	0.0564	−0.0090	−0.0009	−0.0008	−0.0025	6.94

Table B2. Continued

Run	Point	$R/10^6$	M	q	α	β	C_N	C_A	C_L	C_D	C_m	C_l	C_n	C_Y	L/D
122.	8.	4.60	0.22	70.16	8.21	0.00	0.4598	0.0070	0.4540	0.0727	−0.0030	−0.0012	−0.0007	−0.0017	6.32
122.	9.	4.60	0.22	70.16	10.03	0.00	0.5188	−0.0003	0.5110	0.0900	0.0041	−0.0010	−0.0011	−0.0038	5.72
122.	10.	4.60	0.22	70.05	12.03	0.00	0.5995	−0.0075	0.5879	0.1176	0.0124	−0.0005	−0.0014	−0.0046	5.02
122.	11.	4.60	0.22	70.29	14.00	0.00	0.6810	−0.0118	0.6636	0.1532	0.0260	−0.0004	−0.0021	−0.0064	4.34
122.	12.	4.59	0.22	70.06	16.09	0.00	0.7454	−0.0155	0.7205	0.1917	0.0430	0.0020	−0.0076	−0.0170	3.76
122.	13.	4.59	0.22	70.07	18.02	0.00	0.8323	−0.0193	0.7974	0.2391	0.0596	0.0021	−0.0089	−0.0236	3.33
122.	14.	4.58	0.22	69.86	20.07	0.00	0.9233	−0.0204	0.8743	0.2976	0.0784	−0.0008	−0.0077	−0.0153	2.94
123.	2.	4.60	0.22	69.94	−4.00	0.00	0.0246	0.0335	0.0268	0.0317	−0.0322	0.0002	−0.0005	0.0000	0.88
123.	3.	4.60	0.22	70.05	−1.99	0.00	0.0936	0.0315	0.0946	0.0282	−0.0268	0.0001	−0.0005	−0.0010	3.49
123.	4.	4.60	0.22	70.16	0.04	0.00	0.1672	0.0293	0.1671	0.0294	−0.0215	−0.0002	−0.0005	−0.0001	5.92
123.	5.	4.60	0.22	70.16	2.07	0.00	0.2420	0.0258	0.2409	0.0345	−0.0177	−0.0003	−0.0005	0.0002	7.22
123.	6.	4.58	0.22	69.70	4.05	0.00	0.3120	0.0214	0.3098	0.0434	−0.0140	−0.0006	−0.0006	−0.0002	7.31
123.	7.	4.59	0.22	69.93	6.20	0.00	0.3856	0.0142	0.3819	0.0558	−0.0096	−0.0007	−0.0011	−0.0008	6.96
123.	8.	4.58	0.22	70.04	8.09	0.00	0.4514	0.0079	0.4458	0.0714	−0.0028	−0.0013	−0.0010	−0.0013	6.32
123.	9.	4.58	0.22	70.05	10.27	0.00	0.5237	0.0005	0.5152	0.0938	0.0062	−0.0009	−0.0014	−0.0022	5.53
123.	10.	4.59	0.22	70.28	12.26	0.00	0.6073	−0.0046	0.5944	0.1245	0.0147	−0.0003	−0.0015	−0.0012	4.80
123.	11.	4.59	0.22	70.41	14.24	0.00	0.6790	−0.0091	0.6603	0.1582	0.0312	0.0009	−0.0027	−0.0065	4.19
123.	12.	4.58	0.22	70.06	16.12	0.00	0.7398	−0.0144	0.7147	0.1916	0.0473	0.0023	−0.0068	−0.0173	3.74
123.	13.	4.57	0.22	70.08	18.20	0.00	0.8225	−0.0152	0.7861	0.2424	0.0662	0.0022	−0.0100	−0.0224	3.25
123.	14.	4.56	0.22	69.75	20.18	0.00	0.9062	−0.0154	0.8559	0.2981	0.0855	−0.0002	−0.0116	−0.0190	2.87
124.	2.	4.62	0.22	70.05	−4.08	0.00	0.0180	0.0326	0.0202	0.0312	−0.0322	0.0002	0.0002	0.0004	0.67
124.	3.	4.61	0.22	70.05	−2.02	0.00	0.0946	0.0329	0.0957	0.0295	−0.0254	0.0000	0.0001	0.0029	3.37
124.	4.	4.61	0.22	70.28	0.01	0.00	0.1690	0.0289	0.1690	0.0289	−0.0218	−0.0004	−0.0002	−0.0005	6.10
124.	5.	4.60	0.22	70.04	2.13	0.00	0.2440	0.0251	0.2429	0.0341	−0.0180	−0.0005	−0.0003	0.0002	7.39
124.	6.	4.59	0.22	69.93	4.18	0.00	0.3176	0.0203	0.3153	0.0435	−0.0141	−0.0006	−0.0003	−0.0002	7.45
124.	7.	4.59	0.22	70.04	6.15	0.00	0.3869	0.0142	0.3832	0.0555	−0.0099	−0.0006	−0.0007	0.0005	7.03
124.	8.	4.58	0.22	69.70	8.20	0.00	0.4590	0.0071	0.4533	0.0725	−0.0029	−0.0011	−0.0007	0.0011	6.34
124.	9.	4.59	0.22	70.16	10.15	0.00	0.5237	−0.0011	0.5157	0.0912	0.0052	−0.0011	−0.0012	−0.0018	5.70
124.	10.	4.59	0.22	70.17	12.17	0.00	0.6059	−0.0073	0.5938	0.1206	0.0147	−0.0012	−0.0012	−0.0020	4.95
124.	11.	4.60	0.22	70.52	14.10	0.00	0.6900	−0.0106	0.6718	0.1578	0.0265	−0.0007	−0.0021	−0.0046	4.27
124.	12.	4.57	0.22	69.84	16.11	0.00	0.7615	−0.0130	0.7352	0.1989	0.0467	0.0003	−0.0039	−0.0081	3.70
124.	13.	4.57	0.22	69.85	18.16	0.00	0.8467	−0.0149	0.8091	0.2497	0.0636	0.0005	−0.0064	−0.0133	3.24
124.	14.	4.58	0.22	70.22	20.23	0.00	0.9406	−0.0159	0.8880	0.3104	0.0817	−0.0001	−0.0088	−0.0145	2.86
129.	2.	4.75	0.22	70.16	−4.00	0.00	−0.0585	0.0125	−0.0575	0.0165	0.0152	0.0003	0.0002	−0.0016	−3.57
129.	3.	4.75	0.22	70.16	−2.02	0.00	0.0154	0.0173	0.0161	0.0168	0.0226	0.0002	−0.0001	0.0007	0.99
129.	4.	4.74	0.22	70.16	0.06	0.00	0.0882	0.0214	0.0882	0.0215	0.0311	−0.0001	−0.0003	0.0019	4.22
129.	5.	4.74	0.22	70.16	2.03	0.00	0.1512	0.0231	0.1503	0.0285	0.0374	−0.0002	−0.0003	0.0011	5.41
129.	6.	4.74	0.22	70.17	4.19	0.00	0.2404	0.0271	0.2378	0.0446	0.0480	0.0000	−0.0005	0.0021	5.41
129.	7.	4.73	0.22	70.06	6.04	0.00	0.3179	0.0312	0.3128	0.0645	0.0634	−0.0007	−0.0004	0.0001	4.90
129.	8.	4.73	0.22	69.95	8.20	0.00	0.4259	0.0376	0.4162	0.0980	0.0905	−0.0009	−0.0003	−0.0020	4.25
129.	9.	4.73	0.22	69.97	10.09	0.00	0.5088	0.0425	0.4935	0.1309	0.1130	−0.0012	−0.0004	−0.0015	3.77
129.	10.	4.73	0.22	69.98	12.25	0.00	0.6154	0.0486	0.5911	0.1780	0.1371	−0.0009	−0.0007	−0.0007	3.32
129.	11.	4.73	0.22	70.23	14.14	0.00	0.7117	0.0536	0.6770	0.2258	0.1602	−0.0009	−0.0013	−0.0024	2.99
129.	12.	4.72	0.22	69.90	16.09	0.00	0.8131	0.0585	0.7650	0.2816	0.1838	−0.0008	−0.0023	−0.0047	2.71
129.	13.	4.71	0.22	69.92	18.14	0.00	0.9261	0.0644	0.8600	0.3495	0.2095	−0.0002	−0.0046	−0.0061	2.45
129.	15.	4.72	0.22	70.40	20.19	0.00	1.0463	0.0707	0.9576	0.4275	0.2385	0.0010	−0.0099	−0.0133	2.23
130.	2.	4.70	0.22	70.04	−4.06	0.00	−0.0551	0.0133	−0.0540	0.0172	0.0163	0.0006	−0.0001	0.0009	−3.23
130.	3.	4.69	0.22	69.93	−2.00	0.00	0.0221	0.0184	0.0228	0.0176	0.0258	0.0004	−0.0004	0.0023	1.33
130.	4.	4.69	0.22	69.93	0.05	0.00	0.0880	0.0219	0.0880	0.0220	0.0352	0.0001	−0.0004	0.0011	4.13
130.	5.	4.69	0.22	70.05	2.08	0.00	0.1575	0.0250	0.1565	0.0307	0.0438	0.0000	−0.0006	0.0022	5.23

Table B2. Continued

Run	Point	$R/10^6$	M	q	α	β	C_N	C_A	C_L	C_D	C_m	C_l	C_n	C_Y	L/D
130.	6.	4.69	0.22	69.94	4.12	0.00	0.2388	0.0282	0.2362	0.0453	0.0535	−0.0002	−0.0009	0.0022	5.31
130.	7.	4.70	0.22	70.29	6.11	0.00	0.3261	0.0338	0.3206	0.0683	0.0689	−0.0008	−0.0008	0.0021	4.75
130.	8.	4.69	0.22	70.19	8.22	0.00	0.4090	0.0401	0.3991	0.0981	0.0955	−0.0010	−0.0009	0.0027	4.09
130.	9.	4.68	0.22	69.86	10.15	0.00	0.5149	0.0477	0.4984	0.1377	0.1212	0.0012	−0.0007	0.0003	3.62
130.	10.	4.68	0.22	69.98	12.17	0.00	0.6244	0.0538	0.5990	0.1843	0.1448	−0.0003	−0.0008	−0.0016	3.25
130.	11.	4.68	0.22	70.12	14.17	0.00	0.7251	0.0605	0.6882	0.2362	0.1737	−0.0011	−0.0014	−0.0012	2.91
130.	12.	4.69	0.22	70.25	16.21	0.00	0.8392	0.0690	0.7865	0.3006	0.2036	−0.0007	−0.0021	0.0011	2.61
130.	13.	4.68	0.22	70.16	18.22	0.00	0.9462	0.0752	0.8752	0.3673	0.2317	−0.0004	−0.0038	−0.0026	2.38
130.	14.	4.68	0.22	70.18	20.28	0.00	1.0579	0.0820	0.9639	0.4436	0.2628	0.0004	−0.0081	−0.0088	2.17
131.	11.	4.57	0.22	70.16	−4.16	0.00	−0.1198	0.0181	−0.1182	0.0268	0.0041	0.0006	−0.0001	0.0003	−4.46
131.	12.	4.57	0.22	70.16	−1.98	0.00	−0.0369	0.0193	−0.0362	0.0206	0.0146	0.0001	−0.0003	−0.0016	−1.79
131.	13.	4.56	0.22	69.93	0.02	0.00	0.0496	0.0210	0.0496	0.0210	0.0254	0.0000	−0.0003	0.0010	2.42
131.	14.	4.56	0.22	70.05	2.09	0.00	0.1335	0.0207	0.1327	0.0256	0.0349	−0.0002	−0.0003	0.0004	5.33
131.	15.	4.56	0.22	70.05	4.06	0.00	0.2051	0.0199	0.2032	0.0344	0.0461	−0.0004	−0.0005	0.0000	6.03
131.	16.	4.56	0.22	70.05	6.19	0.00	0.2818	0.0201	0.2779	0.0503	0.0627	−0.0004	−0.0006	0.0007	5.60
131.	17.	4.56	0.22	69.94	8.17	0.00	0.3467	0.0170	0.3408	0.0661	0.0779	−0.0006	−0.0008	−0.0011	5.21
131.	18.	4.58	0.22	70.52	10.10	0.00	0.4266	0.0147	0.4174	0.0892	0.0924	−0.0002	−0.0011	0.0001	4.71
131.	19.	4.56	0.22	70.18	12.23	0.00	0.5141	0.0090	0.5005	0.1177	0.1051	−0.0003	−0.0017	−0.0017	4.27
131.	20.	4.56	0.22	70.20	14.33	0.00	0.6032	0.0079	0.5825	0.1569	0.1283	−0.0004	−0.0040	−0.0038	3.72
131.	21.	4.56	0.22	70.09	16.15	0.00	0.6829	0.0104	0.6530	0.2000	0.1512	0.0003	−0.0054	−0.0055	3.27
131.	22.	4.57	0.22	70.34	18.29	0.00	0.7882	0.0152	0.7436	0.2618	0.1777	0.0009	−0.0071	−0.0085	2.84
131.	23.	4.56	0.22	70.01	20.14	0.00	0.8972	0.0188	0.8359	0.3266	0.2027	0.0025	−0.0111	−0.0169	2.56
132.	2.	4.58	0.22	70.28	−4.09	0.00	−0.1177	0.0175	−0.1161	0.0259	0.0020	0.0005	0.0002	−0.0009	−4.55
132.	3.	4.58	0.22	70.39	−2.00	0.00	−0.0386	0.0181	−0.0379	0.0194	0.0110	0.0000	−0.0004	−0.0005	−2.00
132.	4.	4.57	0.22	70.04	−0.03	0.00	0.0425	0.0184	0.0425	0.0184	0.0197	−0.0002	−0.0005	−0.0009	2.40
132.	5.	4.57	0.22	70.16	2.04	0.00	0.1284	0.0174	0.1276	0.0220	0.0259	−0.0004	−0.0005	0.0001	5.99
132.	6.	4.56	0.22	70.04	4.11	0.00	0.2002	0.0152	0.1986	0.0295	0.0339	−0.0007	−0.0006	−0.0015	6.91
132.	7.	4.57	0.22	70.39	6.10	0.00	0.2661	0.0128	0.2632	0.0410	0.0453	−0.0009	−0.0010	−0.0016	6.54
132.	8.	4.57	0.22	70.17	8.12	0.00	0.3403	0.0108	0.3354	0.0587	0.0581	−0.0007	−0.0008	0.0000	5.79
132.	9.	4.56	0.22	70.06	10.18	0.00	0.4156	0.0056	0.4081	0.0790	0.0691	−0.0005	−0.0015	−0.0015	5.22
132.	10.	4.57	0.22	70.18	12.19	0.00	0.5087	0.0024	0.4967	0.1098	0.0781	0.0004	−0.0023	0.0006	4.56
132.	11.	4.57	0.22	70.19	14.21	0.00	0.5866	−0.0023	0.5693	0.1417	0.0946	0.0006	−0.0042	−0.0061	4.03
132.	12.	4.56	0.22	70.08	16.22	0.00	0.6711	−0.0014	0.6447	0.1861	0.1188	0.0012	−0.0059	−0.0088	3.47
132.	13.	4.56	0.22	69.87	18.19	0.00	0.7645	0.0025	0.7255	0.2410	0.1409	0.0010	−0.0070	−0.0148	3.01
132.	14.	4.56	0.22	70.00	20.16	0.00	0.8746	0.0073	0.8185	0.3082	0.1645	0.0024	−0.0109	−0.0211	2.65
133.	6.	4.71	0.22	70.06	−4.03	5.00	−0.1158	0.0181	−0.1143	0.0262	−0.0040	0.0031	−0.0089	−0.0141	−4.45
133.	7.	4.71	0.22	70.05	−2.03	5.00	−0.0400	0.0180	−0.0393	0.0194	0.0065	0.0016	−0.0078	−0.0140	−2.09
133.	8.	4.71	0.22	70.28	−0.01	5.00	0.0418	0.0184	0.0418	0.0184	0.0166	−0.0002	−0.0070	−0.0115	2.36
133.	9.	4.71	0.22	70.17	2.06	5.00	0.1305	0.0194	0.1297	0.0241	0.0247	−0.0031	−0.0061	−0.0045	5.57
133.	10.	4.69	0.22	69.83	4.09	5.00	0.1988	0.0161	0.1971	0.0303	0.0330	−0.0078	−0.0064	−0.0050	6.70
133.	11.	4.69	0.22	69.83	6.10	5.00	0.2723	0.0137	0.2693	0.0425	0.0436	−0.0110	−0.0073	−0.0008	6.47
133.	12.	4.70	0.22	70.07	8.12	5.00	0.3434	0.0105	0.3384	0.0589	0.0561	−0.0127	−0.0084	0.0017	5.85
133.	13.	4.70	0.22	70.08	10.18	5.00	0.4193	0.0066	0.4116	0.0806	0.0688	−0.0146	−0.0115	0.0032	5.18
133.	14.	4.70	0.22	70.10	12.37	5.00	0.5100	0.0040	0.4973	0.1131	0.0830	−0.0181	−0.0163	0.0093	4.44
133.	15.	4.70	0.22	70.12	14.14	5.00	0.5889	0.0030	0.5703	0.1468	0.0971	−0.0218	−0.0164	0.0274	3.91
133.	16.	4.70	0.22	70.15	16.16	5.00	0.6808	0.0033	0.6530	0.1926	0.1169	−0.0237	−0.0160	0.0408	3.40
133.	17.	4.70	0.22	70.31	18.39	5.00	0.7894	0.0058	0.7473	0.2545	0.1443	−0.0264	−0.0115	0.0499	2.95
133.	18.	4.70	0.22	70.34	20.16	5.00	0.8757	0.0065	0.8198	0.3079	0.1667	−0.0268	−0.0125	0.0535	2.67
134.	1.	4.68	0.22	69.94	−4.03	−5.00	−0.1191	0.0172	−0.1176	0.0256	−0.0032	−0.0014	0.0080	0.0124	−4.71
134.	2.	4.68	0.22	69.94	−2.07	−5.00	−0.0413	0.0179	−0.0407	0.0193	0.0067	−0.0003	0.0067	0.0089	−2.17

Table B2. Continued

Run	Point	$R/10^6$	M	q	α	β	C_N	C_A	C_L	C_D	C_m	C_l	C_n	C_Y	L/D
134.	3.	4.68	0.22	69.94	−0.04	−5.00	0.0445	0.0194	0.0445	0.0194	0.0174	0.0012	0.0055	0.0099	2.38
134.	4.	4.69	0.22	70.17	2.09	−5.00	0.1247	0.0169	0.1240	0.0214	0.0243	0.0038	0.0048	0.0036	5.99
134.	5.	4.69	0.22	70.40	4.11	−5.00	0.2033	0.0168	0.2015	0.0313	0.0337	0.0081	0.0051	0.0036	6.60
134.	6.	4.69	0.22	70.17	6.07	−5.00	0.2645	0.0119	0.2617	0.0399	0.0438	0.0107	0.0054	−0.0036	6.70
134.	7.	4.69	0.22	70.19	8.12	−5.00	0.3424	0.0107	0.3374	0.0589	0.0575	0.0118	0.0056	−0.0035	5.80
134.	8.	4.69	0.22	70.20	10.16	−5.00	0.4170	0.0055	0.4095	0.0789	0.0692	0.0141	0.0066	−0.0125	5.25
134.	9.	4.69	0.22	70.21	12.12	−5.00	0.4952	0.0020	0.4838	0.1059	0.0816	0.0190	0.0078	−0.0252	4.59
134.	10.	4.68	0.22	70.12	14.10	−5.00	0.5790	0.0005	0.5614	0.1415	0.0990	0.0248	0.0049	−0.0479	3.98
134.	11.	4.70	0.22	70.49	16.24	−5.00	0.6793	0.0027	0.6514	0.1925	0.1213	0.0303	−0.0022	−0.0661	3.39
134.	12.	4.67	0.22	69.72	18.21	−5.00	0.7719	0.0053	0.7316	0.2463	0.1460	0.0288	−0.0041	−0.0683	2.98
134.	13.	4.69	0.22	70.34	20.25	−5.00	0.8697	0.0062	0.8138	0.3069	0.1718	0.0260	0.0018	−0.0685	2.66
135.	2.	4.68	0.22	70.29	−3.99	5.00	−0.1152	0.0173	−0.1137	0.0253	−0.0037	−0.0010	0.0084	0.0128	−4.60
135.	3.	4.68	0.22	70.28	−2.00	5.00	−0.0370	0.0174	−0.0364	0.0187	0.0052	0.0003	0.0067	0.0100	−2.03
135.	4.	4.68	0.22	70.16	−0.01	5.00	0.0461	0.0168	0.0461	0.0168	0.0102	0.0009	0.0058	0.0096	2.87
135.	5.	4.68	0.22	70.28	2.06	5.00	0.1281	0.0142	0.1275	0.0188	0.0129	0.0029	0.0047	0.0092	7.09
135.	6.	4.67	0.22	70.16	4.03	5.00	0.1960	0.0095	0.1949	0.0233	0.0174	0.0062	0.0048	0.0083	8.68
135.	7.	4.68	0.22	70.40	6.21	5.00	0.2716	0.0048	0.2694	0.0341	0.0245	0.0088	0.0056	0.0095	8.06
135.	8.	4.67	0.22	70.17	8.16	5.00	0.3374	−0.0026	0.3344	0.0454	0.0320	0.0097	0.0066	0.0076	7.46
135.	9.	4.67	0.22	70.07	10.35	5.00	0.4217	−0.0087	0.4164	0.0672	0.0420	0.0098	0.0076	0.0069	6.23
135.	10.	4.66	0.22	69.97	12.47	5.00	0.5074	−0.0153	0.4988	0.0946	0.0516	0.0144	0.0073	−0.0046	5.28
135.	11.	4.68	0.22	70.57	14.51	5.00	0.5857	−0.0170	0.5713	0.1302	0.0690	0.0215	0.0039	−0.0264	4.39
135.	12.	4.67	0.22	70.13	16.52	5.00	0.6770	−0.0169	0.6539	0.1763	0.0874	0.0223	−0.0018	−0.0362	3.71
135.	13.	4.67	0.22	70.28	18.55	5.00	0.7676	−0.0190	0.7338	0.2262	0.1036	0.0177	0.0010	−0.0248	3.24
135.	14.	4.67	0.22	70.08	20.11	5.00	0.8495	−0.0196	0.8044	0.2737	0.1184	0.0153	0.0066	−0.0101	2.93
136.	1.	4.66	0.22	70.06	−4.17	−5.00	−0.1248	0.0174	−0.1232	0.0265	−0.0056	0.0027	−0.0090	−0.0158	−4.77
136.	2.	4.67	0.22	70.17	−2.06	−5.00	−0.0369	0.0185	−0.0362	0.0198	0.0039	0.0015	−0.0081	−0.0110	−1.91
136.	3.	4.67	0.22	70.28	−0.06	−5.00	0.0442	0.0175	0.0442	0.0175	0.0090	0.0008	−0.0070	−0.0094	2.67
136.	4.	4.67	0.22	70.05	1.92	−5.00	0.1152	0.0131	0.1147	0.0169	0.0116	−0.0015	−0.0063	−0.0116	7.16
136.	5.	4.67	0.22	70.16	4.14	−5.00	0.1988	0.0092	0.1976	0.0236	0.0172	−0.0059	−0.0064	−0.0113	8.71
136.	6.	4.67	0.22	70.17	6.14	−5.00	0.2697	0.0043	0.2677	0.0332	0.0233	−0.0081	−0.0074	−0.0114	8.27
136.	7.	4.67	0.22	70.06	8.12	−5.00	0.3382	−0.0026	0.3352	0.0452	0.0310	−0.0092	−0.0092	−0.0125	7.53
136.	8.	4.67	0.22	70.19	10.16	−5.00	0.4179	−0.0072	0.4127	0.0666	0.0411	−0.0084	−0.0114	−0.0129	6.23
136.	9.	4.68	0.22	70.20	12.08	−5.00	0.4962	−0.0130	0.4880	0.0912	0.0496	−0.0103	−0.0151	−0.0153	5.37
136.	10.	4.68	0.22	70.33	14.05	−5.00	0.5731	−0.0178	0.5603	0.1219	0.0619	−0.0142	−0.0162	−0.0077	4.60
136.	11.	4.69	0.22	70.47	16.05	−5.00	0.6554	−0.0198	0.6353	0.1622	0.0785	−0.0161	−0.0165	−0.0029	3.91
136.	12.	4.68	0.22	70.17	18.24	−5.00	0.7617	−0.0157	0.7283	0.2234	0.1014	−0.0171	−0.0105	0.0088	3.26
136.	13.	4.68	0.22	70.20	20.09	−5.00	0.8464	−0.0186	0.8012	0.2733	0.1175	−0.0188	−0.0128	0.0102	2.93
137.	2.	4.65	0.22	70.06	−4.05	0.00	−0.1178	0.0174	−0.1162	0.0256	0.0014	0.0013	0.0002	0.0001	−4.60
137.	3.	4.65	0.22	70.17	−1.99	0.00	−0.0318	0.0195	−0.0311	0.0206	0.0094	0.0010	0.0000	0.0029	−1.55
137.	4.	4.65	0.22	70.17	0.02	0.00	0.0523	0.0190	0.0523	0.0190	0.0168	−0.0001	0.0002	0.0038	2.85
137.	5.	4.65	0.22	70.16	2.09	0.00	0.1308	0.0149	0.1302	0.0197	0.0200	−0.0013	0.0001	0.0029	6.88
137.	6.	4.65	0.22	70.28	4.04	0.00	0.2057	0.0136	0.2042	0.0280	0.0260	−0.0021	0.0006	0.0078	7.49
137.	7.	4.64	0.22	70.17	6.11	0.00	0.2716	0.0095	0.2691	0.0384	0.0352	−0.0031	0.0004	0.0098	7.15
137.	8.	4.65	0.22	70.41	8.08	0.00	0.3364	0.0040	0.3325	0.0513	0.0448	−0.0036	0.0007	0.0090	6.57
137.	9.	4.65	0.22	70.42	10.18	0.00	0.4183	−0.0015	0.4120	0.0725	0.0538	−0.0044	0.0009	0.0110	5.72
137.	10.	4.64	0.22	70.09	12.20	0.00	0.5027	−0.0066	0.4927	0.0998	0.0627	−0.0035	0.0000	0.0093	4.96
137.	11.	4.65	0.22	70.46	14.23	0.00	0.5903	−0.0097	0.5746	0.1357	0.0769	−0.0035	0.0002	0.0041	4.24
137.	12.	4.64	0.22	70.14	16.21	0.00	0.6653	−0.0105	0.6418	0.1757	0.0994	−0.0034	0.0002	0.0071	3.66
137.	13.	4.64	0.22	70.06	18.13	0.00	0.7562	−0.0087	0.7214	0.2270	0.1178	−0.0047	−0.0007	0.0047	3.18
137.	14.	4.64	0.22	69.87	20.23	0.00	0.8582	−0.0072	0.8078	0.2899	0.1419	−0.0072	0.0009	0.0105	2.78

Table B2. Continued

Run	Point	$R/10^6$	M	q	α	β	C_N	C_A	C_L	C_D	C_m	C_l	C_n	C_Y	L/D
138.	2.	4.64	0.22	70.06	−4.12	−5.00	−0.1202	0.0181	−0.1186	0.0267	−0.0044	−0.0011	0.0082	0.0151	−4.52
138.	3.	4.64	0.22	70.17	−2.06	−5.00	−0.0344	0.0195	−0.0337	0.0208	0.0058	0.0009	0.0073	0.0139	−1.67
138.	4.	4.64	0.22	70.17	0.01	−5.00	0.0482	0.0179	0.0482	0.0180	0.0123	0.0008	0.0062	0.0117	2.78
138.	5.	4.64	0.22	70.05	2.03	−5.00	0.1237	0.0154	0.1231	0.0198	0.0162	0.0024	0.0056	0.0110	6.44
138.	6.	4.64	0.22	70.05	4.05	−5.00	0.2026	0.0141	0.2010	0.0284	0.0229	0.0058	0.0062	0.0146	7.27
138.	7.	4.64	0.22	70.06	6.08	−5.00	0.2715	0.0096	0.2690	0.0383	0.0319	0.0075	0.0074	0.0140	7.18
138.	8.	4.64	0.22	70.07	8.13	−5.00	0.3397	0.0042	0.3357	0.0522	0.0427	0.0076	0.0082	0.0128	6.52
138.	9.	4.64	0.22	70.08	10.25	−5.00	0.4235	0.0004	0.4166	0.0757	0.0546	0.0081	0.0106	0.0093	5.57
138.	10.	4.64	0.22	70.09	12.09	−5.00	0.4964	−0.0045	0.4863	0.0996	0.0635	0.0121	0.0112	0.0025	4.91
138.	11.	4.61	0.22	69.31	14.14	−5.00	0.5778	−0.0072	0.5620	0.1342	0.0798	0.0186	0.0090	−0.0154	4.20
138.	12.	4.65	0.22	70.48	16.09	−5.00	0.6599	−0.0083	0.6364	0.1750	0.0973	0.0222	0.0035	−0.0372	3.64
138.	13.	4.64	0.22	70.06	18.20	−5.00	0.7569	−0.0075	0.7214	0.2293	0.1198	0.0208	0.0025	−0.0393	3.15
138.	14.	4.63	0.22	69.86	20.16	−5.00	0.8511	−0.0074	0.8015	0.2864	0.1402	0.0168	0.0092	−0.0277	2.80
139.	1.	4.64	0.22	70.17	−4.05	5.00	−0.1183	0.0178	−0.1168	0.0262	−0.0047	0.0034	−0.0085	−0.0159	−4.57
139.	2.	4.65	0.22	70.51	−2.00	5.00	−0.0365	0.0183	−0.0358	0.0196	0.0058	0.0021	−0.0078	−0.0109	−1.90
139.	3.	4.66	0.22	70.62	0.00	5.00	0.0469	0.0182	0.0469	0.0182	0.0149	−0.0001	−0.0064	−0.0084	2.70
139.	4.	4.64	0.22	70.17	2.07	5.00	0.1264	0.0163	0.1257	0.0208	0.0208	−0.0037	−0.0053	−0.0048	6.30
139.	5.	4.64	0.22	70.17	4.05	5.00	0.1995	0.0136	0.1981	0.0276	0.0275	−0.0085	−0.0050	−0.0008	7.40
139.	6.	4.65	0.22	70.40	6.09	5.00	0.2731	0.0100	0.2705	0.0389	0.0363	−0.0120	−0.0055	0.0032	7.09
139.	7.	4.65	0.22	70.41	8.08	5.00	0.3440	0.0048	0.3399	0.0531	0.0455	−0.0143	−0.0063	0.0083	6.49
139.	8.	4.65	0.22	70.42	10.20	5.00	0.4194	−0.0002	0.4128	0.0741	0.0588	−0.0161	−0.0079	0.0102	5.61
139.	9.	4.64	0.22	70.21	12.11	5.00	0.4990	−0.0044	0.4888	0.1004	0.0686	−0.0192	−0.0117	0.0120	4.89
139.	10.	4.65	0.22	70.46	14.31	5.00	0.5941	−0.0060	0.5772	0.1410	0.0852	−0.0235	−0.0133	0.0262	4.09
139.	11.	4.64	0.22	69.91	16.12	5.00	0.6775	−0.0062	0.6526	0.1822	0.1011	−0.0253	−0.0119	0.0396	3.58
139.	12.	4.65	0.22	70.29	18.20	5.00	0.7786	−0.0037	0.7408	0.2397	0.1225	−0.0266	−0.0058	0.0435	3.09
139.	13.	4.65	0.22	70.11	20.39	5.00	0.8941	−0.0023	0.8389	0.3093	0.1498	−0.0253	−0.0085	0.0461	2.71
140.	2.	4.68	0.22	70.16	−4.05	−5.00	−0.0631	0.0076	−0.0625	0.0120	0.0016	0.0026	−0.0051	−0.0067	−5.46
140.	3.	4.68	0.22	70.39	−1.99	−5.00	0.0158	0.0115	0.0162	0.0109	0.0086	0.0008	−0.0043	−0.0030	1.57
140.	4.	4.67	0.22	70.04	0.03	−5.00	0.0810	0.0132	0.0810	0.0132	0.0135	−0.0018	−0.0044	−0.0051	6.51
140.	5.	4.68	0.22	70.51	2.03	−5.00	0.1549	0.0142	0.1543	0.0197	0.0182	−0.0043	−0.0051	−0.0050	8.14
140.	6.	4.67	0.22	70.17	4.09	−5.00	0.2403	0.0168	0.2385	0.0339	0.0258	−0.0071	−0.0056	−0.0007	7.20
140.	7.	4.67	0.22	70.18	6.11	−5.00	0.3221	0.0175	0.3185	0.0517	0.0354	−0.0111	−0.0058	0.0007	6.24
140.	8.	4.66	0.22	70.08	8.10	−5.00	0.4187	0.0221	0.4114	0.0808	0.0509	−0.0137	−0.0049	0.0006	5.12
140.	9.	4.66	0.22	69.99	10.16	−5.00	0.5127	0.0254	0.5002	0.1155	0.0707	−0.0158	−0.0054	−0.0012	4.34
140.	10.	4.67	0.22	70.13	12.13	−5.00	0.6085	0.0286	0.5889	0.1558	0.0928	−0.0166	−0.0071	−0.0057	3.78
140.	11.	4.67	0.22	70.16	14.21	−5.00	0.7172	0.0344	0.6868	0.2094	0.1180	−0.0193	−0.0053	0.0015	3.28
140.	12.	4.67	0.22	70.20	16.18	−5.00	0.8224	0.0381	0.7792	0.2658	0.1431	−0.0230	−0.0044	0.0041	2.92
140.	13.	4.68	0.22	70.24	18.23	−5.00	0.9405	0.0435	0.8797	0.3355	0.1711	−0.0260	−0.0031	0.0083	2.61
140.	14.	4.67	0.22	70.17	20.22	−5.00	1.0561	0.0481	0.9744	0.4102	0.2014	−0.0289	−0.0062	0.0071	2.37
141.	1.	4.67	0.22	70.27	−4.01	5.00	−0.0587	0.0078	−0.0580	0.0119	0.0026	−0.0007	0.0044	0.0076	−5.14
141.	2.	4.66	0.22	70.04	−1.99	5.00	0.0119	0.0104	0.0123	0.0100	0.0086	0.0010	0.0039	0.0047	1.33
141.	3.	4.67	0.22	70.27	0.04	5.00	0.0825	0.0134	0.0824	0.0134	0.0138	0.0034	0.0035	0.0066	6.49
141.	4.	4.68	0.22	70.39	2.04	5.00	0.1532	0.0137	0.1527	0.0192	0.0193	0.0056	0.0037	0.0028	8.28
141.	5.	4.68	0.22	70.40	4.04	5.00	0.2339	0.0156	0.2322	0.0320	0.0257	0.0080	0.0041	0.0011	7.41
141.	6.	4.68	0.22	70.30	6.05	5.00	0.3191	0.0175	0.3154	0.0510	0.0371	0.0108	0.0041	−0.0012	6.25
141.	7.	4.68	0.22	70.43	8.14	5.00	0.4188	0.0217	0.4115	0.0808	0.0536	0.0137	0.0029	−0.0003	5.12
141.	8.	4.67	0.22	70.10	10.21	5.00	0.5087	0.0240	0.4964	0.1138	0.0716	0.0157	0.0021	−0.0039	4.37
141.	9.	4.68	0.22	70.25	12.20	5.00	0.6084	0.0284	0.5887	0.1564	0.0935	0.0186	0.0001	−0.0076	3.76
141.	10.	4.69	0.22	70.51	14.19	5.00	0.7084	0.0325	0.6788	0.2052	0.1201	0.0223	−0.0042	−0.0178	3.30
141.	11.	4.67	0.22	70.08	16.21	5.00	0.7998	0.0370	0.7577	0.2588	0.1512	0.0227	−0.0085	−0.0239	2.92

Table B2. Continued

Run	Point	$R/10^6$	M	q	α	β	C_N	C_A	C_L	C_D	C_m	C_l	C_n	C_Y	L/D
141.	12.	4.68	0.22	70.23	18.23	5.00	0.8973	0.0400	0.8398	0.3187	0.1774	0.0229	−0.0095	−0.0289	2.63
141.	13.	4.66	0.22	69.71	20.27	5.00	1.0207	0.0462	0.9415	0.3970	0.2067	0.0237	−0.0043	−0.0236	2.36
142.	2.	4.70	0.22	69.95	−4.03	0.00	0.0166	0.0317	0.0188	0.0305	−0.0312	0.0003	0.0001	−0.0008	0.64
142.	3.	4.68	0.22	69.83	−2.00	0.00	0.0913	0.0319	0.0924	0.0287	−0.0217	0.0000	−0.0002	0.0003	3.36
142.	4.	4.67	0.22	69.71	0.07	0.00	0.1731	0.0312	0.1731	0.0314	−0.0144	−0.0004	−0.0005	0.0004	5.75
142.	5.	4.67	0.22	69.83	2.12	0.00	0.2513	0.0296	0.2500	0.0389	−0.0072	−0.0006	−0.0004	−0.0004	6.64
142.	6.	4.67	0.22	70.18	4.13	0.00	0.3229	0.0279	0.3200	0.0511	0.0020	−0.0009	−0.0007	0.0000	6.44
142.	7.	4.66	0.22	69.96	6.09	0.00	0.3927	0.0252	0.3878	0.0667	0.0121	−0.0008	−0.0009	0.0001	5.93
142.	8.	4.67	0.22	70.43	8.11	0.00	0.4663	0.0205	0.4588	0.0861	0.0219	−0.0012	−0.0011	−0.0013	5.42
142.	9.	4.66	0.22	70.33	10.14	0.00	0.5437	0.0166	0.5323	0.1121	0.0327	−0.0011	−0.0012	0.0012	4.82
142.	10.	4.67	0.22	70.57	12.14	0.00	0.6337	0.0122	0.6170	0.1452	0.0419	−0.0008	−0.0022	0.0001	4.29
142.	11.	4.66	0.22	70.48	14.13	0.00	0.7230	0.0115	0.6983	0.1877	0.0593	−0.0010	−0.0031	0.0004	3.75
142.	12.	4.65	0.22	70.29	16.27	0.00	0.8107	0.0130	0.7746	0.2396	0.0858	−0.0007	−0.0030	−0.0027	3.25
142.	13.	4.67	0.22	71.14	18.19	0.00	0.9107	0.0194	0.8591	0.3027	0.1054	0.0002	−0.0058	−0.0066	2.85
142.	14.	4.64	0.22	70.15	20.25	0.00	1.0315	0.0251	0.9591	0.3807	0.1300	0.0001	−0.0070	−0.0104	2.52
146.	2.	3.09	0.14	30.02	−4.04	0.00	−0.1336	0.0122	−0.1324	0.0216	0.0007	0.0001	0.0001	−0.0061	−6.08
146.	3.	3.08	0.14	30.02	−1.98	0.00	−0.0484	0.0139	−0.0478	0.0155	0.0068	−0.0003	−0.0006	−0.0049	−3.07
146.	4.	3.09	0.14	30.13	0.06	0.00	0.0402	0.0134	0.0402	0.0135	0.0121	−0.0005	−0.0006	−0.0020	3.00
146.	5.	3.08	0.14	30.02	2.07	0.00	0.1157	0.0091	0.1153	0.0133	0.0129	−0.0008	−0.0008	−0.0070	8.83
146.	6.	3.08	0.14	30.02	4.05	0.00	0.1925	0.0060	0.1916	0.0195	0.0161	−0.0011	−0.0007	−0.0070	9.86
146.	8.	3.06	0.14	29.79	6.07	0.00	0.2625	0.0023	0.2607	0.0301	0.0228	−0.0009	−0.0011	−0.0051	8.70
146.	9.	3.06	0.14	29.79	8.14	0.00	0.3352	−0.0027	0.3322	0.0448	0.0312	−0.0007	−0.0005	−0.0047	7.41
146.	10.	3.08	0.14	30.14	10.10	0.00	0.4152	−0.0092	0.4103	0.0637	0.0373	−0.0010	−0.0006	−0.0022	6.42
146.	11.	3.07	0.14	29.92	12.19	0.00	0.5013	−0.0161	0.4934	0.0901	0.0471	−0.0021	−0.0006	−0.0019	5.45
146.	12.	3.07	0.14	30.04	14.16	0.00	0.5818	−0.0186	0.5687	0.1243	0.0614	−0.0026	−0.0010	−0.0005	4.55
146.	13.	3.07	0.14	29.94	16.14	0.00	0.6590	−0.0194	0.6384	0.1645	0.0810	−0.0024	−0.0027	−0.0022	3.86
146.	14.	3.06	0.14	29.84	18.16	0.00	0.7434	−0.0213	0.7130	0.2114	0.0986	−0.0022	−0.0066	−0.0097	3.35
146.	15.	3.06	0.14	29.85	20.18	0.00	0.8454	−0.0222	0.8012	0.2708	0.1187	−0.0026	−0.0114	−0.0117	2.94
147.	1.	4.64	0.22	69.94	−4.03	0.00	−0.1198	0.0161	−0.1183	0.0245	0.0016	0.0002	−0.0004	−0.0008	−4.90
147.	2.	4.64	0.22	69.93	−2.07	0.00	−0.0436	0.0167	−0.0430	0.0182	0.0076	0.0000	−0.0002	−0.0003	−2.41
147.	3.	4.63	0.22	70.05	−0.03	0.00	0.0356	0.0143	0.0356	0.0142	0.0124	−0.0003	−0.0005	−0.0019	2.60
147.	4.	4.62	0.22	69.93	2.03	0.00	0.1226	0.0115	0.1221	0.0158	0.0141	−0.0004	−0.0004	−0.0017	8.00
147.	5.	4.62	0.22	69.93	4.04	0.00	0.1958	0.0074	0.1948	0.0212	0.0171	−0.0008	−0.0005	−0.0014	9.43
147.	6.	4.61	0.22	69.71	6.09	0.00	0.2644	0.0027	0.2626	0.0308	0.0238	−0.0005	−0.0008	−0.0003	8.67
147.	7.	4.61	0.22	70.06	8.13	0.00	0.3366	−0.0028	0.3336	0.0448	0.0322	0.0005	−0.0012	−0.0026	7.52
147.	8.	4.61	0.22	70.07	10.12	0.00	0.4082	−0.0105	0.4037	0.0614	0.0385	0.0003	−0.0016	−0.0039	6.60
147.	9.	4.61	0.22	70.20	12.15	0.00	0.4951	−0.0159	0.4874	0.0887	0.0482	0.0008	−0.0024	−0.0049	5.50
147.	10.	4.61	0.22	70.10	14.21	0.00	0.5903	−0.0175	0.5766	0.1279	0.0601	0.0015	−0.0036	−0.0083	4.50
147.	11.	4.60	0.22	70.13	16.16	0.00	0.6537	−0.0216	0.6339	0.1612	0.0813	0.0006	−0.0040	−0.0080	3.93
147.	12.	4.59	0.22	70.05	18.16	0.00	0.7420	−0.0204	0.7114	0.2118	0.0993	0.0010	−0.0063	−0.0120	3.35
147.	13.	4.59	0.22	70.08	20.20	0.00	0.8378	−0.0213	0.7936	0.2694	0.1191	−0.0014	−0.0056	−0.0083	2.94
148.	1.	5.69	0.27	109.86	−4.08	0.00	−0.1212	0.0163	−0.1197	0.0249	0.0013	0.0003	−0.0001	−0.0011	−4.88
148.	2.	5.69	0.27	110.20	−2.02	0.00	−0.0404	0.0170	−0.0398	0.0184	0.0077	0.0001	−0.0003	0.0002	−2.22
148.	3.	5.68	0.27	110.19	−0.05	0.00	0.0395	0.0158	0.0395	0.0157	0.0127	−0.0003	−0.0006	0.0000	2.62
148.	4.	5.67	0.27	110.07	2.06	0.00	0.1267	0.0126	0.1261	0.0172	0.0146	−0.0004	−0.0004	0.0002	7.64
148.	5.	5.66	0.27	109.85	4.08	0.00	0.1962	0.0080	0.1951	0.0219	0.0174	−0.0006	−0.0006	−0.0004	9.18
148.	6.	5.66	0.27	110.20	6.06	0.00	0.2662	0.0038	0.2643	0.0319	0.0236	−0.0005	−0.0008	0.0008	8.46
148.	7.	5.64	0.27	109.75	8.12	0.00	0.3388	−0.0014	0.3357	0.0464	0.0325	0.0002	−0.0011	0.0006	7.32
148.	8.	5.65	0.27	110.34	10.10	0.00	0.4136	−0.0081	0.4086	0.0646	0.0385	0.0003	−0.0014	−0.0006	6.36
148.	9.	5.64	0.27	110.36	12.19	0.00	0.4937	−0.0145	0.4856	0.0901	0.0477	0.0010	−0.0028	−0.0034	5.40

Table B2. Continued

Run	Point	$R/10^6$	M	q	α	β	C_N	C_A	C_L	C_D	C_m	C_l	C_n	C_Y	L/D
148.	10.	5.64	0.27	110.40	14.18	0.00	0.5888	−0.0161	0.5748	0.1286	0.0603	0.0021	−0.0043	−0.0081	4.47
148.	11.	5.63	0.27	110.33	16.20	0.00	0.6583	−0.0190	0.6374	0.1654	0.0829	0.0031	−0.0066	−0.0132	3.85
148.	12.	5.62	0.27	110.38	18.23	0.00	0.7468	−0.0192	0.7153	0.2153	0.0992	0.0042	−0.0110	−0.0223	3.32
148.	13.	5.61	0.27	110.21	20.25	0.00	0.8500	−0.0192	0.8041	0.2762	0.1177	0.0015	−0.0128	−0.0242	2.90
149.	2.	3.05	0.14	30.25	−4.04	0.00	−0.1062	0.0177	−0.1047	0.0251	0.0010	−0.0001	0.0000	−0.0012	−4.16
149.	3.	3.05	0.14	30.25	−2.02	0.00	−0.0155	0.0206	−0.0147	0.0211	0.0076	−0.0001	−0.0005	0.0029	−0.70
149.	4.	3.05	0.14	30.25	0.04	0.00	0.0695	0.0204	0.0695	0.0204	0.0124	0.0000	−0.0004	0.0050	3.43
149.	5.	3.05	0.14	30.14	2.03	0.00	0.1426	0.0168	0.1419	0.0218	0.0151	−0.0002	−0.0002	0.0026	6.58
149.	6.	3.04	0.14	30.14	4.13	0.00	0.2301	0.0157	0.2284	0.0322	0.0189	−0.0001	−0.0003	0.0068	7.14
149.	7.	3.04	0.14	30.14	6.10	0.00	0.3005	0.0112	0.2976	0.0430	0.0252	−0.0001	−0.0007	0.0065	6.92
149.	8.	3.04	0.14	30.03	8.07	0.00	0.3636	0.0060	0.3592	0.0570	0.0333	−0.0003	−0.0003	0.0072	6.30
149.	9.	3.04	0.14	30.03	10.10	0.00	0.4379	−0.0012	0.4313	0.0757	0.0413	−0.0005	−0.0002	0.0065	5.69
149.	10.	3.05	0.14	30.27	12.13	0.00	0.4986	−0.0118	0.4899	0.0932	0.0501	−0.0020	−0.0003	−0.0005	5.23
149.	11.	3.05	0.14	30.27	14.14	0.00	0.5839	−0.0146	0.5697	0.1285	0.0648	−0.0020	−0.0004	0.0052	4.42
149.	12.	3.05	0.14	30.17	16.23	0.00	0.6742	−0.0163	0.6519	0.1728	0.0819	−0.0009	−0.0018	0.0073	3.76
149.	13.	3.03	0.14	29.84	18.15	0.00	0.7481	−0.0188	0.7168	0.2152	0.0987	−0.0018	−0.0059	0.0015	3.32
149.	14.	3.03	0.14	29.85	20.20	0.00	0.8322	−0.0238	0.7892	0.2650	0.1177	−0.0024	−0.0104	−0.0074	2.97
150.	1.	4.60	0.22	70.06	−4.02	0.00	−0.0986	0.0209	−0.0969	0.0278	0.0015	0.0002	−0.0001	0.0032	−3.54
150.	2.	4.59	0.22	69.94	−2.03	0.00	−0.0313	0.0185	−0.0306	0.0196	0.0065	−0.0002	−0.0003	−0.0008	−1.59
150.	3.	4.59	0.22	69.94	0.00	0.00	0.0572	0.0189	0.0572	0.0189	0.0122	−0.0001	−0.0004	0.0035	3.11
150.	4.	4.59	0.22	69.93	2.01	0.00	0.1292	0.0145	0.1286	0.0190	0.0151	−0.0005	−0.0004	0.0012	6.94
150.	5.	4.59	0.22	70.16	4.11	0.00	0.2075	0.0100	0.2062	0.0249	0.0182	−0.0005	−0.0004	0.0008	8.46
150.	6.	4.58	0.22	69.82	6.12	0.00	0.2782	0.0051	0.2761	0.0347	0.0239	−0.0004	−0.0007	0.0012	8.05
150.	7.	4.59	0.22	70.18	8.13	0.00	0.3437	−0.0005	0.3403	0.0481	0.0320	0.0001	−0.0010	−0.0007	7.14
150.	8.	4.58	0.22	70.07	10.13	0.00	0.4169	−0.0061	0.4114	0.0673	0.0410	0.0003	−0.0013	−0.0005	6.14
150.	9.	4.59	0.22	70.43	12.09	0.00	0.4859	−0.0138	0.4780	0.0883	0.0493	0.0004	−0.0022	−0.0045	5.42
150.	10.	4.57	0.22	69.99	14.14	0.00	0.5654	−0.0188	0.5529	0.1199	0.0640	0.0012	−0.0030	−0.0083	4.61
150.	11.	4.56	0.22	69.89	16.13	0.00	0.6439	−0.0235	0.6251	0.1563	0.0793	0.0006	−0.0027	−0.0051	4.00
150.	12.	4.58	0.22	70.38	18.13	0.00	0.7241	−0.0251	0.6960	0.2014	0.0969	0.0019	−0.0068	−0.0139	3.45
150.	13.	4.57	0.22	70.08	20.18	0.00	0.8100	−0.0262	0.7693	0.2548	0.1166	−0.0008	−0.0066	−0.0067	3.01
151.	1.	5.66	0.27	109.98	−4.07	0.00	−0.1046	0.0194	−0.1030	0.0268	0.0008	0.0002	0.0001	0.0001	−3.91
151.	2.	5.65	0.27	109.97	−1.98	0.00	−0.0267	0.0192	−0.0260	0.0201	0.0068	0.0000	−0.0001	0.0004	−1.33
151.	3.	5.63	0.27	109.73	0.03	0.00	0.0554	0.0181	0.0554	0.0181	0.0121	−0.0002	−0.0005	0.0022	3.17
151.	4.	5.64	0.27	110.19	2.03	0.00	0.1325	0.0145	0.1319	0.0192	0.0152	−0.0003	−0.0004	0.0015	7.13
151.	5.	5.63	0.27	109.85	4.07	0.00	0.2028	0.0097	0.2016	0.0240	0.0180	−0.0005	−0.0005	0.0003	8.64
151.	6.	5.62	0.27	110.08	6.13	0.00	0.2717	0.0044	0.2697	0.0334	0.0235	−0.0005	−0.0007	0.0005	8.24
151.	7.	5.61	0.27	109.63	8.13	0.00	0.3380	−0.0015	0.3348	0.0464	0.0318	0.0001	−0.0010	−0.0017	7.30
151.	8.	5.62	0.27	110.34	10.15	0.00	0.4109	−0.0070	0.4057	0.0655	0.0405	0.0002	−0.0015	−0.0011	6.23
151.	9.	5.61	0.27	110.25	12.09	0.00	0.4822	−0.0140	0.4744	0.0873	0.0491	0.0007	−0.0025	−0.0044	5.45
151.	10.	5.61	0.27	110.51	14.12	0.00	0.5609	−0.0192	0.5486	0.1182	0.0641	0.0020	−0.0039	−0.0098	4.65
151.	11.	5.61	0.27	110.43	16.13	0.00	0.6405	−0.0240	0.6219	0.1550	0.0790	0.0029	−0.0055	−0.0127	4.02
151.	12.	5.60	0.27	110.48	18.12	0.00	0.7172	−0.0258	0.6896	0.1985	0.0958	0.0035	−0.0099	−0.0218	3.47
151.	13.	5.60	0.27	110.31	20.19	0.00	0.8072	−0.0264	0.7667	0.2537	0.1175	0.0029	−0.0134	−0.0259	3.02
154.	6.	4.71	0.22	70.17	−4.03	0.00	−0.0545	0.0154	−0.0533	0.0192	0.0194	0.0003	−0.0004	0.0007	−2.82
154.	7.	4.68	0.22	69.82	−2.05	0.00	−0.0058	0.0141	−0.0052	0.0143	0.0285	0.0000	−0.0005	−0.0026	−0.37
154.	8.	4.67	0.22	70.05	0.02	0.00	0.0708	0.0197	0.0708	0.0197	0.0391	−0.0003	−0.0008	0.0003	3.68
154.	9.	4.66	0.22	69.83	2.09	0.00	0.1432	0.0229	0.1423	0.0281	0.0485	−0.0004	−0.0005	0.0003	5.16
154.	10.	4.66	0.22	70.07	4.11	0.00	0.2167	0.0249	0.2143	0.0404	0.0574	−0.0008	−0.0010	−0.0020	5.38
154.	11.	4.66	0.22	70.20	6.10	0.00	0.3050	0.0297	0.3002	0.0619	0.0717	−0.0011	−0.0010	−0.0023	4.89
154.	12.	4.65	0.22	69.98	8.07	0.00	0.3777	0.0356	0.3689	0.0883	0.0971	−0.0012	−0.0013	−0.0024	4.20

Table B2. Concluded

Run	Point	$R/10^6$	M	q	α	β	C_N	C_A	C_L	C_D	C_m	C_l	C_n	C_Y	L/D
154.	13.	4.64	0.22	69.90	10.14	0.00	0.4986	0.0429	0.4833	0.1300	0.1184	−0.0002	−0.0013	−0.0037	3.72
154.	14.	4.64	0.22	70.15	12.17	0.00	0.6095	0.0481	0.5857	0.1755	0.1399	−0.0012	−0.0012	−0.0037	3.33
154.	15.	4.63	0.22	69.95	14.15	0.00	0.7098	0.0523	0.6755	0.2243	0.1655	−0.0013	−0.0024	−0.0037	3.01
154.	16.	4.63	0.22	70.22	16.16	0.00	0.8121	0.0562	0.7644	0.2800	0.1900	−0.0013	−0.0033	−0.0065	2.72
154.	17.	4.63	0.22	70.38	18.21	0.00	0.9296	0.0621	0.8636	0.3495	0.2140	−0.0003	−0.0065	−0.0088	2.46
154.	18.	4.62	0.22	70.20	20.24	0.00	1.0422	0.0659	0.9550	0.4224	0.2404	0.0015	−0.0105	−0.0149	2.25
155.	2.	4.71	0.22	69.93	−4.00	0.00	−0.0579	0.0140	−0.0568	0.0180	0.0215	0.0002	−0.0001	0.0002	−3.21
155.	3.	4.71	0.22	70.17	−2.02	0.00	0.0132	0.0188	0.0138	0.0184	0.0329	−0.0002	−0.0003	−0.0019	0.77
155.	4.	4.69	0.22	70.06	0.03	0.00	0.0876	0.0254	0.0876	0.0254	0.0466	−0.0005	−0.0006	0.0007	3.51
155.	5.	4.69	0.22	70.06	2.07	0.00	0.1595	0.0297	0.1583	0.0355	0.0586	−0.0008	−0.0006	−0.0012	4.53
155.	6.	4.67	0.22	69.73	4.12	0.00	0.2438	0.0354	0.2406	0.0528	0.0715	−0.0009	−0.0005	−0.0007	4.61
155.	7.	4.68	0.22	70.09	6.15	0.00	0.3317	0.0409	0.3254	0.0763	0.0867	−0.0013	−0.0005	−0.0010	4.30
155.	8.	4.67	0.22	69.88	8.11	0.00	0.4127	0.0482	0.4018	0.1059	0.1102	−0.0016	−0.0006	0.0003	3.82
155.	9.	4.66	0.22	69.91	10.19	0.00	0.4994	0.0543	0.4820	0.1417	0.1347	−0.0011	−0.0008	−0.0008	3.41
155.	10.	4.67	0.22	70.17	12.19	0.00	0.6191	0.0624	0.5920	0.1918	0.1596	−0.0017	−0.0006	−0.0001	3.09
155.	11.	4.66	0.22	70.09	14.14	0.00	0.7065	0.0681	0.6684	0.2387	0.1892	−0.0012	−0.0016	−0.0026	2.80
155.	12.	4.66	0.22	70.13	16.20	0.00	0.8270	0.0765	0.7728	0.3043	0.2183	−0.0010	−0.0025	−0.0017	2.53
155.	13.	4.67	0.22	70.52	18.25	0.00	0.9423	0.0832	0.8688	0.3741	0.2475	−0.0007	−0.0049	−0.0040	2.32
155.	14.	4.65	0.22	70.11	20.19	0.00	1.0545	0.0902	0.9585	0.4486	0.2791	−0.0005	−0.0072	−0.0064	2.13
156.	2.	4.68	0.22	70.16	−4.04	0.00	−0.0606	0.0111	−0.0596	0.0154	0.0122	0.0005	−0.0002	0.0011	−3.96
156.	3.	4.68	0.22	70.39	−1.98	0.00	0.0138	0.0151	0.0143	0.0147	0.0195	0.0001	−0.0002	0.0013	1.00
156.	4.	4.66	0.22	70.17	0.03	0.00	0.0837	0.0191	0.0837	0.0192	0.0280	−0.0001	−0.0001	0.0012	4.49
156.	5.	4.66	0.22	70.06	2.03	0.00	0.1550	0.0214	0.1541	0.0269	0.0354	−0.0004	−0.0006	0.0014	5.84
156.	6.	4.65	0.22	70.06	4.02	0.00	0.2328	0.0246	0.2305	0.0408	0.0438	−0.0006	−0.0006	0.0026	5.73
156.	7.	4.64	0.22	69.96	6.15	0.00	0.3257	0.0289	0.3208	0.0636	0.0583	−0.0010	−0.0007	0.0006	5.08
156.	8.	4.65	0.22	69.98	8.19	0.00	0.4167	0.0350	0.4074	0.0940	0.0834	−0.0011	−0.0007	−0.0003	4.35
156.	9.	4.65	0.22	70.24	10.16	0.00	0.5212	0.0401	0.5059	0.1314	0.1049	−0.0012	−0.0011	0.0007	3.85
156.	10.	4.64	0.22	70.15	12.19	0.00	0.6286	0.0456	0.6048	0.1773	0.1276	−0.0009	−0.0012	0.0015	3.41
156.	11.	4.63	0.22	69.95	14.11	0.00	0.7209	0.0478	0.6874	0.2221	0.1484	−0.0004	−0.0028	−0.0039	3.09
156.	12.	4.63	0.22	69.99	16.22	0.00	0.8391	0.0533	0.7908	0.2856	0.1722	−0.0002	−0.0044	−0.0051	2.76
156.	13.	4.63	0.22	70.14	18.24	0.00	0.9469	0.0574	0.8814	0.3510	0.1970	0.0017	−0.0084	−0.0102	2.50
156.	14.	4.63	0.22	70.19	20.17	0.00	1.0555	0.0610	0.9698	0.4212	0.2209	0.0034	−0.0121	−0.0172	2.29
157.	2.	4.65	0.22	69.93	−4.04	0.00	−0.0592	0.0107	−0.0583	0.0148	0.0128	0.0002	−0.0004	0.0005	−4.05
157.	3.	4.65	0.22	70.16	−2.04	0.00	0.0102	0.0147	0.0107	0.0143	0.0206	−0.0001	−0.0005	−0.0011	0.77
157.	4.	4.64	0.22	70.05	0.02	0.00	0.0848	0.0194	0.0848	0.0194	0.0309	−0.0003	−0.0006	−0.0004	4.50
157.	5.	4.64	0.22	69.94	2.13	0.00	0.1601	0.0228	0.1592	0.0288	0.0406	−0.0005	−0.0007	−0.0003	5.66
157.	6.	4.63	0.22	69.95	4.04	0.00	0.2356	0.0261	0.2332	0.0426	0.0500	−0.0007	−0.0008	−0.0004	5.55
157.	7.	4.63	0.22	70.08	6.14	0.00	0.3344	0.0323	0.3290	0.0678	0.0652	−0.0007	−0.0007	0.0010	4.89
157.	8.	4.63	0.22	69.99	8.12	0.00	0.4105	0.0383	0.4009	0.0959	0.0914	−0.0011	−0.0008	0.0011	4.20
157.	9.	4.63	0.22	70.24	10.27	0.00	0.5160	0.0439	0.4999	0.1352	0.1132	−0.0013	−0.0013	−0.0007	3.70
157.	10.	4.63	0.22	70.15	12.10	0.00	0.6096	0.0496	0.5857	0.1762	0.1380	−0.0005	−0.0011	−0.0013	3.32
157.	11.	4.63	0.22	70.30	14.16	0.00	0.7310	0.0547	0.6954	0.2318	0.1617	−0.0010	−0.0023	−0.0039	2.99
157.	12.	4.61	0.22	70.00	16.27	0.00	0.8515	0.0608	0.8004	0.2970	0.1911	−0.0009	−0.0042	−0.0055	2.69
157.	13.	4.62	0.22	70.27	18.25	0.00	0.9637	0.0676	0.8941	0.3660	0.2188	0.0004	−0.0069	−0.0066	2.43
157.	14.	4.61	0.22	70.09	20.21	0.00	1.0818	0.0729	0.9900	0.4422	0.2475	0.0016	−0.0100	−0.0121	2.23

References

1. Robins, A. Warner: Dollyhigh, Samuel M.: Beissner, Fred L., Jr.: Geiselhart, Karl; Martin, Glenn L.: Shields, E. W.; Swanson, E. E.; Coen, Peter G.: and Morris, Shelby J., Jr.: *Concept Development of a Mach 3.0 High-Speed Civil Transport.* NASA TM-4058, 1988.

2. Coe, Paul L., Jr.: and Thomas, James L.: *Theoretical and Experimental Investigation of Ground-Induced Effects for a Low-Aspect-Ratio Highly Swept Arrow-Wing Configuration.* NASA TP-1508, 1979.

3. Coe, Paul L., Jr.; Huffman, Jarrett K.; and Fenbert, James W.: *Leading-Edge Deflection Optimization for a Highly Swept Arrow-Wing Configuration.* NASA TP-1777, 1980.

4. Hoffman, Sherwood: *Bibliography of Supersonic Cruise Research (SCR) Program From 1980 to 1983.* NASA RP-1117, 1984.

5. Hoffman, Sherwood: *Bibliography of Supersonic Cruise Research (SCR) Program From 1977 to Mid-1980.* NASA RP-1063, 1980.

6. Coe, Paul L., Jr.; Kjelgaard, Scott O.; and Gentry, Garl L., Jr.: *Low-Speed Aerodynamic Characteristics of a Highly Swept, Untwisted, Uncambered Arrow Wing.* NASA TP-2176, 1983.

7. Scott, Samuel J.; Nicks, Oran W.; and Imbrie, P. K.: *Effects of Leading-Edge Devices on the Low-Speed Aerodynamic Characteristics of a Highly-Swept Arrow-Wing.* NASA CR-172531, 1985.

8. Darden, Christine M.; and Shepherd, Kevin P.: Assessment and Design of Low Boom Configurations for Supersonic Transport Aircraft. Paper presented at the DGLR/AIAA 14th Aeroacoustics Conference (Aachen, Germany), May 11–14, 1992.

9. Whitehead, Allen H., Jr., compiler: *First Annual High-Speed Research Workshop.* NASA CP-10087, Parts 1–4, 1992.

10. Rao, Dhanvada M.: *Subsonic Flow Investigations on a Cranked Wing Designed For High Maneuverability.* NASA CR-178046, 1986.

11. Rao, Dhanvada M.: *Low-Speed Wind Tunnel Study of Longitudinal Stability and Usable-Lift Improvement of a Cranked Wing.* NASA CR-178204, 1987.

12. Campbell, Bryan A.; Hom, Kam W.; and Huffman, Jarrett K.: *Investigation of Subsonic Maneuver Performance of a Supersonic Fighter Cranked Wing.* NASA TP-2687, 1987.

13. Gentry, Garl L., Jr.; Quinto, P. Frank; Gatlin, Gregory M.; and Applin, Zachary T.: *The Langley 14- by 22-Foot Subsonic Tunnel: Description, Flow Characteristics, and Guide for Users.* NASA TP-3008, 1990.

14. Craidon, Charlotte B., compiler: *A Description of the Langley Wireframe Geometry Standard (LaWGS) Format.* NASA TM-85767, 1985.

15. Rae, William H., Jr.: and Pope, Alan: *Low-Speed Wind Tunnel Testing.* Second ed. John Wiley & Sons, Inc., c.1984.

16. Herriot, John G.: *Blockage Corrections for Three-Dimensional-Flow Closed-Throat Wind Tunnels, With Consideration of the Effect of Compressibility.* NACA Rep. 995, 1950. (Supersedes NACA RM A7B28.)

17. Rao, Dhanvada M.; and Campbell, James F.: Vortical Flow Management Techniques. *Prog. Aerosp. Sci.*, vol. 24, 1987, pp. 173–224.

18. Moskovitz, C. A.; Hall, R. M.; and DeJarnette, F. R.: New Device for Controlling Asymmetric Flowfields on Forebodies at Large Alpha. *J. Aircr.*, vol. 28, no. 7, July 1991, pp. 456–462.

19. Braslow, Albert L.; and Knox, Eugene C.: *Simplified Method for Determination of Critical Height of Distributed Roughness Particles for Boundary-Layer Transition at Mach Numbers From 0 to 5.* NACA TN 4363, 1958.

20. Hall, R. M.; Erickson, G. E.; Banks, D. W.; and Fisher, D. F.: Advances in High-Alpha Experimental Aerodynamics: Ground Test and Flight. *High-Angle-of-Attack Technology*, Volume I, Joseph R. Chambers, William P. Gilbert, and Luat T. Nguyen, eds., NASA CP-3149, Part 1, 1992, pp. 69–115.

21. Lamont, P. J.: Pressure Measurements on an Ogive-Cylinder at High Angles of Attack With Laminar, Transitional, or Turbulent Separation. *A Collection of Technical Papers—AIAA Atmospheric Flight Mechanics Conference*, Aug. 1980, pp. 1–10. (Available as AIAA-80-1556.)

22. Lamont, P. J.: Pressures Around an Inclined Ogive Cylinder With Laminar, Transitional, or Turbulent Separation. *AIAA J.*, vol. 20, no. 11, Nov. 1982, pp. 1492–1499.

23. Campbell, Bryan A.; and Riebe, Gregory D.: An Investigation of the Subsonic Maneuver Characteristics of Two Supersonic Fighter Wing Concepts. *Vortex Flow Aerodynamics*, Volume II, NASA CP-2417, 1986, pp. 185–199.

24. Frink, Neal T.: *Concept for Designing Vortex Flap Geometries.* NASA TP-2233, 1983.

25. Gatlin, Gregory M.: Advanced Fighter Tested for Low-Speed Aerodynamics With Vortex Flaps. *Vortex Flow Aerodynamics*, Volume II, James F. Campbell, Russell F. Osborn, and Jerome T. Foughner, Jr., eds., NASA CP-2417, 1986, pp. 1–16.

REPORT DOCUMENTATION PAGE		Form Approved OMB No. 0704-0188

1. AGENCY USE ONLY (*Leave blank*)	2. REPORT DATE	3. REPORT TYPE AND DATES COVERED
	December 1999	Technical Publication

4. TITLE AND SUBTITLE	5. FUNDING NUMBERS
Subsonic Aerodynamic Assessment of Vortex Flow Management Devices on a High-Speed Civil Transport Configuration	WU 537-03-22-02
6. AUTHOR(S) Bryan A. Campbell, Zachary T. Applin, and Guy T. Kemmerly	

7. PERFORMING ORGANIZATION NAME(S) AND ADDRESS(ES)	8. PERFORMING ORGANIZATION REPORT NUMBER
NASA Langley Research Center Hampton, VA 23681-2199	L-17147

9. SPONSORING/MONITORING AGENCY NAME(S) AND ADDRESS(ES)	10. SPONSORING/MONITORING AGENCY REPORT NUMBER
National Aeronautics and Space Administration Washington, DC 20546-0001	NASA/TP-1999-209693

11. SUPPLEMENTARY NOTES

12a. DISTRIBUTION/AVAILABILITY STATEMENT	12b. DISTRIBUTION CODE
Unclassified–Unlimited Subject Category 02 Distribution: Nonstandard Availability: NASA CASI (301) 621-0390	

13. ABSTRACT (*Maximum 200 words*)

An experimental investigation of the effects of leading-edge vortex management devices on the subsonic performance of a high-speed civil transport (HSCT) configuration was conducted in the Langley 14- by 22-Foot Subsonic Tunnel. Data were obtained over a Mach number range of 0.14 to 0.27, with corresponding chord Reynolds numbers of 3.08×10^6 to 5.47×10^6. The test model was designed for a cruise Mach number of 2.7. During the subsonic high-lift phase of flight, vortical flow dominates the upper surface flow structure, and during vortex breakdown, this flow causes adverse pitch-up and a reduction of usable lift. The experimental results showed that the beneficial effects of small leading-edge vortex management devices located near the model reference center were insufficient to substantially affect the resulting aerodynamic forces and moments. However, devices located at or near the wing apex region demonstrated potential for pitch control with little effect on overall lift.

14. SUBJECT TERMS	15. NUMBER OF PAGES
High-speed civil transport; HSCT; High-speed research; HSR; Vortex flow management	112
	16. PRICE CODE A06

17. SECURITY CLASSIFICATION OF REPORT	18. SECURITY CLASSIFICATION OF THIS PAGE	19. SECURITY CLASSIFICATION OF ABSTRACT	20. LIMITATION OF ABSTRACT
Unclassified	Unclassified	Unclassified	UL

NSN 7540-01-280-5500

Standard Form 298 (Rev. 2-89)
Prescribed by ANSI Std. Z39-18
298-102